UNIVERSITA' DEGLI STUDI DI SIENA

DIPARTIMENTO DI BIOTECNOLOGIA, CHIMICA E FARMACIA

DIPARTIMENTO DI ECCELLENZA 2018-2022

DOTTORATO DI RICERCA IN
CHEMICAL AND PHARMACEUTICAL SCIENCES

CICLO XXXIV

COORDINATORE PROF. MAURIZIO TADDEI

DIVERGENT SYNTHESIS AND MoA INVESTIGATION OF ANTIBACTERIAL ALKYLGUANIDINO UREAS

SETTORE SCIENTIFICO-DISCIPLINARE: **CHIM/08**

DOTTORANDO
Claudia Ardino

TUTOR
Prof.ssa Elena Petricci

ANNO ACCADEMICO: 2021/2022

UNIVERSITA' DEGLI STUDI DI SIENA

DIPARTIMENTO DI BIOTECNOLOGIA, CHIMICA E FARMACIA
DIPARTIMENTO DI ECCELLENZA 2018-2022

DOTTORATO DI RICERCA IN
CHEMICAL AND PHARMACEUTICAL SCIENCES

CICLO XXXIV

COORDINATORE PROF. MAURIZIO TADDEI

DIVERGENT SYNTHESIS AND MoA INVESTIGATION OF ANTIBACTERIAL ALKYLGUANIDINO UREAS

SETTORE SCIENTIFICO-DISCIPLINARE: **CHIM/08**

DOTTORANDO
Claudia Ardino

TUTOR
Prof.ssa Elena Petricci

ANNO ACCADEMICO: 2021/2022

This work is dedicated to the memory of Professor Maurizio Botta,
whose longstanding contribution to chemistry inspired me through the last years.

E però leva sù: vinci l'ambascia
con l'animo che vince ogne battaglia,
se col suo grave corpo non s'accascia.

- ***Dante, Divine Comedy, Inferno XXXIV*** -

External Referees

Prof. Luigi Vaccaro – *University of Perugia*
Research areas/interest: Organic Chemistry

Prof. Lorenzo Botta – *University of Tuscia*
Research areas/interest: Organic Chemistry

Examination Commission

Prof. Lorenzo Botta – *University of Tuscia*

Prof. Silvia Schenone – *University of Genova*

Prof. Stefania Butini – *University of Siena*

Prof. Luigi Vaccaro – *University of Perugia*

Acknowledgments

The past three years were not an easy ride academically speaking. The untimely death of Prof. Maurizio Botta and the recent Covid-19 pandemic outbreak seriously hampered this research work. For these reasons, I will forever be thankful to all the people listed below for helping me completing my research.

The work described in Chapter I was performed at the Department of Biotechnology, Chemistry and Pharmacy of the University of Siena between 2018 and 2021, under the supervision first of Prof. Maurizio Botta and then of Prof. Elena Petricci. Whereas, the work presented in Chapter II was performed at the Van't Hoff Institute for Molecular Sciences (HIMS) of the Universiteeit of Amsterdam, The Netherlands, under the supervision of Prof. Ing. Timothy Noël.

I would like to sincerely thank my supervisor Elena Petricci for the scientific support and for giving me the opportunity to express my scientific creativity with this work, never forcing me in any direction and letting me free to make my own mistakes to improve by myself.
Also, I would like to say a huge thank you to Prof. Jean-Denis Docquier for the antimicrobial susceptibility tests performed on the described compounds and also for its scientific guidance and contribution to all the work.
I would also like to thank Prof. Paolo Visca for the University of Roma Tre for the permeability assays and the hemolysis performed to investigate the MoA of the herein presented compounds. Moreover, I would like to express my gratitude also to Dr. Giulio Poli, from University of Pisa, who performed the Molecular Dynamics simulations, and to Prof. Elena Dreassi for her contribution in setting and performing the LUVs interaction and PAMPA assays and for always being participative in any analytical issues I faced during the thesis.
I am also sincerely grateful to Lead Discovery Siena S.r.l. and to Prof. Lorenzo Botta from the University of Tuscia, for his moral and scientific support, always helping me with everything I needed to complete this work.
I thankfully acknowledge the fundings received from the Erasmus+ for traineeship programme, that were provided to financially support my life in The Netherlands, during my visiting stay at the Universiteeit of Amsterdam.

In the end, a massive thank-you to Dr. Ilaria D'Agostino for being such an inspiring scientist and mentor who guided me through all this work, teaching me with patience all her knowledge, and supporting me every day not only professionally but also on a personal level. This meant everything to me. I feel very blessed that our paths have crossed each other.

Last but not least, I would like to hugely thank Prof. Ing. Timothy Noël who made me feel very welcomed in his laboratory and in his research team in Amsterdam. It was a pleasure to share six months with you and your team, who taught me more than I could have expected. But mostly, I would like to thank you for pushing me day by day to believe in myself and in my capabilities, for your invaluable advices both academical and personal, and for always being so supportive of my work.
Finally, thanks to Dr. Daniele Mazzarella, for his guidance and support, in conceiving and performing the work presented in Chapter II, and to Dr. Luca Capaldo, Dr. Antonio Pulcinella, Dr. Stefano Bonciolini and all team members of Noël research group to have patiently guided me in the field of photochemistry.

A special mention and dedication of this work goes to Prof. Maurizio Botta, who taught me that hard work always pays off even in the darkest days. Thank you.

Table of Contents

CHAPTER I: Divergent synthesis and MoA investigations of novel antibacterial Alkylguanidino Ureas

CHAPTER I:

Divergent Synthesis and MoA investigation of antibacterial Alkylguanidino Ureas

1. Introduction

1.1 The Antimicrobial Resistance: a silent pandemic

Drug-resistant infections are responsible for an ever-increasing pervasive public health threat to human, animal, plant and environmental health and such infections have the potential to become one of the leading causes of death in the foreseeable future.[1] Antimicrobial Resistance (AMR) generally occurs when bacteria, viruses, fungi or parasites tend to no longer respond to medical treatments, consequently increasing the spread of several diseases that can cause severe illness and death.[2] To prevent this scenario it is absolutely crucial the development of a multisectoral action plan focusing global efforts to address this issue. Costs of AMR to the economy is significant, since prolonged illness can cause the need for more expensive and intensive care and longer hospital stays.[2] For these reasons, antimicrobial stewardships, innovations and investment plans across all sectors (agriculture, veterinary and human medicine) are required to mitigate the occurrence of resistant pathogens infections and limit their spread.[3] A wide variety of academic and industrial Research and Development (R&D) projects focusing on bacterial diseases were in the 2020 pipeline[4,5] but several statics highlighted that the pharmaceutical industry needs to reach more people and more countries with both old and new medical treatments, since many of the world's most vulnerable patients are still awaiting to receive their life-saving antibacterial treatments needed.[4] Currently, the Antimicrobial Resistance Multi Partner Trust Fund (AMR MPTF),[6] the Global Antibiotic Research & Development Partnership (GARDP)[7] and other funds and initiatives have been lunched to fill the funding gap in antimicrobial R&D. In fact, research on AMR is extremely underfunded compared to other research areas like cancer or cardiac diseases.[8] Several companies have continued to exit the field due to the low-profit margin of antibacterial research[9], contributing to further weaken this already unstable industrial setting. Hence, there is an urgent need of novel antimicrobial drugs, vaccines and diagnostic tools to tackle the critical spread of multi- and pan-resistant bacteria ("superbugs") or alarming Gram-negative ones, such as carbapenem-resistant Enterobacteriaceae and *Acinetobacter baumannii,* for which only few therapeutic options are still available.[2,10] In fact, any novel antibiotic has been approved by Food and Drugs Administration (FDA) since the launch of Cefiderocol in 2019[11] and Lefamulin represented the last chemical innovation to enter the market.[12,13]

The recent COVID-19 pandemic outbreak proved us that we are still incredibly vulnerable to infections for which we do not have therapies and, despite significant efforts have been made to educate the public opinion about the AMR crisis, its priority remains low on the list when it comes to take action over it.[8] The United Nations Organizations (ONU),[14] the World Health Organization (WHO)[2] and the World Bank (WB)[15] agreed and recognized AMR as a public health and economic concern. Moreover, a 2016 report written by the economist Jim O'Neill and his team, stated that, if left unsolved, the AMR threat will result in one of the leading cause of death by 2050, outperforming cancer and cardiac diseases (Fig.

1).[16] The COVID-19 pandemic and AMR could be considered as parallel and interacting health emergencies since we can consider their measures (handwashing, physical distancing, quarantining and travel restrictions) and consequences comparable.[3] Moreover, COVID-19 outbreak highlighted the potential long-term impact of AMR since its progression is less acute but gradual and constant over time.[3] In addition to well-known factors that can influence AMR (susceptibility and resistance to antimicrobials, drug concentrations, host factors like the serum effect and the impact on gut-microbiota),[17] the overuse and misuse of already existing antimicrobial drugs strengthened AMR during the COVID-19 pandemic.[18] Indeed, hydroxychloroquine and azithromycin[19] along with a wide variety of broad-spectrum antimicrobials were used as experimental therapies in the early stage of the outbreak, with 72% of COVID-19 registered cases receiving an antibacterial therapy.[20] Moreover, secondary bacterial[20–22] or fungal[23–26] infections among patients hospitalized with COVID-19 have been well reported. Indeed, these patients showed primarily Gram-negative bacteria associated infections, like *Pseudomonas aureginosa*, but also late-stage Gram-positive ones, like *Staphilococcus aureus*.[22]

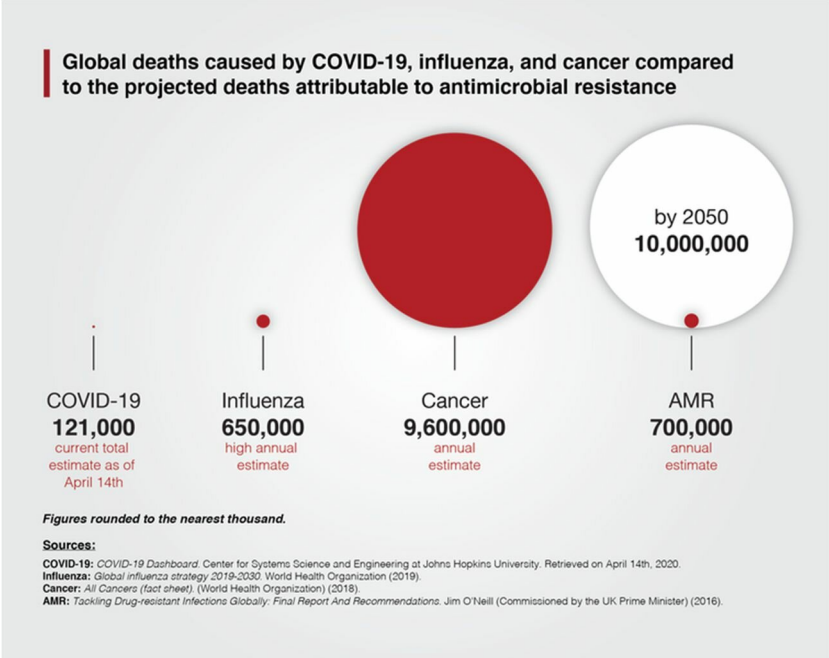

Figure 1. A global thread intensified by the fight against coronavirus.[8]

These evidences arose one again the urgent need of discovering new chemical classes exhibiting innovative mechanisms of action, since few novel chemical scaffolds were proposed in the recent years[27] and the discovery of novel classes has dramatically slowed down.[28]

Known classes of antibiotics and their chemical scaffold have been synthetically modified over the past years into their new-generation version, generally expanding their spectrum of action and reducing side effect.[28] However, the number of derivatives that can be developed from a known molecule could be

limited and the call for greater efforts to identify and synthesize innovative classes of antibiotics is still ongoing.[28]

1.2 The search for novel antibiotics, strategies to overcome AMR and current available therapies

1.2.1 The search for novel antibiotics: a big pharma issue to address

Therapeutic options to treat antibacterial infections are limited due to antibacterial resistance.[29] Among all the bacterial pathogens associated with multi-drug resistance, ESKAPE bacteria are responsible for the ma*J*ority of nosocomial infections and are thus capable to avoid the inhibitory activity of a wide variety of antibacterial drugs.[30] The term "ESKAPE" is an acronym for six bacterial pathogens: *Enterococcus faecium (E. faecium)*, *Staphylococcus aureus* (*S. aureus*), *Klebsiella pneumoniae* (*K. pneumoniae*), *Acinetobacter baumannii* (*A. baumannii*), *Pseudomonas aeruginosa* (*P. aeruginosa*), and *Enterobacter spp.*[31] These bacteria are resistant to more than one antibiotic and along with Extensively Drug-Resistant (XDR) bacteria, which are insusceptible to almost all approved antimicrobials[32], represent the key reason to design novel promising drugs.[33]

As previously outlined, several pharmaceutical companies, such as Novartis, AstraZeneca, Sanofi, Bristol-Meyers Squibb, and Allergan are dropping new antimicrobial research pro*J*ects[33], mainly for economic reasons[34]. Indeed, the costs for R&D and clinical trials represent a big financial risk when it comes to antibacterial drugs, since they only offer moderate investments returns compared to other class of drugs.[35,36] Moreover, novel antimicrobials are typically used for a limited period of time in critically ill patients, due to the rapid rising of resistance against these new drugs.[33] As a result, the last discovery of an entirely original class of antibacterial drugs dates back to 1980s and from 1980 to 2014, in the United States, the number of antibiotic approvals dramatically decreased compared to anticancer drugs approvals (Fig. 2).[37]

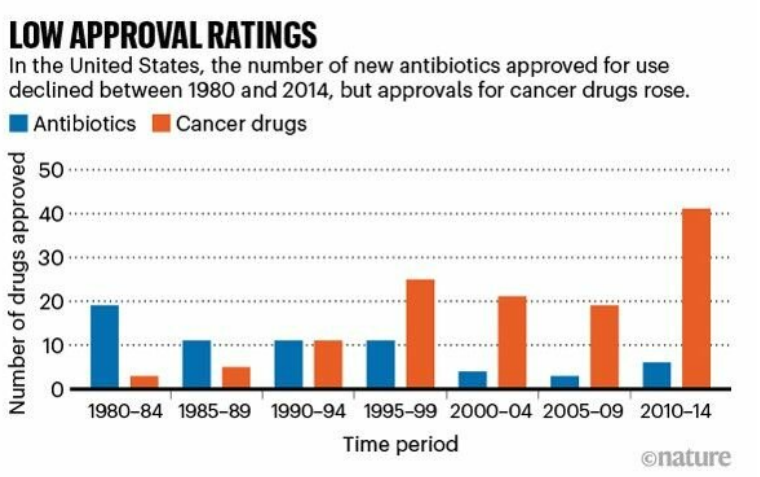

Figure 2. Novel antibacterials approval ratings in the United States.[37]

In fact, as pathogens have acquired more and more mechanisms to evade the antibiotic arsenal, the design of New Chemical Entities (NCE) endowed with antibacterial activity is not trivial and the resulting costs are challenging.[37] Moreover, conventionally, the research for novel antibiotic classes starts from nature[37] and thus the synthetic strategies required for their analogues are generally time and cost-consuming.[38] The price of innovation in the pharmaceutical industry is estimated to be 240-480 million per approved candidate, posing a remarkable barrier to the development of drugs in general.[39] Further, novel antibiotics that finally reach the market have to deal with already approved antimicrobials and health-practitioners could be generally reluctant to employ, on a large scale, antibiotics to which resistance mechanism are yet to be discovered.[28] These factors led big pharmaceutical companies to an exodus from the antibacterial field. Overall, thankfully small pharmaceutical companies and academia continue to focus their efforts addressing AMR, even though only some representatives are currently working on new classes of antibacterial agents.[40]

1.2.2 Synergism and antibiotics adjuvants.

In the past years, health-care leaders tried to improve the management and the therapeutic plans of already existing antibiotics. Several approaches involved drug rotation strategies, in which when resistance to a certain antibiotic reaches critical levels an alternative drug should be rapidly used.[41] In addition, other promising approaches relied on targeting non-essential bacterial pathways by using combination of antibiotics with ad*J*uvants.[42] In fact, synergy and drug combinations actually are the most promising strategies in fighting AMR and the use of adjuvants could be helpful to prevent the activity of already existing antibiotics, avoiding the rising of resistance.[43] For instance, the most successful example of this approach is the combination of the potent β-lactam Amoxicillin, generally inactivated by β-lactamases, and the clavulanic acid.[44] The latter is a β-lactamases inhibitor, also endowed with a slight antibacterial activity, which is able to enhance the inhibitory activity of Amoxicillin, operating on specific secondary pathways that generally lead to resistance mechanism.[43] Adjuvants could be also helpful to lower the dose of viable antibiotics, mitigating their potential side effect, as in the case of the last-resort antibiotic colistin.[45] In Tab. 1 are reported antibiotic adjuvant classes and their representatives.

In general, synergy is a well-known and defined concept in the microbiological field, and it is defined as the microbial growth inhibition operated by at least two bioactive agents exerting a mutual positive interaction.[46] Several fruitful antibiotic combinations are reported and resulted to be successful either in *in vitro* or in *in vivo* models and in clinical trials. Indeed, combination of FDA-approved antibacterial agents proved to be therapeutically effective to treat severe and persistent resistant bacteria infections. As a proof, treatment of *A.baumannii* with a synergistic combination of colistin, meropenem and tygecicline resulted in the resolution of the disease.[47] Moreover, persistent staphylococcal bacteremia can be treated

with a positive outcome using daptomycin plus ceftaroline.[48] Further examples may involve the glycopeptide vancomycin in combination with antistaphylococcal β-lactams to treat severe *Methicillin-Resistant Sthapylococcus aureus* (MRSA), which proved to be a salvage protocol both *in vitro* and in clinical trials.[49] Finally, the synergism of daptomycin with dalbavancin and linezolid is reported to fight MDR pathogens and MRSA.[50] In Tab. 2 are summarized several antibiotics combination and the relative studies that supports the synergism.

Table 1. Overview of some antibiotic adjuvant classes with their representatives.[43]

Antibiotic Adjuvant Class	Compound Name	Bacterium
Efflux Pumps Inhibitors	Phenotiazines, Phenylalanine-arginine-β-naphtylamide (PaβN), Arylpiperazine, Quinolines, Thioridazine (TZ) derivatives	Gram-positive Gram-negative
β-Lactamase inhibitors	Clavulanic acid, Sulbactam, Tazobactam, Diazabicyclooctane (DBO) Boronic acids	Gram-positive Gram-negative
Membrane permeabilizers	Caragenins, Glycine basic peptide (GBP) Menadione, Antimicrobial peptides (AMPs)	Gram-positive Gram-negative

Table 2. Antibiotic combinations.[51]

Antibiotic	Antibiotic in combination	Bacterium	Studies to support synergism
Colistin	Azythromicin	*A.Baumannii, K.Pneumoniae, P.Areuginosa*	Time-kill curves
	Chloramphenicol	*K.Pneumoniae*	Time-kill curves
	Doripenem	*P.areuginosa*	*In vitro* studies
	Rifampim	*A.baumannii*	Time-kill curves
	Tazobactam	*A.baumannii*	Time-kill curves
	Tigecycline	*A.baumannii, K.Pneumoniae, CRE*[a]	Time-kill curves, clinical data
	Vancomycin	*A. baumannii*	Time-kill curves
Daptomycin	Ceftaroline	MRSA	Bacteremic patients
	β-lactams	MRSA, enterococci	Tme-kill curves
	Dalbavancin	MRSA, enterococci	Checkboard
	Gentamicin	MRSA, enterococci	Time-kill curves
	Linezolid	MRSA	Checkboard
	Sulbactam, Tazobactam	MRSA, VISA[b], hVISA[c]	Time-kill curves
	Tigecycline	MRSA	Time-kill curves, surgical site infection model

Levofloxacin	Linezolid	*B.anthracis*	Synergy in checkboard against Sterne strain
Vancomycin	β-lactams	MRSA	In vitro and in vivo models
	Ceftaroline	MRSA	Clinical case studies
	Flucloxacillin	MRSA	Bacteremic patients
	Gentamicin	MRSA	Time-kill curves
	Trimethoprim-sulfamethoxole	MRSA	Clinical studies

[a] CRE: carbapenem-resistant Enterobacteriaceae.
[b] VISA: vamcomycin-intermediate *S.aureus.*
[c] hVISA: heteroresistant vancomycin-intermediate *S.aureus.*

1.2.3 Colistin: the last-resort antibiotic to treat MDR Gram-negative infections.

Colistin (Figure 3) is indeed an old antibiotic belonging to the polymyxin class. Discovered in the late 1940s, its nephron- and neuro-toxicity related issues deterred its prescription for years.[52] The threatening emergency of resistant Gram-negative pathogens in late 1990s caused a renewed interest in the therapeutic use of the this drug.[53] Nowadays, colistin still represents an important treatment option and in some cases the only one still effective to fight MDR *A.baumannii*, *P.aeruginosa* and *K.pneumoniae*.[54] Polymyxins like colistin target the bacterial cell membrane. Particularly, colistin associates to the bacterial membrane through electrostatic interactions between its cationic moieties and the anionic Lipopolysaccharides (LPS) structures in the Gram-negative outer membrane, displacing its stabilizing ions like Mg^{2+} and Ca^{2+}. This lead to permeability changes in the outer cell envelope with consequent leakage of intracellular content and cell death.[55] However, in the last years alarming cases of bacterial resistance to colistin have been reported, either through mutational or adaptive mechanisms.[55] In fact, alteration of the Lipid A and LPS composition, additional expression of efflux pumps or overexpression of membrane proteins represent prevalent resistance mechanisms discovered, resulting in some cases in a change of the bacterial superficial charge with consequent decreasing of the colistin binding affinity for the Gram-negative outer membrane.[56–59]

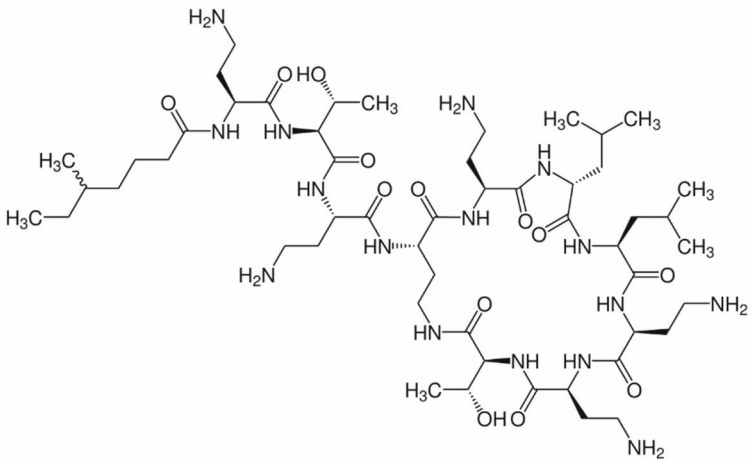

Figure 3. Colistin antibiotic molecular structure.

As previously outlined, the use of antibiotic adjuvants revealed to be helpful to increase the therapeutic efficacy of colistin, by lowering its dose and its related side effects, along with an attenuation of its resistance mechanisms. 2-Aminoimidazoles[60], (E)-2-hexenal[61], indole[61], *N*-acetylcisteine[62], resveratrol[63], niclosamide[64] and pentamidine[65] are in fact known to act as colistin adjuvants, being able to defeat several Gram-negative pathogens. Recently, novel classes have been also discovered. For instance, a class of marine-derivatives analogues is capable to reverse Lipid A modifications, breaking colistin resistance in MDR *A.baumannii*, *K.pneumoniae* and *P.aeruginosa*.[60] Moreover, the synergist combination of the drug with several Small Molecules (SM) proved to be a therapeutically effective strategy to reduce colistin Minimal Bactericidal Concentrations (MBC) by at least 10-fold, attenuating also the evolution of resistance by downregulating the expression of the *pmr*AB system, particularly operons *pmr*CAB and *pmr*H, responsible for some resistance mechanisms.

1.2.4 Innovative therapies that differ from conventional antimicrobials

The biotech scene is rising innovative and radical ideas to tackle the AMR threat. Among the latest strategies, the University of Birminghan in collaboration with the British biotech company Matoke Holdings Ltd are currently proposing a lead pharmaceutical candidate that was based on a natural biological defence mechanism, the reactive oxygen.[66] Initial pre-clinical studies on a gel formulation, revealed that this system showed potent antimicrobial efficacy once reactive oxygen was delivered directly on the site of infection, inhibiting a wide range of highly resistant bacterial pathogens along with the disruption of bacterial biofilms.[67] Aerosol forms are also under investigations.[67]

Another frontier of alternatives antimicrobials could be represented by the phage therapy. Bacteriophages are highly efficient bacteria killers, completely harmful to humans. After seeking out their bacterial targets, bacteriophages enter the cell and using their internal machinery force the bacteria to replicate more and more bacteriophages, bursting out from within and leading to bacteria death.[68] The phage therapy could be also personalized by selecting bacteriophages highly specific for each patient's strain of bacterial infection.[67]

Monoclonal antibodies (mAbs) have also been fruitfully exploited to treat bacterial infections. Recently, the Antibody-Drug-Conjugates (ADC) concept has been applied to antibacterial therapy. In fact, an Antibody-Antibiotic-Conjugate (AAC) combines the selective targeting promoted by the mAb to the bacterial inhibitory activity of the antibacterial.[69] An AAC is generally composed by three component: the antimicrobial drug, connected by a properly designed linker to mAb, which is responsible for the selective delivery of the payload into infected cells.[69] AAC targeting intracellular MRSA in invasive infections have been reported.[70,71] In fact, intracellular MRSA are generally insusceptible to antibiotics, since their location into host-cell macrophages core prevent the drug to reach the bacterium.[70] For this

purpose, specifically targeting the intracellular MRSA with an AAC could prevent cell-to-cell transfer of bacterial infection. After the internalization of the conjugates, the mAb selectively releases the antibiotic that can now exert its inhibitory activity.[70] Moreover, using and AAC it might be possible to overcome poor pharmacokinetics properties and undesired host toxicity, delivering also potent and promising antibacterial compounds or candidates with different or unsuitable profiles as unconjugated drugs.[70]

A key role in non-antibiotic therapies is played by vaccines, being a valuable and effective weapon to fight AMR.[72] In fact, their prophylactic use is helpful to prevent the spread of a bacterial diseases by building an immune host-defense, either before encountering the pathogen or at initial stages of the infection.[72] Furthermore, a crucial advantage of vaccines is represented by the possibility to hit multiple targets, inducing specifically antibody and/or T-cell responses.[72] Vaccines can be also effective against AMR since their implication allows the lowering of inappropriate use of antimicrobials, prescribed for example in case of viral infections.[73] Moreover, vaccines are able to reduce the incidence of resistant serotypes. For instance, before the launch on the market of the 7-valent pneumococcal conjugate vaccine (PCV7), several cases of invasive pneumococcal disease were reported each year in the US. In the early 2000s a 57% reduction in the incidence of penicillin-non-susceptible invasive pneumococcal disease (IPD) was observed along with an 84% of reduction in the rate of MDR strains, outlining that the vaccination was effective regardless of the bacterial resistance phenotype reported.[72]

1.3 Membrane active agents: new weapons to tackle AMR

The bacterial cell membrane represents one of the crucial structures for cell survival, proving to be a promising target for the development of novel antimicrobials in the past two decades.[74] In fact, since the membrane is essential at any stage of the bacterial life cycle, disturbing its functions and altering its structure could be an effective broad-spectrum strategy.[75] Moreover, disrupting the cell membrane will result in alteration of the homeostatic equilibrium, reducing the occurrence of resistance to membrane-active drugs.[76]

The structure and molecular composition of cell membranes differ from Gram-positive and Gram-negative bacteria. Gram-positive bacterial membrane is composed by a cytoplasmic plasma membrane and lipoteichoic acids (LTA), attached to a thick layer of peptidoglycan (Fig. 4).[77] Whereas, Gram-negative bacterial membrane consists of a cytoplasmic inner membrane, a thin layer of peptidoglycan, and an outer membrane containing lipopolysaccharides (Fig. 4).[78] Although structurally different, LTA and LPS are both amphiphilic and anionic, creating the selectivity conditions for membrane-active drugs. Moreover, phosphatidylglycerol (PG) and cardiolipin (CL) are also crucial for the negatively-charged property of the bacterial membrane.[75,79] On the contrary, in mammalian cell membranes, anionic lipids are exposed only to the intracellular environment, and the external surface is prevalently composed by zwitterionic

sphingomyelin and phosphatidylcholine (PC).[80] Generally, agents altering the integrity of the cell membrane are typically both lipophilic and positively-charged, resembling the phospholipid structure with a polar head and a non-polar tail.[81] The cationic moieties interact with the negatively-charged surface of bacterial membranes, and the lipophilic part could be inserted into the bilayer, leading to the alteration of fluidity, packaging and stability of phospholipids, and causing disruption of membrane and eventually cell death.[82] These mechanisms creates the adequate conditions for selectivity since bacterial membranes are endowed with more anionic phospholipids than mammalian bilayers.[75]

Antibiotics membrane-active have already been studied and reported, and some of them entered the market becoming one of the therapeutic options to fight antibacterial infections.

Daptomycin, originally described as an inhibitor of peptidoglycan synthesis, is the only lipopeptide currently approved as an antibacterial agent.[51] Daptomycin was revealed later to be a depolarizing membrane agent due to a calcium-dependent mechanism that results in disruption of the membrane and cell death.[83] Invasive and intensive cocci-related infections, like *S.aureus*-induced bacteremia, can be treated with daptomycin.[84] However, even though it is not widespread, clinical resistance was still observed among enterococcal and staphylococcal clinical isolates.[51]

Moreover, Polymixin B and Colistin entered the market as cyclopeptide antimicrobials, commercially available as last-resort antibiotics for MDR-induced infections.[85] Mechanistic insights about their mode of action were already described in the previous paragraphs.

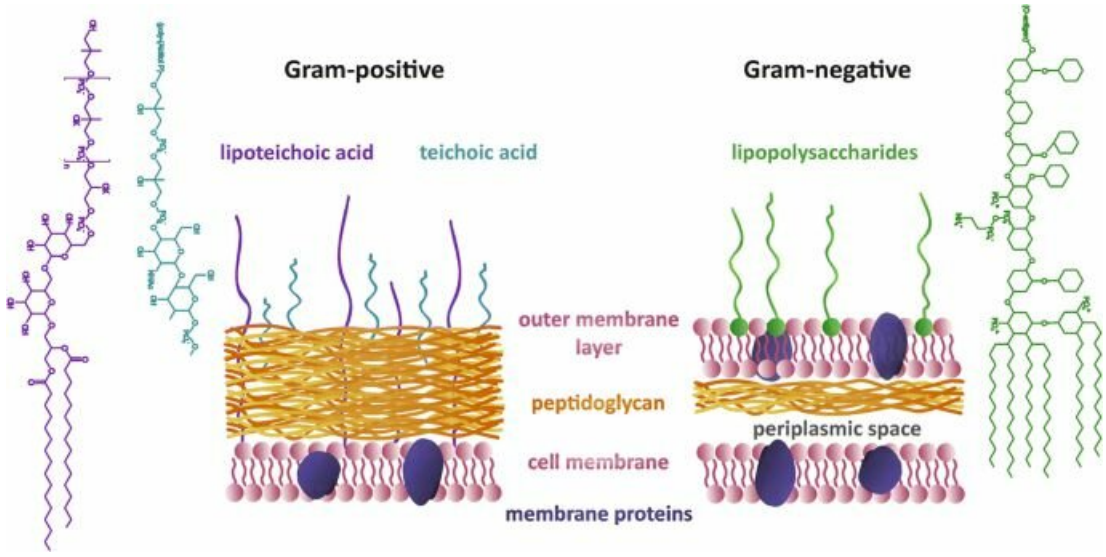

Figure 4. Structural differences between Gram-positive and Gram-negative bacterial membrane. [86]

Several new classes of small molecules interacting with membranes were reported. For instance, the hydantoin pharmacophore has been widely used to develop different antibacterial agents for years, like the antibiotic nitrofurantoin;[87] moreover, the mode of action of these derivatives was still not completely

understood.[88] Recently, a series of membrane-active compounds have been designed and synthesized by combining hydantoin scaffold with hydrophobic tails and positively-charged moieties, targeting the phospholipid bilayer of different MDR strains (MRSA, *P.aeruginosa*, *K.pneumoniae*, vancomycin-resistant-*E.Faecalis* VREF).[88]

Moreover, para-aminobenzensulfonyl oxadiazoles were found to be promising membrane active agents towards MRSA, benefiting also from an additional Mechanism of Action (MoA), by intercalating into deoxyribonucleic acid (DNA).[89]

Antibacterial small molecules endowed with non-peptidic amide bonds, quaternary ammonium groups, and lipophilic alkyl chains were also discovered and reported. In fact, these derivatives proceeded rapidly disrupting the membrane integrity thus preventing resistance.[90]

Bis-guanidine compounds, were widely reported in past decades as antiseptics and disinfectants and can be considered as an attractive molecular scaffold to be developed.[91] In fact, Chlorhexidine (Fig. 5) still represents an important broad-spectrum antimicrobial acting like a disinfectant and its therapeutic effects are related to its ability to disrupt bacterial bilayer.[92] After its adsorption on the cell membrane surface, positively-charged guanidines interact with anionic residues of the bilayer, perfusing into the cytoplasmic environment, producing the leakage or precipitation at a higher dose of cell membrane components.[93]

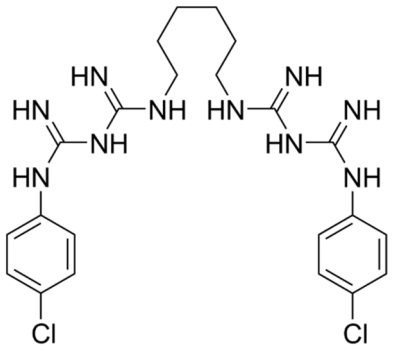

Figure 5. Molecular structure of the biguanide Chlorhexidine.

Similarly to Chlorhexidine, small dimeric cyclic guanidines can display an interesting broad-spectrum antibacterial profile against both Gram-positive and Gram-negative MDR, compromising the bacterial integrity by strongly interacting with the anionic phospholipids in the bilayer. No resistance occurrence has been currently detected and *E.coli* biofilms can be remarkably inhibited. Finally, in vivo studies also confirmed a promising activity towards MRSA-animal models.[94]

1.3.1 Antimicrobial peptides and their MoA

Peptides are a class of pharmaceutical active agents that can be considered a compromise between small molecules and proteins, differing from them in both therapeutical and biophysical terms.[95] They can act

like signaling molecules, potentially playing a key role in therapeutical treatments of altered natural pathways. Antimicrobial Peptides (AMPs) are important natural immunity components widely distributed in insects, mammals, amphibians, fish, plants and bacteria that can be endowed with antiviral, antibacterial, antifungal, or antiparasitic properties.[96,97] While conventional antibiotics are conceived and designed to target specific proteins and receptors, AMPs can act in many different ways but prevalently disrupting the bacterial bilayer leading to cell death. Given this complex and multi-modal MoA, drug resistance to AMPs is rare, due to the wide range of genetic mutations that the pathogen has to get through to change the entire asset of the cell membrane.[74,98,99] More than 3000 AMPs have been identified and discovered with only a few of them being approved by the FDA or currently under clinical trials.[100]

The antimicrobial activity and the specificity of AMPs are generally affected by a wide range of factors: amino-acid constituents, net charge of the molecule and number of positively-charged residues, the length of the peptide, helicity and tridimensional structures.[101,102]

Depending on the amino acid content, AMPs can be categorized as proline-,[103] arginine-,[104] cysteine-,[105] and glycine-rich.[106] The net charge of AMPs strongly affects their activity. In fact, the high affinity of AMPs for the pathogen membranes relies on the strong electrostatic interaction between the positively-charged residues and the anionic phospholipids of the envelope. A secondary driving force in the AMPs antimicrobial activity is represented by the hydrophobic interactions established between the lipophilic domains of the peptide and the acyl chains of the lipids.[100] Due to these particular features, peptides accumulate on the surface of the bacterial membrane outer leaflets, perturbing the asset of the lipids and forming pores or other alterations.[107]

AMPs tend to be almost parallel with respect to the bilayer plane in a *carpet-like mode* (Fig. 6) where their consequent insertion into the membrane results into a modification of lipid ordering and on the penetration of water molecules, with a complex distortion of the curvature and cell death.[108] Higher concentrations of AMPs in the carpet-like model could promote the *detergent-like MoA* (Fig. 6), characterized by the formation of self-assembled AMPs nanostructures interacting with the negatively-charged bacterial membrane, and the generation of surface nanopores followed by cell lysis.[109] Moreover, AMPs can aggregate vertically into the bilayer, packing in a *barrel-stave mode* and creating a rigid pore acting as a sort of ion channel.[110] The pores size depends on the peptide to lipids molar ratio.[110] Finally, in the *toroidal mode* (Fig. 6) AMPs tend to aggregate, inducing the expansion of the head-region of the phospholipids but also the continuous bending of the lipid leaflets. This results in the internal and external leaflets approaching each other, and consequent formation of the toroidal pore.[111]

In addition to the interaction with the cytoplasmic membrane, AMPs can interact with high affinity with the LPS structure, located on the surface of the outer membranes in Gram-negative bacteria. LPS plays also a crucial role in the inflammatory response caused by Gram-negative infections. In fact, LPS can be released after cell lysis or during bacterial cell division, inducing cytokines production, like tumor necrosis

factor-α (TNF-α), interleukin-6 (IL-6), and interleukin-8 (IL-8), by monocytes and phagocytic cells. These cytokines overexpression can cause several organ damages and sepsis. Hence, AMPs can reduce this inflammatory response by directly interacting with LPS.[112] Nevertheless, some AMPs like temporins are also able to form helical oligomeric structures with *N*- and C-termini residues of LPS, rendering the translocation of AMPs into the bacterial inner membrane with consequent inactivation of the peptide.[100] Therefore, certain synthetic modifications of AMPs molecular structure are currently under research and development to reduce the LPS induced aggregation.[100,113]

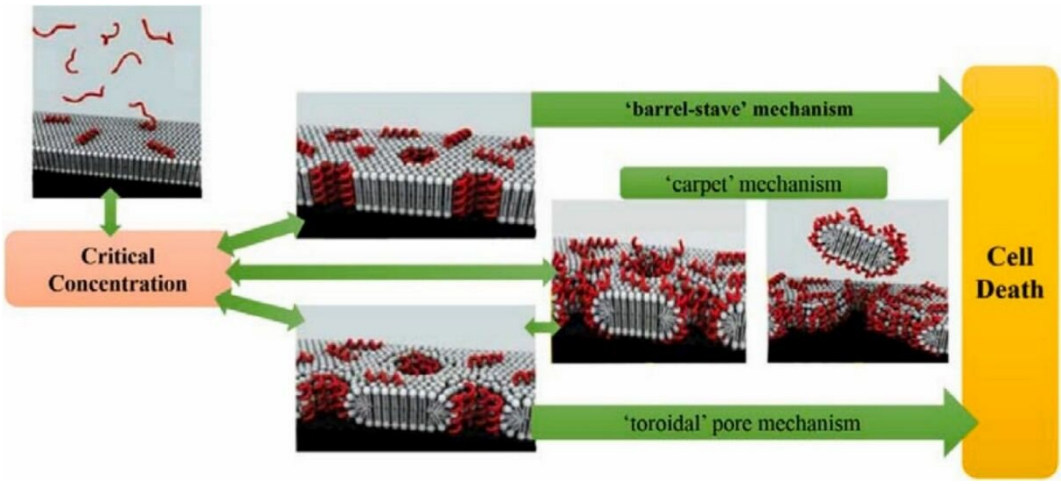

Figure 6. Schematic representation of mechanisms and mode of actions of AMPs. [100]

Several other ancillary mechanisms of action were reported, like interactions with genomic DNA, ribosomes, or other intracellular targets like heat shock proteins or glycoproteins involved in different cytoplasmic pathways. However, literature is still sparse in this field and more effort should be devoted to elucidating these mechanisms.[100]

1.3.2 Investigation and identification of MoA in membrane-active agents.

Investigating AMPs MoA is not trivial as peptides and small molecules, could act with different and synergistic mechanisms.[100] Moreover, because of the high structural and physiological complexity of bacterial membranes, the identification of an accurate MoA could be challenging.[114,115] Nevertheless, the huge biodiversity of bacterial strains also impacts on the composition of lipid bilayers, on the surface charge density, and on the thickness and packaging of the membrane.[114] Additionally, methods to study membrane-active compounds have been scarcely reported in literature in the past and, only recently, the advances in microscopy and in cell biological labeling techniques, provided deeper mechanistic insight of AMPs in unprecedented details.[116]

Recently, several biophysical,[117,118] analytical,[119] and microbiological[120] assays have been reported to evaluate the behavior of compounds targeting the bacterial envelopes. Among them, biomimetic membranes are attracting increasing interest since they allow specific investigation of a given biological phenomenon under very defined and controlled conditions.[121] Moreover, in comparison to microbiological assays, biophysical and analytical studies benefit from a time- and cost-effective protocols, even though they cannot give conclusive data due to the use of oversimplified systems.[122,123]

Thus, artificial bacterial membrane models are widely employed for these studies, along with fluorescence spectroscopy, zeta potential measurements and molecular dynamics (MD).[124] For instance, to investigate membrane-active agents MoA, lipid vesicles or liposomes, Langmuir monolayers, and solid supported lipid monolayers/bilayers are generally used and were widely reported in literature.[122]

Membrane leakage fluorescence assay, using large unilamellar vesicles (LUVs) loaded with self-quenching dyes, could be useful to quantify the antibacterial activity of antimicrobial peptides. In fact, AMPs can permeabilize membranes by disrupting its lipidic asset, providing the leakage of the entrapped dyes content.[125] Several dyes and quenchers, that change fluorescence intensity after membrane leakage, can be used. Among them, different protocols are reported using the pair 8-aminonapthalene-1,3,6 trisulfonic acid (ANTS)/p-xylene-bis-pyridinium bromide (DPX) along with calcein and carboxyfluorescein.[122,126]

The development of a wide number of theoretical and computational simulation approaches arises in interest as an useful tools to describe membrane-agents/lipid interactions. One of these *in silico* approaches is MD, in which it is possible to predict the behavior and investigate the dynamics of a given molecule into the lipid bilayer.[125] For instance, MD was recently reported as a crucial tool to characterize Polymyxin B1 interactions with a heterogeneous model of *E. coli* outer membrane, revealing that the lipopeptide aggregates in the headgroup region of LPS instead of showing an affinity for the Lipid A as believed.[127]

However, to get a comprehensive understanding of drug-membrane interactions, several additional analytical tools could also be required. Techniques like ultraviolet (UV)[128] or fluorescence[116] spectroscopy, circular dichroism,[129] dynamic light scattering,[130] transmission electron microscopy (TEM) or scanning electron microscopy (SEM)[131] have been reported to investigate the mechanism of action of AMPs. Particularly, spectroscopic techniques proved to be very versatile and several case studies reported also the use of electron paramagnetic resonance (EPR),[132] nuclear magnetic resonance (NMR)[133] or infrared spectroscopy (IR)[134] to assess lipid ordering, membrane-drug interactions and/or disruption.

Different labeling approaches have been also developed to detect and localize compounds in either cytosolic, membrane or cell wall fractions, gaining a first hint towards the understanding of the drug target.[116] However, chemical labeling could affect physiochemical properties and thus MoA or antimicrobial activity.[135,136] Label-free technologies could be a valuable alternative, even though they cannot allow visualization of compounds.[116]

Finally, detailed assessment of MoA could be performed with living cells using *in vitro* microbiological protocols and fluorescent dyes, useful to asses alteration of the permeabilization,[137] fluidity,[138] or to evaluate pore-sizing,[139] or depolarization, that can be generally induced by the membrane-active agents even without generating pores.[140]

Elucidating the MoA of membrane active agents could be thus very challenging. Over the last years, several and different methods and protocols have been developed, adapted, and refined to give proper and deeper understandings of antibiotic mechanisms in model and living bacterial cells. This proved to be essential since sometimes the *in vivo* mechanisms could be found different from *in vitro* models or the drug candidate may hit more targets, which is a realistically common feature for membrane active agents.[141–143]

2. State of the Art

2.1 Guanidine moiety in medicinal chemistry: the case of antibacterial drugs.

The guanidine group is a common chemical features of several natural and synthetic compounds that display a broad biological activity.[144] Recently, chemists focused their efforts on guanylated polyamines as they resulted very promising in terms of bioactive properties.[145] When the amine functional group is replaced with a guanidine moiety physicochemical properties of the molecules are generally amplified compared to the corresponding amine. In fact, guandine is a stronger base (pKa of guanidinium cation ≈ 13.5, pKa of ammonium cation is 9.25), suggesting that at physiological or basic pH this moiety is protonated, originating the guanidinium cation.[146] These changes in chemical and physical properties could reflect also in improving the biological activity. In fact, notably, when the amino moiety in neomycin B and kanamycin A is replaced with a guanidine one, the antimicrobial spectrum of activity is extended toward gentamicin resistant *P.aeruginosa* and MRSA.[147] Moreover it is common knowledge that proteins and ezymes, endowed with guanidinium terminals on lateral chains of amino acid like arginine, are able to recognize and bind with high affinity other anionic residues, like carboxylates, phosphates or metals. Hence, due to ion pairing and Hydrogen Bonding (HB), these interactions can results in improving potency and selectivity.[148]

From 2008 onwards, numerous guanidine-containing compounds emerged for their promising biological profiles, making guanidine scaffold one of the most widely investigated in medicinal chemistry for the design of peptides, peptidomimetics and small molecules.[149] The therapeutic applications for guanidine bearing drug candidates are numerous.[150] In fact, clonidine and amiloride entered the market as treatments for central nervous systems and cardiovascular disorders respectively.[151,152] Biguanides like metformin instead have been approved to treat diabetes, whereas cimetidine and famotidine to treat ulcer and stomach acidity.[153–155] Several guanidine endowed drug candidate have also been approved to treat ischemic, inflammatory and autoimmune diseases and they can also act like anticancer and antimicrobial agents (streptomycin, bleomycin, capreomycin and proguanil).[149,156] In Fig. 7 are represented some guanidine-related drugs examples.

Guanidine are also preferred functional groups in antibacterial agents design and development, benefiting from electrostatic interactions that may occur between the guanidinium cations and bacterial targets like negatively-charged envelopes, leading to disruption of bilayers as for AMPs.[157] Indeed, antibacterial hydrazones bearing an aminoguanidine have been reported as putative inhibitors of NorA efflux pump in *S.aureus*, also modulating norfloxacin resistance.[158]

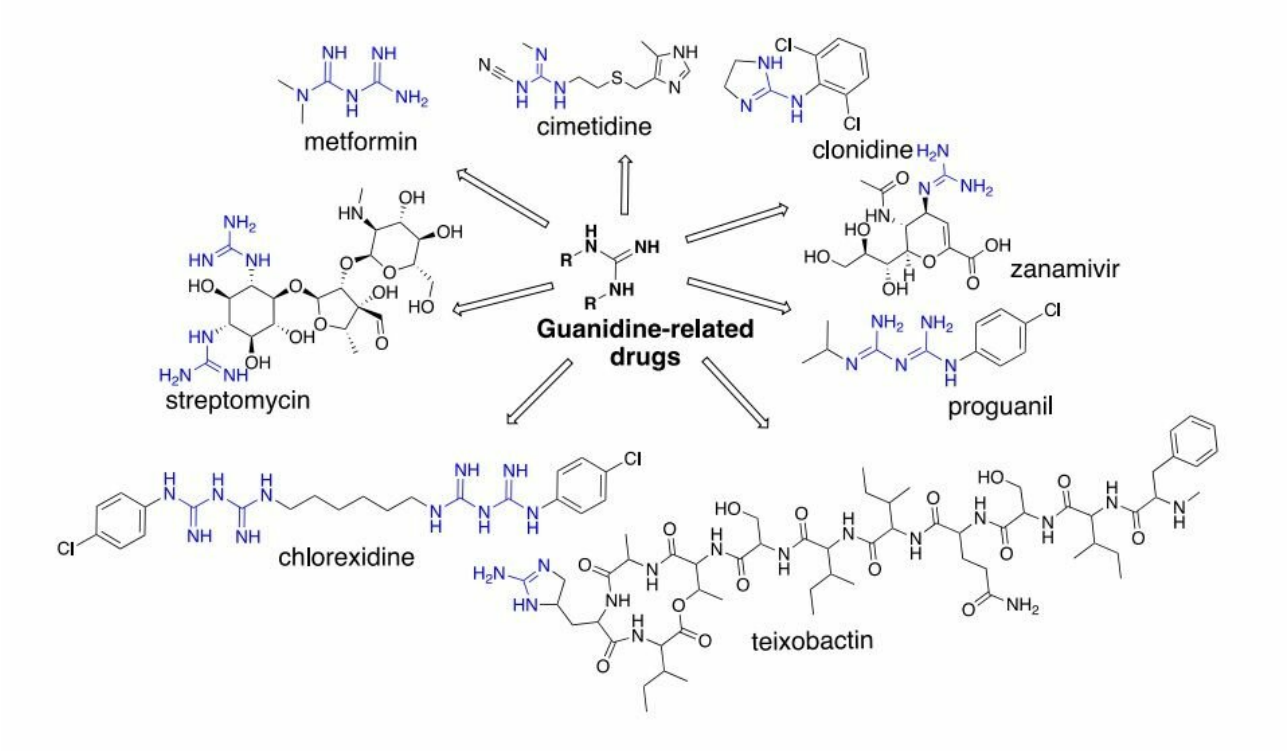

Figure 7. Representative guanidine-related drugs

Guanidinomethyl biaryl compounds were also identified as potent broad-spectrum antibacterial agents, targeting the cell division protein FtsZ thanks to fruitful interactions between the guanidinium moiety and the anionic side chain of E185 residue and the Van der Waals forces between the alkyl chain of I228 and the biaryl compounds phenyl ring.[159]

Natural guanidine alkaloids isolated from *Pterogyne nitensis* and their synthetic analogues derivatives proved to be promising antibiotic candidates to target MRSA strains.[160] Additionally, an improved activity towards MRSA strains was also achieved by replacing the amino and hydroxy groups of amynoglicosides amikacin and kanamycin with guanidine moieties, as recently reported.[161]

Finally, small dimeric cyclic guanidines exhibited interesting antibacterial profiles towards multi-resistant *Staphylococcus epidermidis* (MRSE), MRSA, *K.Penumoniae* and resistant *Enterococcus faecalis* (VRE).[94]

These were only few representative examples of how deeper the medicinal chemistry research is investigating the guanidine function for its antimicrobial properties in the design of small molecules. However, guanidine also affected positively the design of AMPs. In fact, guanylated glyoxamine-based peptidomimetics showed improved antibacterial and antibiofilm profiles, compared to the parent AMP endowed with quaternary ammonium functional group.[162,163] Moreover, synthetic AMPs incorporating guanidine moieties exhibited pronounced membrane disruption in DPPG monolayers as Gram-positive cytoplasmic model membranes.[164] Finally, arginine-rich AMPs also displayed interesting antibacterial profile due to the presence of the guanidinium cation.[165]

2.2 Insight on properties and interactions of guanidinium cation.

Guanidine was first isolated in 1861 but, although known for more than 150 years, the first solid-state structure was solved only in late 2007.[166,167]

At physiological pH guanidine exists as protonated form, originating the guanidinium cation, a highly symmetric planar trigonal functionality[168], characterized by a strongly stabilized Y-shape that can form two strong parallel HBs with biological components. This geometry can exert favorable HBs alignments compared to the parent ammonium cations as guanidine maintains its protonated form over a wide range of pH.[169]

Hydrogen bonding is a ubiquitous phenomenon in nature of remarkably importance in living organism functionalities. Due to the mobility of the proton involved in HB, this interaction proved to be very useful for electron transfer processes in significant biological pathways.[170]

The chemical systems able to exert HBs are typically positively or negatively charged at physiological pH. Thus, generally HBs established between two or more systems could be enhanced or assisted by electrostatic forces.[171] These Charged-Assisted HBs (CAHBs) have been widely reported in literature,[172,173] and play a key role in guanidinium moiety interactions. The ionic pairs and the hydrogen bonding interactions do not work independently but they reinforce each other. When the ionic interactions are strong, like in systems with a cation and anion interacting, the relative HBs are stronger though.[171] Additionally, unlike ammonium cations where the charge is localized on nitrogen atom, guanidinium cations can benefit from an excellent delocalization of the positive charge thanks to their Y-shape, namely *Y-aromaticity*,[174] which can favor ion pairing with phosphate, carboxylate or sulfate anions.[169]

Comparing the binding energies reported in literature respectively for ammonium and guanidinium cations, high binding affinities were found for both the functional groups, with a greater selectivity for phosphates and arsenates over other anions. However, binding affinity constants are greater for guanidinium group rather that ammonium one, outlining that the former could bind strongly and more efficiently these anions.[175] The phosphate binding ability could be ascribed to the rigid and planar guanidinium structure that results to be complementary to that of phosphate oxoanion, allowing the formation of a two-point HB chelate motif.[176,177]

These evidences point out the great relevance that embedding a guanidine moiety in a drug candidate could have. In fact, its introduction into multifunctional chemical scaffolds has proven to be a very useful and efficient strategy to reinforce interactions with biological counterparts. Due to these promising physicochemical features, membrane targeted guanidine-based drug candidates show a wide range of biological activities and, among them, interesting antibacterial,[178,179] antifungal,[180] and antiviral[181] profiles.

Given these strong multifaced noncovalent interactions that guanidinium cation can exert, including bidentate HBs but also cation-π interactions with aromatic moieties, this functional group could modulate adhesion of several biomolecules.[182]

As previously described, embedding the guanidine moiety to replace the amine functional group could result in an improved activity profile. Particularly referring to the antibacterial activity, due to the set of interactions established by guanidine-based membrane-active agents, it is likely that the association with anions is more efficient with guanidinium than with ammonium cations. In fact, the association constants (K_{assoc}) of butylammonium chloride and guanidinium chloride, as model compounds for ammonium (NH^{3+}) and Gu^{+} ions, respectively, were found to be 0.31 and 0.37 M1 for NH^{3+} and Gu^{+} respectively (Fig. 8) , when salt-bridges are formed with carboxylate anions.[183] Whereas, K_{ass} were reported 0.93 and 1.37 M1 , respectively (Fig. 8), for phosphate anions salt-bridges, indicating that guanidinium ions exhibit greater binding affinity for oxyanions than ammonium.

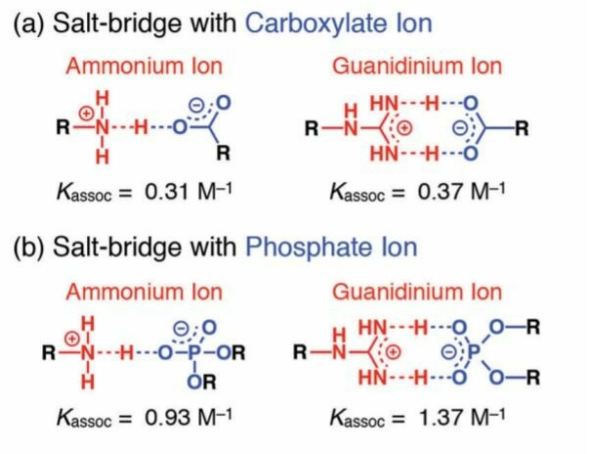

Figure 8. Association constants (K_{assoc}) of salt-bridge interactions of ammonium and guanidinium ions with (a) carboxylate and (b) phosphate anions. [182]

Transferring this concerns in drug-membrane interactions field, association of guanidine moieties with phosphate groups in bacterial bilayers represent one of the mechanisms that could explain disruption effects operated by membrane-active agents towards bacterial membranes.

2.3 Alkylguanidino ureas: a promising class of antibacterials

As previously mentioned, polyguanidines have attracted considerable attention for their antibacterial activity.[184]

For several years, the research group of Prof. Botta investigated a series of alkylguanidino ureas (AGUs) endowed with promising antibacterial profiles against both Gram-positive and Gram-negative bacteria.[185–187] Compound **1** (Tab.3) was identified as the most promising derivative of the series, with Minimum Inhibitory Concentration (MIC) values ranging from 0.5 to 8 μg/mL on Gram-positive and Gram-negative representative strains. Moreover, the antibacterial properties of hit compound **1** were also further investigated on recent antibiotic-resistance clinical isolates (Tab. 3).[185]

Table 3. Antibacterial profile of alkylguanidino ureas series hit compound. In blue, antibacterial activity towards clinical resistant isolates with pandrug-resistant phenotype.[185]

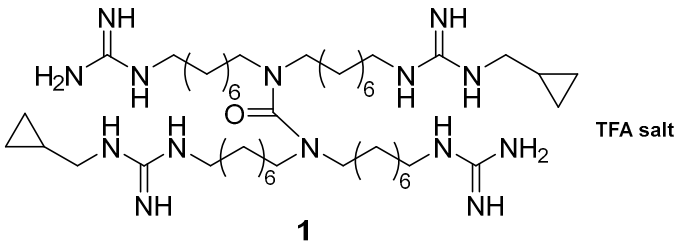

1

Bacterial strains	MIC [μg/mL]
B. subtilis ATCC 6633	0.5
E. faecalis ATCC 19433	2
S. aureus ATCC 25923 SEP	2
S. pyogenes ATCC 12344	1
A. baumannii ATCC 17978	8
E. coli CCUG^{T}	2
K. pneumoniae ATCC 13833	2
P. aeruginosa ATCC 27853	8
A. baumannii AC-54/97	2
B. cepacia SI-R2	16
E. cloacae VA-417/02	1
K. pneumoniae SI-081	2
S. maltophilia 634/08	16

The interesting antibacterial profile of compound **1** encouraged the research group to better investigate the AGUs chemical class. Hence, structural analogue of derivative **1** were designed and synthesized to obtain a small chemical library to do some preliminary considerations about structure-activity relationships (SARs). With this purpose, the synthetic efforts of the group were initially directed towards the modification of the alkyl chains length and of the guanidine moieties substitutions.[185]

Concerning the alkyl chains, the length of the spacer between the central urea moiety and the guanidines was investigated. In fact, the optimal number of carbon atoms in the methylene chains were found to be 8 since the increase of two carbon atoms (10) produced a slight reduction in activity, whereas decreasing the length to six methylene resulted in a complete loss of potency, particularly against Gram-negative strains.[185]

Then, the cyclopropylmethyl substitution was replaced with other small alkyl or hindered aromatic moieties, in order to evaluate the impact of guanidine substitutions on antibiotic activity. As reported in Tab.4 and Tab.5, these new derivatives (**2-16**) basically retained the antibacterial profile of hit compound **1**. Hence, the nature of substituents on guanidine moiety seemed to not affect significantly the biological activity.

Table 4. MICs [μg/mL] of AGUs derivatives (obtained as trifluoroacetate salts) and control antibiotics (colistin, vancomycin and daptomycin) on representative Gram-positive and Gram-negative bacteria. MICs [μg/mL] are expressed as median values calculated from experiments performed at least in triplicate.[185]

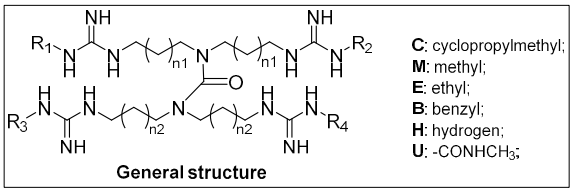

Cpd	n_1	n_2	R_1	R_2	R_3	R_4	*B.subtilis* ATCC 6633	*E.faecalis* ATCC 19433	*S.aureus* ATCC 25923 SEP	*S.pyogenes* ATCC 12344	*A.baumannii* ATCC 17978	*E..coli* CCUG^T	*K.pneumoniae* ATCC 13833	*P.aeruginosa* ATCC 27853
1	6	6	H	C	C	H	0.5	2	2	1	8	2	2	8
2	8	8	H	C	H	C	2	4	8	4	64	16	8	64
3	4	4	H	C	H	C	4	32	4	2	128	16	32	256
4	6	6	H	E	H	E	1	1	1	0.5	16	2	2	16
5	6	6	H	M	H	M	0.5	1	0.5	0.5	8	1	4	8
6	6	6	H	B	H	B	2	2	2	2	8	4	2	16
7	6	6	C	C	C	C	8	4	16	2	8	16	4	64
8	6	6	E	E	E	E	0.5	1	0.5	0.25	16	2	4	32
9	6	6	B	B	B	B	4	4	8	1	16	4	4	8
10	6	6	H	H	H	H	32	2	2	1	16	4	32	32
11	6	6	C	C	H	H	2	8	8	4	16	4	4	16
12	4	4	C	C	H	C	4	16	4	2	64	8	16	128
13	4	4	E	E	H	E	16	64	32	4	256	64	128	>256
14	6	4	C	C	C	C	4	8	2	1	64	4	4	128
15	6	6	C	C	U	U	2	4	2	2	8	4	4	16
16	6	6	U	C	U	C	8	16	8	16	16	8	8	32
			Vancomycin				0.5	1	1	0.5				
			Colistin								1	0.5	0.5	0.5
			Daptomycin				1	1	0.5	0.12				

Particularly, after MICs comparation with hit compound **1**, the activity profiles of analogues **2-16** resulted to be in some cases worsened, although not significantly in terms of order of dilutions differences. Exceptions in the trend were represented by the inhibition profiles of derivatives **5** and **8** on Gram-positive strains, where the antibacterial activity resulted improved compared to compound **1**, particularly on *E. faecalis*, *S. aureus*, and *S. pyogenes* bacteria.

Table 5. MICs of selected compounds on Gram-negative antibiotic-resistant clinical isolates with pandrug-resistant phenotype. MICs [μg/mL] are expressed as median values calculated from experiments performed at least in triplicate.[185]

Cpd	*A. baumannii* AC-54/97	*B. cepacia* SI-R2	*E. cloacae* VA-417/02	*K. pneumoniae* SI-081	*S. maltophilia* 634/08
1	2	16	1	2	16
4	n.d.	32	4	4	16
5	4	32	4	8	16
6	n.d.	16	4	8	8
7	8	32	4	4	8
8	8	32	2	8	32

The influence of the number of substituted and unsubstituted guanidines was also evaluated. Despite the interesting Gram-positive inhibition profile of compound **8**, bearing four ethyl-substituted guanidines, the optimal combination was still represented by two unsubstituted guanidines and two substituted ones, bearing small alkyl functional groups. Structural simmetry was considered when designing derivative **11** and, unexpectedly, this structural inversion compromised the biological activity, although superficial charge remained unvaried. Finally, analogues **15** and **16** were designed as it was assumed that their lower predicted pKa, due to the presence of an *N*-methyl amidinourea functionality, would have increased the selectivity towards bacterial cells.[185] However, although active towards almost all tested strains, derivative **15** and **16** showed a worsened antibacterial profile towards Gram-negative bacteria, particularly *A. baumannii* and *P. aeruginosa*.

The Minimal Bactericidal Concentration (MBC) evaluation of most active compounds, although measured only for *E. coli* and *A. baumannii*, showed identical values to that of the MIC, indicating a strong bactericidal activity of these compounds (data here not reported). This was further confirmed by a time-kill curve analysis, in which the bactericidal activity of hit compound **1** (4 μg /mL, 2 fold MIC) was found to be ≥4 log10 in one hour and thus superior to that of colistin (Fig. 9). Furthermore, the bacterial load, measured after 24 hours of exposure to 2 fold MIC of these antibiotics, was comparable.[185]

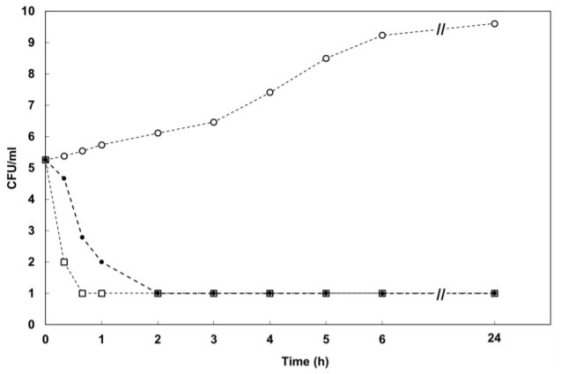

Figure 9. Time-kill curve experiments performed with E. coli CCUG^{T} . These experiments were performed in the absence (growth control, empty circles) or presence of 2 fold MIC of compound 1 (solid circles) or colistin (empty squares), used as a comparator for the experiment.[185]

2.3.1 ADME properties of AGUs and preliminary MoA investigations.

In order to estimate the possible effect of Plasma Protein Binding (PPB) on antibacterial activity of AGUs derivatives, compound **1** was tested on *E. coli* strain in Mueller Hinton Broth (MHB) supplemented with 10% complement-free Human Serum (HS). Data collected (not showed here)[185] revealed that HS can reduce, but not inhibit, the biological activity of hit compound **1**. Since the most abundant component of HS is human serum albumin (HSA) and, given the 76% homology sequence of Bovine Serum Albumin (BSA) with HSA,[188] the susceptibility of *E. coli* MG1655 to compound **1** was again tested in MHB supplemented with increasing concentrations of BSA. Remarkably, no alteration of the antibacterial profile of compound **1** was reported (data not shown),[185] suggesting that maybe other serum proteins could affect the activity of **1** in HS. These results highlighted that AGUs are effectively suitable for future development as drug candidates.

Concerning first investigations of AGUs MoA, due to their polycationic nature, the impairment of bacterial bilayers was assessed. An enzyme-based assay was set up to evaluate disruption of membranes. A colorless chromogenic substrate poorly permeable, like o-nitrophenyl-βD-galactoside (ONPG), was selected as it is able to release the yellowish o-nitrophenol (ONP) upon enzymatic hydrolysis. However, due to its scares permeability profile ONPG reaches the cytoplasm, where the enzyme is located, only when the bilayers show permeability defects, such as those promoted by membrane-active agents.[189,190] Hit compound **1** and derivative **2**, **7** and **10** were tested in three bacterial strains (*E. coli* MG1655, *A. baumannii* ATCC19606T harboring plasmid pMP220::PrrnB, *P. aeruginosa* ATCC15692 harboring plasmid pMP220::PrrnB), characterized by physiological or induced high-level of β-galactosidase. Sodium Dodecyl Sulfate (SDS), acting like a disrupting agent, was used as positive control and remarkably, none of the tested compounds produced the conversion of the ONPG in ONP, suggesting that no macroscopic alteration of the membranes occurred. However, microstructural damages could not be excluded since different disrupting mechanisms could promote the bacterial cell death.[185]

Additionally, a specific fluorescence assay was set up to evaluate the possible disruption of the Gram-negative outer membrane. Three Gram-negative bacteria were exposed to increasing concentrations of test compounds, colistin or dimethylsulfoxide (DMSO), as positive and negative controls, respectively, followed by the addition of 1-*N*-phenylnaphthylamine (NPN). LPS in the outer membrane structure acts like a permeability barrier for this lipophilic dye, that is able to emit fluorescence in hydrophobic environments. Hence, due to the presence of LPS, in case of permeability defects, this dye enables the detection of a potential outer membrane damage.[126] Test compounds revealed a dose-dependent increase in NPN fluorescence emission for all Gram-negative tested species, *P. aeruginosa* ATCC15692, *E. coli* MG1655 and *A. baumannii* ATCC19606T (data not shown). These results outlined that AGUs tested were able to perturb Gram-negative outer membrane.[185]

Finally, the depolarization of cytoplasmic membrane was assessed as another potential MoA of AGUs. Thus, compound **1** was tested for its ability to depolarize *E.coli* membrane using the fluorescent dye 3,3'-dipropylthiacarbocyanine ($DiSC_3$-5),[191,192] although compound **1** was found unable to restore any fluorescence after incubation of bacterial cells at the concentration of 2 fold MIC(**1**), highlighting that membrane depolarization is not the prevalent MoA of AGUs.

In depth analysis were also carried out to evaluate the impact of AGUs on biofilm formation. Crystal violet assay revealed that they were unable neither to inhibit the formation of biofilm, nor to alter its three-dimensional structure.[185]

The propensity of compound **1** to select resistant mutants was assessed, investigating also its potential mechanism of resistance in E. coli $CCUG^T$. The phenotypic analysis of these isolates did not reveal any acquisition of novel resistant phenotype, indicating that the compound was unable to select stable mutants with acquired mutations.[185]

Finally hemolytic activity of **1**, **2**, **7** and **10** was tested on red blood cells. Data collected are reported in Tab.6. With the exception of compound **2**, derivatives **1**, **7** and **10** displayed no hemolytic effects. Compound **1** was further investigated for its cytotoxicity effect on HeLa cells, showing only a minimal cytotoxicity after 24 hours when tested at 16 μg/mL (Fig.10) that became more evident at 256 μg/mL even though it did not exceed the 60% after 24 hours (Fig.10).

Table 6. Hemolytic activity of selected compounds with positive and negative controls.[185]

Cpd	Haemolysis (%)			
64 μg/mL in DMSO	**0 Rh+**	**A Rh+**	**B Rh+**	**A Rh-**
1	3	4	5	5
2	54	41	44	44
7	3	2	2	3
10	3	4	6	7
0.2% TRITON-X 100 [a]	100	100	100	100
1.6% DMSO [b]	0	0	0	0

[a] Positive control.

[b] Negative control.

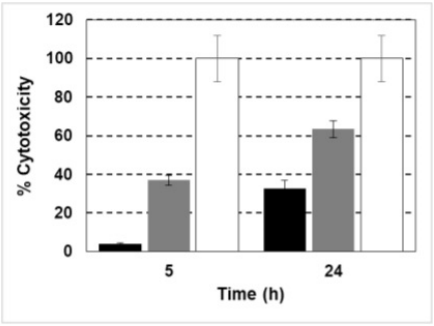

Figure 10. Cytotoxicity of compound **1,** after 5 and 24 hours, at 16 μg/mL (black) and 256 μg/mL (grey). In white the cytotoxicity control.[185]

Preliminary ADME characterization of hit compound **1**, reassumed in Tab.7, revealed that the AGU derivative is metabolically stable, as measured by means of human liver microsomial proteins, and also very soluble in water, probably due to its polycationic nature. Furthermore, the distribution constant logD at pH 7.4 displayed a good value in agreement with those of daptomycin and vancomycin and consistent with the experimental solubility found. Low percentage of bond (B_{max}) values to α-1-acid glycoprotein (AGP) were found for compound **1**, thus indicating only a moderate affinity for this serum protein, as expected for positively-charged compounds.[185] The parallel artificial membrane permeability assay (PAMPA), validated with rifamixin and chloramphenicol (CAF), revealed low apparent permeability (P_{app}) for compound **1** at physiological pH as expected for polycationic compounds (Tab. 8). Caco-2 permeability assay was also performed since it is known from literature that endogenous substances, bearing guanidines and amines, could cross the membrane benefiting from apical transport mechanisms, like H^+ antiports and P-glycoprotein G (P-gp), and the less investigated basolateral ones. The P_{app} apical-to-basolateral ($P_{app\ (A>B)}$) and basolateral-to-apical ($P_{app\ (B>A)}$) were found very low (Tab. 8), indicating that the AGUs hit compound was not absorbed through passive diffusion, paracellular permeation or active transport. These evidences outlined a low oral bioavailability that can be overcame by intravenous administration.[185]

Table 7. Preliminary ADME data collected for hit compound **1**.[185]

ADME	Cpd	Metabolic stability (%) [a]	Solubility [g/L] [b]	logD (pH 7.4) [c]	HSA		AGP	
					K_d [μM] [d]	Bmax (%) [d]	K_d [μM] [d]	Bmax (%) [d]
	1	> 99	0.292 ± 0.022	-0.79	23.27 ± 14.6	14.0	0.11 ± 0.06	30.2

[a] The human liver microsome stability is expressed as a percentage of the unmodified parent drug. [b] The human liver microsome stability is expressed as a percentage of the unmodified parent drug. Aqueous solubility was determined by means of the LC-MS method. [c] Distribution coefficient 1-octanol/ TRIS buffer pH 7.4 . [d] K_d and Bmax values are measured by means of the indirect fluorescence method.

Table 8. Permeability studies of compound **1** (PAMPA and Caco-2 cell line experiments and efflux ratio). Rifamixin and CAF (low permeability) as reference compounds for PAMPA. Atenolol (low permeability) and propranolol (highly permeable compound), as reference compounds for Caco-2 cells.

Permeability	Cpd	P_{app} (PAMPA) [10^{-6} cm/s]	P_{app} (Caco-2) [e] $P_{app\ (A>B)}$ [10^{-6} cm/s]	Efflux ratio [f] $P_{app\ (A>B)}/P_{app\ (B>A)}$
	1	1.60 ± 0.43	0.19 ± 0.09	0.65
	Rifamixin	0.06 ± 0.01	n.d.	n.d.
	CAF	0.30 ± 0.50	n.d.	n.d.
	Atenolol	n.d	0.13 ± 0.04	0.37
	Propanolol	n.d	22.4 ± 5.4	0.40

[e] A, apical; B, basolateral; $P_{app(A>B)}$ is the P_{app} in the apical-to-basolateral direction. [f] B>A/A>B is the ratio of the basolateral-to-apical and the apical-to-basolateral permeation rate. Results are obtained from the average values of $P_{app\ (A>B)}$ and $P_{app\ (B>A)}$.

2.4 Searching for SARs by molecular simplification

As previously described, the development of the first AGUs series revealed interesting preliminary information about the SARs features. Particularly, the optimal spacer length was established to be eight methylene groups and the nature of the guanidino substitutions did not affect significantly the antibacterial profile. Structurally isomerism proved to have a potential relevance on the inhibitory activity, and thus the position of the guanidino substitutions could play a key role in potency. However, these evidences were only preliminary findings and the data collected about the putative MoA and SARs analysis, were not exhaustive or conclusive enough to guide a rational design of novel analogues.[193] Moreover, the synthetic pathway built up to achieve the first AGUs derivatives was limited by the high degree of complexity and by the number of reaction steps. Particularly, the guanylation procedures and the coupling with the secondary amines to furnish the central urea, took up to 48 hours and the purification of intermediates resulted not trivial.[185,194] Thus the research group resorted to a chemical strategy, generally involved in the design of compounds acting on unknown targets or binding modes and common to several natural products derivatives, the structural simplification.[193] In fact, the concept of molecular simplification, as a drug design strategy, could be useful to shorten the synthetic route, while trying to understand the chemical features required for biological activity.[195] This approach consist in reducing the high molecular weight of a compound, dissecting step-by-step its original chemical structure.[193] Therefore, the molecular simplification strategy benefits from more accessible syntheses and improved drug-like properties, enhancing positively the balance between pharmacological activity and toxicity issues.[196]

Thus, leaving the central urea moiety unvaried, due to its well-known capability to form stable HBs with biological targtes,[197] four classes of novel AGUs were synthesized. In Tab. 9 are schematically resumed all new analogues for each chemical class, with their general formulas and some representative derivatives chemical structures. The design of each class has been inspired by a parent compound, listed in the table. First, six derivatives were designed, characterized by the removal of the *N*-substitutions on the urea function (*arm-removed* series). Compound **7** was selected as model compound for this structural simplification, being a totally symmetric compound. One, two or three alkylguanidino arms were replaced with hydrogens or methyl groups, furnishing tris-, bis-, or mono-substituted ureas (**17-22**).[193]

Then, the guanidino moiety was shut down and completely truncated from the selected parent compound **7** (*guanidino turned-off* series), leaving the octyl linker unsubstituted and deprived of its guanidino function (**23-27**). Furthermore, the encouraging biological results collected for derivative **23**, bearing only one guanidine turned-off octyl linker, drove us also to investigate the length of the alkyl chain of the truncated spacer (compounds **28-31**).

Table 9. Schematically representation of novel AGUs derivatives. Parent compounds that inspired the design of these derivatives, along with their structural characteristics and general formulas are listed in the table. All compounds were obtained as trifluoroacetate salts.

Series	*Parent cpd*	*Representative Molecular Structures*	**Cpd**	*Urea Substitution*			
				R¹	**R²**	**R³**	**R⁴**
Arm-Removed	7	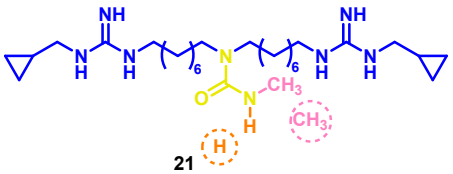 21	17	A	A	A	H
			18	A	H	A	H
			19	A	A	H	H
			20	A	H	H	H
			21	A	A	H	CH_3
			22	A	H	H	CH_3
Guanidino-Turned Off	7	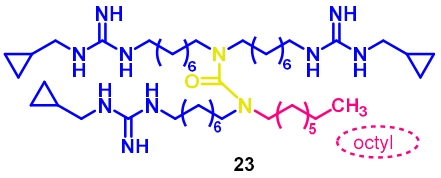 23	23	A	A	A	octyl
			24	A	octyl	A	octyl
			25	A	A	octyl	octyl
			26	A	octyl	octyl	octyl
			27	octyl	octyl	octyl	octyl
	23	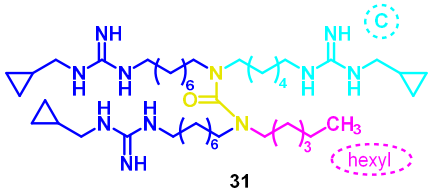 31	28	A	A	A	hexyl
			29	A	A	C	octyl
			30	C	C	A	octyl
			31	A	C	C	hexyl
Amidino-Cut Off	10	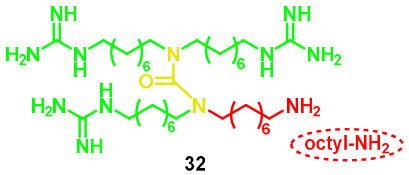 32	32	B	B	B	octyl-NH_2
			33	B	octyl-NH_2	B	octyl-NH_2
			34	B	B	octyl-NH_2	octyl-NH_2
			35	B	octyl-NH_2	octyl-NH_2	octyl-NH_2
			36	octyl-NH_2	octyl-NH_2	octyl-NH_2	octyl-NH_2
	33	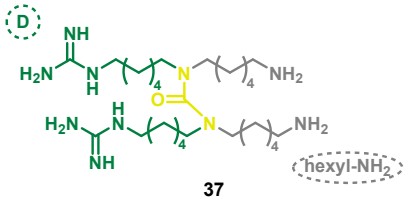 37	37	D	hexyl-NH_2	D	hexyl-NH_2
Traditional	1	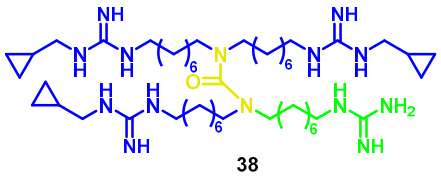 38	38	A	A	A	B
			39	A	B	B	B

A (blue) and B (green) represent urea substituents characterized by an 8-methylenes spacer and a terminal cyclopropylmethyl (A) or unsubstituted (B) guanidino moiety.
C (cyan) and D (dark green) represent urea substituents characterized by a 6-methylenes spacer and a terminal cyclopropylmethyl (C) or unsubstituted (D) guanidino moiety.

Then, the amidino part of the guanidine moiety was cut off (*amidino-cut off series*) from the selected parent compound **10**, being a symmetrically unsubstituted tetraguanidino derivates. This simplification furnished derivatives with one, two, three or four primary amines (**32-36**) and also in this case, the length of the alkylamine spacer was investigated (**37**). In the end, the number of cyclopropylmethyl-substituted guanidines on hit compound **1** was investigated by designing derivatives **38** and **39** (*traditional series*).

2.4.1 Arm-removed series

The design of arm-removed series led to less substituted ureas compared to the firs AGUs series. Switching to tris-, bis-, mono-substituted ureas could change the topological polar surface (tPSA) of compounds, increasing the number of hydrogen bond donors (HBD) and acceptors (HBA), allowing more interactions with pharmacological targets. However, this strategy involves also the reduction of both the lipophilic part of the molecule, namely the polymethylene linker, and also the polycationic terminals endowed with guanidino moieties that play a key role in bilayer interactions. This could led to a decrease of molecular hydrophobicity (calculated partition coefficient, clogP), HBD + HBA and tPSA. As reported in Tab.10, the biological activities of derivatives **17-22** reflects all these evidences. In fact, only the tri-*N*-substituted derivative **17** retains a certain activity on all the tested strains, particularly on *B. subtilis*, *S. pyogenes*, and *S. epidermidis*. The antibacterial profiles of other tris- and bis-substituted ureas analogues resulted worsened compared to that of their parent compound. Remarkably, compound **20** (Fig. 11), being a monosubstituted urea analogue, showed an interesting and enhanced antibacterial profile, on both Gram-positive and Gram-negative strains, compared to its parent compound.[193]

Table 10. MICs [μg/mL] of *arm-removed* derivatives and their parent compounds, on Gram-positive and Gram-negative representative strains. MICs are expressed as the average values calculated from experiments performed at least in triplicate.

Cpd	*B. subtilis ATCC 6633*	*E. faecalis ATCC 19433*	*S. pyogenes ATCC 12344*	*S. epidermidis ATCC 14990*	*S. aureus ATCC 25923 SEP*	*E. coli CCUGT*	*K. pneumoniae ATCC 13833*	*A. baumannii ATCC 17978*	*P. aeruginosa ATCC 27853*
1	0.5	2	1	2	2	2	2	8	8
7	8	4	2	-	16	4	4	8	64
17	1	8	1	1	-	8	8	64	64
18	> 128	64	8	> 128	-	64	> 128	-	> 128
19	8	16	2	-	16	32	32	128	128
20	1	1	1	-	0.5	2	1	16	16
21	32	64	8	8	-	128	128	> 128	> 128
22	64	64	128	-	32	128	128	> 128	> 128
Colistin	-	-	-	-	-	0.5	0.5	1	0.5
Vancomycin	0.5	1	1	-	0.5	-	-	-	-
Daptomycin	1	1	0.5	-	0.12	-	-	-	-

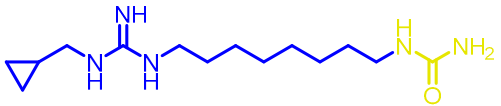

20

Figure 11. Molecular Structure of compound 20, the most promising derivative from arm-removed AGUs series.

Furthermore, derivatives **21** and **22**, endowed respectively with one or two methyl groups as urea substituents, exherted a worsened activity profile when compared to that of the corresponding demethylated derivatives (**19** and **20**), outlining the key role of the urea HBD capability.

2.4.2 Guanidino-turned off series

The interest in investigating the guanidine role in AGUs derivatives relies in the enormous chemical and biological portfolio of functionalities in both natural and synthetic fields.[149]
Given all the advantageous properties of guanidino functional groups,[198] their progressive removal from the AGUs structure could allow us to understand how many of these groups are essential for biological activity. Moreover, truncating the guanidines from the alkyl spacer, the HBD capability dramatically decreased along with an increase in clogP.[193] The collected data from biological evaluation are listed in Tab.11.

Table 11. MICs [μg/mL] of *guanidino-turned off* derivatives and their parent compounds, on Gram-positive and Gram-negative representative strains. MICs are expressed as the average values calculated from experiments performed at least in triplicate.

Cpd	*B. subtilis ATCC 6633*	*E. faecalis ATCC 19433*	*S. pyogenes ATCC 12344*	*S. epidermidis ATCC 14990*	*S. aureus ATCC 25923 SEP*	*E. coli CCUGT*	*K. pneumoniae ATCC 13833*	*A. baumannii ATCC 17978*	*P. aeruginosa ATCC 27853*
1	0.5	2	1	2	2	2	2	8	8
7	8	4	2	-	16	4	4	8	64
23	2	2	1	2	-	4	4	4	8
24	128	32	8	16	-	> 128	128	> 128	> 128
25	128	128	4	128	-	128	64	128	> 128
26	64	128	16	64	-	> 128	> 128	> 128	> 128
27	> 128	> 128	> 128	> 128	> 128	> 128	> 128	> 128	> 128
28	2	1	1	0.5	-	4	8	8	16
29	2	2	1	-	1	2	2	4	8
30	0.5	0.5	1	1	-	4	4	16	16
31	1	2	1	4	-	4	8	32	64
Colistin	-	-	-	-	-	0.5	0.5	1	0.5
Vancomycin	0.5	1	1	-	0.5	-	-	-	-
Daptomycin	1	1	0.5	-	0.12	-	-	-	-

Turning off the guanidino moieties in AGUs compounds proved to be generally detrimental for MIC values towards all tested bacterial strains. An exception is represented by the tris-guanidino endowed derivative **23**, that showed a slightly improved profile compared to the parent compound **7**, maintaining a similar antibacterial spectrum to that of the hit compound **1**. On the other hand, truncating two (**24** and **25**), three (**26**), or all (**27**) guanidino moieties resulted in a significant worsening or loss of antibacterial activity. However, encouraged by the biological results collected for derivative **23**, different chain lengths were designed, furnishing derivatives **28-31**. This tris-guanidino derivatives endowed with different chain lengths exhibit good antibacterial profiles, retaining the MICs of the parent compound **23** either on Gram-positive or on Gram-negative strains.[193]

Overall, the *arm-removed* and the *guanidino-turned off* series provided interesting SARs consideration about the number of positive electrostatic charges required for the activity. Three-charges endowed compounds (**17**, **23** and **28-31**), displayed high potency, while divalent one (**18**, **19**, **21**, **24** and **25**) showed a moderate-low activity. In the end, monocharged and/or neutral derivatives (**22**, **26** and **27**) were found almost or totally inactive.

2.4.3 Amidino-cut off series

The role of primary amines was also investigated by cutting the aminidino portion of the guanidino moiety. Like guanidines, primary amines are protonated at physiological pH but the number of hydrogen bondings decreases dramatically. For this series, derivative **10**, characterized by four unsubstituted guanidines, was chosen as parent compound due to the great difference with the corresponding free-amino derivatives in terms of the number of hydrogen bonds. In fact, for each unsubstituted guanidine-amine switch, there is a lack of two hydrogen bond donors and two acceptors.

Beyond the HB capability, another effect of the replacement of guanidines with amines was considered. In fact, larger K_{ass} for phosphate-bearing molecules were estimated for guanidinium than for primary ammonium,[182] hence a lower antibacterial activity of polyamines would be expected when compared to AGUs.[193]

Amidino-cut off and their biological profiles are listed in Tab.12. Evaluating the collected data, mono- and diamino-eight membered ureas derivatives (**32-34**) displayed an interesting antibacterial profile compared to the parent compound **10**, particularly on *B. subtilis*, *S. pyogenes*, *S. aureus* and *E. coli*. On the contrary, polyamines **35** and **36** resulted overall less active than **10**. Whereas, six-membered diamino ureas **37** was found almost inactive.[193]

Overall, switching one or two guanidines with primary amines seemed to improve the activity on selected bacterial strains, highlighting that the activity could be related also to specifical bacterial features that characterize each strain.

Table 12. MICs [μg/mL] of *amidino-cut off* derivatives and their parent compounds, on Gram-positive and Gram-negative representative strains. MICs are expressed as the average values calculated from experiments performed at least in triplicate.

Cpd	*B. subtilis ATCC 6633*	*E. faecalis ATCC 19433*	*S.pyogenes ATCC 12344*	*S. epidermidis ATCC 14990*	*S. aureus ATCC 25923 SEP*	*E. coli CCUGT*	*K. pneumoniae ATCC 13833*	*A. baumannii ATCC 17978*	*P. aeruginosa ATCC 27853*
1	0.5	2	1	2	2	2	2	8	8
10	32	2	1	-	-	4	32	16	32
32	1	4	0.25	-	1	2	8	16	16
33	0.5	8	0.25	-	0.5	2	16	16	32
34	0.5	8	0.25	-	0.5	2	16	16	32
35	4	32	16	-	2	32	64	64	128
36	4	16	4	-	8	32	16	16	32
37	32	>128	128	128	128	>128	>128	>128	>128
Colistin	-	-	-	-	-	0.5	0.5	1	0.5
Vancomycin	0.5	1	1	-	0.5	-	-	-	-
Daptomycin	1	1	0.5	-	0.12	-	-	-	-

2.4.4 Traditional series

Hit compound **1** was chosen as parent compound for the design and synthesis of traditional series derivatives **38** and **39**. In fact, the impact of substitutions on guanidines was evaluated. Hence, derivative **38** bearing three *N*-cyclopropylmethyl guanidines, and derivative **39**, endowed with only one *N*-cyclopropylmethyl guanidine, were synthesized. Compound **38** showed a slightly worsened profile compared to hit compound **1**, whereas compound **39** displayed an interesting antibacterial profile with an enhanced inhibitory activity towards almost all the tested strains compared to hit compound **1**, while maintaining unvaried MICs on B. subtilis and P. aeruginosa strains. Biological data collected are reported in Tab. 13.[193]

Table 13. MICs [μg/mL] of *traditional* derivatives and their parent compounds, on Gram-positive and Gram-negative representative strains. MICs are expressed as the average values calculated from experiments performed at least in triplicate.

Cpd	*B. subtilis ATCC 6633*	*E. faecalis ATCC 19433*	*S. pyogenes ATCC 12344*	*S. epidermidis ATCC 14990*	*S. aureus ATCC 25923 SEP*	*E. coli CCUGT*	*K. pneumoniae ATCC 13833*	*A. baumannii ATCC 17978*	*P. aeruginosa ATCC 27853*
1	0.5	2	1	2	2	2	2	8	8
38	2	2	1	-	2	8	4	8	16
39	0.5	1	0.25	-	0.5	0.5	1	4	8
Colistin	-	-	-	-	-	0.5	0.5	1	0.5
Vancomycin	0.5	1	1	-	0.5	-	-	-	-
Daptomycin	1	1	0.5	-	0.12	-	-	-	-

2.5 The impact of trifluoroacetate counterion: synthesis of the hydrochloride derivative.

The whole AGUs were obtained and tested as trifluoroacetate salts. Therefore, in order to investigate the impact of the counterion on the biological activity, compound **40** (Fig. 12) was synthesized.

Briefly, all the reported synthetic routes for AGUs derivatives relies on the tert-butoxycarbonyl (Boc) protecting group, particularly to enhance the accessibility and handling of AGUs synthetic intermediates. Hence, final Boc-cleavage were performed in trifluoroacetic acid (TFA) solutions and compounds were thus generally endowed with guanidines bearing trifluoroacetate (TF-Acetate) counterions.

To evaluate the impact of TF-Acetate counterion, a different salt analogue of hit compound **1** was achieved, compound **40**, bearing an hydrochloride counterion.[199]

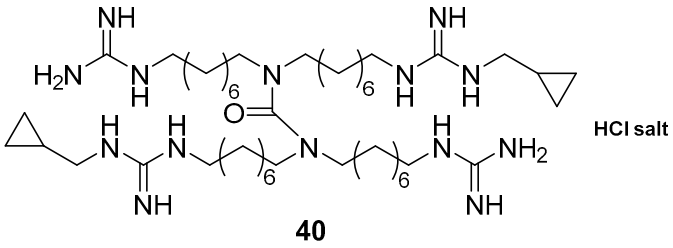

40

Figure 12. Molecular structure of compound **40**, the hydrochloride derivative of hit compound **1**.

The presence of residual TFA or TF-Acetate anions are known to interfere with cellular assays by inhibiting cell proliferation or favoring cell viability unspecifically.[200–202] Moreover, in view of *in vivo* experiments and potential application in clinical tests, a protocol to prepare more pharmaceutically suitable salts was developed by the research group.[199]

Briefly, first attempts involved the final Boc-cleavage with concentrated hydrochloride acid in dry dioxane[203] or preparation of the acid *in situ* with an acetyl chloride/dry methanol solution.[204] However, the obtained final products did not respect the acceptable purity for biological evaluation (>95%). Therefore, the TF-Acetate salt was converted into the chloride corresponding form by stirring a methanol solution with an anion-exchange resin, the Amberlite IRA 400 resin chloride form,[205–207] furnishing the desired compound **40**. The conversion was checked by fluorine ^{19}F-NMR spectrometry, that actually revealed the disappearing of the characteristic signal of TF-Acetate anions.[199]

Generally, no significant evidences could emerge by testing a compound as different organic or inorganic salt forms. However, moderate discrepancies could be highlighted for antibacterial agents when tested as salt form of different counterions,[208,209] even though the changes in MIC values were fond not higher that 2-fold and can be conventionally accepted as not significant differences.[210–212] This motivation relies on the difference in terms of molecular weights of hydrochloride and TF-Acetate forms, being MICs

reported as μg/mL, thus could not be considered as a direct influence of the counterion type on antimicrobial activity.[210]

Therefore, antibacterial activity of compound **40** will be evaluated and the discrepancies in terms of biological profile are expected not significant compared to the TF-Acetate parent compound **1**.[199]

3. Aim of this work

The majority of current antibacterial drugs hit old well-acquainted targets and bacteria have already developed resistance strategy for them. Therefore, there is a rising interest in discovering new classes of bioactive compounds exhibiting novel mechanisms of action.

Encouraged by the interesting SARs considerations collected with first series of AGUs[185,194] and with the molecular simplification strategy,[193] during my PhD work we decided to better investigated some other chemical features that could result crucial for the activity of this polycationic antibacterials.

The synthetic strategy, that was recently developed and reported by the group,[193] was based on Fukuyama's approach for polyamines preparation.[213–215] Briefly, the achievement of orthogonally protected polyamine ureas in large amount, bearing azido and trityl (Tr) groups, proved to be helpful for the preparation of several derivatives, benefiting from subsequent and selective removal of the *N*-protecting groups, followed by appropriate *N*-guanylation reactions at the end of the synthetic route.[193] Thanks to this fruitful divergent approach, new AGUs derivatives could be thereby prepared in a more accessible and versatile way, with high yielding steps, since the synthetically challenging guanylation reactions could be performed at the end of the pathway.

3.1 Synthesis of derivatives of compound 1: varying the chain lengths, symmetry and *N*-substitutions

SARs collected for the first series of AGUs outlined that the optimal biological activity was achieved when the alkyl spacer was composed by eight methylene. Increasing the number of carbon atoms from 8 to 10 or decreasing it to 6, resulted in a consistent fall of activity.[185]

Hence, we decided to investigate additional chain lengths to fill the gap in the AGUs library. Thus, the synthesis and the biological activities of new analogues, endowed with either seven or nine carbon atoms alkyl spacers (compounds **41** and **42**, Fig. 13) will be discussed.

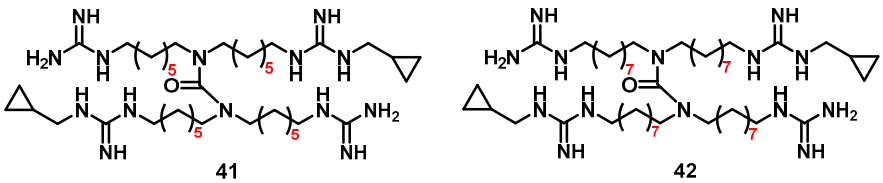

Figure 13. Molecular structures of new analogues of compound **1**, derivatives **41** and **42**, endowed respectively with seven or nine methylene alkyl spacers.

Furthermore, biological data displayed by first AGUs derivatives suggested that the symmetry and the position of the *N*-substituted guanidine on the alkyl spacer could play a key role in the antibacterial

activity.[185] Thus, derivatives **43-46** (Fig. 14) were synthesized to gain a deeper understanding about the effect of asymmetric methylene linkers on the molecule and the hydrocarbon distance, between the urea and the guanidino functionalities, required for activity.

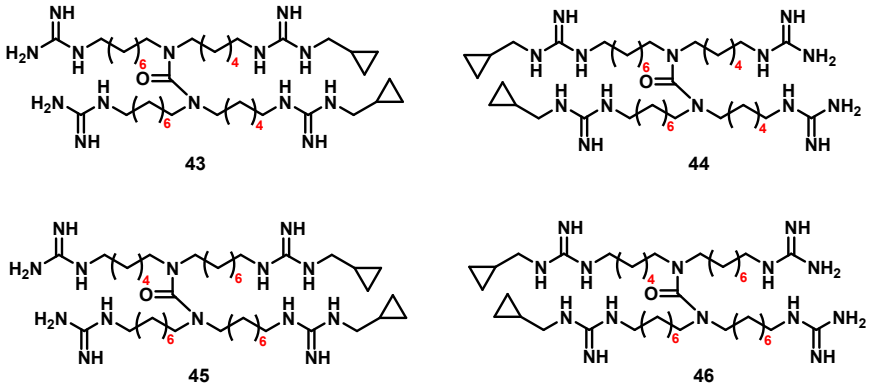

Figure 14. Molecular structure of derivatives **43-46** endowed with asymmetric chain lengths.

The kind of *N*-substitution on guanidine moieties seemed to not affect significantly the antibacterial activity.[185] Hence, we directed our chemical efforts towards the synthesis of novel AGUs derivatives to define more accurate SARs. With this purpose, compounds **47a-m** and **48a-b** were designed (Fig.15), to evaluate the role of guanidine moiety and the impact of *N*-substitutions involving saturated or unsaturated alkyl moieties, non-polar and polar functional groups, that were selected either considering their steric effects or their electronic contributions.

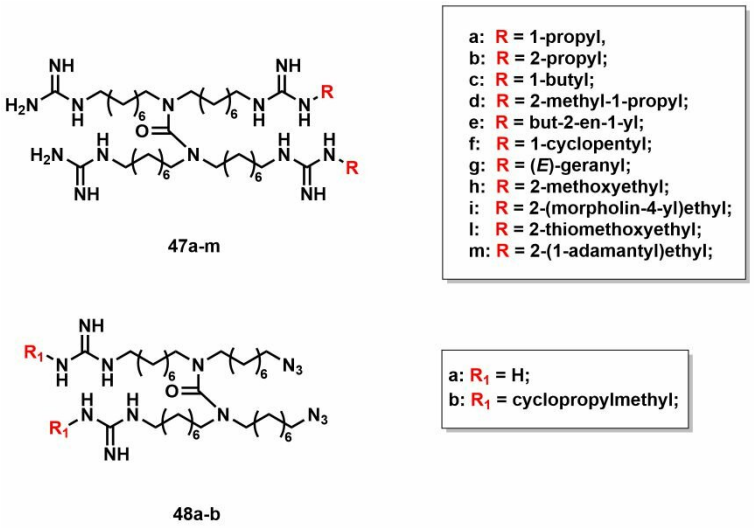

Figure 15. Molecular structure of derivatives **47a-m** and **48a-b** endowed with different *N*-substitutions or azido moieties to replace guanidines.

3.2 Synthesis of derivatives of compound 20: the impact of *N*-substitutions and the length of the alkyl spacer on the biological activity

As previously outlined, compound **20** proved to be the most active of the *arm-removed* series in the AGUs library. Encouraged by this interesting evidence and by its promising antibacterial profile,[193] we focused on the synthesis of a small library of derivatives.

Briefly, being the synthetic route of compound **20** easy and accessible, with few high yielding steps we synthesized derivatives **49-54** (Fig.16).

Since the effect of substitutions on the urea moiety was already investigated by designing compound **22**, bearing a methyl group with a worsened antibacterial profile,[193] we directed our chemical efforts towards the synthesis of different *N*-alkyl guanidino analogues (**50-54**, Fig. 16).

Moreover, the hydrocarbon distance between the guanidino group and the urea functionality was also evaluated, designing derivative **49** endowed with a different chain length (Fig. 16).

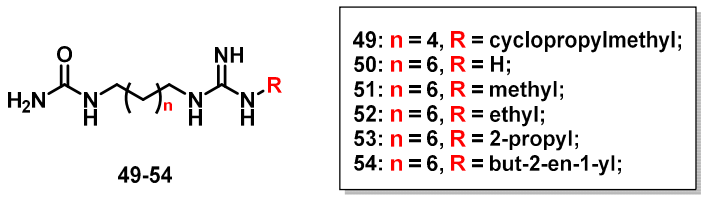

Figure 16. Molecular structures of derivatives **49-54** as analogues of compound **20**.

3.3 The role of urea moiety: unsuccessful attempts to achieve the thiourea derivative

The whole AGUs library, along with new derivatives synthesized and presented in this work, were achieved leaving unvaried the urea functionality. This relies on the enormous number of urea containing bioactive compounds, including a variety of clinically approved therapies. Indeed, urea functionality has been widely employed in medicinal chemistry and drug discovery, to establish crucial drug-target interactions and fine-tune important drug-like properties.[197] Moreover, urea-endowed compounds have also been reported in literature as antimicrobials and more specifically antibacterial agents.[216]

Concerning the putative AGUs mode of action, we supposed that the urea functionality could be also crucial to establish additional HB interactions with bacterial membrane as another contact point with the bilayers, thus an useful strategy to assess its role in biological activity could be its replacement with a thiourea functionality. In fact, switching from oxygen to sulfur, HB between thiourea and other bioactive components could involve only two hydrogen bond acceptors provided by the coplanar nitrogen atoms, whereas urea functionality could benefit also from another additional HBA represented by the oxygen.

Therefore, several synthetic attempts were made to achieve this potentially interesting derivative. Unfortunately, challenging synthetic routes, along with several undefined byproducts and impurities, limited significantly the handling of the synthetic intermediates and thus preventing the achievement of the desired compound.
The synthetic attempts will be discussed in results and discussion part of this thesis.

3.4 AGUs MoA investigation

Compounds **1**, **20** and **39** were selected for further and deeper investigations about the MoA of AGUs, as their antibacterial profile and chemical diversity resulted very promising. Hence, the synthesis of this three compounds was performed to achieve larger amounts for biological assays.
Given the complexity of membrane-active agents MoA evaluation,[116] the first approach we selected to investigate their mode of action was resorting to artificial and simulated model membrane.
Thus, LUVs endowed with bacterial phospholipids were employed to assess the AGUs interactions with artificial bilayers, that were monitored through the versatile and easily accessible UV-spectroscopy. Then, traditional PAMPA experiments were performed, both with mammalian and bacterial phospholipids, along with a modified PAMPA protocol, involving scarce permeable molecule, like caffeine ad CAF, as probes for evaluation of membrane damage. Furthermore, MD simulations provided interesting and additional information about the chemical features required for the interaction with the membranes.
Cell-based assays were also needed to validate the analytical and computational protocols since, being experiments on model membranes, they could not furnish exhaustive and conclusive data about the mechanism of action. Hence, permeabilization assays were performed exposing three Gram-positive representative strains, *B. subtilis* ATCC 6633, *E. faecalis* ATCC 29212 and *S. aureus* ATCC 25923, and three Gram-negative ones, *A. baumannii* ATCC 17978, *E. coli* MG1655 and *P. aeruginosa* ATCC 27853, to AGUs selected derivatives. The uptakes of two fluorophores, namely SYTO9 and propidium iodide (PI), were monitored to evaluate potential loss of membrane integrity.
In fact, the green-fluorescent dye SYTO9 could permeate all bacterial cells, whereas PI enters only cells presenting damaged membranes, resulting in a red fluorescence emission upon intracellular DNA binding.[217] Moreover, loss of membrane integrity was also additionally confirmed by confocal laser scanner microscopy (CLSM).
In the end, hemolytic activity of test compounds was considered as a means of assessing cytotoxicity of AGUs derivatives.

3.5 The effect of counterions on AGUs antibacterial properties

An estimated 50% of all drug molecules are generally administered as salts. This evidence indicates that the salification, or salt formation, of a drug substance could be a crucial step in drug development.[218]
As previously outlined, the research group already focused his efforts on investigating the role of the counterion on the biological activity, since the whole library has been obtained as TF-Acetate salt form. Following this purpose, compound **40**, the hydrochloride salt analogue of hit compound **1**, was prepared to exploit this chemical feature.[199]
Herein we also reported the synthetic attempts to achieve the free-base derivative of **1**, compound **55** (Fig.17), and the biological comparison of activity profiles of **1**, **40** and **55**. In fact, it is noteworthy that the selected counterions do not have to alter the biological profile of the parent drug candidate.[219] Hence, we decided to evaluate the antibacterial activities of these two new analogues considering them as new chemical entities.

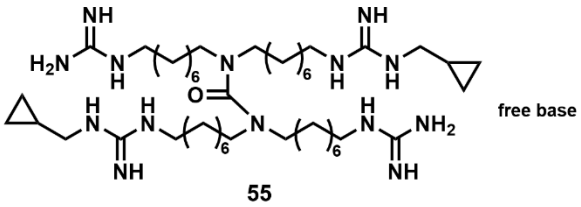

55

Figure 17. Molecular structure of the free-base analogue of compound **1**, derivative **55**.

4. Results and Discussion

4.1 Chemistry

*4.1.1 Preparation of derivatives **41** and **42**: varying the chain length*

Several preparation methodologies are reported in literature to achieve symmetrical tetrasubstituted urea derivatives. Among them, different approaches involve the use of phosgene and its safer derivative triphosgene, as they could provide high yielding and scalable reactions.[220] In the past, the research group selected the latter approach to afford *N*-carbamoyl derivatives of properly synthesized secondary amines, that were then coupled with the same or different secondary amines through a nucleophilic addition and subsequent elimination, to furnish the desired ureas. The followed retrosynthetic approach is showed in Fig. 18.

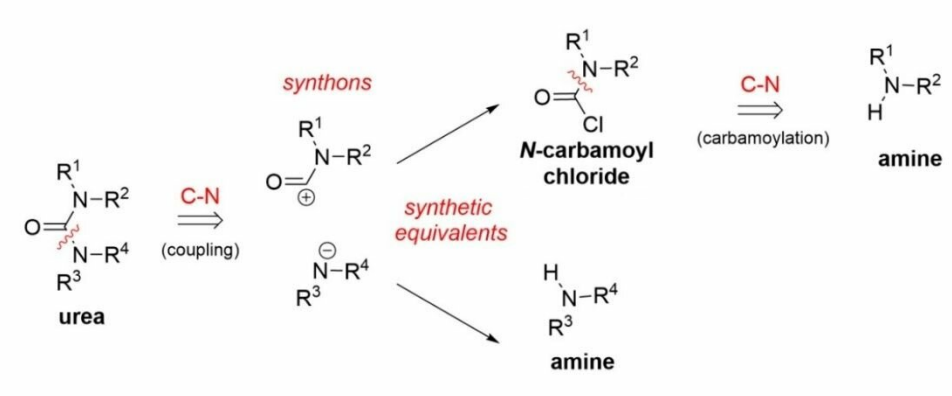

Figure 18. Retrosynthetic plan for AGUs derivatives.

The synthetic procedure adopted for the preparation of compounds 41 and 42 was already reported by the research group.[185,186] Briefly, the route was based on the subsequent two guanylation steps with properly commercially available or synthesized *N*-substituted S-methyl or *1H*-pyrazolecarboxamidine guanylating agents, respectively, on a triamine derivative. Then the *N*-carbamoyl derivative of this bis-guanylated monomeric unit could be prepared and then coupled as previously described. Unfortunately, triamine derivatives endowed with 7 or 9 carbon atoms are not commercially available, thus a suitable synthetic strategy have been developed and optimized by the group to afford these intermediates.

In Scheme 1 the synthesis of derivatives **41** and **42** is summarized.

Briefly, commercially available 1,7-dibromoheptane and 1,9-dibromononane are reacted with sodium azide to furnish bromoazides **56a-b**. A bis-alkylation of benzylamine with **56a-b** is performed to obtain diazide derivatives **57a-b**. Subsequent reductions of the azido moieties with a Staudinger protocol afford diamine derivatives **58a-b** in quantitative yields. Then, a debenzylation of the central amine is

accomplished through an acid-catalyzed hydrogenation over palladium, furnishing the triamine derivatives **59a-b**.

Scheme 1. Preparation of compounds **41** and **42**.

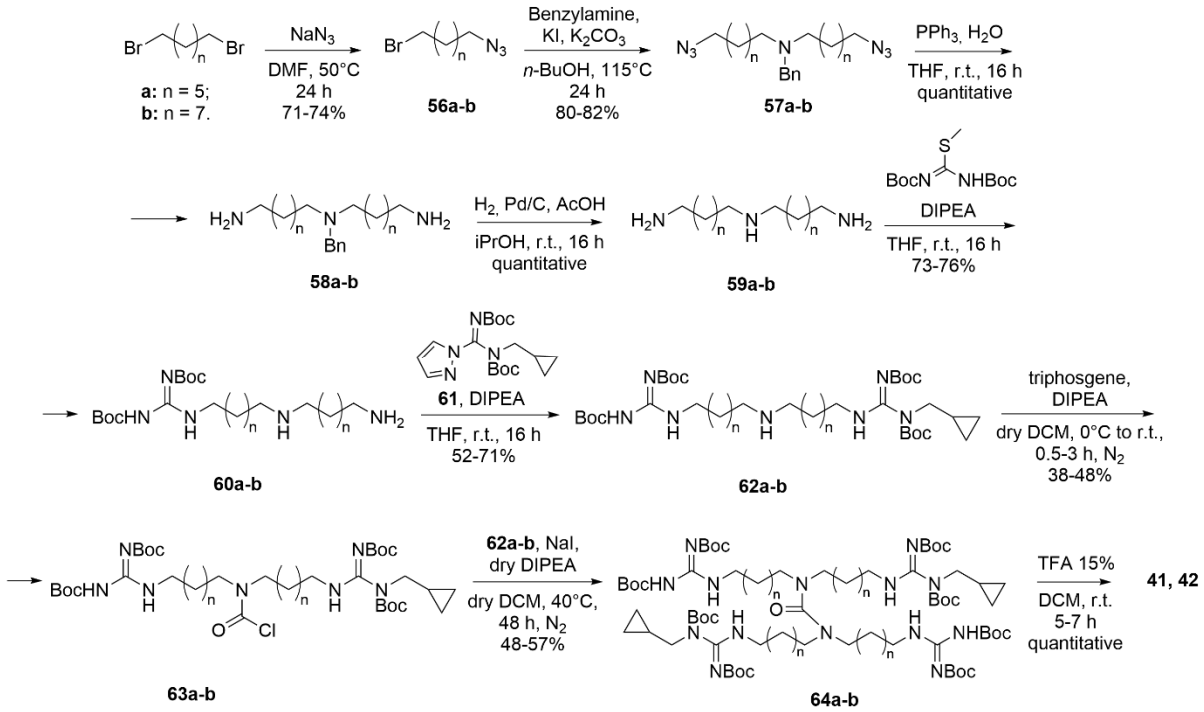

Then, triamine derivatives **59a-b** are subjected to a bis-guanylation, first with the commercially available 1,3-Bis(tert-butoxycarbonyl)-2-methyl-2-thiopseudourea, and then with the properly synthesized compound **61**, whose synthesis have already been reported and described by the group.[185,186] The monomeric derivative **62a-b** are then submitted to a carbamoylation reaction to afford the corresponding *N*-carbamoyl chloride derivatives **63a-b** which are then coupled with intermediated **62a-b** to furnish the tetraguanidino urea derivatives **64a-b**. A final deprotection with TFA allow the cleavage of Boc protecting groups and the achievement of compounds **41** and **42** as TF-Acetate salts.
Characterizations of derivatives **56-62a** have been already reported by the group[199] and will not be described in the material and methods section.

4.1.2 Divergent synthesis as a tool to achieve novel AGUs derivatives

To improve the efficiency of AGUs chemical synthesis, a divergent approach was previously developed and optimized by the research group. Briefly, divergent synthesis aims to generate a key intermediate, namely the central core of the molecular structure, from which successive generation of building blocks

could be added. Thus, divergent synthesis proved to be an effective strategy to quickly access to derivative libraries, focusing on chemical skeletal diversity.[221]

Previously reported procedures for AGUs preparation consisted of very polar intermediates whose purification resulted not trivial.[185,186] Indeed, the first series of AGUs derivatives were obtained through the final coupling reactions between already bis-guanlylated substrates.[185,186] Moreover, the overall yield of final compounds was limited by the challenging guanlyation reactions and purifications.[185]

Hence, to improve the handling of the synthetic pathways, the research group resorted to the Fukuyama's strategy for polynitrogenated alkyl compounds.[215,222] Following this approach, a tetrasubstituted urea orthogonally protected could be achieved, in large amounts, as key intermediated to provide further derivatization at the end of the synthetic route.[193]

As orthogonal protecting groups for amines, azido, p-Nosyl (p-Ns) and trityl groups were selected, since they resulted easy to cleave in a selective way and could provide the proper lipophilicity to favor the purification and isolation of the key intermediate. In fact, the previously required triamine, whose synthesis resulted fundamental as not commercially available, has been now converted in a tri-protected substrate, where the primary and secondary amine moieties are masked as azido, nosyl or trityl amine functional groups. Following this approach, the key tetrasubstituted urea is now endowed with strategically protected and orthogonally cleavable amines: indeed, azido moieties could be converted through simple hydrogenation heterogeneously catalyzed or by Staudinger reaction with milder conditions into the corresponding amines, whereas trityl group could be cleaved in acid environment.

Therefore, this approach proved to fruitful to obtain a wider variety of new AGUs derivatives presenting interesting chemical diversity.

*4.1.3 Preparation of derivatives **43-46** endowed with asymmetric alkyl spacers*

First AGUs SARs previously collected pointed out that structural symmetry could play a key role in antibacterial activity. In fact, compound **11**, showed a worsened antibacterial profile compared to its parent compound **1**, proving that the structural inversion operated actually affected the potency and the activity. This results encouraged us to deeper investigate this chemical feature and thus derivatives **43-46** were designed, being ureas endowed with asymmetrical arms with different chain lengths.

The innovative synthetic strategy optimized by the group proved to be very helpful for this purpose. Scheme 2 shows the synthesis of the key intermediate **70a-b**. Briefly, the amino moieties of proper commercially available diamino alkane are submitted to two subsequent protection, first with trityl chloride and then with *p*-Nosyl chloride to afford with high yield derivatives **66a-b**.

Scheme 2. Synthesis of the key intermediate **70a-c**.

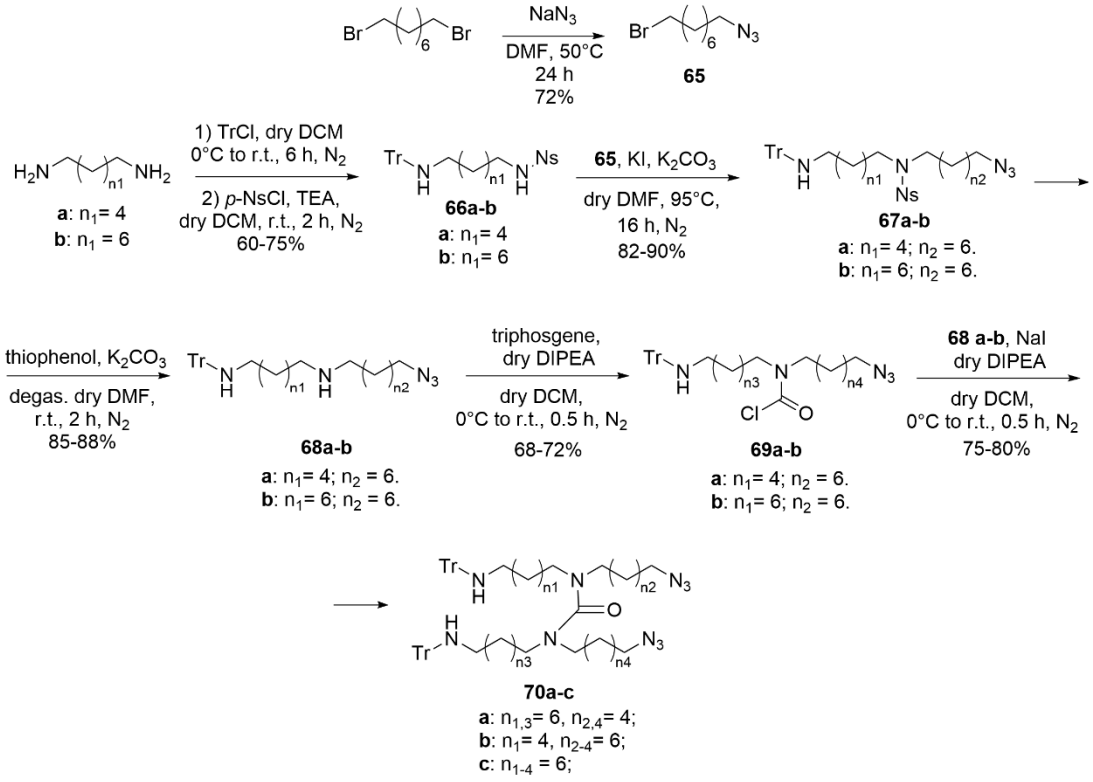

The nosyl strategy was conceived to promote the *N*-alkylation with the bromo azide **65**, which synthesis has been widely reported by the group[185,223] and thus will not be discussed. Moreover, being an hindering protecting group, nosyl moiety prevents also from bis-alkylation. Hence, the furnished derivatives **67a-b** are then submitted to a selective cleavage to free the central secondary amine, affording derivatives **68a-b**. Briefly, the deprotection of Ns groups involve the addition of a thiolate on the sulfonyl-bearing carbon, promoting the formation of the *Meisenheimer complex* (Fig. 19). The following elimination of sulfur dioxide provides the free amine as desired (Fig. 19).

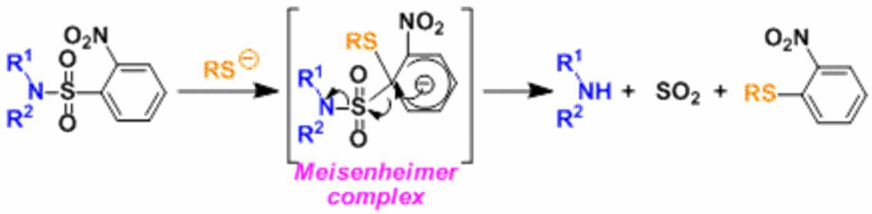

Figure 19. Mechanism of Ns group cleavage.[224]

Carbamoyl chlorides **69a-b** are obtained by reacting **68a-b** with triphosgene. Then, the coupling with the corresponding amines **68a-b** could occur, furnishing with high yields the orthogonally tetra-protected urea intermediate **70a-c** (Scheme 2).

Scheme 3. Synthesis of asymmetrical derivatives **43-46**.

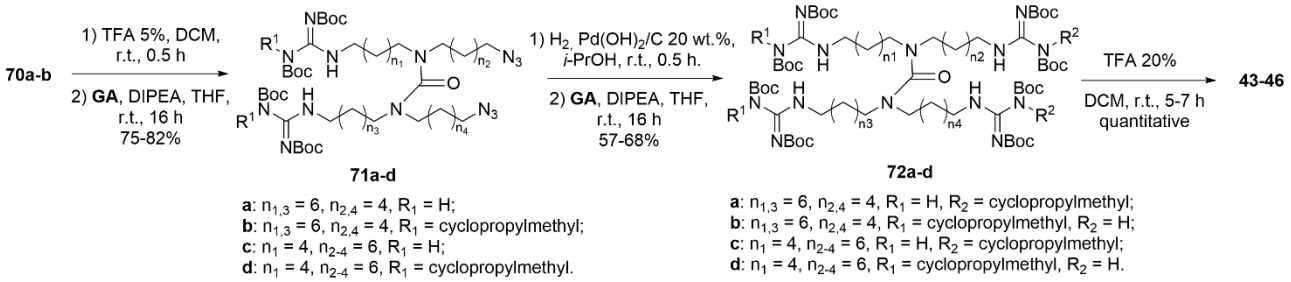

Cleavage of trityl groups could be performed in acid environment using a 5% solution of TFA in dichloromethane (DCM), then the proper guanylating agent (GA) between the commercially available *N,N*-DiBoc-*1H*-pyrazolecarboxamidine or compound **61**, is selected for the first guanylation step (**71 a-d**, Scheme 3). Conversion of the azido moieties in the corresponding amines is achieved by catalytic hydrogenation with palladium hydroxide on carbon, then second guanylation with the suitable GA is performed to obtain derivatives **72a-d**. Final deprotection with TFA furnish the TF-Acetate salts **43-46**.

*4.1.4 Preparation of derivatives **1**, **47a-m** and **48a-b**: the role of the guanidine moieties and their N-substitutions*

Investigation on AGUs MoA required larger amounts of hit compound **1** and its interesting derivatives **20** and **39**. Thus, the new divergent synthetic strategy revealed to be useful to achieve **1** in moderately-high quantity, compared to the previous reactions plan.

Moreover, preliminary investigations about the role of the substitutions on guanidine moieties provided flat SARs and almost all equipotent derivatives (**2-16**, Tab. 4). Thus, we decided to get a deeper understanding of this chemical features by synthesizing compounds **47a-m** (Scheme 4).

Proper substituents were selected according to their contributions in terms of electronic or steric effects and to their hydro-/lipophilic balance.

First, cyclopropylmethyl group of hit compound **1** was spatially deconstructed or simplified, furnishing linear and/or branched *N*-substituted guanidino derivatives. Hence, 1-propyl (**47a**), 2-propyl (**47b**), 1-butyl (**47c**), 2-methyl-1-propyl (**47d**), and but-2-en-1yl (**47e**) compounds were synthesized (Scheme 4).

Then, a cycloalkyl substituent was embedded, due to its ability to establish larger hydrophobic interactions with lipophilic counterparts (**47f**).[225] Furthermore, a geranyl chain was also selected as a representative unsaturated substituent, giving its known antimicrobial activity (**47g**).[226,227]

In the end, substituents endowed with different degrees of polarity were explored, achieving polar (**47h** and **47i**, Scheme 4) and apolar (**47l** and **47m**, Scheme 4) analogues.

Scheme 4. Synthesis of derivative **1**, **47a-m** and **48a-b**.

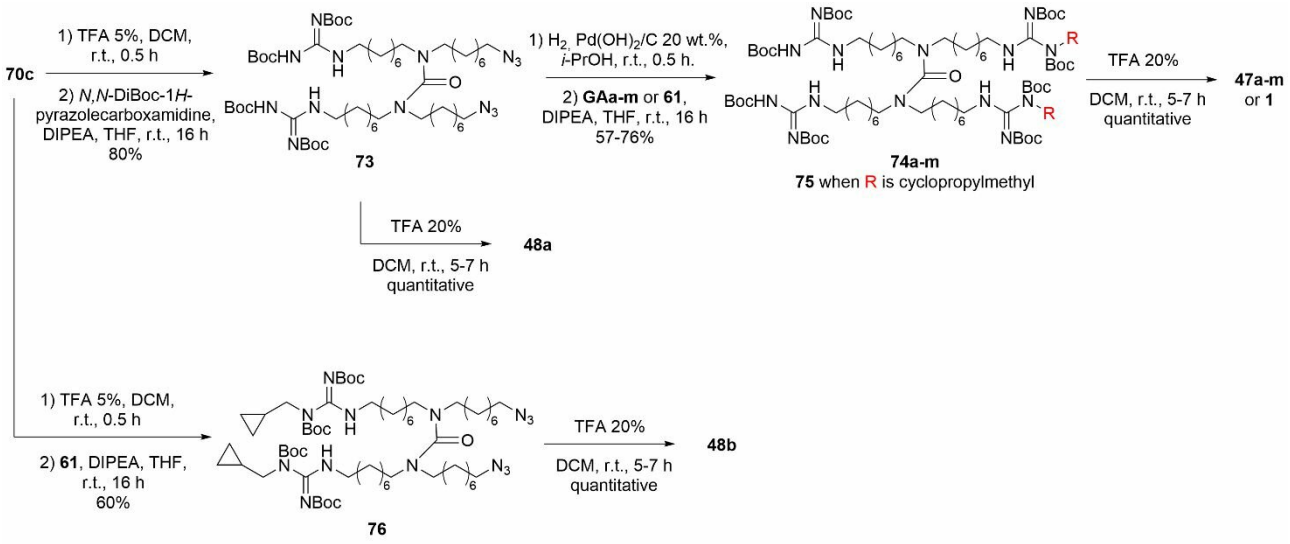

R = **a**: 1-propyl; **b**: 2-propyl; **c**: 1-butyl; **d**: 2-methyl-1-propyl; **e**: but-2-en-1-yl; **f**:1-cyclopentyl; **g** (*E*)-geranyl; **h**: 2-methoxyethyl; **i**: 2-(morpholin-4-yl)ethyl; **l**: 2-thiomethoxyethyl; **m**: 2-(1-adamantyl)ethyl.

Additionally, the role of guanidine moiety itself was evaluated. Indeed, starting from the synthetic intermediates **73** and **74** (Scheme 4), derivatives **48a** and **48b** were respectively obtained. Hence, two guanidines are replaced by azido moieties to ultimately confirm if the number of charges are strictly relevant for the potency.

Briefly, the previously described key intermediate **70c**, bearing eight methylene alkyl spacers, is first detritylated and then guanylated with the proper guanylating agent, either the commercially available *N,N*-DiBoc-*1H*-pyrazolecarboxamidine or compound **61**, to afford respectively derivatives **73** and **76**.

The bis-guanylated compounds **73** and **76** are then treated with TFA to afford respectively compounds **48a** and **48b,** after cleaving Boc protecting groups. Intermediate **73** has also been used as starting material to prepare derivatives **47a-m** and **1**. In fact, through this optimized synthetic approach, hit compound **1** has been obtained in larger amount, in order to perform MoA investigations. Hence, after palladium-catalyzed hydrogenation of azido moieties, the second guanylation could occur using the properly synthesized guanylating agents **GAa-m** or **61**, furnishing derivatives **74a-m**. In the end, final compounds **47a-m** and **1** are furnished as TF-Acetate salt after Boc-cleavage in acid environment.

Guanilating agents **GAa-m** (Scheme 5) are obtained by reacting *N,N*-DiBoc-*1H*-pyrazolecarboxamidine with the suitable alcohol under Mitsunobu conditions. Compound **GAe** has been already characterized and reported by the group,[228] thus will not be described in the experimental session of this thesis.

Scheme 5. Synthesis of guanylating agents **GAa-m**.

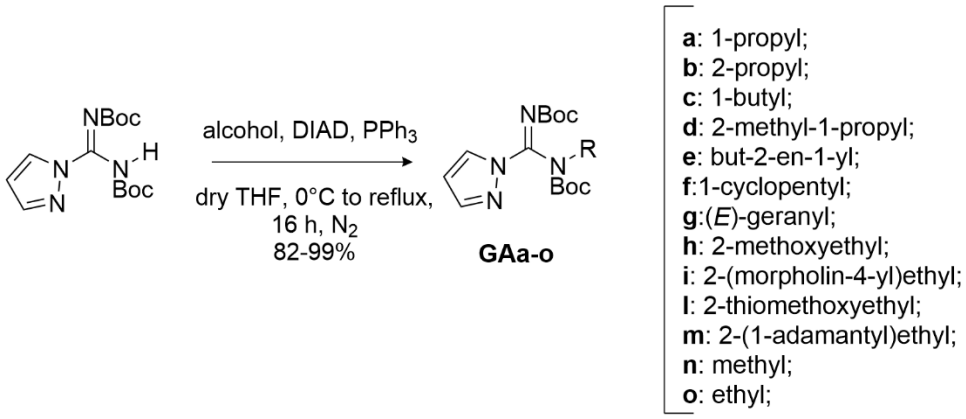

*4.1.5 Synthesis in larger scale of compound **39***

As previously mentioned, MoA investigations required hit compound **1**, but also derivatives **20** and **39**, in larger amount to perform different analytical and cell-based assays.

The synthtetic route to achieve compound **39** is resumed in Scheme 6 and has been already reported by the group,[193] thus intermediates will not be characterized and discussed in this work.

Briefly, commercially available 2-nitrobenzenesulfonamide is submitted to a bis-*N*-alkylation with bromoazide **65**, affording the nosyl amine **77**. After sulfonamide cleavage with sodium methanethiolate and subsequent carbamoyl formation, derivative **78** is obtained. Secondary amine **68b**, bearing one azido moiety and one trityl group, is now coupled with **78**. Hence, the selected key intermediate to obtain **39** is a tetrasubstituted urea bearing three azido moieties and one trityl group, that can be selectively cleaved, freeing the amine, which is subsequently guanylated, affording derivative **79.**

Azido moieties are then reduced in the corresponding primary amines resorting to a palladium-catalyzed hydrogenation and after second guanylation and final Boc-cleavage with TFA, compound **39** is obtained.

Scheme 6. Reported synthesis for compound **39.**[193]

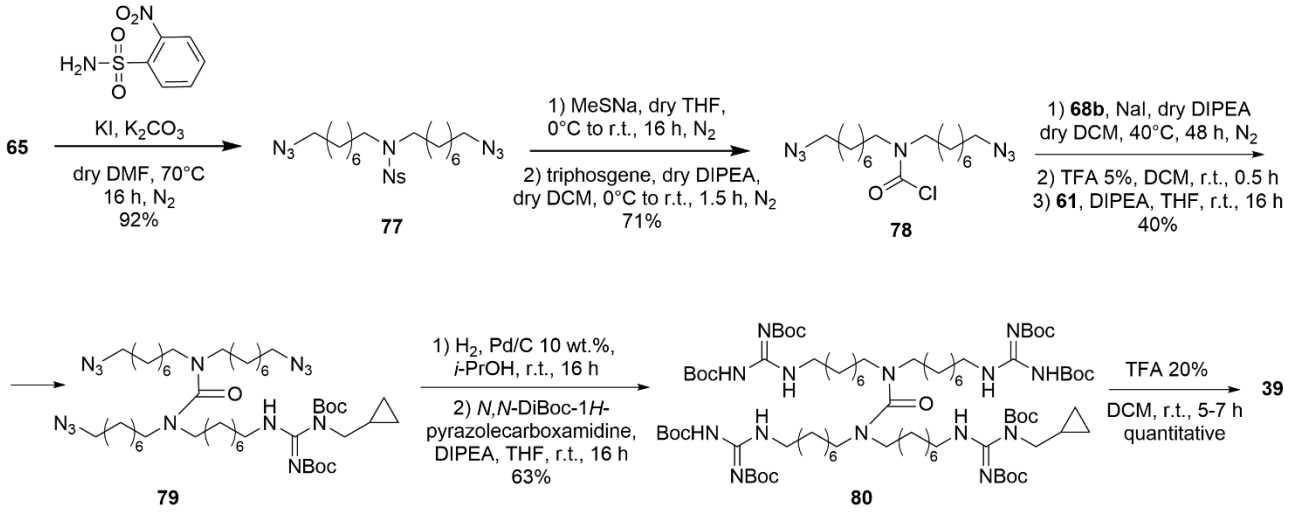

*4.1.6 Failed synthetic attempts to achieve compound thiourea analogue**1***

Shedding light on the role of urea functionality in AGUs antibacterial profiles prove to be an interesting option to get a deeper understanding about the chemical features required for the activity. For this purpose, the thiourea derivative was conceived. Notably, the synthesis and the antibacterial studies of thiourea derivatives endowed with antimicrobial activity have been widely reported in literature.[229]

Investigations concerning its potential role in membrane-active antibacterials revealed that C=S and N-H groups in thiourea moieties can be easily protonated under acidic conditions and react with the carboxyl and phosphate groups of the bacterial surface, contributing to enhance the antibacterial activity.[230,231] Moreover the incorporation of alkyl chains as substituents in thiourea derivatives proved to exert interesting biological properties.[232,233] Indeed, the presence of long alkyl chains were reported to improve the biological profile of thiourea derivatives.[234]

However, the challenging design of a suitable synthetic approach limited so far the achievement of the desired thiourea analogue. In Scheme 7 are summarized several failed attempts that outline the synthetic inaccessibility of this compound.

Briefly, first strategy involves the use of a thiation agent, namely the Lawesson's reagent,[235] to convert either the urea **70c** or **75** into their thio analogues. Unfortunately, both reactions display only a mixture of byproducts difficult to identify, along with starting material degradation that occurs mainly with tetraguanylated urea **75**.

Then, the azido/trityl amine **68b** is first converted into its thiocarbonyl imidazole derivative **83** with very poor yield and subsequently coupled with the amine counterpart. During this reaction only degradation of the imidazoyl derivative **83** is observed but no coupling occurs.

Inspired by the Tomkinson's approach,[236,237] compound **68b** is converted into the dithiocarbamic acid **84** with very good yield and then coupled with the nosyl amine **67b**. The supposed mechanism of reaction, that has been hypothesized relying on Tomkinson's approach, is reported in Fig. 20.

Scheme 7. Synthetic attempts to achieve the thiourea derivative of **1**.

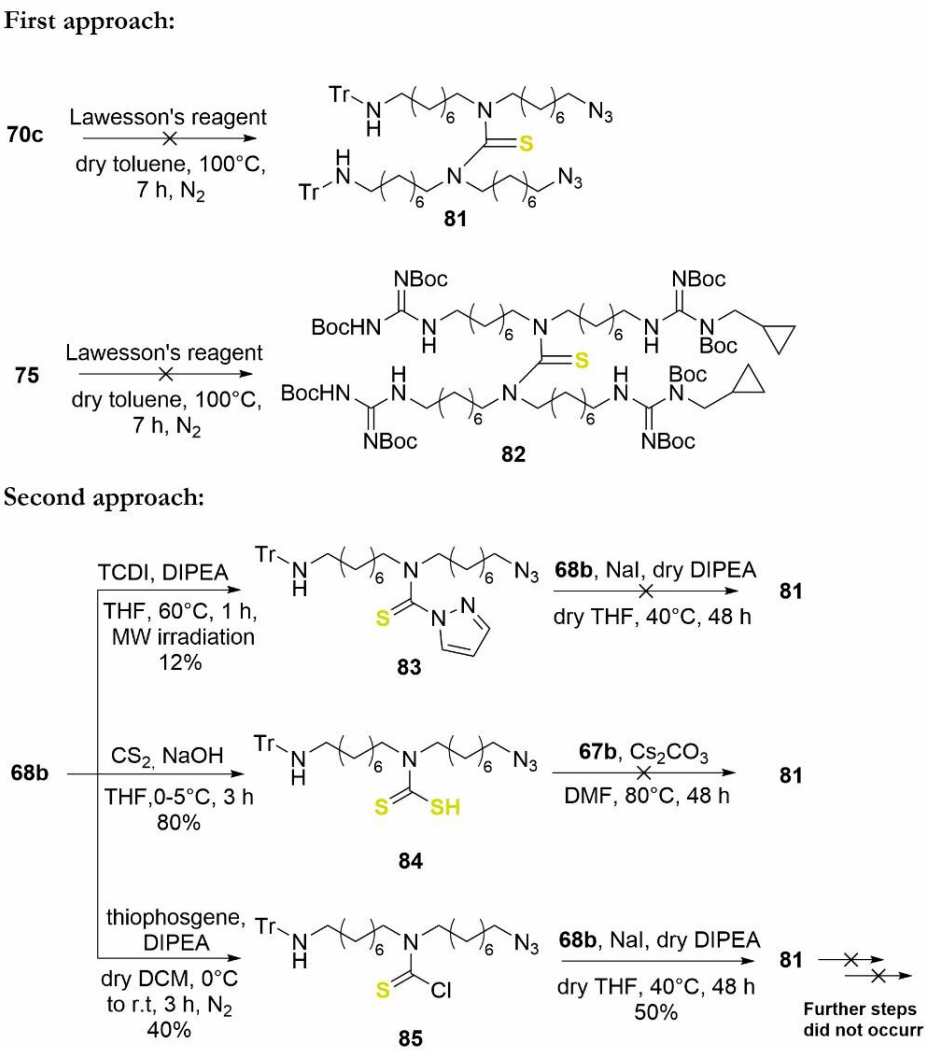

Therefore, the thio nucleophile **84** displays an *ipso* attack to form the initial Meisenheimer complex type which, after loss of sulfur dioxide, gives the final thiourea derivative in a deprotection/functionalization sequence (Fig. 20). However, only the deprotected amine and the nosyl byproduct are observed but no coupled thiourea is formed.

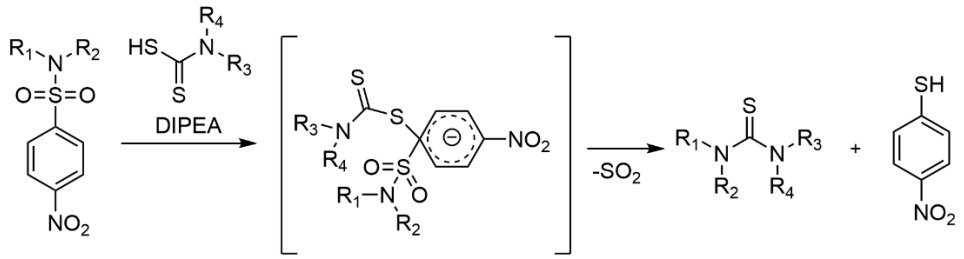

Figure 20. Hypothesized mechanism of reaction according to Tomkinson's approach.

Final approach we resort is the formation of the thiocarbamoyl derivative **85**, that occurs with moderate yields using thiophosgene. Then **85** was coupled with **68b** affording thiourea **81** as desired. However further functionalizations of compound **81** promote the formation of several unknow byproducts, challenging to isolate and identify, along with degradation of starting materials. Thus, the achievement of the thiourea analogue of **1** failed. Moreover, the formation of the thiocarbamoyl derivative **85** lacks in reproducibility. In fact, while performing the reaction under controlled conditions in terms of temperature, exposure to light and/or air, inert atmosphere and time, the reaction outcome results not reproducible, due to degradation of thiocarbamoyl chloride, along with the rapid formation of several byproducts (Table 14). Among them, the major byproduct is supposed to be the thiuram oxides **86** (Figure 21).

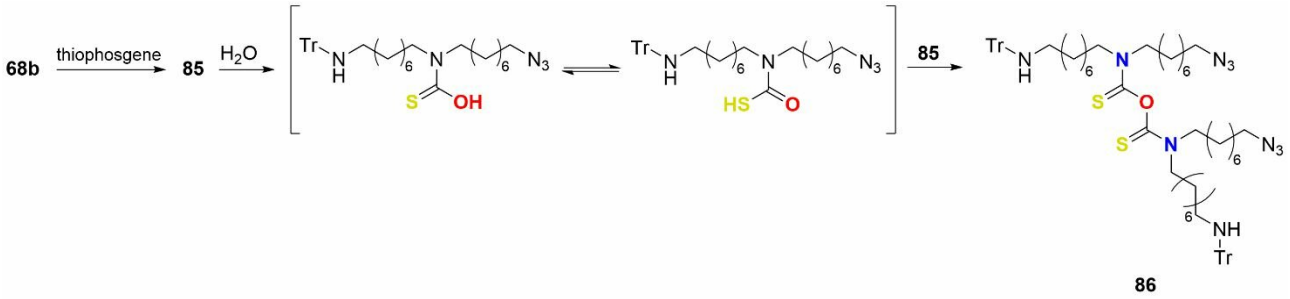

Figure 21. Hypothesized mechanism of thiuram oxide formation.

Briefly, a recurring unidentified dimer has been isolated during the thiocarbamoyl formation reaction. According to literature,[238] thiocarbamoyl chlorides could react with alcohols or water, furnishing the corresponding carbamothioic acid, which could afford thiuram oxide **86** after coupling with thiocarbamoyl chloride **85**. Although the reaction with thiophosgene was performed under inert atmosphere, the detected LC-MS signals and the ^{1H}-NMR spectra collected for the isolated byproduct **86**, seems to confirm that the formation of the thiuram oxide could occur.

As a further proof, **86** has been synthesized according to the synthetic pathway presented in Scheme 8. Hence, the amine **68b** was converted into its corresponding thiocarbamic acid and then coupled with the carbamoyl chloride **69b** in a *one pot-two step* protocol, as reported in literature.[239,240]

Scheme 8. Synthesis of derivative **86**.

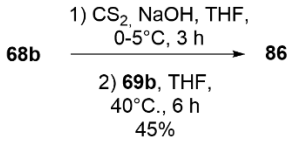

Experimental analytical data collected were consistent with those of the isolated byproduct (Figure 22). This evidence could properly explain the observed rapid consumption of the thiocarbamoyl chloride and the formation of several byproducts during the reaction. Moreover, **85** revealed to be also air-sensitive, since desulfuration after air exposure is observed (entry 8, Table 14). The formation of this unknown derivative occurs not only in DCM, but also when the reaction is performed in anhydrous toluene or tetrahydrofuran (THF) (entries 4-5, Table 14). Presumably, traces of water in solvents or poorly dried glassware could have contributed to this transformation. Even though the structure of this derivative has not been completely confirmed, this evidence outlines the instability of thiocarbamoyl chloride intermediate and thus the resulting scarce handling of this substrate.

Table 14. failed attempts to achieve compound **85**.

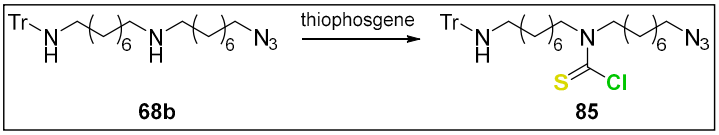

Entry	Solvent	Base	Temperature	Exposure	Time	Yield	Comments
1	dry DCM	dry DIPEA	0°C to r.t.	light	3 h	40%	**85** was purified and isolated
2	dry DCM	dry DIPEA	0°C to r.t.	light	5 h	n.d.	**68b** did not react completely, observing **85** consumption and formation of the thiuram oxide.
3	dry DCM	DMAP	0°C to r.t.	light	3 h	traces	After 0.5 h **85** formed but **68b** was still present. After 3h only traces of **85** were visible.
4	dry THF	dry DIPEA	0°C to r.t.	light	2 h	traces	Several byproducts, thiuram oxide present, only traces of **85**.
5	dry toluene	dry DIPEA	0°C to r.t.	light	3 h	traces	Traces of **85**, huge amount of thiuram oxide.
6	degas. dry DCM	dry DIPEA	0°C to r.t.	light	3.5 h	11%	Several byproducts, **85** observed only in traces, thiuram oxide detected.
8	degas, dry DCM	dry DIPEA	0°C to r.t.	light	3 h	23%	After isolation, desulfuration occurred due to air exposure
9	degas, dry DCM	dry DIPEA	0°C to r.t.	dark	3 h	n.d.	After 0.5 h **85** formed. Then its consumption was observed along with thiuram oxide formation.
10	degas, dry DCM	DMAP	0°C to r.t.	dark	4 h	n.d.	Reaction did not occurr

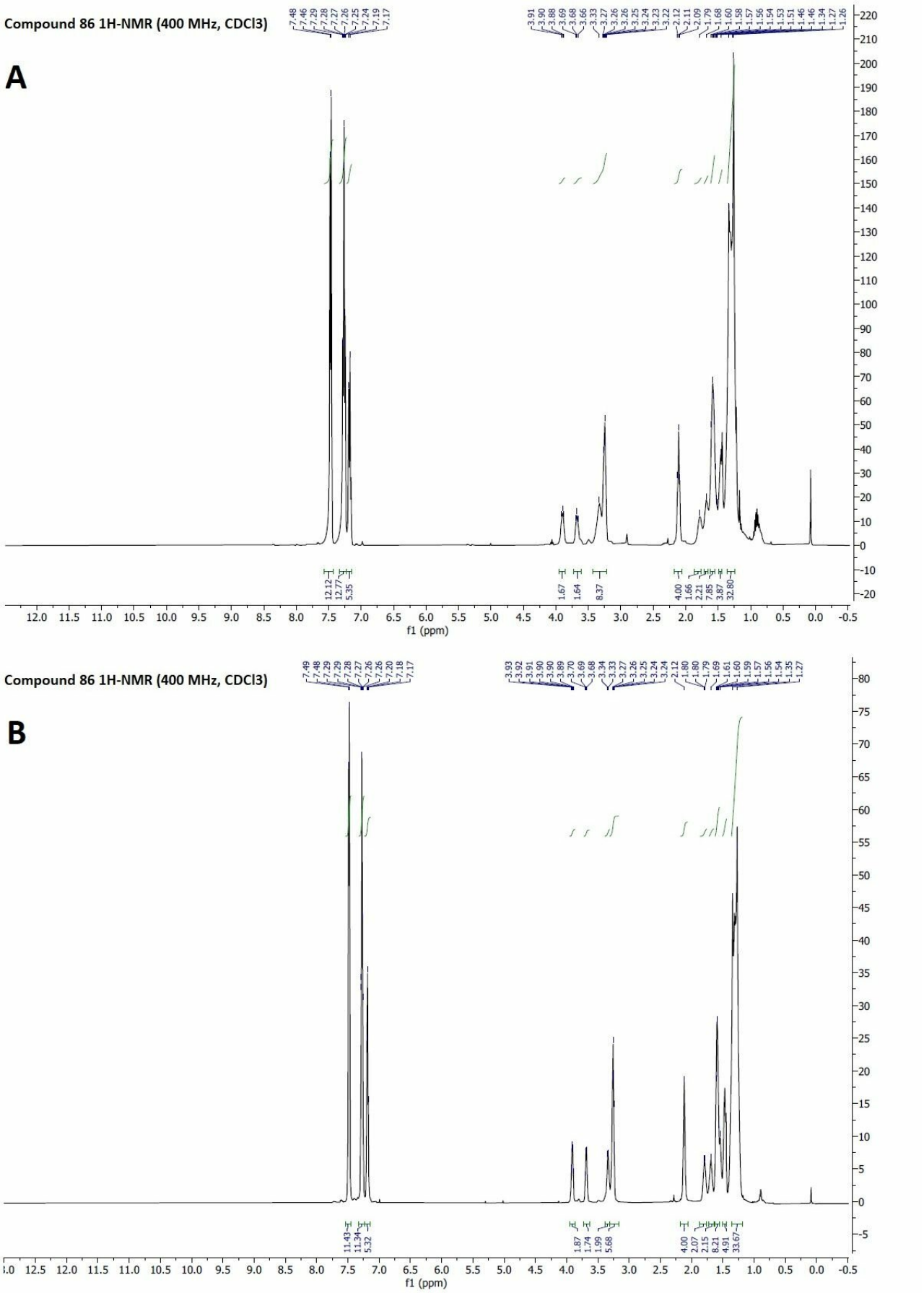

Figure 22. ^{1H}-NMR spectra for derivative **86**. A) ^{1H}-NMR spectra of derivative **86** isolated from thiocarbamoylation reaction. B) ^{1H}-NMR spectra of derivative **86** synthesized according to Scheme 8.

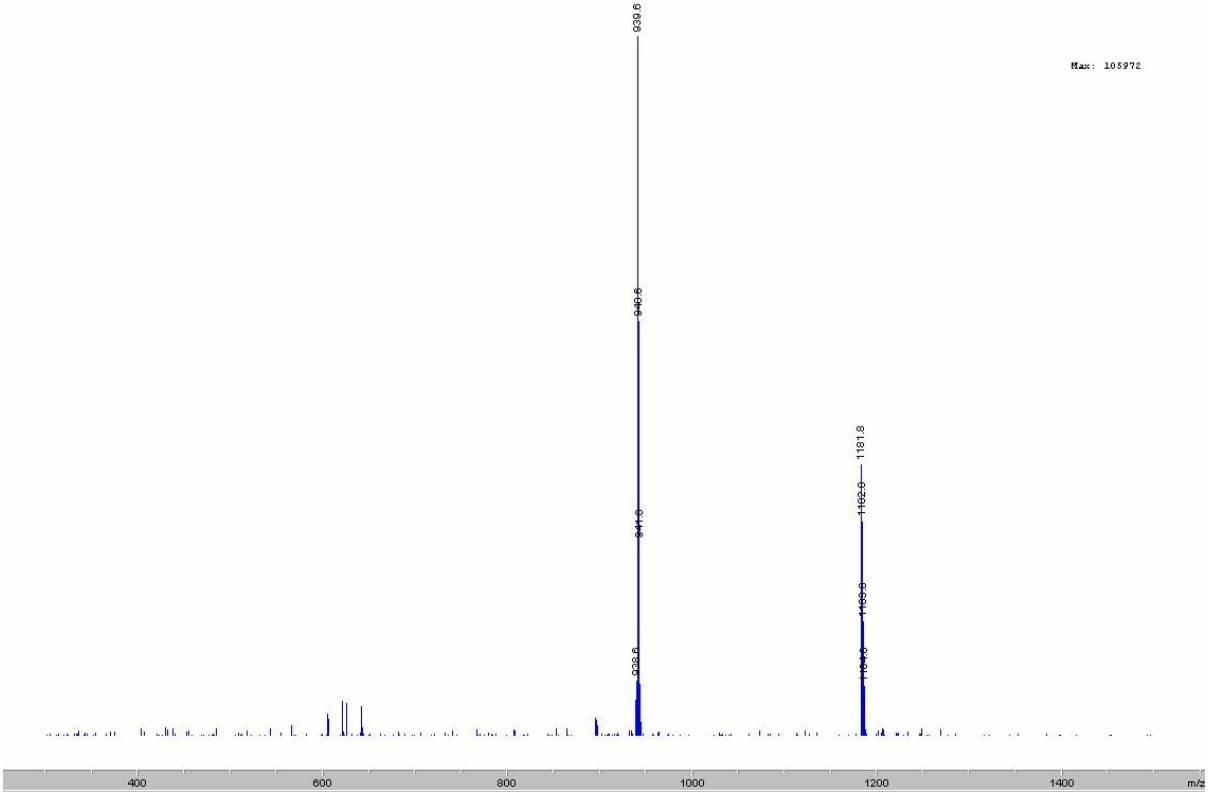

Figure 23. LC-MS (ESI+) spectra of compound **86**. Sample was prepared in MeOH. This mass spectra was acquired using a binary solvent system 95/5 MeOH/H2O, in positive mode scanning over the mass range 300-1500 m/z, using a variable fragmentor voltage of 10-70 mV. $[M+H]^+$ = 1181.8, [M+H-Trityl fragment]+ = 936.6 mass artefact.

*4.1.7 Preparation of compound **20** and its analogues **49-54***

Compound **20** emerged as the most promising derivative of the arm-removed AGUs serie. Given its interesting antibacterial profile, that represented an outlier data among all the SARs collected, a focused library was developed and compound **20** was synthesized in larger scale to perform MoA studies, according to the synthetic plan presented in Scheme 9.

Scheme 9. Synthesis of compounds **20** and **49-54**.

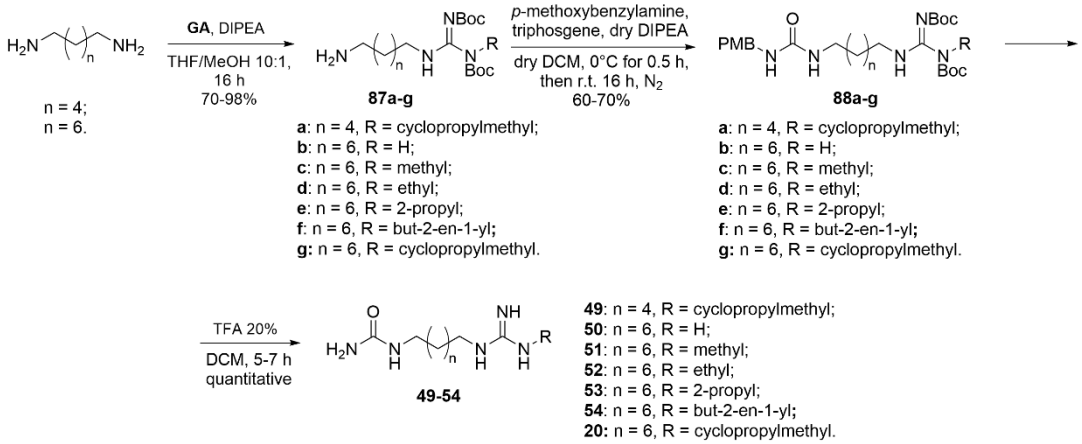

The length of the alkyl spacer and the *N*-substitutions on guanidine moiety were varied.

Briefly, the commercially available 1,6-diaminohexane or 1,8-diaminooctane are submitted to a monoguanylation reaction with the suitable GA among the properly synthesized **GAa-m**, compound **61** or the 1,3-Bis(*tert*-butoxycarbonyl)-2-methyl-2-thiopseudourea, affording the monoguanylated derivatives **87a-g**. Then, the *in situ* generated *p*-methoxybenzyl isocyanate (not showed) reacts with compounds **87a-g** furnishing intermediated **88a-g**. In the end, the final Boc cleavage with a 20% TFA solution affords derivatives **20** and **49-54** as TF-Acetate salts.

*4.1.8 Preparation of compound **55**, the free-base analogue of hit compound **1***

As previously mentioned, the research group was already investigating the effect of the counterion on biological activity and toxicity profile of AGUs. Hence, the hydrochloride analogue **40** was synthesized. Preparing the free-base derivative **55** is not trivial and several attempts were made to remove the TF-Acetate anion from the compound. Hence, different synthetic strategies were developed to obtain derivative **55**, by exploring both in batch and microwave (MW)-assisted acid or base-free conditions, along with salt-exchange procedures (Scheme 10).

Scheme 10. Synthetic attempts to obtain free-base derivative **55**.

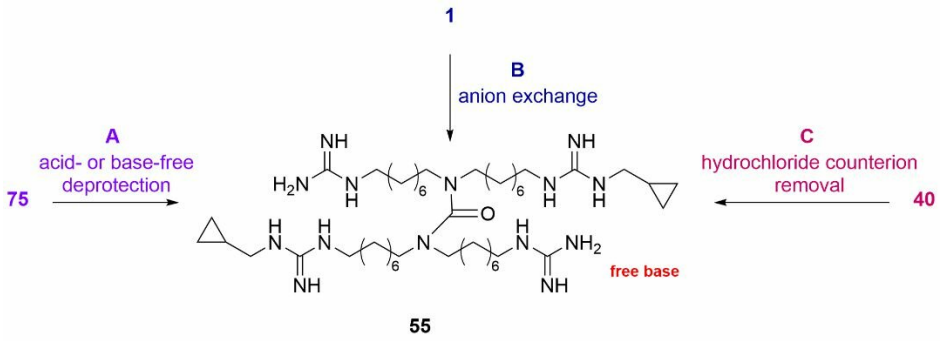

First synthetic strategy adopted relies on acid- or base-free protocols to obtain compound **55** starting from the Boc-protected derivative **75** (Scheme 10, **A**). Initially, we resorted to a classical *in batch* approach, exploiting the traditional heating. Then, MW irradiation protocols were adopted[241,242] to shorten long Boc deprotection reaction time, as MW is known to promote yield improvements, favoring reactions completion.[243] Unfortunately this approaches led mostly to different undesired byproducts, along with starting material degradation. Hence, anion exchange resins were employed to convert directly the TF-Acetate form, compound **1**, in the free-base **55** (Scheme 10, **B**). Nonetheless, this approach resulted unsuccessful and thus a different strategy was developed, relying on the conversion of the hydrochloride salt derivative **40** into the corresponding salt-free form **55** (Scheme 10, **C**), which proved to be resolutive. In Tab X are resumed all the synthetic attempts made with the purpose to achieve derivative **55**.

Table 15. Synthetic attempts to achieve derivative **55**.

Entry	Strategy Type	Starting material	Conditions	Results	Byproducts [a]
1	A, *in batch*	75	I_2, DCM , r.t. for 96 h, then reflux for 24 h.	Cleavage partially occurred.	Intermediate with two Boc-groups left.
2	A, *in batch*	75	Thermal Neat, 185 °C, 48 h.	Cleavage occurred. Not isolated.	Several unidentified byproducts along with urea degradation.
3	A, *in batch*	75	H_2O Milli-Q 1.3 µM, 100 °C, 48 h.	Cleavage occurred. Not isolated.	Several unidentified byproducts.
4	A, MW	75	MW, MeOH , 120 °C, ramp time 2.5 min, 100 W, 2 h.	Cleavage partially occurred.	**A** and **B** (R = CH_3); **C** and **D**.
5	A, MW	75	MW, TFE , 100 °C, ramp time 2.5 min, 100 W, 2 h.	Cleavage occurred. Not isolated.	**A** and **B** (R = CH_2CF_3).
6	A, MW	75	MW, THF , 100 °C, ramp time 2.5 min, 100 W, 1 h.	Cleavage occurred. Not isolated.	Several unidentified byproducts.
7	A, MW	75	MW, neat, open vessel, 40 °C, ramp time 1 min, 50 W, 1.5 h.	Cleavage partially occurred.	Several unidentified byproducts.
8	B	1	Amberlite IRA-67 (3 fold in weight), MeOH, r.t., 48 h.	^{19}F NMR confirmed the presence of TF-Acetate.	-
9	B	1	Amberlite IRA-67 (3 fold in weight), DCM, r.t., 1 week.	^{19}F NMR confirmed the presence of TF-Acetate.	-
10	B	1	Amberlyst A-21 (10 fold in weight), MeOH, r.t., 1 week.	^{19}F NMR confirmed the presence of TF-Acetate.	-
11	C	40	Na°, dry EtOH, r.t., 6 h, N_2.	Cleavage occurred. Isolated.	-

[a] Structure of byproducts **A**, **B**, **C**, and **D**. R is one between CH_3 or CH_2CF_3. The molecular structures were hypnotized based on literature and LC-MS analyses.

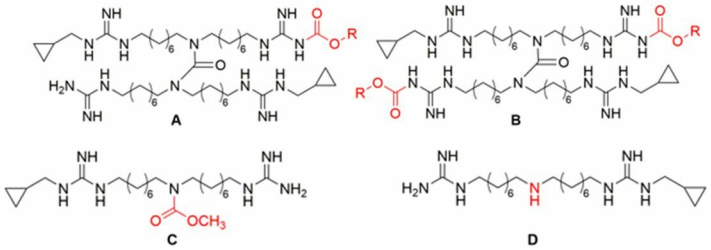

In brief, an *in batch* (Scheme 10, **A**) iodine-mediated deprotection is first performed (entry 1, Table 15): according to the reported mechanism of reaction, iodine can activate the carbonylic oxygen freeing the *N*-Boc protected guanidines after an E_1 elimination.[244] Unfortunately, the consumption of the starting material **75** is not observed, even after several days of stirring, heating at reflux and progressive addition of iodine equivalents to the reaction mixture, probably due to the complexity of Boc-protected polyguanidines cleavage. Then, a thermal-induced deprotection at 185°C is performed (entry 2, Table 15) through an open-vessel/solvent-free approach, leading to reaction completion. However, several unknown byproducts are detected during the reaction by LC-MS related to the degradation of the urea moiety. A milder approach is then explored, resorting to an high temperature water-mediated Boc cleavage (entry 3, Table 15).[245] Fully deprotection occurs but a wide variety of byproducts and unknow purities are detected.

MW protocols has been then set up to achieve **55** in an operationally simple way (Scheme 10, **A**). Indeed, the cleavage occurs under MW irradiation varying solvents, reaction time and temperature. When methanol is selected as a solvent, heating the reaction at 120°C (entry 4, Table 15),[246] no evidence of product is observed. Additioanlly, byproducts with one or two *N*-(methoxycarbonyl) guanidines are

formed (see Table 15, general structure **A** and **B**) as a result of methanol transesterification over the Boc carbamate moiety.[247] Furthermore, traces of urea degradation are detected at LC-MS analysis showing peaks corresponding to the *N*-methoxycarbamate, due to the presence of methanol (Table 15, general structure **C**),[199] and the resulting free secondary amine (Table 15, general structure D). Therefore, trifluoroethanol (TFE) is then selected as a solvent to overcome the methanol nucleophilic addition to the Boc carbonyl moiety (entry 5, Table 15),[248] benefiting also from its unique properties, like strong HBD capability, high ionizing power, and a mild acidic behavior (pK_a = 12.4).[249] Thus, TFE is supposed to facilitate the protecting group cleavage.[248,249] However, even though urea degradation is not observed, *N*- and *N,N'*-(trifluoroethoxyethylcarbonyl)guanido derivatives are generated (Table 15, general structure **A** and **B**). Despite THF (entry 6, Table 15) provides the complete cleavage of the protected polyguanidines, the presence of several byproducts limited isolation and characterization of derivative **55**. In the end, an open-vessel solvent-free approach (entry 7, Table 15) results in an incomplete Boc cleavage overall, even after several MW cycles.

Another investigated synthetic strategy, adopted to obtain free-base derivative **55**, relies on the treatment of the TF-Acetate salt **1** with exchange resins (Scheme 10, **B**). Unfortunately, exchange resins Amberlyst A-21 (OH-form)[250,251] and Amberlite IRA-67 (OH-form),[252] or their addition directly in the crude mixture after TFA Boc cleavage-mediated, proves to be an unsuccessful approach (entries 8-10, Table 15).

TF-Acetate anions strongly interacts with positively charged guanidines, thus its displacement is not trivial.[253] An efficient strategy to remove the TF-Acetate counterion could be its replacement with another counterion associated to a stronger acid like HCl (pK_a = -5.9).[254] Following this approach, the TF-Acetate counterion could be reprotonated by HCl after its displacement, facilitating its removal by simple rotary evaporation.[253] Then, the hydrochloride counterion can be then removed with a strong base. Following this strategy, derivative **40** is treated with sodium ethoxide (entry 11, Table 15) in anhydrous ethanol under inert atmosphere, due to the high hygroscopic nature of free-base guanidines.[255] The resulting NaCl has least solubility in ethanol,[256] and thus tends to precipitate. Filtering-off the so formed salt from the crude mixture leads to the obtainment of derivative **55**, as desired. Moreover, a precipitation assay with silver nitrate has been performed to confirm the total absence of hydrochloride counterion.

4.2 Biology

4.2.1 Antibacterial activity on representative Gram-positive and Gram-negative strains

The antibacterial activity of the newly synthesized compounds **41-46**, **47a-m**, **48a-b**, and **49-55** was evaluated on a panel of representative Gram-positive and Gram-negative type strains (Table 16). Colistin, vancomycin and daptomycin MICs value were added as reference. The analysis of data reported in Table

16 provided some interesting observations, adding value to the already collected SAR information about the AGUs library.

Biological results here reported for compounds **41-46**, **47a-m**, **48a-b**, and **55** highlighted further chemical features that play a key role in activity, confirming the rising interest in developing analogues of hit compound **1** as antibacterial agents. Moreover, preliminary findings acquired about derivatives **49-54**, as structural analogues of compound **20**, were fundamental to gain a better understanding of their supposed behavior towards membranes and to hypothesize a putative MoA.

Table 16. MIC [μg/mL] values on Gram-positive and Gram-negative representative strains. MICs are expressed as the average values calculated from experiments performed at least in triplicate. n.a.: not active, MIC value> 256 μg/mL; -: not determined.

	Compound	Chemical modifications	*B. subtilis* ATCC 6633	*E. faecalis* ATCC 19433	*S. pyogenes* ATCC 12344	*S. aureus* ATCC 25923 SEP	*E. coli* CCUGT	*K. pneumoniae* ATCC 13833	*A. baumanni* ATCC 17978	*P. aeruginosa* ATCC 27853
Traditional AGUs serie	**1**	-	0.5	2	1	2	2	2	8	8
	41	chain lenght	2	8	4	2	8	8	32	32
	42	chain lenght	4	4	2	4	8	16	8	16
	43	chain lenght	1	4	1	0.25	2	2	32	32
	44	chain lenght	1	8	1	0.25	4	4	64	128
	45	chain lenght	0.5	1	0.5	0.25	1	1	16	16
	46	chain lenght	4	4	4	1	8	4	64	128
	47a	*N*-substitution	1	1	1	0.5	0.5	1	8	8
	47b	*N*-substitution	0.5	0.5	0.5	0.25	0.5	1	8	8
	47c	*N*-substitution	1	2	2	1	2	2	4	8
	47d	*N*-substitution	2	4	4	2	4	4	8	16
	47e	*N*-substitution	2	2	2	1	2	2	8	16
	47f	*N*-substitution	1	1	1	0.25	1	1	4	8
	47g	*N*-substitution	2	2	2	1	2	2	4	8
	47h	*N*-substitution	0.5	1	0.5	0.5	1	2	8	16
	47i	*N*-substitution	1	2	1	1	4	4	32	64
	47l	*N*-substitution	1	2	1	0.5	2	4	16	32
	47m	*N*-substitution	16	16	16	8	32	32	64	128
	48a	Guanidine replacement	8	16	8	2	32	32	64	n.a.
	48b	Guanidine replacement	32	8	8	4	16	16	64	128
	55	free-base	8	8	4	8	16	16	32	64
Analogues of 2	**2**	-	1	1	1	0.5	2	1	16	16
	49	chain lenght	128	128	128	128	n.a.	n.a.	n.a.	n.a.
	50	*N*-substitution	64	n.a.	64	16	n.a.	n.a.	n.a.	n.a.
	51	*N*-substitution	128	128	64	32	n.a.	n.a.	n.a.	n.a.
	52	*N*-substitution	64	128	64	32	n.a.	n.a.	n.a.	n.a.
	54	*N*-substitution	64	128	64	32	n.a.	n.a.	n.a.	n.a.
	Vancomycin		0.5	1	1	0.5	-	-	-	-
	Colistin		-	-	-	-	0.5	0.5	1	0.5
	Daptomycin		1	1	0.5	0.12	-	-	-	-

Biological data collected for symmetric derivatives **41** and **42** (Table 16), characterized by alkyl spacers composed of 7 and 9 carbon atoms respectively, confirmed that eight is the optimal length of the methylene spacer, even though the potency displayed is only slightly decreased compared to **1**. Moreover, asymmetric derivatives **7-10**, endowed with different alkyl spacers, exerted interesting biological profiles. In fact, a significant reduction in activity against Gram-negative bacteria was observed for derivatives **43** and **44**. Compound **46**, bearing a cyclopropylmethyl guanidine on the 6 membered arm, showed

worsened MIC values. However, its structural isomer **45**, bearing an unsubstituted guanidine on the 6 membered arm, displayed an enhanced antibacterial profile, particularly on Gram-positive strains. These evidences state that a 6 methylenes spacer endowed with an unsubstituted guanidine is a good feature for the antibacterial activity.

Moreover, these data outlined that presumably the distance between the urea moiety and the unsubstituted guanidine might plays a crucial role in the activity. Indeed, although compounds **45** and **46** are structural isomers and their predicted physicochemical properties[257] (data not shown) are comparable, their biological profiles presented significant differences. This seems to suggest that the guanidinium moieties should be placed at a certain distance from the urea to properly reach and interact with the negatively charged phospholipids heads present in specific regions of the bilayer leaflet. In fact, the typical distribution of bacterial phospholipids in the inner and outer leaflets of the bilayer is known to affect properties like membrane potential, permeability, shape, and surface charge[258] and also the interaction with membrane-active compounds. Thus, the differences in biological activity for membrane-active compounds could be related to the natural bacterial membranes asymmetry.[259]

A further investigation on AGUs molecular scaffold was performed by exploring the *N*-substitution on the guanidino moieties. In fact, properly substituents were selected according to their contribution to the total steric hindrance, lipophilicity, and electronic distribution of the whole structure. Initially, cyclopropylmethyl group of hit compound **1** was spatially deconstructed or simplified to furnish linear and branched substituents saturated or unsaturated, affording respectively 1-propyl (**47a**), 2-propyl (**47b**), 1-butyl (**47c**), 2-methyl-1-propyl (**47d**) and but-2-en-1yl (**47e**) guanidino derivatives. These modifications are supposed to provide both a slight reduction in lipophilicity and a mild change in steric hindrance,[225] aiming at understanding how the physicochemical properties could affect the biological activity. To this concern, while **47b** showed an enhanced broad-spectrum antibacterial activity, derivatives **47a** and **47c-e** displayed a biological profile comparable to hit compound **1** (Table 16). *N*-cyclopentyl guanidines in derivative **47f** were conceived since cycloalkyl substituents are supposed to establish a larger number of hydrophobic interactions with lipophilic moieties,[225] and interestingly these features actually improved the antibacterial activity (Table 16), probably due to additional interactions with phospholipid bacterial bilayers. Geranyl chain was then selected as a representative unsaturated substituent to evaluate the impact of extended unsaturated and branched chains on AGUs potency, benefiting also from its known antimicrobial activity.[226,227,260] Thus, compound **47g** was synthesized and tested, resulting in an overall retained broad-spectrum antibacterial activity (Table 16). In the end, guanidino substituents with different degrees of polarity were explored, by preparing polar **47h** and **47i** and non-polar **47l** and **47m** representatives. Interesting considerations can be deducted by observing biological data reported in Table 16. In fact, polar substituents seemed to promote a retention of biological activity. As a proof, methoxyethyl derivative **47h**, benefiting from a big H-bonding capability, showed an improved

antibacterial profile. Also morpholinoethyl derivative **47i**, endowed with an increased number of positive charges and conceived to be more selective towards Gram-positive and Gram-negative bacteria,[81] exerted a promising activity especially against Gram-positive strains. However, no significant information could be gained from data of thiomethoxyethyl compound **47l,** since it basically retained the antibacterial profile of **1**. On the contrary, the presence of bulky and hindered substituents such as adamantaneethyl group (**47m**) was clearly not tolerated (Table 16).

Furthermore, two of the four guanidines on traditional AGUs were substituted with the uncharged azido moieties in derivatives **48a** and **48b** respectively, to evaluate also the activity of synthetic intermediates of this series, providing additional information about the role of guanidines. As expected, both of the bis-guanylated derivative **48a** and **48b** exerted only a moderate activity against Gram-positive strains due to the reduction in terms of number of charges (Table 16).

Inspired by the promising biological profile of the *arm-removed* series hit, compound **20**, a focused library was prepared by performing chemical derivatizations in terms of the spacer length and the guanidine moiety substitutions. First, the length of the linker chain was shortened from 8 to 6 methylene, providing derivative **49**, which resulted in a complete loss of biological activity (Table 16). Then, the guanidine moiety was first undressed and left unsubstituted (**50**), then methyl (**51**), ethyl (**52**), isopropyl (**53**), and crotyl (**54**) groups were selected to evaluate the impact on potency of *N*-substitutions. With some exceptions of Gram-positive strains, that resulted still susceptible to these derivatives, all compound **20** analogues (**49-54**) proved to be overall inactive towards Gram-negative strains (Table 16). These findings seemed to suggest that compound **20** might hit a specific target, besides the interaction with bacterial membranes. Hence, further studies are required to elucidate the mode of action of compound **20** to proceed with a rational design of novel derivatives.

The antibacterial activity was also evaluated for derivatives **40** and **55**, to understand the counterion effect on biological activity. In fact, AGUs were all tested as TF-Acetate form and thus the hydrochloride derivative **40** and the free-base **55** were conceived with an eye towards a potential clinical use and for *in vivo* experiments.

In fact, *in vivo* TFA is reported to trifluoroacetylate proteins, causing hepatitis, while TF-Acetate anions can interfere or disrupt membrane function, enzymatic catalysis, secondary structures of proteins, and protein stability[261] and lead to immune response-inductions.[262–264] Also, compounds as TF-Acetate salts were reported to exert a low pharmacological efficacy compared to the same compounds with other counterions.[265] Hence, each case should be considered individually and more than one counterion should be investigated to achieve the optimal biological profile.[266]

MIC values for **40** and **55** were determined first in μg/mL and then data were converted in mM to better compare their biological profiles with that of compound **1**, excluding by this way the influence of molecular weight, as reported in Table 17.

The Clinical & Laboratory Standards Institute (CLSI)[267] and the European Committee on Antimicrobial Susceptibility Testing (EUCAST)[268] do not provide guidelines on the unit system for reporting MIC values. Thus, both weight/volume (μg/mL) and molarity (mol/L) systems were employed. In general, in clinical use, a relevant parameter to understand the potency of an antibiotic is the ratio between MIC value and blood concentration, that is conventionally expressed as weight/volume. However, MICs are usually expressed as weight/volume for unknown substances, such as extracts or mixtures, while when the test substance is a fully characterized molecule, molarity is preferred. Mechanistically, the biological activity is due to the number of the compound moles and not to the weight of the test substance. Thus, to compare the biological activity of compounds with different molecular weights, MICs are preferred to be indicated through the molar system. The hydrochloride salt compound **40** and the free-base **55** weight approximately 24 and 35% less than the corresponding TF-Acetate form **1**, resulting in a no significant difference. To this concern, observing biological data reported in Table 17 expressed in μg/mL of compound **40** are in agreement with those of hit compound **1**, while a slight but not significant difference can be outlined when data are converted in molarity, resulting overall in a lower potency for compound **40**. Concerning derivative **55**, a lower potency could be observed particularly on Gram-negative strains, considering data as both weight/volume or molarity. However, compound **55** still retained overall a good antibacterial profile on Gram-positive strains, since the detected MIC values differ from that of compound **1** by only 2 fold dilutions (Table 17), which could not be considered as a significant loss of activity.

Table 17. MICs comparation between compounds **1**, **40**, and **55**. MICs were determined in μg/mL and are expressed as the average values calculated from experiments performed at least in triplicate. Colistin (COL), Vancomycin (VAN), and Daptomycin (DAP) antibiotics were used as control in these assays. -: not determined.

Bacterial strains	MICs Evaluation [μg/mL]						MICs Conversion [μM] [a]		
	COL	VAN	DAPT	1	40	55	1	40	55
B. subtilis ATCC 6633	-	0.5	1	2	1	8	1.54	1.18	9.46
E. faecalis ATCC 19433	-	1	1	2	2	8	1.54	2.02	9.46
S. aureus ATCC 25923	-	0.5	0.125	2	2	8	1.54	2.02	9.46
S. epidermidis ATCC 14990	-	-	-	1	1	4	0.77	1.01	4.73
S. pyogenes ATCC 12344	-	0.5	0.125	1	0.5	4	0.77	0.50	4.73
E. coli CCUGT	0.5	-	-	2	2	16	1.54	2.02	18.92
K. pneumoniae ATCC 13833	0.5	-	-	2	2	16	1.54	2.02	18.92
A. baumannii ATCC 17978	1	-	-	8	8	32	6.15	8.07	37.85
P. aeruginosa ATCC 27853	0.5	-	-	8	8	64	6.15	8.07	75.71

[a] MICs conversion in molarity (mM) was calculated through the formula: $\frac{MIC(\mu g/mL)}{m.w.} * 1000$, considering 1301.42, 991.16 and 845.33 g/mol as the molecular weight for **1**, **40**, and **55** respectively.

4.2.2 Antibacterial activity on drug-resistant clinical isolates

Synthesizing in larger scale derivatives **20** and **39** proved to be crucial for further investigations about their SARs and to get a reliable insight about their MoA.

Thus, derivatives **20** and **39** were selected to further evaluate their antibacterial properties on recent antibiotic-resistant clinical isolates with a pan drug-resistant drug phenotype. Remarkably, all test compounds retain much of their activity on specific pathogens regardless of the resistance phenotype, as displayed by MIC and MBC values reported in Table 18.

Table 18. MICs of Selected Compounds on Gram-Negative Antibiotic-Resistant Clinical Isolates. MIC values (μg/mL) are expressed as median values calculated from experiments performed at least in triplicate.

Cpd	*E. cloacae* VA-417/02	*K. Pneumoniae* SI-081Rb	*A. baumannii* AC-54/97
1	1	2	2
20	4	4	16
39	2	2	8

4.2.3 MBC of selected compounds

Table 19. MBC values of test compounds. MBCs are expressed as the average values calculated from experiments performed at least in triplicate.

	Compound	Chemical modifications	*B. subtilis* ATCC 6633	*E. faecalis* ATCC 19433	*S. pyogenes* ATCC 12344	*S. aureus* ATCC 25923 SEP	*E. coli* CCUGT	*K. pneumoniae* ATCC 13833	*A. baumannii* ATCC 17978	*P. aeruginosa* ATCC 27853
Traditional AGUs serie	**40**	hydrochloride salt of **1**	2	2	1	4	2	4	8	8
	41	chain lenght	2	8	4	2	8	8	32	32
	42	chain lenght	4	8	4	4	8	16	8	16
	43	chain lenght	4	16	2	1	16	4	64	64
	44	chain lenght	1	16	0.5	1	4	16	64	128
	45	chain lenght	1	4	0.5	1	4	4	64	16
	46	chain lenght	4	16	1	4	8	16	64	128
	47a	*N*-substitution	1	4	0.5	8	0.5	1	16	8
	47b	*N*-substitution	0.5	4	0.25	1	0.5	2	8	16
	47c	*N*-substitution	1	4	1	2	2	2	4	8
	47d	*N*-substitution	2	8	2	4	4	4	8	16
	47e	*N*-substitution	2	4	1	2	2	2	8	16
	47f	*N*-substitution	1	4	1	1	1	1	4	8
	47g	*N*-substitution	2	2	1	4	4	2	4	16
	47h	*N*-substitution	1	2	1	1	2	2	8	32
	47i	*N*-substitution	2	4	1	2	4	8	32	128
	47l	*N*-substitution	2	8	2	2	4	2	16	128
	47m	*N*-substitution	32	32	32	32	64	64	128	256
	48a	Guanidine replacement	8	16	8	8	32	32	64	n.a.
	48b	Guanidine replacement	32	32	8	16	64	32	64	128
	55	free-base	8	8	4	8	16	16	32	> 64
Analogues of 2	**49**	chain lenght	256	256	256	256	n.a.	n.a.	n.a.	n.a.
	50	*N*-substitution	128	n.a.	16	16	256	n.a.	n.a.	n.a.
	51	*N*-substitution	128	256	32	64	128	128	n.a.	n.a.
	52	*N*-substitution	128	256	64	128	n.a.	n.a.	n.a.	n.a.
	54	*N*-substitution	64	128	32	64	128	128	n.a.	n.a.

The biological profile of the synthesized library was further investigated through MBC assay to distinguish whether their MoA is bactericidal or bacteriostatic. In Table 19 are reported the collected data.

According to the CLSI standard,[267] the MBC/MIC ratio is essential to understand how the antibiotic acts. In particular, when the ratio is equal or minor than 2, it is considered indicative of bactericidal action, whereas antibiotics with a ratio higher than 8 are bacteriostatic. The found MBC values for compounds **40-46**, **47a-m**, **48a-b**, and **49-55** resulted most of the cases identical or comparable to those of the MICs, indicating a strong bactericidal activity, except for compounds **49-54**. The MBC values for compounds **1**, **20**, and **39** were already reported.[185,193]

4.2.4 Hemolytic activity

As part of the investigation conducted on AGUs properties, activity, and MoA the hemolytic activities of selected compounds were evaluated. Compound **1**, **20** and **39**, being synthesized in larger scale, were selected for the study, aiming also at gaining a better insight on their selectivity index.

Hemolytic activity was tested on human erythrocytes from healthy 0 Rh-negative donors. Briefly, a suspension of 5% erythrocytes in PBS was incubated in presence of increasing concentrations (from 1 to 64 μg/mL) of DMSO solution of test compound (**1**, **20**, or **39**) to match the active concentration determined in antibacterial susceptibility tests. The highest concentration of DMSO (0.4% v/v) was also tested to exclude any solvent-induced hemolytic activity. Assays were conducted in triplicate. Hemolysis was expressed in percentage, relative to 0% of lysis of erythrocytes in the negative control (blank with PBS) and 100% of lysis of erythrocytes in the presence of 0.2% Triton X-100 (total lysis), according to the formula:

$$Hemolysis\ (\%) = \frac{A_{\text{sample}} - A_{\text{blank}}}{A_{\text{total lysis}} - A_{\text{blank}}} \times 100$$

As reported in Table 20, no hemolysis was observed in the negative control. Additionally, all test compounds showed any or weak, dose-dependent, hemolytic activities (<8.1% at 64 μg/mL). Remarkably, no hemolysis was observed for compound **20**. This results encouraged the interest in deeply investigating its MoA. For this reason, giving also its promising antibacterial profile, further studies will be conducted also on compound **20** analogues, derivatives **49-54,** to better understand if the loss of activity is concomitant with an enhancement in compounds safety profiles. In the end also the most promising derivatives presented in this work, besides the previously mentioned, will be evaluated for their hemolytic tendency as a preliminary method to asses cytotoxicity and their selectivity towards bacterial membranes.

Table 20. Hemolytic activity of selected AGUs.

Cpd	Hemolysis (%) at cpd concentration [μg/mL]							
	0[a]	1	2	4	8	16	32	64
1	0.0 ± 0.0	0.0 ± 0.0	0.2 ± 0.1	0.4 ± 0.2	0.8 ± 0.3	1.2 ± 0.5	2.0 ± 0.8	3.4 ± 0.5
20	0.0 ± 0.0	0.0 ± 0.0	0.0 ± 0.0	0.0 ± 0.0	0.0 ± 0.0	0.0 ± 0.0	0.0 ± 0.0	0.0 ± 0.0
39	0.0 ± 0.0	0.0 ± 0.0	0.0 ± 0.0	0.0 ± 0.0	0.0 ± 0.0	1.1 ± 0.1	3.3 ± 0.2	8.1 ± 0.6

[a] 0.4 % (v/v) DMSO, equivalent to the maximum test concentration with 64 μg/mL of tested compounds.

4.3 MoA investigations

4.3.1 LUVs interactions

A preliminary understanding of compound-membrane interactions could be achieved *via* bilayer models. In fact, although they could not be considered conclusive studies, model membranes-based experiments prove to be valuable and reliable studies, benefiting from controlled and reproducible experimental conditions.[125] Hence, interactions with phospholipids could be monitored in a fast and inexpensive manner,[122,123,269] through a simplified bilayer model in which non-lipid components are excluded to avoid lipid-proteins interferences.[270]

Due to their similar size to living prokaryotic cells,[271] LUVs could be used to mimic several cell types bilayers,[272,273] benefiting from easy preparation and a wide variety of phospholipid mixtures that could be employed to model particular membranes.

Anionic phospholipids are predominant in Gram-positive strains while, on the contrary, the inner membrane of Gram-negative ones is prevalently composed by different ratios of zwitterionic phospholipids.[122,274,275] Particularly, LUVs endowed with 1-Palmitoyl-2-Oleoyl-PhosphatidylGlycerol (POPG) are widely reported as a model to evaluate AMPs ability to disrupt or perturb Gram-positive membranes.[276]

To get a preliminary understanding of the AGUs ability to interact with membranes, UV spectra of selected compounds were recorded in presence and in absence of a LUVs suspension. In fact, it is common knowledge that UV-Vis spectra of a molecule could be affected by either its chemical features or the environmental polarity.[277] The latter depends on the kind of interaction displayed with the phospholipid vesicles.

AGUs **1**, **20** and **39** were selected for their promising biological profile, to elucidate how the structural modification is reflected in the interaction with the phospholipid bilayers. Hence, the maximum absorption wavelengths (λ_{max}) of each compound (125 μM in 4-(2-hydroxyethyl)-1-piperazineethanesulfonic acid (HEPES)-buffered solution (25 mM, 140 mM NaCl, pH 7.4)) were detected by scanning the samples from 200 to 900 nm. Then, test compound solutions were added to a 1 mM suspension of POPG-LUVs and the UV-Vis spectra were recorded at time 0 (t_0) and after 1 hour.[278]

Test compounds showed all three the same trend, displaying at t_0 a bathochromic (red) shift along with a hyperchromic effect. Moreover, the signals intensities increased after 1 hour from the addition. In Figure 24 is reported the UV-Vis spectra recorded for compound **1**, as representative for all test compounds. Moreover, in Table 20 are resumed the λ_{max} and the absorbance band shift ($\Delta\lambda_{max}$) found in POPG-LUVs experiments with selected AGUs.

Figure 24. UV-Vis spectra of compound **1** in absence or in presence of a POPG-LUVs suspension.

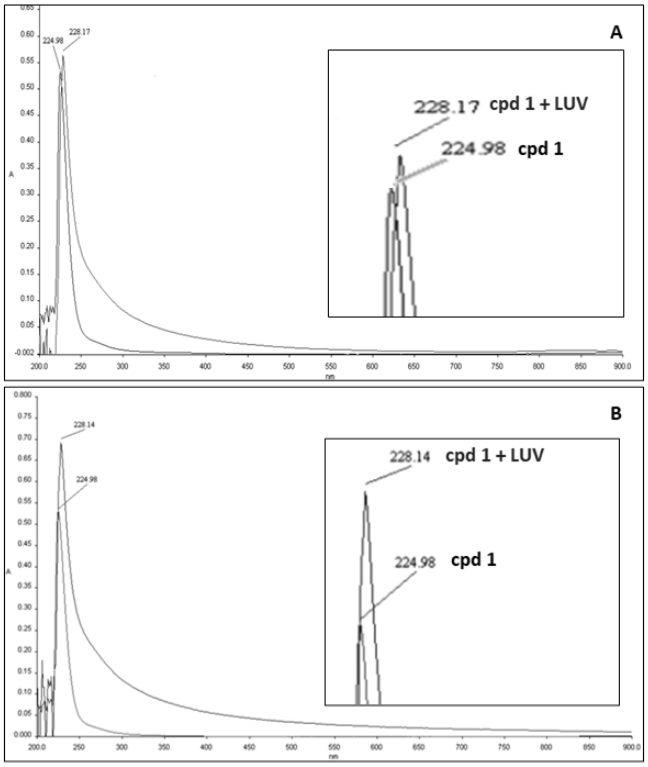

Table 21. Maximum Absorption and absorbance band shift found in POPG-LUVs experiments with selected AGUs. [a] The absorbance band shifts were calculated using the formula $\Delta\lambda_{max} = \lambda_{max}$(cpd+LUV)- λ_{max}(cpd)

Cpd	Maximum Absorption λ_{max} [nm]	Absorbance band shift $\Delta\lambda_{max}$ [a] [nm]
1	225.0	3.2
20	224.6	0.9
39	225.5	2.5

The UV-Vis spectra of compound **1** alone and in presence of a POPG-LUVs suspension showed λ_{max} values of 225.0 and 228.2 nm, respectively, and a maximum absorption band shifts ($\Delta\lambda_{max}$) of 3.2 nm. A moderate-high red shift was also observed for compound **39** (Table 20), bearing only one

cyclopropylmethyl-substituted guanidine. On the contrary, compound **20**, surrounded by only one guanidino function compared to **1**, displayed the smaller shift in absorbance band (Table 20). Moreover, a hyperchromic effect was also detected and found higher after 1 hour from the compound addition to POPG-LUVs, as shown in Figure 24 for compound **1**. No detailed clarifications were previously reported in literature concerning this behavior, therefore could be explained as a stable and strong interaction in the time between guanidine moieties and phospholipids.

These results collected suggested overall the inability of test compounds to entirely insert into the bilayer[278] or to partition into a more hydrophilic microenvironment,[279] which generally could occur due to compounds internalization into the LUVs aqueous core or to the establishment of salt-bridges-like interaction between guanidines and anionic phospholipids.[170]

4.3.2 Traditional and modified PAMPA

Further experiments were required to confirm that the alterations of the UV-Vis absorbance bands, provided by the AGUs tested, could be the result of effective electrostatic interactions with the phospholipids, stating the affinity for the bilayers. Thus, traditional and modified PAMPA were performed also aiming at validate the POPG-LUVs experimental conditions and the reliability of this fast and inexpensive analytical method.

Briefly, standard PAMPA protocols involved the use of phosphatidylcholine (PC)-endowed phospholipids to generate a protein-free bilayer miming mammalian membranes.[280,281] However, any research work explored before the application of bacterial bilayers in PAMPA experiments, even though literature reports bilayers composed of pure POPG and of 1-palmitoyl-2-cafoleoyl-phosphatidylethanolamine (POPE) and POPG, in ratio 6:4, as mimics of Gram-positive and Gram-negative bacterial membranes respectively.[276,282,283] Hence, the permeability of each test compound was first assessed towards the mammalian and bacterial membrane models. Then, the AGUs capability to alter the membrane integrity and functionality was investigated by using CAF and caffeine as small-sized (323 and 194 Da respectively) and scarce permeable probes.[283,284] Test compounds, caffeine and CAF were incubated in the donor wells alone or as a mixture of each compound/each probe in a 1:1 molar ratio. Donor and acceptor wells were then analyzed by UV-Vis spectroscopy, after 5 hours of room temperature incubation, thanks to a plate reader, benefiting from its versatility and high-throughput capability.[285,286] AGUs **1**, and **39** were scanned at their λ_{max} of 225 nm, compound **20** at 224 nm, whereas CAF and caffeine at 280 and 275 nm, respectively. The protocol was properly optimized to reduce the background noise and the buffer solution interferences during the UV measurements. Apparent permeability (P_{app}) and Membrane Retention (MR) values are reported in Table 21.

Table 22. P_{app} from traditional and modified PAMPA experiments. Values are reported as the mean of at least two experiments. [a] P_{app} values and MR% are referred to the probe. [b] Data already reported.[185]

Cpd	P_{app} [10^{-6} cm/sec] (MR%)		
	PC-phospholipids	pure POPG	POPE/POPG 6:4
1	1.60[b]	1.88 (46.1)	0.74 (42.4)
20	3.17 (7.7)	6.10 (16.0)	3.48 (3.2)
39	1.85 (0)	0.26 (56.0)	0.30 (40.8)
Chloramphenicol	0.54	0.06	1.12
Chloramphenicol[a] + 1	6.12	2.18	1.39
Chloramphenicol[a] + 20	0.04	0.08	1.67
Chloramphenicol[a] + 39	4.67	3.78	6.98
Caffeine	1.84 (3.2)	1.95 (4.5)	1.98 (3.3)
Caffeine[a] + 1	3.54 (12.6)	2.49 (13.5)	3.03 (12.6)
Caffeine[a] + 20	2.04 (12.8)	2.09 (13.4)	2.10 (17.5)
Caffeine[a] + 39	12.03 (8.1)	6.13 (14.6)	4.28 (19.0)

As expected, test compounds resulted to be low permeable in all the bilayers. Furthermore, derivatives **1**, and **39** were strongly retained by bacterial phospholipids, with > 40% MR. These results were perfectly in agreement with LUVs experiments previously performed, indicating a strong affinity for the bilayers. P_{app} values of CAF and caffeine were also determined to confirm their scarce permeability profile on bacterial bilayers. Permeability of CAF was found higher in PC- and POPG-bilayers in presence of compounds **1**, and **39**, pointing out that perturbation of these membranes actually occurs. Whereas the same permeability was found in POPE/POPG model when bilayers are exposed to **1**, while resulted highly increased with derivative **39**. However, a selectivity towards phospholipids could be noticed: P_{app} values of CAF increased up to sixteenfold in PC bilayers and sixtyfold in the POPG one. Moreover, compound **39** displayed a good enhancement of probe permeability on POPE/POPG bilayers, whereas compound **1** showed no significant differences (Table 21).

On the contrary, compound **20** exerted a different trend compared to **1** and **39**, being apparently not able in increasing probes permeability, as shown by data collected and reported in Table 21. These evidence, along with its low retention and its not-significant red shift in LUVs experiments, outlined a less effective membrane-active agent profile. As further proof, trypan blue, a non-permeable dye,[287] was added to the bilayer microfilters at the end of all the PAMPA experiments to ensure the bilayer macroscopic integrity. On the other hand, enhancement of probe permeabilization was also observed when caffeine was co-incubates with test compounds. While AGUs **1** and **20** do not affect significantly the caffeine P_{app}, compound **39** induced a relevant permeabilization of caffeine in PC bilayers, suggesting a narrower selectivity index compared to **1** and **20**. Also caffeine MR was monitored and evaluated during the experiments, given its known propensity to be retained by membranes.[288] Actually, an increase ranging from 4% (intrinsic MR) up to higher values was observed in presence of all the tested compounds. This could be explained by a combo of interactions occurring: those among phospholipids, AGUs, and

caffeine (salt-bridges between guanidinium cations and phosphates of phospholipids),[182] and the cation-π interactions established by the guanidinium and the caffeine aromatic ring.[289,290] Hence, since AGUs are presumed to be close to phospholipid heads or to fit into the membrane, guanidino derivatives could create an additional hindrance for caffeine permeabilization, increasing its retention.
However, at the end of the experiments, Trypan Blue was added, even in this case, on the top of bilayers and no characteristic absorbance at 590 nm was detected in the acceptor wells, confirming a non-macroscopic membranes alterations.

4.3.3 In silico studies

In order to rationalize the results obtained for compounds **1**, **20**, and **39,** with LUVs and PAMPA experiments, computational studies, particularly MD, were involved to further investigate MoA of AGUs. Two simulated membranes reproducing the bilayers used in the PAMPA were generated using the CHARMM-GUI Membrane Builder tool.[291] The two different systems were solvated by a layer of explicit water molecules above both membrane leaflets. Test compounds **1**, **20**, and **39** were complexed with both solvated lipid systems and subjected to a 600 ns MD simulation protocol to evaluate the interactions between ligands and phospholipid membranes.
First MD studies were conducted on a POPG simulated membrane, in the attempt of mimicking the Gram-positive bacterial bilayers. Thereby, compound **1** showed a marked propensity for binding to anionic POPG phospholipids. In fact, during the MD simulation, **1** rapidly generates HBs and salt-bridge interactions with the polar phospholipid heads. Indeed, after 80 ns, the compound results fully bounded to the membrane and also partially embedded within one of the two leaflets in a sort of *carpet-like* behavior. In this model compound **1** guanidine moieties lay around the plane defined by the phospholipid heads while the central urea, being a more lipophilic moiety, significantly protrudes toward the center of the bilayer (Figure 25A). This model of interaction is averagely preserved for the rest of the simulation. Although the central portion of the compound oscillates up and down within the membrane leaflet during the MD, it predominantly resides below the level of the lipids phosphate groups. This evidence could be demonstrated by the distribution of the ligand electron density during the simulation, with respect to the bilayer center. In fact, as depicted in Figure 25C, the electron density of compound **1** shows a peak around 15.0 Å from the bilayer center, which is below the density peak related to the lipids phosphate groups, corresponding to about 19.5 Å (Figure 26). Moreover, the analysis of the ligand-phospholipid HBs revealed that compound **1** generates strong and long-lasting interactions with the lipid heads. In fact, despite the fluidity of the membrane system and the mobility of the phospholipids around **1**, being the system a mono-lipid simulated membrane, the compound forms 7 HB interactions with 5 different lipid molecules. These directional interactions are averagely preserved for more than 200 ns, suggesting that the compound can establish strong interactions with the phospholipid bilayers, being retained within it.

Similar results were obtained for compound **39** in terms of both internalization and dispositions within the membrane, as well as interactions with the phospholipid heads. Moreover, the evaluated electron density of the **39** is comparable to that of **1**, with a peak around 15.7 Å (Figure 27).

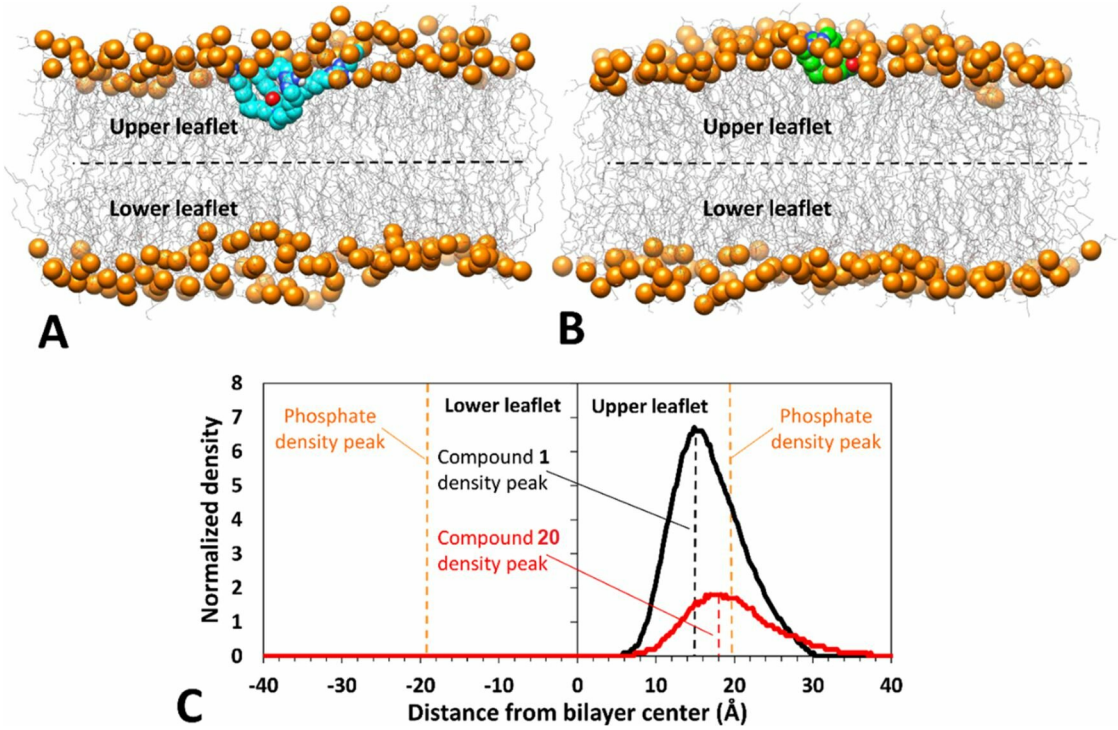

Figure 25. Representative snapshots extracted after 300 ns from the MD simulation of the pure POPG membrane in presence of selected compounds. Compounds **1** (A) and (B) **20** are shown as cyan and green spheres, respectively, while the phospholipids are represented as gray wires, and their phosphorous atoms are highlighted as orange spheres. C) Electron density profile of compounds **1** and **20** with the corresponding peaks highlighted by dashed lines (black and red, respectively). Whereas, the density peaks of the lipid phosphate groups are indicated with orange dashed lines.

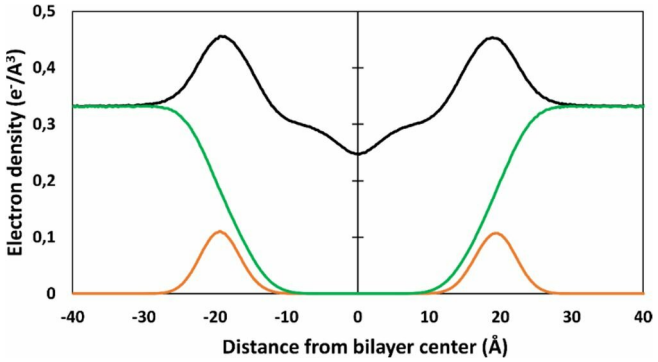

Figure 26. Electron density profiles for pure POPG systems. In green the density profiles related to the solvent molecules, in orange to the lipid phosphate groups, and in black to the whole system.

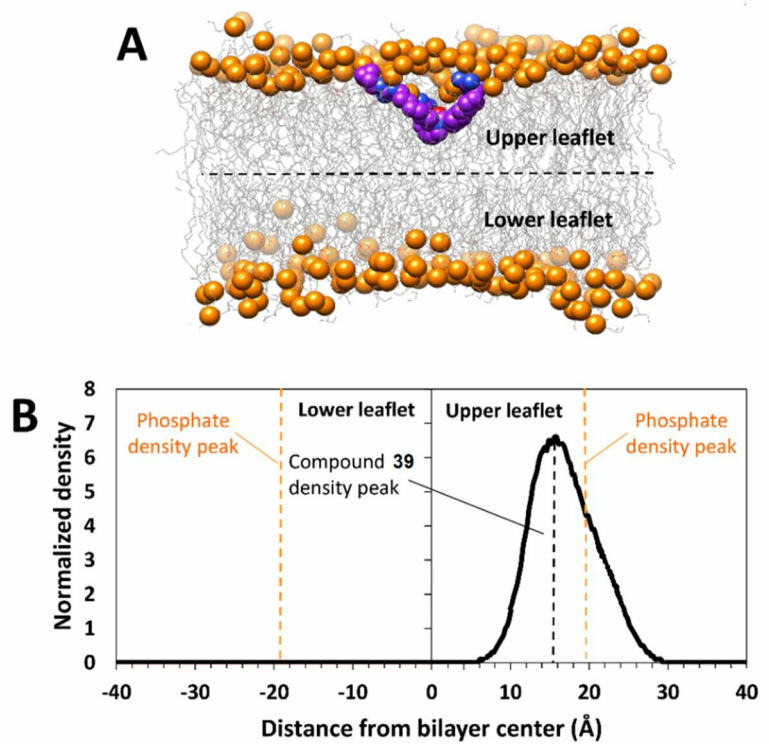

Figure 27. Representative snapshots extracted after 300 ns from the MD simulation of the pure POPG membrane in presence of compounds **39** (A) and its electron density profile (B).
Compound **39** is shown as purple spheres, while phospholipids are represented as gray wires, and their phosphorous atoms are highlighted as orange spheres. Electron density profile of compounds **39** with the corresponding peaks highlighted by black dashed lines.The density peaks of the lipid phosphate groups are indicated with orange dashed lines.

On the contrary, compound **20** shows overall less stable and less strong interactions with the POPG bilayer. In fact, compound **20** tends to fluctuates within the solvent layer in the proximity of the membrane for about 40 ns before being able to establish interactions with the negatively charged phospholipid heads and anchor to the membrane leaflet. Moreover, **20** stabilizes its binding in about 200 ns, assuming the *carpet-like* interaction model previously described for compound **1** and **39**. Compared to the other teste compounds, **20** maintains a shallower disposition within the membrane leaflet, (Figure 25B), as outlined by its density peak around 18.0 Å from the bilayer center (Figure 25C). In fact, the density peak is significantly closer to that of the phosphate groups compared to **1** and **39**. In the end, HBs established by **20** are preserved for about 50 ns of MD (less than 10% of the whole simulation) and are displayed with a single phospholipid unit. Hence, considering these evidences, **20** presumably exerts less affinity for the POPG lipid bilayer compared to other tested AGUs. Thus **20** is less likely to establish strong interactions with the phospholipid heads, and to be stably retained within the membrane.
Results reported for all test compounds revealed to be in agreement with the experimental data collected with LUVs and traditional and/or modified PAMPA, proving the reliability of these selected analytical tools.
With respect to the Gram-negative model membrane, a phospholipid bilayer composed by mixed POPE/POPG (6:4 molar ratio) was simulated.

Compound **1** shows results similar to those observed with the Gram-positive model membrane. However, the selected AGU employs 1.5 fold more time before embedding within the membrane leaflet and assuming the *carpet-like* interaction model, which is then preserved for the rest of the simulation (Figure 28A). Compound **1** forms 9 HBs interactions, established for more than 200 ns of simulation, with three different phospholipids units, two POPE and one POPG, pointing out how the AGU can stably interact with both lipids. Moreover during the MD, the core portion of **1** is proves to be predominantly located below the polar layer of the phospholipid heads, showing an electron density peak around 18.0 Å from the bilayer center that is again lower than the 21.0 Å lipids phosphate groups peak (Figure 28C), (Figure 29). Compound **39** shows a trend comparable to that observed for **1**. In fact, it can be internalized within the membrane after around 150 ns of MD, maintaining its core below the level of the phosphate groups, as showed by their density peaks around 18.5 Å (Figure 30) In this case, **39** shows a broad peak (in the range between 15 to 20 Å) since part of the molecule stays deeper within the membrane and the remaining part of its molecular scaffold lays closer to the leaflet surface. However, AGU **39** well interact with both types of phospholipids, POPE and POPG, and stably maintains its disposition within the membrane.

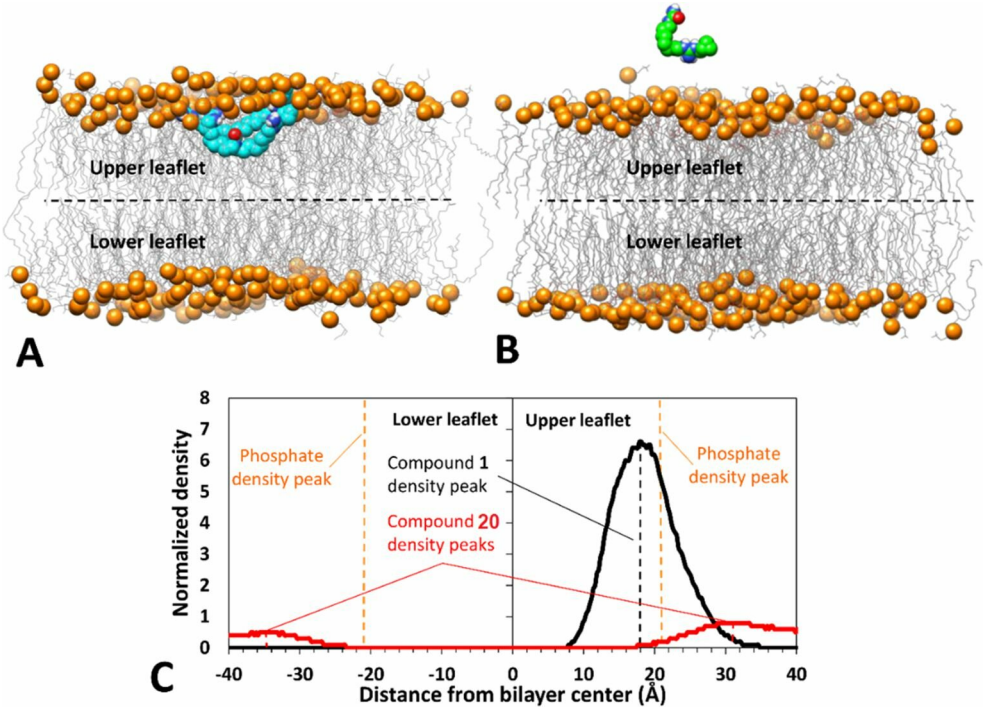

Figure 28. Representative snapshots extracted after 300 ns from the MD simulation of the mixed POPE/POPG membrane in presence of AGUs selected compounds. Compound **1** (A) and **20** (B) are shown as cyan and green spheres, respectively, while the phospholipids are represented as gray wires, and their phosphorous atoms are highlighted as orange spheres. C) Electron density profile of compounds **1** and **20** with the corresponding peaks highlighted by dashed lines (black and red, respectively). The density peaks of the lipid phosphate groups are indicated with orange dashed lines.

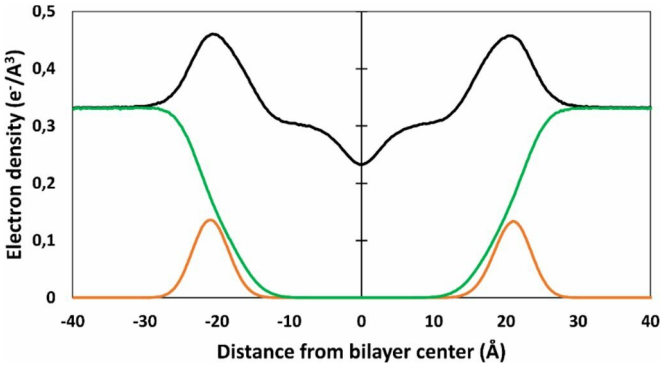

Figure 29. Electron density profiles obtained for the mixed POPE/POPG membrane systems. The density profiles related to the solvent molecules, the lipid phosphate groups, and the whole system are shown in green, orange, and black, respectively.

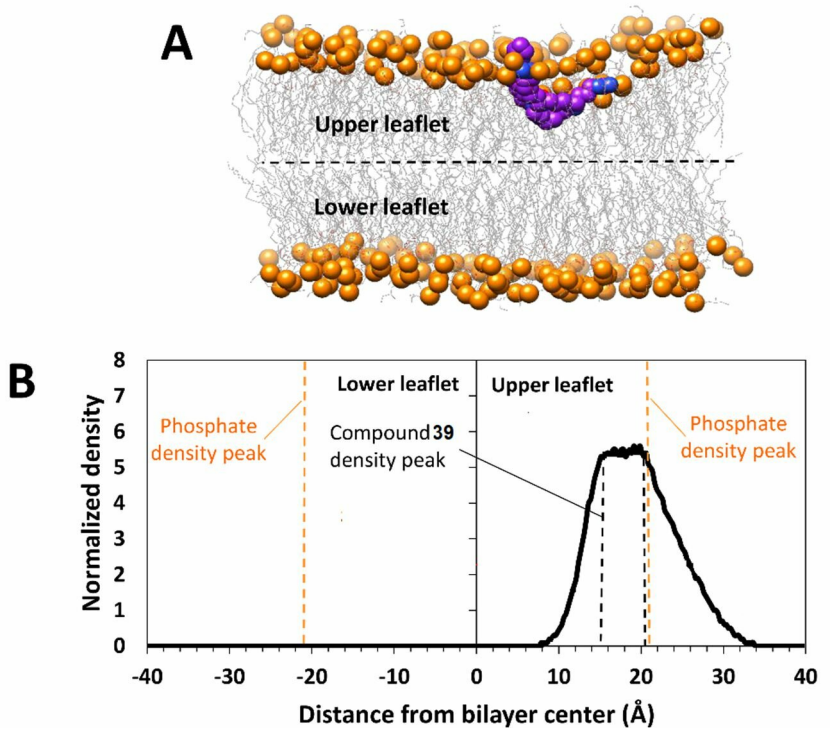

Figure 30. Representative snapshots extracted after 300 ns from the MD simulation of the mixed POPE/POPG membrane in presence of compounds **39** (A) and its electron density profiles (B).
Compound is shown as purple spheres, while the phospholipids are represented as gray wires, and their phosphorous atoms are highlighted as orange spheres. Electron density profile of compounds **39** with the corresponding peaks is highlighted by black dashed lines. The density peaks of the lipid phosphate groups are indicated with orange dashed lines.

However, compound **20** proved to be almost unable to interact with the mixed lipid bilayer, not even at the level of the lipid heads layer, as displayed in POPG simulated membranes. In fact, the test compound stays within the bulk solvent (Figure 28B) at an average distance of about 30-35 Å from the bilayer center. Therebye, it remains at least 10 Å away from the lipids phosphate groups, as outlined by its electron density profile (Figure 28C). Moreover, Figure 28C shows the presence of two different density peaks at opposite sides of the membrane bilayer. These evidence suggests that the AGU occasionally moves far away from the membrane to cross the boundaries of the periodic system box and appear at the other side

of the bilayer, as it is generally displayed by water molecules. Among the total 600 ns of MD simulation, AGU **20** establishes stable interactions with the phospholipid heads layer, for only about 40 ns (about 7% of the whole MD) after which the compound moves back away into the bulk solvent. These results are consistent with the experimental value of membrane retention in the mixed POPE/POPG membrane determined for compound **20**.

Overall, MD results provided a structure-based rationale for the interpretation of experimental assays.

4.3.4 Cell-based permeabilization of bacterial membranes

Cell-based experiments were needed to investigate the complex phenomena occurring at the membrane level. Moreover, they proved to be crucial to assess the reliability of the preliminary experimental data collected with LUVs, PAMPA and MD protocols.

Thereby, cells of three different Gram-positive reference strains, namely *B. subtilis* ATCC 6633, *E. faecalis* ATCC 29212, and *S. aureus* ATCC 25923, and three representatives Gram-negative ones, namely *A. baumannii* ATCC 17978, *E. coli* MG1655, and *P. aeruginosa* ATCC 27853, were exposed to selected AGUs **1**, **20** and **39**. The membrane integrity was monitored during time. Briefly, bacterial suspensions in phosphate-buffered saline (PBS) were individually exposed to test compounds, and the uptake of SYTO 9 and PI fluorophores was monitored. The assay is based on the assumption that the SYTO 9 green-fluorescent dye enters all bacterial cells, whereas PI enters only cells presenting with a damaged cytoplasmic membrane, resulting in red fluorescence emission upon DNA binding. Thus, the ratio between green- and red-fluorescent cells indicates the extension of membrane damages on the bacterial population.[217,292] Figure 31 shows that all the tested compounds were capable to alter membrane permeability, although the extent of membrane damage (PI uptake) varied depending on the bacterial strain, AGU, and exposure time. In fact, a strain-dependent trend was highlighted in the initial number of PI-permeable cells, being lowest for *A. baumannii* ATCC 17978 and highest for *B. subtilis* ATCC 6633 (Figure 31). Membrane perturbation observed was particularly rapid in *A. baumannii*, *B. subtilis*, and *S. aureus,* as outlined by the low green/red fluorescence observed 15 min after exposure to AGUs (Figure 31). Notably, compound **39** showed the highest activity on both Gram-positive and Gram-negative species, whereas the activity of **1** and **20** proved to be susceptible upon tested bacterial species. However, compound **20** showed the narrower range of activity, among all test compounds, provoking membrane disruption only in *A. baumannii*, *B. subtilis*, and *E. faecalis*. On the contrary, AGUs **1** and **39** compromised membrane integrity in all tested strains, although with slower kinetics in *E. coli* and *P. aeruginosa* (Figure 31).

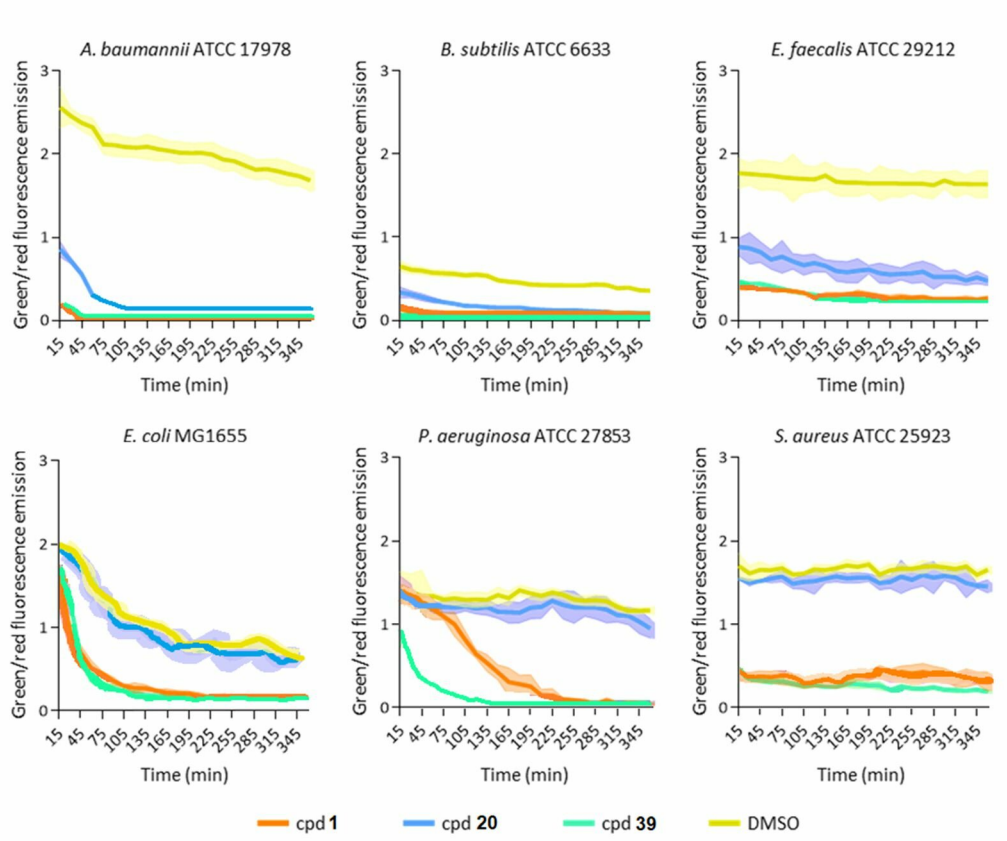

Figure 31. Time-course analysis of bacterial membrane permeabilization by selected AGUs. Bacterial cells from 16-h cultures in Luria-Bertani broth (LB) were washed with PBS and suspended at OD_{600}= 0.1 in PBS supplemented with SYTO 9 (6 μM), PI (30 μM), and tested compound (16 μg/mL in DMSO, 16 mg/mL stock concentration). An equal concentration of DMSO (0.1% v/v) was used in the untreated control (yellow plot). Bacterial suspensions were dispensed in 96-well microtiter plates, and the fluorescence emission at 498 and 617 nm wavelength (emission λ_{max} of SYTO 9 and PI, respectively) was recorded every 15 min for 6 h at 37 °C in a Spark 10M (Tecan) microplate reader. The ratio between SYTO 9 (green) and PI (red) fluorescence emissions denotes membrane integrity. Data are the mean of three independent experiments ± standard deviation, indicated as shaded area.

Moreover, loss of membrane integrity was confirmed by CLSM imaging of bacterial cells, prior to SYTO 9 and PI staining. Indeed, CLSM observations were in agreement with fluorometry results obtained with live/death staining, both showing an increase in the number of PI-positive cells, compared to the total number of SYTO 9-positive cells, for all test compounds (Figure 32-34).

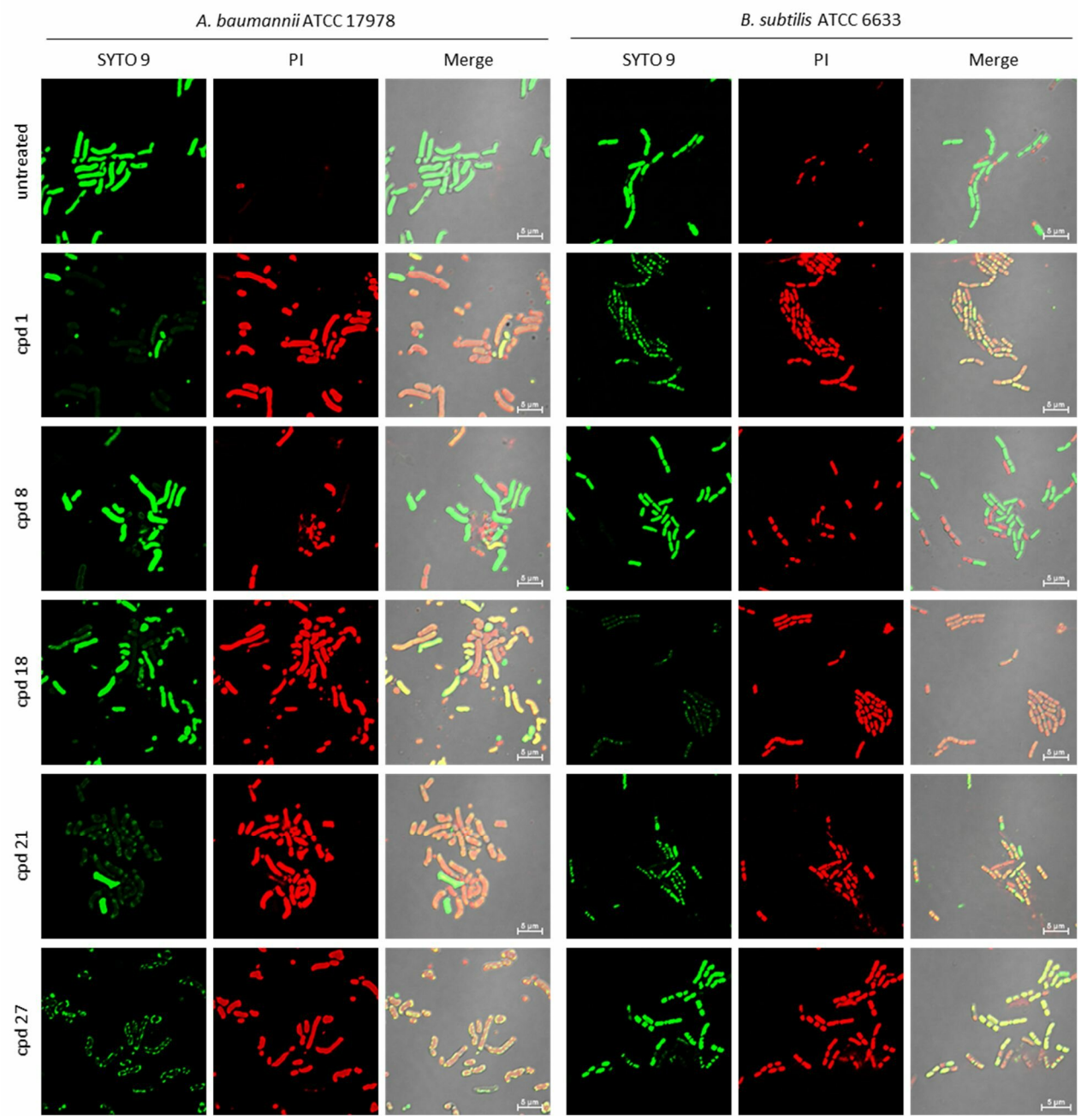

Figure 32. Confocal laser scanning microscopy imaging of *A. baumannii* and *B. subtilis* cells treated with different AGUs. Bacterial cells from 16-h cultures in LB were washed with PBS and suspended at OD_{600}= 0.1 in PBS supplemented with 6 μM of SYTO 9, 30 μM PI, and 16 μg/mL of each cpd in DMSO (16 mg/mL stock concentration). An equal concentration of DMSO (0.1% v/v) was used in the untreated control. The bacterial suspensions were incubated for 1 h at 37 °C, then visually inspected using the NikonA1+ CLSM equipped with 100× oil immersion objective (NA 1.4). SYTO 9 fluorescence, PI fluorescence, and fluorescence-DIC merged channels are shown. Scale bar: 5 μm.

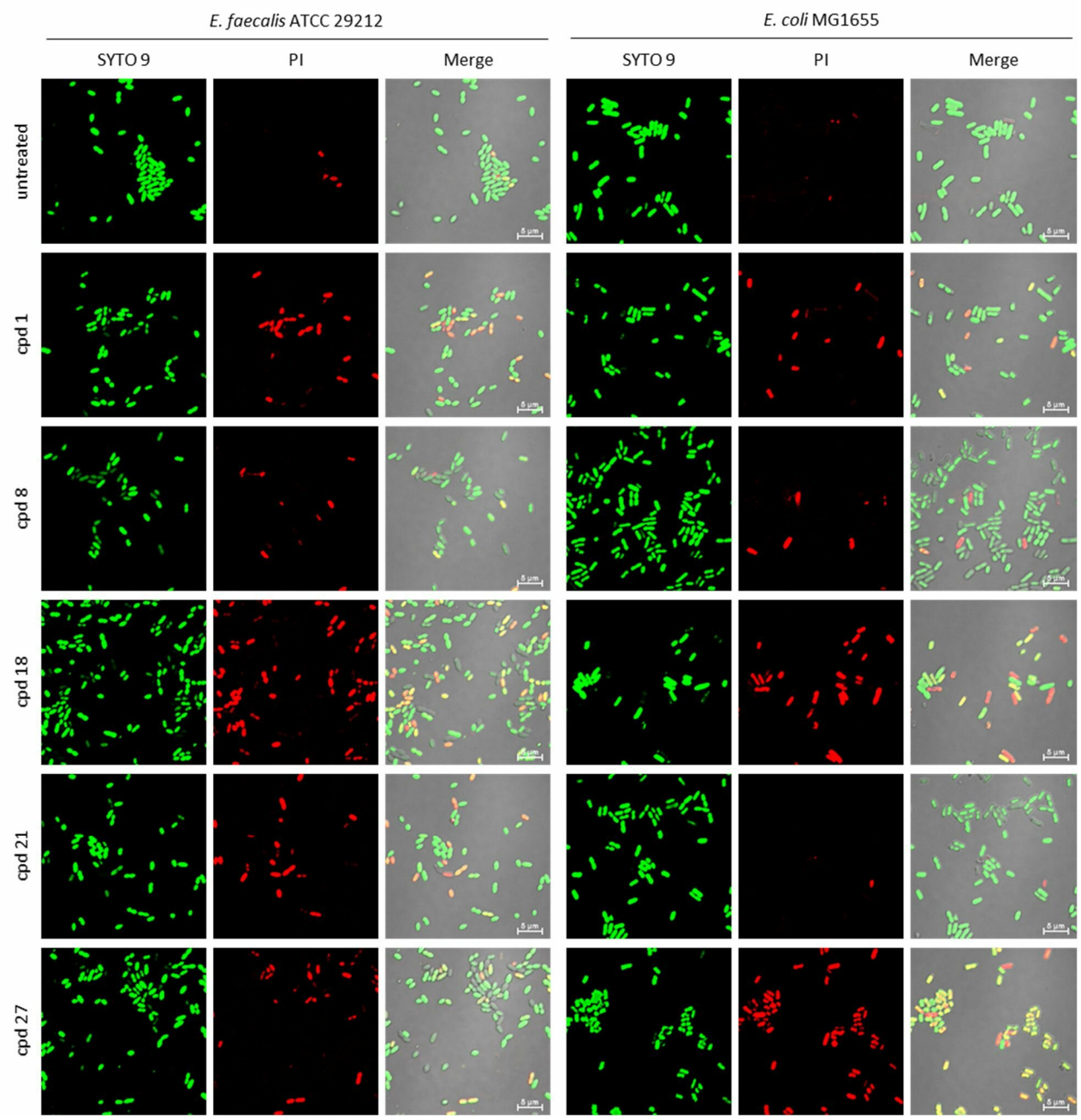

Figure 33. Confocal laser scanning microscopy imaging of E. faecalis and E. coli cells treated with different AGUs. Bacterial cells from 16-h cultures in LB were washed with PBS and suspended at OD600= 0.1 in PBS supplemented with 6 μM of SYTO 9, 30 μM PI, and 16 μg/mL of each cpd in DMSO (16 mg/mL stock concentration). An equal concentration of DMSO (0.1% v/v) was used in the untreated control. The bacterial suspensions were incubated for 1 h at 37 °C, then visually inspected using the NikonA1+ CLSM equipped with 100× oil immersion objective (NA 1.4). SYTO 9 fluorescence, PI fluorescence, and fluorescence-DIC merged channels are shown. Scale bar: 5 μm.

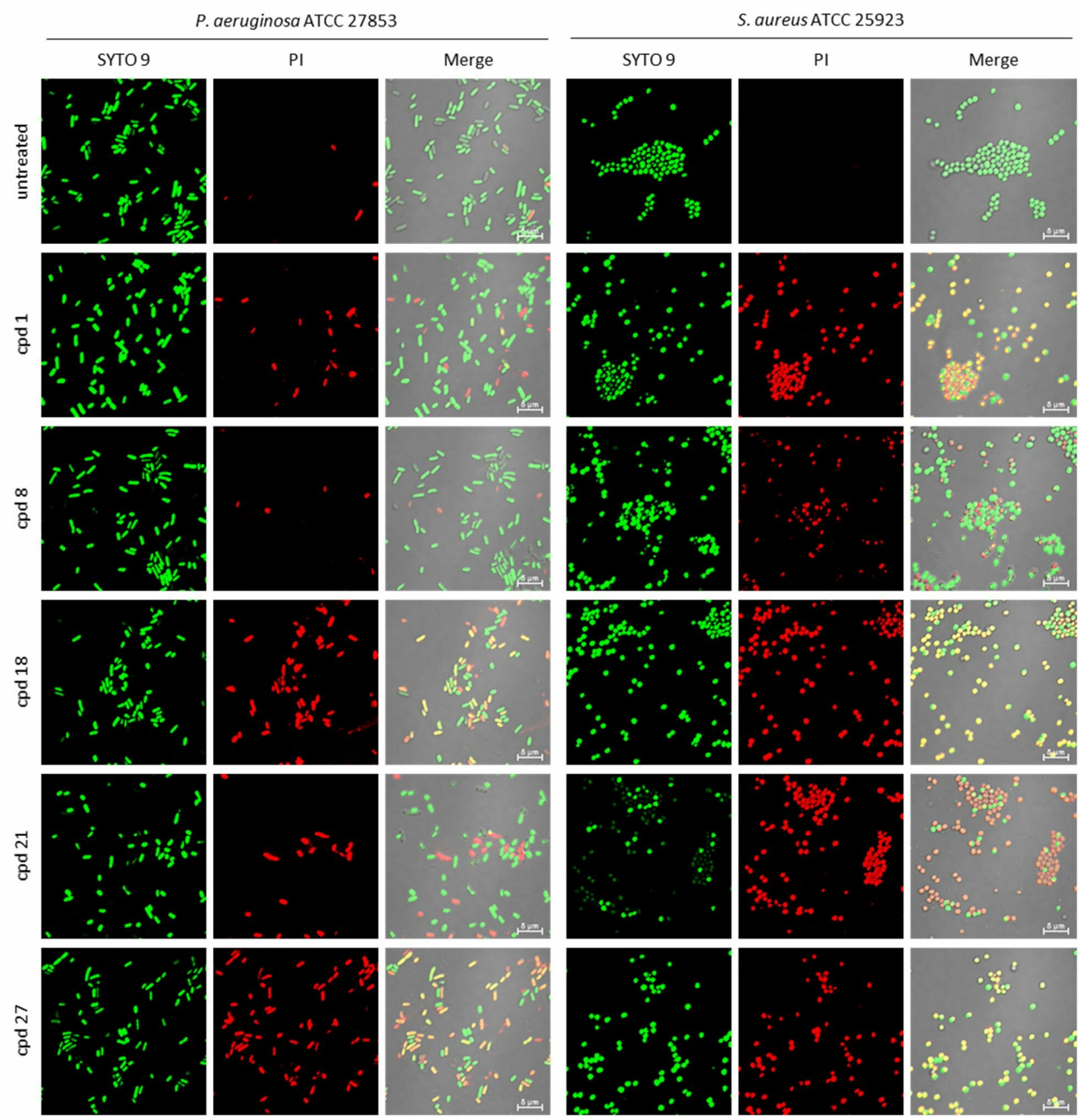

Figure 34. Confocal laser scanning microscopy imaging of *P. aeruginosa* and *S. aureus* cells treated with different AGUs. Bacterial cells from 16-h cultures in LB were washed with PBS and suspended at OD_{600}= 0.1 in PBS supplemented with 6 μM of SYTO 9, 30 μM PI, and 16 μg/mL of each compound in DMSO (16 mg/mL stock concentration). An equal concentration of DMSO (0.1% v/v) was used in the untreated control. The bacterial suspensions were incubated for 1 h at 37 °C, then visually inspected using the NikonA1+ CLSM equipped with 100× oil immersion objective (NA 1.4). SYTO 9 fluorescence, PI fluorescence, and fluorescence-DIC merged channels are shown. Scale bar: 5 μm.

5. Conclusion

Encouraged by the results obtained with the molecular simplification approach,[193] this work was mainly conceived to extend the previously defined SARs and to explore more thoroughly their mechanism of action.

In fact, nineteen new derivatives were synthesized, compounds **41-46**, **47a-m** and **48a-b**, varying the length of the alkyl spacer, the guanidino moieties and their *N*-substitutions. Observing the biological data collected, 8-methylenes is still the optimal length for AGUs linker, although at least one 6-methylenes spacer bearing an unsubstituted guanidine could be required to boost the antibacterial activity, as evidenced by MIC values of compound **45**. The decrease in number of guanidino functionalities in derivatives **48a-b** led to a reduction of potency. Branched saturated or unsaturated (**47b,d,g**) and cyclic (**47f**) alkyl *N*-substituents improved the antibacterial activity, particularly against Gram-positive strains. Moreover, tested Gram-positive bacteria proved to be significantly susceptible also to linear or cyclic polar guanidino substituents (**47h-i**), as further confirmed by the worsened antibacterial profiles of AGUs endowed with small or bulky non-polar substituents (**47l-m**).

Additionally, this work also focused on the development of a novel library, inspired by the *arm-removed* hit, compound **20**. Thus, derivatives **49-54** were synthesized to further explore the newly developed molecular scaffold. Shortening the chain (**49**) led in a complete loss of potency. However, Gram-positive strains resulted still susceptible to unsubstituted guanidines (**50**) or to ones endowed with small linear/branched alkyl substituents (**51-54**), although a dramatically decrease in activity was observed. Overall, chemical modification of the *N*-substitutions pattern in molecular scaffold of **20** led to a total loss of activity against Gram-negative strains.

These preliminary findings suggested that compound **20** might hit a specific target, besides the interaction with bacterial membranes. Hence, aiming to proceed with a rational design of novel derivatives, compound **20** along with compound **1** and **39** were synthesized in larger scale and MoA investigations were made to properly describe the antibacterial behavior of these selected AGUs. Thus analytical, *in silico* and cell-based experiments were performed on AGUs **1**, **20** and **39**. Briefly, the UV-Vis spectra of suspensions of test compounds and POPG-LUVs suggested that interactions between AGUs and phospholipids are likely to occurr. PAMPA performed on three model bilayers, mimicking mammalian and bacterial phospholipids, showed a significant MR (> 40%) for compounds **1**, and **39**, particularly on bacterial ones, highlighting a stronger affinity to bilayers than that of compound **20**, in accordance with LUVs experiments. Then, membrane integrity of the three bilayers was preliminarily assessed by monitoring alterations in P_{app} values of poorly permeable probes, CAF and caffeine, with a modified PAMPA protocol. Both these molecules showed enhanced values when incubates with compounds **1**, and **39**, revealing a moderate perturbation of the 3 bilayers. On the contrary, derivative **20** exerted no

significant alteration in membrane functionality, being in agreement with what highlighted its low MR and the small redshift caused by the interaction with LUVs suspension. Additionally, MD simulations also confirmed a strong interaction between AGUs **1**, and **39** on both the simulated bacterial membranes employed for the MD. Whereas, **20** seemed to display less affinity for mammalian phospholipids and a scarce ability to interact with POPG and POPE/POPG mixed bilayers.

To confirm these preliminary evidences, permeability assays on living bacterial cells were also performed to validate the reliability of membrane model approaches. Briefly, representative Gram-positive and Gram-negative bacterial species were exposed to selected AGUs, monitoring the uptake of the fluorescent dyes SYTO9 and PI. Compound **39** provoked the highest membrane perturbation, whereas the effect of **1** varied depending on tested strains. However, compound **20** showed the narrowest activity profile among the three tested AGUs, promoting membrane disruption only on a few bacterial strains. These evidence were also confirmed by CLSM imaging, leading to hypothesize additional MoAs for compound **20** as in accordance with the preliminary SARs acquired. In the end, hemolytic activity assays were performed to evaluate the selectivity of AGUs library and as a means for assessing their cytotoxicity. AGUs **1**, and **39** showed limited hemolytic activity. However, AGU **20** was remarkably not hemolytic at all, in agreement with the scarce phospholipids affinity highlighted by LUVs, PAMPA and MD experiments. Further evaluation of the hemolytic activity will be performed on the novel synthesized derivatives although, since being structurally analogues of compounds **1** and **39**, it is likely to suppose a comparable hemolytic trend.

Moreover, the impact of the counterion was evaluated preparing the free-base derivative **55** and assessing its biological activity along with that of the hydrochloride salt **40**. Comparing both their antibacterial profiles with that of AGUs hit compound **1** emerged that **40** provided only a slight increase of MIC values, whereas greater differenced could be observed for **55**. Anyway, the free-base compound exerted a good antibacterial activity but with low potency overall, particularly on Gram-negative strains. However, salt form of drug candidates are generally preferred,[218] especially with guanidines bearing molecules due to their instability and their tendency to carbonation.[293] Thereby, salt selection investigations will be further pursue to discover counterions with a positive impact on both the safety profile and the drugability properties of AGUs library.

6. Matherials and Methods

6.1 General Chemistry

All commercially available chemicals and solvents were used as purchased. DCM was dried over calcium hydride and THF was dried over sodium and benzophenone before use. Degassed dry DMF was prepared from dry DMF through cycles of atmosphere exchange under sonication and purging (nitrogen bubbling). Anhydrous reactions were performed into flame-dried glassware after three cycles of vacuum/ dry nitrogen and were run under a positive pressure of dry nitrogen. Chromatographic separations were performed on columns packed with silica gel (230-400 mesh, for flash technique). TLCs were visualized under UV light and stained with Ninhydrin or basic permanganate stains. ^{1H} NMR and ^{13}C NMR were recorded on a Bruker Avance 400 spectrometer at 400 MHz and 100 MHz respectively or a Bruker Avance 600 spectrometer at 600 MHz and 150 MHz respectively. Spectra are reported in parts per million (δ scale) and internally referenced to the $CDCl_3$, CD_3OD, and DMSO-D_6 signal, respectively at δ 7.26, 3.31, and 2.50 ppm. Chemical shifts for carbon are reported in parts per million (δ scale) and referenced to the carbon resonances of the solvent ($CDCl_3$ at δ 77.00, CD_3OD at δ 49.00, and DMSO-D_6 at δ 39.00 ppm). Data are shown as following: chemical shift, multiplicity (s = singlet, d = doublet, t = triplet, q = quartet, qi = quintet, m = multiplet and/or multiplet resonances, br = broad signal), integration and coupling constants (*J*) in Hertz (Hz). Mass spectra (LCMS) were acquired using an Agilent 1100 LC-MSD VL system (G1946C) by direct injection with a 0.4 mL/min flow rate using a binary solvent system of 95/5 MeOH/H_2O. UV detection was monitored at 221 or 254 nm. Mass spectra were acquired in positive or negative mode scanning over the mass range 100-1500 m/z, using a variable fragmentor voltage of 0-70 V.

6.2 Determination of purity

The purity of final products (≥95%) and was assessed by HPLC-UV-MS analysis using an Agilent 1260 Infinity-II HPLC-DAD interfaced with Agilent 6130 MSD (Agilent Technologies, Palo Alto, CA) constituted by a vacuum solvent degassing unit, an injection with the volume ranging from 1 to 100 µL, a binary high-pressure gradient pump, a 1260 series diode-based UV detector, and a thermostated column housing an autosampler. The Agilent 6130 series mass spectra detection (MSD) single-quadrupole instrument was equipped with a multimode ESI/atmospheric pressure chemical ionization (APCI) source (Agilent Technologies, Palo Alto, CA). Nitrogen was used as the nebulizing and drying gas. The pressure of the nebulizing gas, the flow of the drying gas, the capillary voltage, the fragmentor voltage, and the vaporization temperature were set at 40 psi, 9 L/min, 3000 V, 10 V, and 350 °C,

respectively. Chromatographic analyses were performed using a Phenomenex Kinetex EVO C18 100Å column (150 × 4.6 mm, 5 μm particle size) at room temperature and gradient elution with a binary solution (eluent A: H_2O/CH_3COONH_4 0.05% w/v, eluent B: ACN). The analysis started with 5% of B (from t = 0 to t = 3 min), then B was increased to 95% (from t = 3 to t = 12 min), then kept at 95% (from t = 12 to t = 18 min) and finally return to 5% of eluent B in 2.0 min. The flow rate was 0.6 mL/min and the injection volume was 10 μL (sample concentration was 1 mg/mL). UV detection was monitored at 254 and 225 nm. Mass spectra were acquired in positive mode scanning over the mass range 100-1500 m/z using a step size of 0.1.

6.3 Chemical procedures

6.3.1 General synthesis of bromoazide derivatives 56a-b and 65

To a solution of dibromoalcane (32.4 mmol) in DMF (60.0 mL), NaN_3 (17.8 mmol) was added and the reaction mixture was stirred at 50 °C overnight. After cooling, the reaction mixture was concentrated and then diluted with AcOEt (20.0 mL). The organic phase was extracted twice with H_2O (20.0 mL) and then with Brine (20.0 mL). The combined organic layers were dried over Na_2SO_4 and then evaporated under reduced pressure. The crude product was purified through flash chromatography to afford the corresponding bromoazide derivatives as oils.

1-azido-7-bromoheptane (56a):

Starting material: 1,7-dibromoeptane. The crude was purified by silica gel flash chromatography (Hexane).^{1H} NMR (400 MHz, $CDCl_3$) δ (ppm): 1.35 (m, 4H); 1.43 (m, 2H); 1.56 (m, 2H); 1.84 (m, 2H); 3.24 (t, 2H, J = 6.8 Hz); 3.38 (t, 2H, J= 7.2 Hz). ^{13}C NMR (100 MHz, $CDCl_3$) δ (ppm): 26.5; 27.9; 28.5; 28.6; 32.4; 33.5; 51.0. Colorless oil. Yield: 74%

1-azido-9-bromononane (56b):

Starting material: 1,9-dibromononane. The crude was purified by silica gel flash chromatography (Hexane).^{1H} NMR (600 MHz, $CDCl_3$) δ (ppm): 1.32 (m, 6H); 1.47 (m, 6H); 1.82 (m, 2H); 3.26 (*t*, 2H, J = 7.0 Hz); 3.40 (*t*, 2H, J = 7.2 Hz). ^{13}C NMR (100 MHz, $CDCl_3$) δ (ppm): 26.6; 28.1; 28.7; 29.5; 29.7; 30.3; 32.4; 33.8; 51.2. Colorless oil. Yield: 71%.

1-azido-8-bromoctane (65):

Starting material: 1,8-dibromoctane. ^{1H} NMR (400 MHz, CDCl3) δ (ppm): 1.33 (m, 6H); 1.43 (m, 2H); 1.60 (m, 2H); 1.85 (m, 2H); 3.25 (m, 2H); 3.40 (m, 2H). ^{13}C NMR (100 MHz, CDCl3) δ (ppm): 26.5; 27.9; 28.5; 28.7; 28.8; 32.6; 33.7; 51.3 Yield: 72%

6.3.2 General synthesis of bis-azidobenzylamine derivatives 57a-b

Benzylamine (3.67 mmol), K_2CO_3 (11.01 mmol) and KI (1.28 mmol) were dissolved in 1-Butanol (8.4 mL). The mixture was heated at 115 °C and a solution of **56a-b** (9.18 mmol) in 1-Butanol (21.0 mL) was added dropwise. The reaction mixture was stirred at 115°C for 48h. After cooling, the reaction mixture was filtered and the white solid was washed with AcOEt (20.0 mL). The organic phase was washed with Brine, dried over Na_2SO_4 and then evaporated under reduced pressure. The crude product was purified trough flash chromatography (eluent: DCM/MeOH 95/5), affording the compounds as yellow oils.

bis(7-azidoheptyl)(benzyl)amine (57a):

Starting material: **56a**. The crude was purified by silica gel flash chromatography (DCM/MeOH 95/5). ^{1H} NMR (400 MHz, $CDCl_3$) δ (ppm): 1.29 (m, 12H); 1.52 (m, 8H); 2.44 (m, 4H); 3.23 (t, 4H, J = 6.8 Hz); 3.6 (s, 2H); 7.29 (m, 5H). ^{13}C NMR (100 MHz, $CDCl_3$) δ (ppm): 26.4; 27.2; 28.5; 29.1;29.3; 51.4; 53.7; 58. 7; 126.54; 128.6; 129.0; 140.2. LCMS m/z (ES+) = 386.0 $[M + H]^+$; 408 $[M + Na]^+$. Colorless oil. Yield: 80%.

bis(9-azidononyl)(benzyl)amine (57b):

Starting material: **56b**. The crude was purified by silica gel flash chromatography (DCM/MeOH 95/5). ^{1H} NMR (400 MHz, $CDCl_3$) δ (ppm): 1.31 (m, 20H); 1.55 (m, 8H); 2.44 (m, 4H); 3.25 (t, 4H, J = 6.6 Hz); 3.63 (s, 2H); 7.31 (m, 5H). ^{13}C NMR (100 MHz, $CDCl_3$) δ (ppm): 26.2; 27.5; 28.7; 29.0; 29.1; 51.2; 53.9; 60.1; 126.6 128.9; 129.0; 140.5. LCMS m/z (ES+) = 442.6 $[M + H]^+$; 464.6 $[M + Na]^+$. Colorless oil. Yield: 82%.

6.3.3 General synthesis of bis-aminobenzylamine derivatives 58a-b

To a solution of **57a-b** (5.06 mmol) in THF (40.0 mL), triphenylphosphine (15.18 mmol) was added and the mixture was stirred for *1H* at room temperature. Then H_2O (202.4 mmol) was added and the reaction mixture was stirred at room temperature overnight. The reaction mixture was diluted with AcOEt (20.0 mL) and extracted three times with HCl 2N (20.0 mL). The aqueous phase was carefully basified with NaOH 2N (20.0 mL) and back-extracted three times with AcOEt (40.0 mL). The combined organic phases were washed with Brine (120.0 mL) and after drying over Na_2SO_4, solvent was evaporated under reduced pressure. The products were obtained without any further purification as colorless oils.

bis(7-aminoheptyl)(benzyl)amine (58a):

Starting material: **57a**. No further purification. ^{1H} NMR (400 MHz, CD_3OD) δ (ppm): 1.25 (m, 12H); 1.45 (m, 8H); 2.39 (t, 4H, J = 7.2 Hz); 2.58 (t, 4H, J = 7.2 Hz); 3.53 (s, 2H); 7.21 (m, *1H*); 7.29 (m, 4H). ^{13}C NMR (100 MHz, CD_3OD) δ (ppm): 26.2; 26.6; 27.1; 29.0; 32.3; 41.1; 53.3; 58.2; 126.5; 127.7; 128.9; 138.9. LCMS m/z (ES+) = 334.0 $[M + H]^+$. Yellowish oil. Yield: quantitative.

bis(9-aminononyl)(benzyl)amine (58b):

Starting material: **57b**. No further purification. ^{1H} NMR (400 MHz, CD_3OD) δ (ppm): 1.27 (m, 20H); 1.46 (m, 8H); 2.43 (t, 4H, J = 7.0 Hz); 2.61 (t, 4H, J = 7.0 Hz); 3.47 (s, 2H); 7.22 (m, *1H*); 7.31 (m, 4H). ^{13}C NMR (100 MHz, CD_3OD) δ (ppm): 26.1; 26.8; 26.9; 29.3; 32.6; 40.9; 53.5; 58.1; 126.7; 127.9; 129.1; 139.3. LCMS m/z (ES+) = 404.7 $[M + H]^+$; 426.6 $[M + Na]^+$. Yellowish oil. Yield: quantitative.

6.3.4 General synthesis of triamine derivatives 59a-b

To a solution of **58a-b** (1.18 mmol) in *i*-PrOH (19.0 mL), Pd/C (10%, 0.06 mmol) and AcOH (6.1 mL) were added. The reaction mixture was sub*J*ected to three cycles of vacuum followed by flux of H2, and it was stirred under a strong flux of H_2 overnight. Then the reaction mixture was diluted with MeOH (20.0 mL) and filtered through a plug of celite. The filtrate was concentrated and NaOH 2N (40.0 mL) was added until the formation of a precipitate. The aqueous phase was extracted three times with AcOEt (40.0 mL) and the combined organic layers were dried over Na_2SO_4 and concentrated under reduced pressure. The triamine derivatives were obtained as white solids without any further purification.

bis(7-aminoheptyl)amine (59a):

Starting material: **58a**. No further purification. ^{1H} NMR (400 MHz, CD_3OD) δ (ppm): 1.33 (s, 12H); 1.50 (m, 8H); 2.57 (t, 4H, J = 7.2 Hz); 2.64 (t, 4H, J = 7.2 Hz). ^{13}C NMR (100 MHz, CD_3OD) δ (ppm): 26.5; 26.9; 28.9; 29.3; 32.2; 41.1; 49.3. LCMS m/z (ES+) = 244.0 $[M + H]^+$. Off-white solid. Yield: quantitative.

bis(9-aminononyl)amine (59b):

Starting material: **58b**. No further purification. ^{1H} NMR (400 MHz, CD_3OD) δ (ppm): 1.31 (s, 20H); 1.52 (m, 8H); 2.55 (t, 4H, J = 7.0 Hz); 2.67 (t, 4H, J = 7.0 Hz). ^{13}C NMR (100 MHz, CD_3OD) δ (ppm): 26.9; 27.2; 29.1; 29.3; 32.4; 41.3; 49.6. LCMS m/z (ES+) = 300.6 $[M + H]^+$. Yiellowish solid. Yield: quantitative.

6.3.5 General synthesis for the monoguanylated derivatives 60a-b

Triamine derivative **59a-b** (2.24 mmol) was dissolved in THF/MeOH 5/3 (11.0 mL) and the temperature was increased to 50 °C. When the compound was completely solubilized, a solution of 1,3-Bis(tert-butoxycarbonyl)-2-methyl-2-thiopseudourea (0.75 mmol) in THF (11.0 mL) was added dropwise over 2h through a syringe pump and the reaction mixture was stirred at 50°C overnight. Solvent was then evaporated and the crude product was purified through flash chromatography, affording desired compounds as yellowish oils.

tert-butyl *N*-[({7-[(7-aminoheptyl)amino] heptyl}amino)({[(tert-butoxy)carbonyl]amino})methylidene]carbamate (60a) :

Starting material: **59a**. The crude was purified by silica gel flash chromatography (DCM/MeOH/TEA 8/2/0.5). ^{1H} NMR (400 MHz, CD_3OD) δ (ppm): 1.30 (m, 12H); 1.47 (s, 9H); 1.50 (s, 9H) 2.55 (m, 4H); 2.63 (m, 2H); 3.34 (m, 2H). ^{13}C NMR (100 MHz, CD_3OD) δ (ppm): 25.1; 26.0; 26.2; 27.0; 27.5; 28.0;

28.8;28.9;29.0; 32.2; 40.3; 41.0; 48.0; 79.0; 82.5; 152.8; 156.3; 161.1. LCMS m/z (ES+) = 486.0 $[M + H]^+$. Colorless oil. Yield: 76%.

tert-butyl *N*-[({9-[(9-aminononyl)amino]nonyl}amino)({[(tert-butoxy)carbonyl]amino})methylidene]carbamate (60b):

Starting material: **59a**. The crude was purified by silica gel flash chromatography (DCM/MeOH/TEA 8/2/0.5). ^{1H} NMR (400 MHz, CD_3OD) δ (ppm): 1.30 (m, 20H); 1.48 (s, 9H); 1.52 (s, 9H) 2.52 (m, 4H); 2.64 (m, 2H); 3.36 (m, 2H). ^{13}C NMR (100 MHz, CD_3OD) δ (ppm): 24.8; 26.2; 26.4; 27.2; 27.6; 28.1; 28.9; 29.1; 29.2; 32.3; 40.5; 41.3; 48.1; 79.0; 82.6; 153.0; 156.2; 161.4. LCMS m/z (ES+) = 542.8 $[M + H]^+$. Colorless oil. Yield: 73%.

6.3.6 General synthesis for bisguanylated derivatives 61a-b

A solution of **61** (0.45 mmol) in THF (2.5 mL) was added to derivatives 60a-b (0.18 mmol), solubilized in the minimum MeOH required. DIPEA (0.06 mL, 0.36 mmol) was added and the reaction mixture was stirred at room temperature overnight. Then the reaction mixture was diluted with AcOEt and washed with $NaHCO_3$ s.s. and Brine. The crude product was purified through flash chromatography, affording compounds as yellowish oils.

***tert*-butyl *N*-({[7-({7-[({[(*tert*-butoxy)carbonyl]amino}({[(*tert*-butoxy)carbonyl]imino})methyl)amino]heptyl}amino)heptyl]amino}({[(*tert*-butoxy)carbonyl]imino})methyl)-*N*-(cyclopropylmethyl)carbamate (62a):**

Starting material: **60a**. The crude was purified by silica gel flash chromatography (DCM/MeOH 9/1). ^{1H} NMR (400 MHz, $CDCl_3$) *δ* (ppm): 0.21 (m, 2H); 0.43 (m, 2H); 1.01 (m, *1H*); 1.42 (m, 12H); 1.48 (m, 36H); 1.57 (m, 4H); 1.83 (m, 4H); 2.87 (m, 4H), 3.27 (m, 2H); 3.35 (m, 2H); 3.59 (m, 2H); 8.25 (br, *1H*); 11.46 (br, *1H*). ^{13}C NMR (100 MHz, $CDCl_3$) *δ* (ppm): 3.4; 10.5; 26.0; 26.6;26.7; 27.7; 28.0; 28.1; 28.5; 29.0; 40.6; 44.8; 47.8; 52.0; 79.1; 82.0; 82.5; 153.0; 156.1; 163.0. LCMS *m/z* (ES+) = 782.0 $[M + H]^+$; 804.0 $[M + Na]^+$. Colorless oil. Yield: 52%.

tert-butyl *N*-({[9-({9-[({[(tert-butoxy)carbonyl]amino}({[(tert-butoxy)carbonyl]imino})methyl)amino]nonyl}amino)nonyl]amino}({[(tert-butoxy)carbonyl]imino})methyl)-*N*-(cyclopropylmethyl)carbamate (62b):

Starting material **60b**. The crude was purified by silica gel flash chromatography (DCM/MeOH 9/1). ^{1H} NMR (400 MHz, $CDCl_3$) *δ* (ppm): 0.19 (m, 2H); 0.41 (m, 2H); 1.03 (m, *1H*); 1.45 (m, 20H); 1.51 (m, 36H); 1.59 (m, 4H); 1.81 (m, 4H); 2.89 (m, 4H), 3.26 (m, 2H); 3.37 (m, 2H); 3.61 (m, 2H); 8.20 (br, *1H*); 11.40 (br, *1H*). ^{13}C NMR (100 MHz, $CDCl_3$) *δ* (ppm): 3.1; 10.3; 26.2; 26.8; 26.9; 27.4; 28.0; 28.2; 28.7; 29.1; 40.5; 44.3; 47.9; 52.1; 79.1; 82.2; 82.6; 151.0; 156.3; 163.2. LCMS *m/z* (ES+) = 839.2 $[M + H]^+$; 861.2 $[M + Na]^+$. Colorless oil. Yield: 71%.

6.3.7 General synthesis for carbamoyl derivatives 63a-b

To a solution of monomers **62a-b** (0.12 mmol) in dry THF (5.0 mL) DIPEA (0.021 mL, 0.12 mmol) and triphosgene (29.7 mg, 0.10 mmol) were added at 0 °C under nitrogen atmosphere. The mixture was stirred 10 min at 0°C and then warmed to room temperature for *1H*. Then $NaHCO_3$ s.s. was added to quench the reaction mixture and it was stirred for 10 min. The aqueous phase was extracted three times with AcOEt and the combined organic layers were washed with Brine, dried over Na2SO4 and concentrated. The solvent was removed under reduced pressure and the crude product was purified through flash chromatography, affording compounds as oils.

tert-butyl *N*-({[7-({7-[({[(tert-butoxy)carbonyl]amino}({[(tert-butoxy)carbonyl]imino})methyl)amino]heptyl}(chlorocarbonyl)amino)heptyl]amino}({[(tert-butoxy)carbonyl]imino})methyl)-*N*-(cyclopropylmethyl)carbamate (63a):

Starting material: **62a**. The crude was purified by silica gel flash chromatography (PE/AcOEt 7/3). ^{1H} NMR (400 MHz, $CDCl_3$) δ (ppm): 0.24 (m, 2H); 0.46 (m, 2H); 1.05 (m, *1H*); 1.34 (m, 12H); 1.47 (m, 36H); 1.58 (m, 8H); 3.31 (m, 4H); 3.35 (m, 4H); 3.54(m, 2H); 8.29 (br, *1H*); 11.49 (br, *1H*). ^{13}C NMR (100 MHz, CDCl3) δ (ppm): 3.5; 10.6; 22.6; 26.5; 26.6; 26.7; 27.4; 28.0; 28.2; 28.3; 28.8; 29.0; 29.6; 31.8; 33.7; 40.8; 43.8; 49.8; 51.1; 52.1; 79.1; 81.9; 82.9; 85.2; 131.6; 148.9; 153.2; 158.1; 164.5. LCMS m/z (ES+) = 422.5 $[M + 2H]^{2+}$. Colorless oil. Yield: 48%.

tert-butyl *N*-({[9-({9-[({[(tert-butoxy)carbonyl]amino}({[(tert-butoxy)carbonyl]imino})methyl)amino]nonyl}(chlorocarbonyl)amino)nonyl]amino}({[(tert-butoxy)carbonyl]imino})methyl)-*N*-(cyclopropylmethyl)carbamate (63b):

Starting material: **62b**. The crude was purified by silica gel flash chromatography (PE/AcOEt 7/3). ^{1H} NMR ($CDCl_3$) δ (ppm): 0.21 (m, 2H); 0.43 (m, 2H); 1.01 (m, *1H*); 1.31 (m, 20H); 1.49 (m, 36H); 1.60 (m, 8H); 3.29 (m, 4H); 3.37 (m, 4H); 3.55 (m, 2H); 8.29 (br, *1H*); 11.49 (br, *1H*). ^{13}C NMR (CDCl3) δ (ppm): 3.2; 10.9; 22.6; 26.5; 26.6; 26.7; 27.2; 28.1; 28.2; 28.6; 28.8; 29.2; 29.9; 31.7; 33.8; 41.2; 44.5; 50.1; 51.1; 52.3; 79.2; 82.0; 82.9; 85.4; 131.7; 150.1; 153.2; 158.6; 164.7. LCMS m/z (ES+) = 901.7 $[M + 2H]^{2+}$. Colorless oil. Yield: 57%.

6.3.8 General synthesis for the urea coupling

To the carbamoyl derivatives (0.06 mmol) and sodium iodide (0.006 mmol, previously dried in oven) in a tube, a solution of the proper amine derivatives (0.08 mmol) in dry DCM (6.2 mL) and dry DIPEA (21 μL) were added under nitrogen atmosphere. Then, the tube was sealed and the reaction mixture was stirred at 40 °C for 24 h under nitrogen atmosphere. After cooling, DCM and $NaHCO_3$ s.s. were added to the mixture and it was stirred for 10 min. The aqueous phase was extracted three times with DCM and the combined organic layers were washed with brine, dried on Na_2SO_4, filtered and evaporated under reduced pressure. The crude product was purified through flash column chromatography (silica gel).

tert-butyl *N*-[({7-[(7-{[amino({[(tert-butoxy)carbonyl]imino})methyl][(tert-butoxy)carbonyl]amino}heptyl)[(7-{[amino({[(tert-butoxy)carbonyl]imino})methyl][(tert-butoxy)carbonyl]amino}heptyl)({7-[({[(tert-butoxy)carbonyl](cyclopropylmethyl)amino}({[(tert-butoxy)carbonyl]imino})methyl)amino]heptyl})carbamoyl]amino]heptyl}amino)({[(tert-butoxy)carbonyl]imino})methyl]-*N*-(cyclopropylmethyl)carbamate (64a):

Starting materials **63a** and **62a**. Flash chromatography on sílica gel. (DCM/MeOH 98/2).[1H] NMR (400 MHz, $CDCl_3$) δ (ppm): 0.22 (m, 4H); 0.43 (m, 4H); 1.02 (m, 2H); 1.29 (m, 24H); 1.47 (m, 72H); 1.52 (m, 16H); 3.04 (m, 8H); 3.29 (m, 4H); 3.39 (m, 4H); 3.52 (m, 4H); 8.26 (br, 2H); 11.49 (br, 2H). ^{13}C NMR (100 MHz, $CDCl_3$) δ (ppm): 3.4; 10.5; 26.7; 26.9; 27.0; 27.9; 28.0; 28.3; 28.9; 29.1; 29.6; 40.9; 43.7; 48.1; 48.4; 52.1; 79.3; 81.8; 82.9; 153.2; 156.1; 163.9; 165.0. LCMS m/z (ES+) = 796.1 $[M + 2H]^{2+}$; 531.7 $[M + 3H]^{3+}$ YIELD: 57%

tert-butyl *N*-[({9-[(9-{[amino({[(tert-butoxy)carbonyl]imino})methyl][(tert-butoxy)carbonyl]amino}nonyl)[(9-{[amino({[(tert-butoxy)carbonyl]imino})methyl][(tert-butoxy)carbonyl]amino}nonyl)({9-[({[(tert-butoxy)carbonyl](cyclopropylmethyl)amino}({[(tert-butoxy)carbonyl]imino})methyl)amino]nonyl})carbamoyl]amino]nonyl}amino)({[(tert-butoxy)carbonyl]imino})methyl]-*N*-(cyclopropylmethyl)carbamate (64b):

Starting materials **63b** and **62b**. Flash chromatography on sílica gel. (DCM/MeOH 98/2).[1H] NMR (400 MHz, $CDCl_3$) δ (ppm): 0.25 (m, 4H); 0.46 (m, 4H); 1.06 (m, 2H); 1.31 (m, 24H); 1.49 (m, 72H); 1.55 (m, 16H); 3.07 (m, 8H); 3.36 (m, 4H); 3.42 (m, 4H); 3.56 (m, 4H); 8.27 (br, 2H); 11.48 (br, 2H). ^{13}C NMR (100 MHz, $CDCl_3$) δ (ppm): 3.2; 10.6; 26.8; 26.8; 27.2; 27.9; 28.1; 28.4; 29.0; 29.3; 29.6; 41.1; 43.8; 48.1; 48.5; 52.1; 79.3; 81.8; 83.0; 153.3; 156.1; 164.2; 165.1. LCMS. LCMS m/z (ES+) = 852.2 $[M + 2H]^{2+}$; 568.5 $[M + 3H]^{3+}$ YIELD: 48%.

1,3-bis(8-azidooctyl)-1,3-bis({6-[(triphenylmethyl)amino]hexyl})urea (70a):

Starting materials: amine **68a** and carbamoyl chloride **69a**. The crude was purified by silica gel flash chromatography (PE/Et_2O 7/3). ^{1H} NMR (400 MHz, $CDCl_3$) δ (ppm): 1.28-1.34 (m, 24H); 1.46 (m, 8H); 1.57 (m, 8H); 2.11 (m, 4H); 3.06 (m, 8H); 3.23 (t, 4H, J = 6.8 Hz); 7.18 (t, 6H, J = 7.2 Hz); 7.27 (t, 12H, J = 8 Hz); 7.47 (d, 12H, J = 8 Hz). ^{13}C NMR (100 MHz, $CDCl_3$) δ (ppm): 26.6; 26.9; 27.1; 27.2; 28.7; 29.1; 29.2; 30.83; 43.4; 48.2; 51.3; 70.8; 126.1; 127.6; 128.6; 145.4; 163.4. LCMS m/z (ES+) = 243.0 [trityl fragment + H]$^+$; 1049.6 [M + H]$^+$; 1071.6 [M + Na]$^+$. Colorless oil. Yield:75%.

1,3-bis(8-azidooctyl)-3-{6-[(triphenylmethyl)amino]hexyl}-1-{8[(triphenylmethyl)amino]octyl}urea (70b):

Starting materials: amine **68a** and carbamoyl chloride **69a**. The crude was purified by silica gel flash chromatography (PE/Et_2O 7/3). ^1H NMR (400 MHz, $CDCl_3$) δ (ppm): 1.27-1.34 (m, 28H); 1.46 (m, 8H); 1.57 (m, 8H); 2.11 (m, 4H); 3.07 (m, 8H); 3.24 (t, 4H, *J* = 6.8 Hz); 7.18 (t, 6H, *J* = 7.2 Hz); 7.26 (t, 12H, *J* = 7.2 Hz); 7.47 (d, 12H, *J* = 7.6 Hz). ^{13}C NMR (100 MHz, $CDCl_3$) δ (ppm): 26.6; 27.1; 27.9; 28.7; 29.0; 29.2; 48.2; 51.3; 59.2; 126.1; 127.6; 128.6; 146.3; 165.5. LCMS *m/z* (ES+) = 243.0 [trityl fragment + H]$^+$; 1077.8 [M + H]$^+$; 1099.8 [M + Na]$^+$. Colorless oil. Yield:76%.

1,3-bis(8-azidooctyl)-1,3-bis({8-[(triphenylmethyl)amino]octyl})urea (70c):

Starting materials **68b** and **69b**. Flash chromatography on sílica gel. (PE/Et_2O 7/3).^1H NMR (400 MHz) (400 MHz, $CDCl_3$) δ = 1.30 (m, 32H), 1.49 (m, 12H), 1.59 (m, 4H), 2.13 (t, 4H, *J*= 6.8 Hz), 3.09 (m, 8H), 3.25 (t, 4H, *J*= 6.8 Hz), 7.19 (t, 3H, *J*= 7.2 Hz), 7.28 (t, 6H, *J*= 7.6 Hz), 7.49 (d, 6H, *J*= 7.6 Hz). ^{13}C NMR (100 MHz) ($CDCl_3$) *δ* (ppm): 26.6, 26.9, 27.0, 27.2, 27.9, 28.7, 29.1, 29.2, 29.4, 29.6, 30.8, 43.5, 48.1, 51.4, 79.4, 126.1, 127.7, 128.6, 129.6, 146.3, 165.3. LCMS *m/z* (ES+) = 1127.4 [M + Na]$^+$, 1105.4 [M + H]$^+$, 553.2 [M + 2H]$^{2+}$, 369.2 [M + 3H]$^{3+}$, 863.4 [artifact without trityl fragment + H]$^+$, 243.0 [trityl fragment + H]$^+$. Colorless oil. Yield: 80%.

1,3-bis(8-azidooctyl)-1,3-bis({8-[(triphenylmethyl)amino]octyl})thiourea (81):

Starting materials: amine **68a** and thiocarbamoyl chloride **85**. The crude was purified by silica gel flash chromatography (PE/Et_2O 7/3). The crude was purified by silica gel flash chromatography (PE/Et_2O 8/2). ^1H NMR ($CDCl_3$) δ (ppm): 1.26-1.30 (m, 32 H); 1.44 (m, 4H); 1.56 (m, 12H); 2.11 (t, 4H, *J* = 6.8 Hz); 3.23 (t, 4H, *J* = 6.8 Hz); 3.43 (q, 8H, *J* = 7.6 Hz); 7.18 (t, 6H, *J* = 7.2 Hz); 7.27 (t, 12H, *J* = 7.2 Hz); 7.47 (d, 12H, *J* = 7.6 Hz). ^{13}C NMR ($CDCl_3$) δ (ppm): 26.7; 26.8; 27.1; 27.3; 29.3; 29.5; 32.2; 42.2; 50.3; 70.8; 126.6; 128.2; 145.3; 185.7. LCMS *m/z* (ES+) = 1049.6 [M + H]$^+$; 1071.6 [M + Na]$^+$. Yield: 50%. Pale yellow oil.

6.3.9 Synthesis of {8-[(8-azidooctyl)({[(8-azidooctyl)({8-[(triphenylmethyl)amino]octyl})carbamoyl]sulfanyl}methanethioyl)amino]octyl}(triphenylmethyl)amine (86):

To a solution of amine **68b** (0.35 mmol) in THF (23 mL), NaOH (0.42 mmol) was added. The reaction was then cooled down to 0°C and then carbon disulfide (21 μL) was added. The resulting mixture was stirred ad 0-5°C for 3 h. Then, a solution of 69b (0.083 mmol) in THF (1mL) was added and the resulting mixture was stirred at 40°C for 6 hours. The crude was then diluted with $NaHCO_3$ ss. and extracted three times with DCM. The organic layers was then dryed over Na_2SO_4, filtered and evaporated under reduced pressure. The crude mixture was purified by gel silica flash chromatography (PE/Et_2O 8/2). ^1H NMR

($CDCl_3$) δ (ppm): 1.29 (m, 32H); 1.45 (m, 4H); 1.58 (m, 8H); 1.69 (m, 2H); 1.77 (m, 2H); 2.12 (t, *J* = 6.9 Hz, 4H); 3.24 (m, 6H); 3.33 (m, 2H); 3.69 (m, 3.69); 3.91 (dt, *J* = 10.5, 5.0 Hz, 2H); 7.17 (t, *J* = 7.3 Hz, 6H); 7.26 (m, 12H); 7.47 (d, *J* = 7.7 Hz, 12H). ^{13}C NMR ($CDCl_3$) δ (ppm): 26.6; 26.7; 26.9; 27.3; 28.8; 29.0; 29.1; 29.2; 29.5; 29.6; 29.7; 30.8; 43.6; 51.4; 51.5; 54.5; 54.6; 55.7; 55.8; 70.8; 76.8; 77.0; 77.2; 126.2; 127.7; 128.6; 128.7; 146.3; 161.5; 185.5. LCMS *m/z* (ES+) = 1181.7 $[M + H]^+$; 1203.7 $[M + Na]^+$; 936.7 [M – trityl fragment + H]$^+$. Yield: 45%. Pale yellow oil.

6.3.10 General synthesis for trityl-nosyl-amines 66a-b

To a stirred solution of proper diaminoalcane (57.46 mmol) in dry DCM (27.5 mL) in ice bath, a solution of triphenylmethyl chloride (14.35 mmol) in dry DCM (27.0 mL) was added dropwise through a dropping funnel over 4 h at 0 °C under nitrogen atmosphere. Then, the reaction mixture was stirred at room temperature for 2 h. The solvent was evaporated under reduced pressure and the crude was treated with Et_2O and filtered over a celite plug to remove the fine powder of starting material. Then the filtrate was evaporated under reduced pressure and purified by flash column chromatography (silica gel) affording the trityl amine derivative. Then, to a solution of the so obtained trityl amine (10.10 mmol) and freshly distilled TEA (2.75 mL) in dry DCM (36.0 mL), a solution of 4-Nitrobenzenesulfonyl chloride (10.60 mmol) in dry DCM (36.0 mL) was added via cannula at room temperature under nitrogen atmosphere. The reaction mixture was stirred at room temperature for 2 h, then the solvent was evaporated under reduced pressure. The crude was purified by flash column chromatography (silica gel).

4-nitro-N-{6-[(triphenylmethyl)amino]hexyl}benzene-1-sulfonamide (66a):

First step: trityl amine. Starting material: 1,6-diaminohexane. The crude was purified by silica gel flash chromatography (DCM/MeOH 95/5). ^{1H} NMR ($CDCl_3$) δ (ppm): 1.28 (m, 4H); 1.47 (m, 4H); 1.74 (br, 3H); 2.12 (t, 2H, *J* = 6.8 Hz); 2.67 (t, 2H, *J* = 6.8 Hz); 7.18 (t, 3H, *J* = 7.2 Hz); 7.27 (t, 6H, *J* = 7.6 Hz); 7.48 (d, 6H, *J* = 8.0 Hz). ^{13}C NMR ($CDCl_3$) δ (ppm): 26.7; 27.1; 30.7; 33.2; 41.9; 43.4; 70.8; 126.1; 127.6; 128.6; 146.3. LCMS *m/z* (ES+) = 243.0 [trityl fragment + H]$^+$; 381.2 $[M + Na]^+$. Pale yellow oil. Yield: 80%.

Second step: trityl-nosyl-amine. The crude was purified by silica gel flash chromatography (DCM). ^{1H} NMR (400 MHz, $CDCl_3$) δ (ppm): 1.24 (m, 4H); 1.46 (m, 4H); 1.60 (br, *1H*); 2.11 (t, 2H, *J* = 6.8 Hz); 2.99 (m, 2H); 4.68 (br, *1H*); 7.19 (t, 3H, *J* = 6.8 Hz); 7.27 (t, 6H, *J* = 8.0 Hz); 7.47 (d, 6H, *J* = 8.0 Hz); 8.05 (d, 2H, *J* = 8.4 Hz); 8.35 (d, 2H, *J* = 8.4 Hz). ^{13}C NMR (100 MHz, $CDCl_3$) δ (ppm): 26.3; 26.6; 27.0; 29.5; 30.4; 43.3; 43.3; 78.8; 124.3; 126.2; 127.7; 128.5; 146.0; 151.3. LCMS m/z (ES+) = 243.0 [trityl fragment + H]$^+$. LCMS *m/z* (ES-)= 541.9 $[M - H]^-$; 578.0 $[M + Cl]^-$. Pale yellow foam. Yield: 75%.

4-nitro-N-{8-[(triphenylmethyl)amino]octyl}benzene-1-sulfonamide (**66b**):

First step: trityl amine. Starting material: 1,8-diaminoctane. The crude was purified by silica gel flash chromatography (DCM/MeOH 9/1). ^{1H} NMR (400 MHz, CD_3OD) δ (ppm): 1.20 (m, 10H), 1.47 (m, 4H), 1.46 (m, 4H), 2.12 (t, 2H, *J*= 7.2 Hz), 2.60 (t, 2H, *J*= 6.8 Hz), 7.17 (t, 3H, *J*= 6.8 Hz), 7.24 (d, 6H, *J*= 7.6 Hz), 7.43 (d, 6H, *J*= 7.6 Hz). ^{13}C NMR (100 MHz, CD_3OD) δ (ppm): 26.5, 27.0, 29.0, 29.1, 30.0, 32.3, 41.0, 43.5, 78.0, 125.8, 127.2, 128.4, 146.2. LCMS *m/z* (ES+) = 409.0 $[M + Na]^+$, 243.0 [trityl fragment + H]$^+$. Colorless oil. Yield: 89%.

Second step: trityl-nosyl amine. The crude was purified by silica gel flash chromatography (DCM). ^{1H} NMR (400 MHz, $CDCl_3$) δ (ppm): 1.20 (m, 8H), 1.45 (m, 4H), 2.09 (m, 2H), 2.99 (m, 2H), 4.63 (br, *1H*), 7.17 (t, 3H, *J*= 6.8 Hz), 7.24 (t, 6H, *J*= 7.6 Hz), 7.43 (d, 6H, *J*= 7.6 Hz), 8.05 (d, 2H, *J*= 8.0 Hz), 8.34 (d, 2H, *J*= 8.0 Hz).^{13}C NMR (100 MHz, $CDCl_3$) δ (ppm): 26.4, 26.7, 27.2, 28.9, 29.3, 29.6, 43.4, 43.7, 48.3, 124.4, 126.3, 127.8, 128.2, 128.3, 128.7, 142.2, 150.0. LCMS *m/z* (ES+) = 594.0 $[M + Na]^+$, 571.9 $[M + H]^+$, 243.0 [trityl fragment + H]$^+$. LCMS *m/z* (ES-) = 570.1 $[M - H]^-$, 606.2 $[M + Cl]^+$. Off-white powder. Yield: 84%.

6.3.11 General synthesis for masked azido-nosyl-trityl triamines 67a-b

Sulphonamides **66a-b** or commercial 2-Nitrobenzene-1-sulfonamide (5.24 mmol), potassium carbonate (15.72 mmol, previously dried in oven), and potassium iodide (2.62 mmol, previously dried in oven) were dissolved in dry DMF (17.5 mL) under nitrogen atmosphere. The mixture was heated at 95 °C and a solution of **65** (6.28 mmol) in dry DMF (17.5 mL) was added. The reaction mixture was stirred at 95°C for 16 h. After cooling, the reaction mixture was diluted with AcOEt, filtered over cotton, washed with AcOEt, and concentrated under reduced pressure. The residue was treated with $NaHCO_3$ and extracted three times with AcOEt. The combined organic layers were washed with H_2O, an aqueous solution of LiCl 5% and brine, dried on Na_2SO4, filtered, and then evaporated under reduced pressure. The crude product was purified through flash column chromatography.

{6-[N-(8-azidooctyl)4-nitrobenzenesulfonamido]hexyl}(triphenylmethyl)amine (67a):

Starting materials: **65** and **66a**. The crude was purified by silica gel flash chromatography (PE/EtOAc 8/2). ^{1H} NMR (400 MHz, $CDCl_3$) δ (ppm): 1.28 (m, 12H); 1.52 (m, 8H); 2.11 (m, 2H); 3.13 (m, 4H); 3.25 (t, 3H, *J* = 6.8 Hz); 7.19 (t, 3H, *J* = 7.2 Hz); 7.28 (t, 6H, *J* = 7.2 Hz); 7.48 (d, 6H, *J* = 7.6 Hz); 7.97 (d, 2H, *J* = 8.4 Hz); 8.34 (d, 2H, *J* = 8.8 Hz). ^{13}C NMR (100 MHz, $CDCl_3$) δ (ppm): 26.5; 28.6; 28.70; 28.9; 42.6; 48.0; 51.3; 78.8; 124.2; 127.3; 128.1; 145.9; 151.0. LCMS *m/z* (ES+) = 243.0 [trityl fragment + H]$^+$; 719.3 $[M + Na]^+$. Yellow oil. Yield: 82%.

{8-[N-(8-azidooctyl)4-nitrobenzenesulfonamido]octyl}(triphenylmethyl)amine (67b):

Starting materials: **65** and **66b**. The crude was purified by silica gel flash chromatography (PE/EtOAc 8/2). ^{1H} NMR (400 MHz, CD_3OD) δ (ppm): 1.28 (m, 24H), 1.52 (m, 8H), 2.11 (m, 2H), 3.14 (m, 4H), 3.25 (t, 2H, *J*= 6.8 Hz), 7.19 (m, 3H), 7.27 (m, 6H), 7.48 (m, 6H), 7.97 (d, 2H, *J*= 8.4 Hz), 8.33 (d, 2H,

J= 8.4 Hz).^{13}C NMR (100 MHz, $CDCl_3$) δ (ppm): 26.5, 27.2, 28.6, 28.7, 28.9, 29.0, 29.4, 44.3, 48.2, 51.3, 78.3, 124.2, 126.1, 127.7, 128.1, 128.6, 146.1, 146.3, 149.8. LCMS *m/z* (ES+) = 763.0 $[M + K]^+$, 747.2 $[M + Na]^+$, 243.2 [trityl fragment + H]$^+$. Pale yellow oil. Yield: 90%.

N,N*-bis(8-azidooctyl)-2-nitrobenzene-1-sulfonamide *(77):

The crude product was purified through silica gel flash chromatography (PE/AcOEt 75/25). ^{1}H NMR (400 MHz, $CDCl_3$) δ (ppm): 1.24 (m, 12H), 1.31 (m, 4H), 1.53 (m, 8H), 3.23 (m, 8H), 7.58 (m, 1H), 7.67 (m, 2H), 7.96 (m, 1H). ^{13}C NMR (100 MHz, $CDCl_3$) δ (ppm): 26.3, 26.4, 28.0, 28.7, 28.9, 47.1, 51.3, 124.0, 130.5, 131.5, 133.3, 133.6, 147.9. LCMS *m/z* (ES+) = 547.2 $[M+ K]^+$, 531.2 $[M + Na]^+$. Colorless oil. Yield: 92%.

6.3.12 General synthesis for nosyl cleavage in derivatives 68a-b

To a stirred solution of the proper nosyl derivative **67a-b** (0.79 mmol) and potassium carbonate (1.58 mmol, previously dried in oven) in degassed dry DMF (3.6 mL), thiophenol (242 μL, 2.36 mmol) was added under nitrogen atmosphere and the reaction mixture was stirred at room temperature for 2 h with a bleach trap outlet. Then, the reaction mixture treated with DCM and NaH_2CO_3 s.s.. The aqueous phase was extracted three times with DCM and the combined organic layers were washed with brine, dried on Na_2SO_4 and then evaporated under reduced pressure. The crude product was purified through silica gel flash chromatography.

{6-[(8-azidooctyl)amino]hexyl}(triphenylmethyl)amine (68a):

Starting material: **67a**. The crude was purified by silica gel flash chromatography (DCM/MeOH 95/5). ^{1H} NMR (400 MHz, $CDCl_3$) δ (ppm): 1.31 (m, 12H); 1.46 (t, 2H, *J* = 6.8 Hz); 1.57 (t, 2H, *J* = 6.8 Hz); 1.72 (m, 4H); 2.11 (t, 2H, *J* = 6.8 Hz); 2.78 (q, 4H, *J* = 6.4 Hz); 3.23 (t, 2H, *J* = 6.8 Hz); 7.18 (t, 3H, *J* = 7.2 Hz); 7.27 (t, 6H, *J* = 7.6 Hz); 7.47 (d, 6H, *J* = 7.6 Hz). ^{13}C NMR (100 MHz, $CDCl_3$) δ (ppm): 26.6; 27.1; 29.2; 29.9; 30.4; 31.1; 44.1; 48.9; 50.7; 78.1; 125.9; 127.2; 128.7; 145.3. LCMS *m/z* (ES+) = 243.0 [trityl fragment + H]$^+$; 534.3 $[M + Na]^+$. Yellow oil. Yield: 75%.

{8-[(8-azidooctyl)amino]octyl}(triphenylmethyl)amine (68b)

Starting material: **67b**. The crude was purified by silica gel flash chromatography (DCM/MeOH 95/5). ^{1H} NMR (400 MHz, $CDCl_3$) δ = 1.30 (m, 16H), 1.46 (m, 2H), 1.59 (m, 2H), 1.69 (m, 2H), 3.25 (t, 2H, *J*= 6.8 Hz), 7.18 (t, 3H, *J*= 7.2 Hz), 7.27 (t, 6H, *J*= 7.2 Hz), 7.48 (d, 6H, *J*= 7.6 Hz). ^{13}C NMR (100 MHz), $CDCl_3$) δ (ppm): 26.6, 27.0, 27.1, 27.3, 28.9, 29.0, 29.3, 30.0, 30.5, 31.1,44.3, 48.7, 50.3, 77.4, 126.2, 127.0, 129.3, 145.0. LCMS *m/z* (ES+) = 562.0 $[M + Na]^+$, 540.3 $[M + H]^+$, 243.0 [trityl fragment + H]$^+$. Yellow oil. Yield: 88%.

6.3.13 General synthesis for the carbamoyl derivatives

To a solution of the proper secondary amine (0.96 mmol) in dry DCM (16.0 mL), DIPEA (334 μL) was added under nitrogen atmosphere. Then, a solution of triphosgene (0.48 mmol) in dry DCM (30.0 mL) was added dropwise at 0 °C. The mixture was stirred at 0 °C for 30 min and then at room temperature for 0.5-1 h. $NaHCO_3$ s.s. was added to the reaction mixture and it was stirred for 10 min. The aqueous phase was extracted three times with DCM and the combined organic layers were washed with brine, dried on Na_2SO_4, filtered and evaporated under reduced pressure. The crude product was purified through flash column chromatography.

N-(8-azidooctyl)-N-{6-[(triphenylmethyl)amino]hexyl}carbamoyl chloride (69a):

Starting material: **68a**.The crude was purified by silica gel flash chromatography (PE/Et_2O 8/2). ^{1H} NMR (400 MHz, $CDCl_3$) δ (ppm): 1.34 (m, 12H); 1.59 (m, 8H); 2.13 (m, 2H); 3.31 (m, 6H); 7.19 (t, 3H, J = 7.2 Hz); 7.28 (t, 6H, J = 7.2 Hz); 7.48 (d, 6H, J = 8 Hz). ^{13}C NMR (100 MHz, $CDCl_3$) δ (ppm): 26.5; 28.7; 29.0; 30.6; 42.3; 49.8; 51.3; 126.1; 127.7; 128.6; 148.7. LCMS m/z (ES+) = 243.0 [trityl fragment + H]$^+$; 574.3 [M + H]$^+$; 596.3 [M + Na]$^+$. Colorless oil. Yield: 68%.

N-(8-azidooctyl)-N-{8-[(triphenylmethyl)amino]octyl}carbamoyl chloride (69b):

Starting material **68b**. The crude product was purified through silica gel flash column chromatography (PE/AcOEt 9/1). ^{1H} NMR (400 MHz, $CDCl_3$) δ = 1.16 (m, 16H), 1.55 (m, 8H), 3.01 (m, 2H), 3.29 (m, 6H), 7.30 (m, 9H), 7.57 (m, 6H). ^{13}C NMR (100 MHz, $CDCl_3$) δ (ppm): 26.4, 27.1, 27.4, 28.3, 28.7, 28.9, 29.0, 29.6, 46.2, 49.8, 51.1, 51.3, 78.4, 127.8, 128.1, 128.4, 129.1, 146.3, 148.2. LCMS m/z (ES+) = 624.2 [M + Na]$^+$, 243.0 [trityl fragment + H]$^+$. Colorless oil Yield: 72%.

6.3.14 Synthesis of *N,N*-bis(8-azidooctyl)carbamoyl chloride 78:

First step: nosyl deprotection. To sulphonamide **77** (0.21 mmol) in dry THF (7.0 mL), anhydrous sodium methanethiolate (58.8 mg, 0.84 mmol) was added at 0 °C under nitrogen atmosphere and the reaction mixture was stirred at room temperature for 4 h with a bleach trap outlet. Then, the reaction mixture was treated with AcOEt and NaH_2CO_3 s.s.. The aqueous phase was extracted three times with AcOEt and the combined organic layers were washed with brine, dried on Na_2SO_4, and then evaporated under reduced pressure. The crude product was purified through silica gel flash chromatography (AcOEt/MeOH 9/1). ^{1}H NMR (400 MHz, $CDCl_3$) δ = 31 (m, 16H), 1.51 (m, 4H), 1.58 (m, 4H), 2.49 (br, 1H), 2.61 (t, 4H, J= 7.2 Hz), 3.24 (t, 4H, J= 6.8 Hz). ^{13}C NMR (100 MHz, $CDCl_3$) δ (ppm): 26.6, 27.1, 28.7, 29.0, 29.2, 29.6, 49.7, 51.4. LCMS m/z (ES+) = 324.2 [M + H]$^+$. Yellow oil. Yield: quantitative.

Second step: carbamoylation. Procedure of carbamoylation as reported in **6.3.12** using the nosyl-deprotected bis azide previously described. The crude product was purified through silica gel flash column chromatography (PE/AcOEt 9/1). ^{1}H NMR (400 MHz, $CDCl_3$) δ = 1.37 (m, 16H), 1.60 (m, 8H), 3.26 (t, 4H, J= 6.4 Hz), 3.33 (m, 2H), 3.38 (m, 2H). ^{13}C NMR (100 MHz, $CDCl_3$) δ (ppm): 26.5, 26.5, 27.4,

28.3, 28.7, 28.9, 29.0, 49.8, 51.1, 51.4, 149.2. LCMS *m/z* (ES+) = 424.1 $[M + K]^+$, 408.1 $[M + Na]^+$, 404.1 [MeOH-adduct artifact + $Na]^+$, 386.1 $[M + H]^+$, 382.1 [MeOH-adduct artifact + $H]^+$. Yellow oil. Yield: 71%.

6.3.15 Synthesis of {8-[(8azidooctyl)(chloromethanethioyl)amino]octyl}(triphenylmethyl)amine (85):

To an ice-cold solution of secondary amine **68b** (0.37 mmol) and dry DIPEA (0.19 mL) in dry DCM (9 mL) a solution of thiophosgene (57 μL) in dry DCM (9 mL) was slowly added dropwise via *canula* under N_2 atmosphere. The reaction mixture was stirred at 0°C for 30 minutes and then at room temperature for 30 min. Then, it was quenched with aqueous $NaHCO_3$ s.s. and extracted three times with DCM. The organic phases were reunited, washed with brine, dried over Na_2SO_4, filtered, and evaporated under reduced pressure. The crude was purified by silica gel flash chromatography (PE/Et_2O 9/1). ^{1}H NMR (400 MHz, $CDCl_3$) δ (ppm): 1.33 (m, 16H); 1.47 (m, 2H); 1.60 (m, 2H); 1.74 (m, 4H); 3.26 (t, 2H, *J* = 6.8 Hz); 3.68 (m, 2H); 3.83 (m, 2H); 7.19 (t, 3H, *J* = 6.8 Hz); 7.28 (t, 6H, *J* = 7.6 Hz); 7.48 (d, 6H, *J* = 7.6 Hz). ^{13}C NMR (100 MHz, $CDCl_3$) δ (ppm): 25.6; 26.5; 27.8; 28.7; 28.9; 29.4; 30.7; 31.4; 43.3; 51.3; 55.8; 126.1; 127.6; 128.6; 173.7. LCMS *m/z* (ES+) = 243.0 [trityl fragment + $H]^+$; 640.1 $[M + Na]^+$. Brown oil. Yield: 40%.

6.3.16 General synthesis of monoguanylated azido dimers

To a solution of the proper urea derivatives **70a-c** (0.14 mmol) in DCM (13.3 mL), freshly distilled TFA (final concentration 5%, 700 μL) was added. The resulting mixture was stirred at room temperature for 0.5 h. The reaction completion was verified through direct LCMS in*J*ection. Then, the mixture was treated with toluene and methanol, evaporating under reduced pressure. The crude was then dissolved in THF (2.8 mL) and DIPEA (122 μL) was added. The mixture was stirred at room temperature for 10 min and then the suitable **61** or commercially available *N,N*-DiBoc-*1H*-pyrazolecarboxamidine was added. The reacting mixture was then stirred at room temperature for 16 h. The crude was purified through silica gel flash chromatography.

***tert*-butyl *N*-[({6-[(8-azidooctyl)[(8-azidooctyl)(8-[({[(*tert*-butoxy)carbonyl]amino}({[(*tert*-butoxy)carbonyl]imino})methyl]amino}octyl)carbamoyl]amino]hexyl}amino)({[(*tert*-butoxy)carbonyl]amino})methylidene]carbamate (71a):**

Starting material **70a**. After detritylation LCMS *m/z* (ES+) = 593.5 $[M+H]^+$; 615.5 $[M+Na]^+$. Guanylating agent used: *N,N*'-Di-Boc-*1H*-pyrazole-1-carboxamidine (commercial). The crude was purified by silica gel flash chromatography (PE/AcOEt 8/2). ^{1H} NMR (400 MHz, $CDCl_3$) δ (ppm): 1.31 (m, 28H); 1.51 (s, 36H); 1.55-1.60 (m, 16H); 3.07 (m, 8H); 3.25 (t, 4H, *J* = 6.8 Hz); 3.39 (m, 4H); 8.28 (br, 2H); 11.50 (br,

2H). ^{13}C NMR (100 MHz, $CDCl_3$) δ (ppm): 26.6; 26.9; 28.0; 28.2; 28.7; 29.0; 29.2; 40.8; 48.2; 51.3; 78.8; 82.9; 156.0; 165.2. LCMS *m/z* (ES+) = 1077.3 $[M + H]^+$; 1199.7 $[M + Na]^+$. Colorless oil. Yield:75%.

***tert*-butyl *N*-[({6-[(8-azidooctyl)[(8-azidooctyl)(6-[({[(*tert*-butoxy)carbonyl](cyclopropylmethyl)amino}({[(*tert*-butoxy)carbonyl]imino})methyl]amino}hexyl)carbamoyl]amino]hexyl}amino)({[(*tert*-butoxy)carbonyl]imino})methyl]-*N*- (cyclopropylmethyl)carbamate (71b):**

Starting material **70a**. After detritylation LCMS *m/z* (ES+) = 565.9 $[M + H]^+$. Guanylating agent used: **61**. The crude was purified by silica gel flash chromatography (PE/AcOEt 9/1). ^{1H} NMR (400 MHz, $CDCl_3$) δ (ppm): 0.23 (m, 4H); 0.46 (m, 4H); 1.04 (m, 2H); 1.30 (m, 24H); 1.46 (s, 18H); 1.48 (s, 18H); 1.58 (m, 16H); 3.06 (m, 8H); 3.25 (t, 4H, *J* = 6.8 Hz); 3.32 (m, 4H); 3.53 (m, 4H); 8.28 (br, 2H). ^{13}C NMR (100 MHz, $CDCl_3$) δ (ppm): 3.5; 10.4; 26.6; 26.8; 26.9; 28.1; 28.7; 29.0; 29.2; 40.9; 43.9; 48.0; 48.5; 51.3; 78.8; 82.9; 156.0; 163.2; 165.2. LCMS *m/z* (ES+) = 1156.7 $[M + H]^+$; 1179.3 $[M + Na]^+$. Colorless oil. Yield: 78%.

***tert*-butyl *N*-[({6-[(8-azidooctyl)[(8-azidooctyl)(8-[({[(*tert*-butoxy)carbonyl]amino}({[(*tert*-butoxy)carbonyl]imino})methyl]amino}octyl)carbamoyl]amino]hexyl}amino)({[(*tert*-butoxy)carbonyl]amino})methylidene]carbamate (71c):**

Starting material **70b**. After detritylation LCMS *m/z* (ES+) = 593.5 $[M+H]^+$; 615.5 $[M+Na]^+$. Guanylating agent used: *N,N'*-Di-Boc-*1H*-pyrazole-1-carboxamidine (commercial). The crude was purified by silica gel flash chromatography (PE/AcOEt 8/2). ^{1H} NMR (400 MHz, $CDCl_3$) δ (ppm): 1.31 (m, 28H); 1.51 (s, 36H); 1.55-1.60 (m, 16H); 3.07 (m, 8H); 3.25 (t, 4H, *J* = 6.8 Hz); 3.39 (m, 4H); 8.28 (br, 2H); 11.50 (br, 2H). ^{13}C NMR (100 MHz, $CDCl_3$) δ (ppm): 26.6; 26.9; 28.0; 28.2; 28.7; 29.0; 29.2; 40.8; 48.2; 51.3; 78.8; 82.9; 156.0; 165.2. LCMS *m/z* (ES+) = 1077.3 $[M + H]^+$; 1199.7 $[M + Na]^+$. Colorless oil. Yield:75%.

tert-butyl *N*-[({6-[(8-azidooctyl)[(8-azidooctyl)({8-[({[(tert-butoxy)carbonyl](cyclopropylmethyl)amino}({[(tert-butoxy)carbonyl]imino})methyl)amino]octyl})carbamoyl]amino]hexyl}amino)({[(tert-butoxy)carbonyl]imino})methyl]-*N*-(cyclopropylmethyl)carbamate (71d):

Starting material used **70b**. After detritylation LCMS *m/z* (ES+) = 593.5 $[M+H]^+$; 615.5 $[M+Na]^+$. Guanylating agent used: **61**. The crude was purified by silica gel flash chromatography (PE/AcOEt 7/3). ^{1H} NMR (400 MHz, $CDCl_3$) *δ* (ppm): 0.25 (m, 4H); 0.45 (m,4H); 1.31 (m, 36H); 1.47 (s, 18H); 1.49 (s, 18H); 1.58 (m, 8H); 3.08 (m, 8H); 3.25 (t, 4H, *J* = 7.2 Hz); 3.30 (m, 4H); 3.55 (m, 4H). ^{13}C NMR (100 MHz, $CDCl_3$) *δ* (ppm): 3.5; 10.5; 26.6; 26.7; 26.8;26.9; 27.0; 27.8; 27.9; 28.1; 287; 29.0; 29.2; 29.6; 43.8; 48.0; 48.3; 48.5; 51.4; 52.1; 79.1; 81.8; 151.3; 155.2; 165.2. LCMS *m/z* (ES+) = 543.5 $[M-1Boc\ artifact + 2H]^{2+}$; 593.5 $[M + 2H]^{2+}$; 604.5 $[M + H + Na]^{2+}$; 615.5 $[M + 2Na]^{2+}$; 1185.9 $[M + H]^+$; 1208.9 $[M + Na]^+$. Colorless oil. Yield: 82%.

tert-butyl *N*-[({8-[(8-azidooctyl)[(8-azidooctyl)({8-[({[(tert-butoxy)carbonyl]amino}({[(tert-butoxy)carbonyl]imino})methyl)amino]octyl})carbamoyl]amino]octyl}amino)({[(tert-butoxy)carbonyl]amino})methylidene]carbamate (73):

Starting material: **70c**. After detritylation LCMS *m/z* (ES+) = 621.5 $[M + H]^+$; 643.5 $[M + Na]^+$. Guanylating agent used: *N,N'*-Di-Boc-*1H*-pyrazole-1-carboxamidine (commercial). The crude was purified by silica gel flash chromatography (PE/ Et_2O 7/3). ^{1H} NMR (400 MHz, $CDCl_3$) δ (ppm): 1.30 (m, 32H); 1.49 (s, 18H); 1.50 (s, 18H); 1.59 (m, 16H); 3.08 (m, 8H); 3.25 (t, 4H, *J* = 6.8 Hz); 3.39 (m, 4H); 8.28 (br, 2H); 11.50 (br, 2H). ^{13}C NMR (100 MHz, $CDCl_3$) δ (ppm): 26.6; 26.8; 26.9; 27.0; 27.9; 28.0; 28.2; 28.7; 28.9; 29.0; 29.2; 29.3; 40.9; 48.2; 51.3; 78.8; 79.1; 82.9; 151.3; 153.3; 156.0; 164.2; 165.3. LCMS *m/z* (ES+) = 1105.7 $[M + H]^+$; 1127.7 $[M + Na]^+$. Colorless oil. Yield: 80%.

tert-butyl *N*-[({8-[(8-azidooctyl)[(8-azidooctyl)({8-[({[(tert-butoxy)carbonyl](cyclopropylmethyl)amino}({[(tert-butoxy)carbonyl]imino})methyl)amino]octyl})carbamoyl]amino]octyl}amino)({[(tert-butoxy)carbonyl]imino})methyl]-*N*-(cyclopropylmethyl)carbamate (76):

Starting material: **70c**. After detritylation LCMS *m/z* (ES+) = 311.3 $[M + 2H]^{2+}$; 621.5 $[M + H]^+$; 643.5 $[M + Na]^+$. Guanylating agent used: **61**. The crude was purified by silica gel flash chromatography (PE/AcOEt 8/2). ^{1H} NMR (400 MHz, $CDCl_3$) *δ* (ppm): 0.25 (m, 4H); 0.45 (m, 4H); 1.05 (m, 2H); 1.32 (m, 32H); 1.47 (s, 36H); 1.50 (s, 36H); 1.59 (m, 16H); 3.08 (m, 8H); 3.26 (t, 4H, *J* = 6.8 Hz); 3.31 (m, 4H); 3.56 (m, 4H). ^{13}C NMR (100 MHz, $CDCl_3$) δ (ppm): 3.6; 10.4; 26.6; 26.9; 27.0;27.9; 28.1; 28.7; 29.1; 29.2; 48.2; 51.3; 78.8; 82.9; 153.2; 156.0; 163.4; 165.2. LCMS *m/z* (ES+) = 303.5 $[M + 4H]^{4+}$; 607.5 $[M + 2H]^{2+}$; 618.5 $[M + H + Na]^{2+}$; 629.7 $[M + 2Na]^{2+}$; 1214.7 $[M + H]^+$; 1235.7 $[M + Na]^+$. Colorless oil. Yield: 60%.

***tert*-butyl *N*-[({8-[(8-azidooctyl)[bis(8-azidooctyl)carbamoyl]amino]octyl}amino)({[(*tert*-butoxy)carbonyl]imino})methyl]-*N*-(cyclopropylmethyl)carbamate (79):**

The synthesis of derivatives **79** proceeded first with coupling between carbamoyl chloride **78** and amine **68b** following the *coupling procedure* **6.3.8**. Then, trityl-deprotection and guanylation with guanylating agents **61** as reported in **6.3.14**. The crude product was purified through silica gel flash chromatography (PE/AcOEt 8/2). ^{1}H NMR (400 MHz, $CDCl_3$) *δ* (ppm): 0.22 (m, 2H), 0.44 (m, 2H), 1.03 (m, 1H), 1.29 (m, 32H), 1.45 (s, 9H), 1.47-1.50 (overlapped, m, 17H), 1.87 (m, 8H), 3.06 (m, 8H), 3.23 (t, 6H, *J*= 6.8 Hz), 3.30 (m, 2H), 3.52 (m, 2H ^{13}C NMR (100 MHz, $CDCl_3$) *δ* (ppm): 3.5, 10.1, 23.9, 26.6, 26.9, 27.9, 28.2, 28.7, 29.0, 29.2, 43.7, 48.2, 51.3, 78.8, 81.9, 83.1, 151.7, 155.3, 165.3. LCMS *m/z* (ES+) = 965.7 $[M + Na]^+$, 943.7 $[M + H]^+$. Colorless oil. Yield: 71%.

6.3.17 General synthesis of bisguanylated dimers

To a solution the proper azido-bearing urea (0.11 mmol) in *i*-PrOH (12.2 mL), $Pd(OH)_2/C$ (20%, 0.04 mmol) was added. The reaction mixture was sub*J*ected to three cycles of vacuum followed by a flux of hydrogen, then it was stirred under a flux of 1 atm hydrogen for 1-16 h. The reaction completion was verified through direct LCMS in*J*ection. The reaction mixture was diluted with MeOH and filtered through a plug of celite. Then, to the crude in THF (3.3 mL), The appropriate guanylating agent (*N,N*'-Di-Boc-*1H*-pyrazole-1-carboxamidine, **61** or compounds **GAa-m**) (0.28 mmol) and DIPEA (0.55 mmol) were added. The reaction was stirred at room temperature for 24 h. Then, the mixture was treated with $NaHCO_3$ s.s. and extracted three times with DCM. The combined organic phases were dried over Na_2SO_4, filtered and evaporated under reduced pressure. The crude was purified by silica gel flash chromatography.

***tert*-butyl *N*-[({8-[({8-[({[(*tert*-butoxy)carbonyl](cyclopropylmethyl)amino}({[(tert-butoxy)carbonyl]imino})methyl)amino]octyl}({6-[({[(*tert*-butoxy)carbonyl]amino}({[(*tert*-butoxy)carbonyl]imino})methyl)amino]hexyl})carbamoyl)({6-[({[(*tert*-butoxy)carbonyl]amino}({[(*tert*-butoxy)carbonyl]imino})methyl)amino]hexyl})amino]octyl}amino)({[(*tert*-butoxy)carbonyl]imino})methyl]-*N*-(cyclopropylmethyl)carbamate (72a):**

Starting material **71a**. After hydrogenation LCMS *m/z* (ES+) = 997.3 $[M + H]^+$. Guanylating agent used: 61. The crude was purified by silica gel flash chromatography (PE/AcOEt 7/3). ^{1H} NMR (400 MHz, $CDCl_3$) δ (ppm): 0.24 (m, 4H); 0.46 (m, 4H); 1.05 (m, 2H); 1.34-1.27 (m, 24H); 1.48 (s, 36H); 1.50 (s, 36H); 1.59 (m, 16H); 3.06 (m, 8H); 3.41 (m, 8H); 8.30 (br, 2H); 11.50 (br, 2H). ^{13}C NMR (100 MHz, $CDCl_3$) δ (ppm): 3.8; 10.1; 26.7; 27.0; 28.0; 28.2; 28.9; 29.2; 29.6; 40.9; 43.7; 48.3; 52.1; 79.2; 83.0; 153.2; 156.0 163.4; 165.2. LCMS *m/z* (ES+) = 795.6 $[M + 2H]^{2+}$; 817.5 $[M + 2Na]^{2+}$. Colorless oil. Yield: 67%.

***tert*-butyl *N*-[({6-[({6-[({[(*tert*-butoxy)carbonyl](cyclopropylmethyl)amino}({[(*tert*-butoxy)carbonyl]imino})methyl)amino]hexyl}({8-[({[(*tert*-butoxy)carbonyl]amino}({[(*tert*-butoxy)carbonyl]imino})methyl)amino]octyl})carbamoyl)({8-[({[(*tert*-butoxy)carbonyl]amino}({[(*tert*-butoxy)carbonyl]imino})methyl)amino]octyl})amino]hexyl}amino)({[(*tert*-butoxy)carbonyl]imino})methyl]-*N*-(cyclopropylmethyl)carbamate (72b):**

Starting material: **71b** . After hydrogenation LCMS *m/z* (ES+) = . Guanylating agent used: *N,N'*-DiBoc-*1H*-pyrazole-1-carboxamidine. The crude was purified by silica gel flash chromatography (PE/AcOEt 7/3). ^{1H} NMR (400 MHz, $CDCl_3$) δ (ppm): 0.24 (m, 4H); 0.46 (m, 4H); 1.04 (m, 2H); 1.31 (m, 26H); 1.46 (s, 36H); 1.49-1.50 (m, 36H); 1.61 (m, 16H); 3.07 (m, 8H); 3.31 (m, 4H); 3.40 (m, 4H); 3.54 (m, 4H); 8.28 (br, 2H); 11.50 (br, 2H). ^{13}C NMR (100 MHz, $CDCl_3$) δ (ppm): 3.5; 10.5; 26.7; 27.0; 28.0; 28.2; 28.9; 29.2;

29.6; 40.9; 43.7; 48.0; 48.6; 52.1; 79.2; 83.0; 153.2; 156.0; 163.6; 165.2. LCMS *m/z* (ES+) = 795.6 $[M + 2H]^{2+}$; 817.5 $[M + 2Na]^{2+}$. Colorless oil. Yield: 67%

***tert*-butyl *N*-[({8-[({8-[({[(*tert*-butoxy)carbonyl](cyclopropylmethyl)amino}{[(*tert*-butoxy)carbonyl]imino})methyl)amino]octyl}{8-[({[(*tert*-butoxy)carbonyl]amino}{[(*tert*-butoxy)carbonyl]imino})methyl)amino]octyl})carbamoyl){6-[({[(*tert*-butoxy)carbonyl]amino}{[(*tert*-butoxy)carbonyl]imino})methyl)amino]hexyl})amino]octyl}amino){[(*tert*-butoxy)carbonyl]imino})methyl]-*N*-(cyclopropylmethyl)carbamate (72c):**

Starting material: **71c**. After hydrogenation LCMS *m/z* (ES+) = 513.5 $[M + 2H]^{2+}$; 1025.5 $[M + H]^{+}$. Guanylating agent used: **61**. The crude was purified by silica gel flash chromatography (PE/AcOEt 7/3). ^{1H} NMR (400 MHz, $CDCl_3$) δ (ppm): 0.23 (m, 4H); 0.45 (m, 4H); 1.04 (m, 2H); 1.26-1.30 (m, 28H); 1.46 (s, 36H); 1.49-1.50 (m, 36H); 1.49-1.59 (overlapped, m, 16H); 3.08 (m, 8H); 3.32 (m, 4H); 3.39 (m, 4H); 3.54 (m, 4H); 8.28 (br, 2H); 11.50 (br, 2H). ^{13}C NMR (100 MHz, $CDCl_3$) δ (ppm): 3.4; 10.5; 26.7; 26.9; 27.0; 28.0; 28.2; 28.9; 29.2; 40.8; 43.8; 48.3; 52.1; 79.1; 81.8; 82.9; 153.2; 156.0; 163.5; 165.2. LCMS *m/z* (ES+) = 809.5 $[M + 2H]^{2+}$; 831.5 $[M + 2Na]^{2+}$. Colorless oil. Yield: 68%.

tert-butyl *N*-[({6-[({8-[({[(tert-butoxy)carbonyl](cyclopropylmethyl)amino}{[(tert-butoxy)carbonyl]imino})methyl)amino]octyl}{8-[({[(tert-butoxy)carbonyl]amino}{[(tert-butoxy)carbonyl]imino})methyl)amino]octyl})carbamoyl){8-[({[(tert-butoxy)carbonyl]amino}{[(tert-butoxy)carbonyl]imino})methyl)amino]octyl})amino]hexyl}amino){[(tert-butoxy)carbonyl]imino})methyl]-*N*-(cyclopropylmethyl)carbamate (72d):

Starting material: **71d**.After hydrogenation LCMS *m/z* (ES+) = . Guanylating agent used: *N,N'*-DiBoc-*1H*-pyrazole-1-carboxamidine.The crude was purified by silica gel flash chromatography (PE/AcOEt 1/1). ^{1H} NMR (400 MHz, $CDCl_3$) *δ* (ppm):0.25 (m, 4H); 0.46 (m,4H); 1.31 (m, 28H); 1.47-1.51 (m, 72H); 1.60 (m, 6H); 3.08 (m, 8H); 3.31 (m, 4H); 3.40 (m, 4H); 3.55 (m, 4H); 8.29 (br, 2H); 11.51 (br, 2H). ^{13}C NMR (100 MHz, $CDCl_3$) *δ* (ppm): 3.2; 10.6; 26.6; 26.8; 27.1; 28.2; 28.4; 28.9; 29.3; 41.2; 44.1; 48.3; 52.2; 79.3; 81.9; 82.9; 153.4; 156.2; 163.9; 165.5. LCMS *m/z* (ES+) = 473.5 [M-2Boc artifact + 3H]$^{3+}$; 506.2 [M-1Boc artifact + 3H]$^{3+}$; 540.2 [M + 3H]$^{3+}$; 809.7 [M + 2H]$^{2+}$._820.8 [M + 2Na]$^{2+}$._Colorless oil. Yield: 57%.

tert-butyl *N*-[({8-[({8-[({[(tert-butoxy)carbonyl](propyl)amino}{[(tert-butoxy)carbonyl]imino})methyl)amino]octyl}{8-[({[(tert-butoxy)carbonyl]amino}{[(tert-butoxy)carbonyl]imino})methyl)amino]octyl})carbamoyl){8-[({[(tert-butoxy)carbonyl]amino}{[(tert-butoxy)carbonyl]imino})methyl)amino]octyl})amino]octyl}amino){[(tert-butoxy)carbonyl]imino})methyl]-*N*-propylcarbamate (74a):

Starting material: **73**.After hydrogenation LCMS *m/z* (ES+) = 527.5 $[M+2H]^{2+}$; 1053.8 $[M+H]^{+}$. Guanylating agent used: **GAa.** The crude was purified by silica gel flash chromatography (PE/AcOEt 1/1). ^{1H} NMR (400 MHz, $CDCl_3$) δ (ppm): 0.89 (t, 6H, J = 8.0 Hz); 1.21-1.31 (m, 32H); 1.46 (s, 18H); 1.49-1.50 (overlapped s, 54H); 1.57 (m, 20H); 3.07 (m, 8H); 3.22 (m, 4H); 3.40 (m, 4H); 3.61 (m, 4H); 8.29 (br, 2H); 11.51 (br, 2H). ^{13}C NMR (100 MHz, $CDCl_3$) δ (ppm): 11.2; 22.3; 23.8; 26.7; 26.8; 27.0; 27.1; 28.0; 28.1; 28.2; 28.2; 28.9; 29.2; 29.6; 40.9; 43.8; 48.2; 48.3; 58.1; 68.5; 79.1; 82.9; 153.3; 156.0; 163.6; 165.3. LCMS *m/z* (ES+) = 541.5 $[M + 3H]^{3+}$; 811.8 $[M + 2H]^{2+}$. Colorless oil. Yield: 76%.

***tert*-butyl N-[({8-[({8-[({[(*tert*-butoxy)carbonyl](propan-2-yl)amino}({[(*tert*-butoxy)carbonyl]imino})methyl)amino]octyl}({8-[({[(*tert*-butoxy)carbonyl]amino}({[(*tert*-butoxy)carbonyl]imino})methyl)amino]octyl})carbamoyl)({8-[({[(*tert*-butoxy)carbonyl]amino}({[(*tert*-butoxy)carbonyl]imino})methyl)amino]octyl})amino]octyl}amino)({[(*tert*-butoxy)carbonyl]imino})methyl]-N-(propan-2-yl)carbamate (74b):**

Starting material: **73**. After hydrogenation LCMS *m/z* (ES+) = 527.5 $[M+2H]^{2+}$; 1053.8 $[M+H]^{+}$. Guanylating agent used: **GAa.** The crude was purified by silica gel flash chromatography (PE/AcOEt 7/3). ^{1H} NMR (400 MHz, $CDCl_3$) δ (ppm): 1.26-1.30 (m, 32H); 1.30 (overlapped, d, 12H, J = 6.8 Hz); 1.46 (s, 36H); 1.48 (s, 36H); 1.48-1.54 (overlapped, m, 16H); 3.06 (m, 8H); 3.20 (t, 4H, J = 6.8 Hz); 3.38 (m, 4H); 4.16 (m, 2H); 8.26 (br, 2H); 11.48 (br, 2H). ^{13}C NMR (100 MHz, $CDCl_3$) δ (ppm): 20.4; 20.6; 26.7; 26.8; 27.0; 27.9; 28.0; 28.1; 28.3; 28.9; 29.2; 40.9; 43.6; 48.3; 49.9; 79.2; 81.3; 82.9; 153.2; 156.0; 163.5; 165.2. LCMS *m/z* (ES+) = 811.8 $[M + 2H]^{2+}$; 833.5 $[M + 2Na]^{2+}$. Colorless oil. Yield: 66%.

tert-butyl *N*-[({8-[({8-[({[(tert-butoxy)carbonyl](butyl)amino}({[(tert-butoxy)carbonyl]imino})methyl)amino]octyl}({8-[({[(tert-butoxy)carbonyl]amino}({[(tert-butoxy)carbonyl]imino})methyl)amino]octyl})carbamoyl)({8-[({[(tert-butoxy)carbonyl]amino}({[(tert-butoxy)carbonyl]imino})methyl)amino]octyl})amino]octyl}amino)({[(tert-butoxy)carbonyl]imino})methyl]-*N*-butylcarbamate (74c):

Starting material: **73**. After hydrogenation LCMS *m/z* (ES+) = 527.5 $[M+2H]^{2+}$; 1053.8 $[M+H]^{+}$.. Guanylating agent used: **GAc.** The crude was purified by silica gel flash chromatography (PE/AcOEt 1/1). ^{1H} NMR (400 MHz, $CDCl_3$) δ (ppm): 0.92 (t, 6H, J = 7.2 Hz); 1.32 (m, 36H); 1.47 (s, 18H); 1.50-1.51 (overlapped s, 54H); 1.59 (overlapped, m, 16H); 1.66 (m, 4H); 3.08 (m, 8H); 3.22 (m, 4H); 3.40 (m, 4H); 3.65 (m, 4H); 8.29 (br, 2H); 11.51 (br, 2H). ^{13}C NMR (100 MHz, $CDCl_3$) δ (ppm): 13.7; 14.0; 20.0; 22.6; 26.8; 27.0; 28.0; 28.2; 28.2; 28.9, 29.2; 29.6; 31.2; 40.9; 43.8; 48.2; 48.4; 79.1; 82.9; 151.5; 153.4; 156.0; 163.6. LCMS *m/z* (ES+) = 825.5 $[M + 2H]^{2+}$; 836.5 $[M + H + Na]^{2+}$. Colorless oil. Yield: 71%.

tert-butyl *N*-[({8-[({8-[({[(tert-butoxy)carbonyl](2-methylpropyl)amino}({[(tert-butoxy)carbonyl]imino})methyl)amino]octyl}({8-[({[(tert-butoxy)carbonyl]amino}({[(tert-

butoxy)carbonyl]imino})methyl)amino]octyl})carbamoyl)({8-[({[(tert-butoxy)carbonyl]amino}({[(tert-butoxy)carbonyl]imino})methyl)amino]octyl})amino]octyl}amino)({[(tert-butoxy)carbonyl]imino})methyl]-*N*-(2-methylpropyl)carbamate (74d):

Starting material: 73. After hydrogenation LCMS m/z (ES+) = 527.5 $[M+2H]^{2+}$; 1053.8 $[M+H]^{+}$. Guanylating agent used: **GAd.** The crude was purified by silica gel flash chromatography (PE/AcOEt 1/1). ^{1H} NMR (400 MHz, $CDCl_3$) δ (ppm): 0.89 (d, 12H, J = 6.8 Hz); 1.26-1.32 (m, 32H); 1.47 (s, 18H); 1.49-1.50 (overlapped s, 54H); 1.52-1.66 (m, 16H); 1.82 (m, 2H); 3.07 (m, 8H); 3.25 (m, 4H); 3.39 (m, 4H); 3.54 (d, 2H, J = 7.2 Hz); 8.29 (br, 2H); 11.51 (br, 2H). ^{13}C NMR (100 MHz, $CDCl_3$) δ (ppm): 14.0; 20.2; 22.6; 26.8; 26.8; 27.0; 28.0; 28.1; 28.2; 28.2; 28.5; 28.9; 29.2; 29.6; 40.9; 43.9; 48.2; 48.4; 54.7; 79.1; 82.9; 153.2; 156.0; 163.6; 165.5, 167.1. LCMS m/z (ES+) = 551.0 $[M + 3H]^{3+}$; 826.2 $[M + 2H]^{2+}$. Colorless oil. Yield: 76%.

tert-butyl *N*-[(2E)-but-2-e*N*-1-yl]-*N*-[({8-[({8-[({[(2E)-but-2-e*N*-1-yl][(tert-butoxy)carbonyl]amino}({[(tert-butoxy)carbonyl]imino})methyl)amino]octyl}({8-[({[(tert-butoxy)carbonyl]amino}({[(tert-butoxy)carbonyl]imino})methyl)amino]octyl})carbamoyl)({8-[({[(tert-butoxy)carbonyl]amino}({[(tert-butoxy)carbonyl]imino})methyl)amino]octyl})amino]octyl}amino)({[(tert-butoxy)carbonyl]imino})methyl]carbamate (74e):

Starting material: **73**. After hydrogenation LCMS m/z (ES+) = 527.5 $[M+2H]^{2+}$; 1053.8 $[M+H]^{+}$. Guanylating agent used: **GAf.** The crude was purified by silica gel flash chromatography (PE/AcOEt 1/1). ^{1H} NMR (400 MHz, $CDCl_3$) δ (ppm): 1.30 (m, 32H); 1.46-1.51 (m, 72H); 1.56 (m, 16H); 1.67 (d, 6H, J = 6.0 Hz); 3.07 (m, 8H); 3.20 (m, 4H); 3.39 (m, 4H); 4.16 (m, 4H); 5.49 (m, 2H); 5.65 (m, 2H); 8.29 (br, 2H); 11.51 (br, 2H). ^{13}C NMR (100 MHz, $CDCl_3$) δ (ppm): 17.6; 21.9; 26.87; 26.8; 27.1; 28.0; 28.1; 28.2; 28.9; 29.2; 40.9; 43.7; 48.2; 48.4; 49.3; 79.1; 82.9; 126.2; 129.6; 152.1; 153.2; 155.5, 157.1; 163.6. LCMS m/z (ES+) = 412.0 $[M + 4H]^{4+}$; 549.0 $[M + 3H]^{3+}$; 823.0 $[M + 2H]^{2+}$; 834.0 $[M + H + Na]^{2+}$. Colorless oil. Yield: 60%.

***tert*-butyl *N*-[({8-[({8-[({[(*tert*-butoxy)carbonyl](propan-2-yl)amino}({[(*tert*-butoxy)carbonyl]imino})methyl)amino]octyl}({8-[({[(*tert*-butoxy)carbonyl]amino}({[(*tert*-butoxy)carbonyl]imino})methyl)amino]octyl})carbamoyl)({8-[({[(*tert*-butoxy)carbonyl]amino}({[(*tert*-butoxy)carbonyl]imino})methyl)amino]octyl})amino]octyl}amino)({[(*tert*-butoxy)carbonyl]imino})methyl]-*N*-cyclopentylcarbamate (74f):**

Starting material: **73**. After hydrogenation LCMS m/z (ES+) = 527.5 $[M+2H]^{2+}$; 1053.8 $[M+H]^{+}$. Guanylating agent used: **GAe.** The crude was purified by silica gel flash chromatography (PE/AcOEt 7/3). ^{1H} NMR (400 MHz, $CDCl_3$) δ (ppm): 1.30 (m, 32H); 1.44 (s, 36H); 1.49 (s, 36H); 1.49-1.54

(overlapped, m, 16H); 1.71 (s, 12H); 1.96 (m, 4H); 3.06 (m, 8H); 3.20 (t, 4H, *J* = 6.8 Hz); 3.38 (m, 4H); 4.09 (m, 2H); 8.27 (br, 2H); 11.49 (br, 2H). ^{13}C NMR (100 MHz, $CDCl_3$) δ (ppm): 23.6; 26.7; 26.9; 27.0; 28.0; 28.1; 28.2; 28.9; 29.2; 30.1; 40.8; 43.5; 48.1; 48.3; 58.9; 79.3; 81.2; 82.9; 153.2; 156.0; 163.3; 165.2. LCMS *m/z* (ES+) = 837.8 $[M + 2H]^{2+}$; 859.6 = $[M + 2Na]^{2+}$. Colorless oil. Yield: 66%.

tert-butyl *N*-[({8-[({8-[({[(tert-butoxy)carbonyl][(2E)-3,7-dimethylocta-2,6-die*N*-1-yl]amino}({[(tert-butoxy)carbonyl]imino})methyl)amino]octyl}({8-[({[(tert-butoxy)carbonyl]amino}({[(tert-butoxy)carbonyl]imino})methyl)amino]octyl})carbamoyl)({8-[({[(tert-butoxy)carbonyl]amino}({[(tert-butoxy)carbonyl]imino})methyl)amino]octyl})amino]octyl}amino)({[(tert-butoxy)carbonyl]imino})methyl]-*N*-[(2E)-3,7-dimethylocta-2,6-die*N*-1-yl]carbamate (74g):

Starting material: **73**. After hydrogenation LCMS *m/z* (ES+) = 527.5 $[M+2H]^{2+}$; 1053.8 $[M+H]^{+}$. Guanylating agent used: **GAg**. The crude was purified by silica gel flash chromatography (PE/AcOEt 1/1). ^{1H} NMR (400 MHz, $CDCl_3$) *δ* (ppm): 1.30 (m, 32H); 1.46-1.56 (overlapped m, 78H); 1.59 (s, 6H); 1.68 (s, 12H); 2.00 (m, 4H); 2.03 (m, 4H); 3.07 (m, 8H); 3.21 (m, 4H); 3.40 (m, 4H); 4.26 (m, 4H); 5.07 (m, 2H); 5.19 (m, 2H); 8.29 (br, 2H); 11.51 (br, 2H). ^{13}C NMR (100 MHz, $CDCl_3$) *δ* (ppm): 16.2; 17.9; 20.7; 25.6; 26.4; 26.8; 26.9; 27.0; 28.0; 28.1, 28.2; 28.9; 29.3; 29.6; 39.5; 40.9; 43.8; 45.2; 48.4; 52.6; 55.4; 79.1; 82.9; 1195; 123.8; 129.8; 131.3; 151.3; 153.4; 156.3; 165.3. LCMS *m/z* (ES+) = 453.2 $[M + 4H]^{4+}$; 604.1 $[M + 3H]^{3+}$; 905.5 $[M + 2H]^{2+}$; 916.5 $[M + H + Na]^{2+}$. Colorless oil. Yield: 61%.

***tert*-butyl N-[({8-[({8-[({[(*tert*-butoxy)carbonyl](2-methoxyethyl)amino}({[(*tert*-butoxy)carbonyl]imino})methyl)amino]octyl}({8-[({[(*tert*-butoxy)carbonyl]amino}({[(*tert*-butoxy)carbonyl]imino})methyl)amino]octyl})carbamoyl)({8-[({[(*tert*-butoxy)carbonyl]amino}({[(*tert*-butoxy)carbonyl]imino})methyl)amino]octyl})amino]octyl}amino)({[(*tert*-butoxy)carbonyl]imino})methyl]-N-(2-methoxyethyl)carbamate (74h):**

Starting material: **73**. After hydrogenation LCMS *m/z* (ES+) = 527.5 $[M+2H]^{2+}$; 1053.8 $[M+H]^{+}$. Guanylating agent used: **GAh.** The crude was purified by silica gel flash chromatography (DCM/MeOH 99:1). ^{1H} NMR (400 MHz, $CDCl_3$) *δ* (ppm): 1.31 (m, 32H); 1.47 (s, 18H); 1.50 (s, 54H); 3.07 (t, 8H, *J* = 7.6 Hz); 3.26 (t, 4H, *J* = 7.2 Hz); 3.33 (s, 6H); 3.39 (q, 4H, *J* = 7.2 Hz); 3.51 (m, 4H); 3.81 (m, 4H); 8.30 (br, 2H); 11.50 (br, 2H). ^{13}C NMR (100 MHz, $CDCl_3$) *δ* (ppm): 26.7; 26.8; 27.0; 28.0; 28.1; 28.2; 28.3; 28.9; 29.3; 29.6; 40.8; 43.8; 48.2; 58.4; 79.1; 81.9; 82.9; 153.2; 156.0; 163.5; 165.4. LCMS *m/z* (ES+) = 552.3 $[M + 3H]^{3+}$; 827.6 $[M + 2H]^{2+}$; 839.5 $[M + H + Na]^{2+}$. Colorless oil. Yield: 62%.

***tert*-butyl N-[({8-[({8-[({[(tert-butoxy)carbonyl][2-(morpholin-4-yl)ethyl]amino}({[(*tert*-butoxy)carbonyl]imino})methyl)amino]octyl}({8-[({[(*tert*-butoxy)carbonyl]amino}({[(*tert*-butoxy)carbonyl]imino})methyl)amino]octyl})carbamoyl)({8-[({[(*tert*-butoxy)carbonyl]amino}({[(*tert*-**

butoxy)carbonyl]imino})methyl)amino]octyl})amino]octyl}amino)({[(*tert*-butoxy)carbonyl]imino})methyl]-N-[2-(morpholin-4-yl)ethyl]carbamate (74i):

Starting material: **73**. After hydrogenation LCMS *m/z* (ES+) = 527.5 $[M+2H]^{2+}$; 1053.8 $[M+H]^{+}$. Guanylating agent used: **GAi.** The crude was purified by silica gel flash chromatography (DCM/MeOH 99:1). ^{1H} NMR (400 MHz, $CDCl_3$) δ (ppm): 1.31 (m, 32H); 1.47 (s, 18H); 1.48 (s, 18H); 1.50 (s, 36H); 2.49 (m, 12H); 3.07 (m, 8H); 3.26 (m, 4H); 3.39 (q, 4H, J = 8 Hz); 3.65 (m, 8H); 3.80 (m, 4H); 8.28 (br, 2H); 11.50 (br, 2H). ^{13}C NMR (100 MHz, $CDCl_3$) δ (ppm): 26.7; 27.1; 27.9; 28.1; 28.2; 28.3; 28.9; 29.3; 40.8; 48.4; 53.7; 57.8; 66.8; 79.1; 81.9; 82.9; 153.2; 156.0; 163.6; 165.2. LCMS *m/z* (ES+) = 882.8 $[M + 2H]^{2+}$; 893.7 $[M + H + Na]^{2+}$; 904.5 $[M + 2Na]^{2+}$. Colorless oil. Yield: 57%.

tert-butyl N-[({8-[({8-[({[(tert-butoxy)carbonyl][2-(methylsulfanyl)ethyl]amino}({[(tert-butoxy)carbonyl]imino})methyl)amino]octyl}({8-[({[(tert-butoxy)carbonyl]amino}({[(tert-butoxy)carbonyl]imino})methyl)amino]octyl})carbamoyl)({8-[({[(tert-butoxy)carbonyl]amino}({[(tert-butoxy)carbonyl]imino})methyl)amino]octyl})amino]octyl}amino)({[(tert-butoxy)carbonyl]imino})methyl]-N-[2-(methylsulfanyl)ethyl]carbamate (74l):

Starting material: **73**. After hydrogenation LCMS *m/z* (ES+) = 527.5 $[M+2H]^{2+}$; 1053.8 $[M+H]^{+}$. Guanylating agent used: **GAl.** The crude was purified by silica gel flash chromatography (DCM). ^{1H} NMR (600 MHz, $CDCl_3$) δ (ppm): 1.27 (m, 32H); 1.43 (m, 36H); 1.47 (m, 36H); 1.54 (m, 8H); 1.57 (m, 8H); 2.86 (s, 6H); 3.07 (m, 8H); 3.17 (m, 4H); 3.31 (m, 4H); 3.81 (t, J =7.2 Hz, 2H); 4.01 (t, J = 7.2, 2H). ^{13}C NMR (100 MHz, $CDCl_3$) δ (ppm): 15.6; 27.1; 27.3; 27.4; 28.2; 28.3; 28.5; 29.3; 29.5; 41.0; 41.1; 47.6; 48.1; 80.4; 81.0; 147.4; 151.5; 153.0; 163.0; 165.5. LCMS *m/z* (ES+) = 844.2 $[M + 2H]^{2+}$; 855.2 $[M + H + Na]^{2+}$; 866.3 $[M + 2Na]^{2+}$. Colorless oil. Yield: 62%.

tert-butyl N-[2-(adamantan-1-yl)ethyl]-N-[({8-[({8-[({[2-(adamantan-1-yl)ethyl][(tert-butoxy)carbonyl]amino}({[(tert-butoxy)carbonyl]imino})methyl)amino]octyl}({8-[({[(tert-butoxy)carbonyl]amino}({[(tert-butoxy)carbonyl]imino})methyl)amino]octyl})carbamoyl)({8-[({[(tert-butoxy)carbonyl]amino}({[(tert-butoxy)carbonyl]imino})methyl)amino]octyl})amino]octyl}amino)({[(tert-butoxy)carbonyl]imino})methyl]carbamate (74m):

Starting material: **73**. After hydrogenation LCMS *m/z* (ES+) = 527.5 $[M+2H]^{2+}$; 1053.8 $[M+H]^{+}$. Guanylating agent used: **GAm.** The crude was purified by silica gel flash chromatography (DCM). ^{1H} NMR (600 MHz, $CDCl_3$) δ (ppm): 1.28 (m, 32H);1.31 (m, 4H); 1.47 (s, 36H); 1.51 (m, 46H); 1.59 (m, 24H); 1.63 (m, 8H); 1.68 (m, 8H); 1.93 (s, 6H); 3.06 (m, 8H); 3.20 (m, 4H); 3.38 (m, 4H); 3.64 (m, 4H); 8.29 (bs, *1H*); 11.49 (br, *1H*). ^{13}C NMR (150 MHz, $CDCl_3$) δ (ppm): 26.4; 27.1; 27.3; 27.4; 28.2; 28.3; 28.2; 28.3; 28.9; 29.3; 29.5; 33.6; 37.5; 41.0; 41.1; 41.9; 42.2; 47.6; 80.4; 80.6; 80.9; 81.0; 147.4; 147.5; 151.5;

152.9; 161.9; 165.2. LCMS m/z (ES+) = 932.3 $[M + 2H]^{2+}$; 943.3 $[M + H + Na]^{2+}$; 954.3 $[M + 2Na]^{2+}$. Colorless oil. Yield: 60%.

1,3-bis({8-[N'-(cyclopropylmethyl)-N',N''-di-Boc-carbamimidamido]octyl})-3-[8-(N',N''-di-Boc-carbamimidamido)octyl]- 1-[8-(N''-Boc-carbamimidamido)octyl]urea (75):

Starting material: **73**. After hydrogenation LCMS m/z (ES+) = 527.5 $[M+2H]^{2+}$; 1053.8 $[M+H]^{+}$. The crude product was purified by silica gel flash chromatography (DCM/CH3OH 98/2). ^{1}H NMR (400 MHz, $CDCl_3$): δ 0.26 (d, J = 4.8 Hz, 4H); 0.43 (d, J = 7.6 Hz, 4H); 1.09 (m, 2H); 1.31 (m, 48H); 1.48 (s, 72H); 3.07 (m, 8H); 3.29 (m, 4H); 3.32 (m, 4H); 3.51 (m, 4H); 8.26 (br, 2H); 11.49 (br, 2H). ^{13}C NMR (100 MHz, $CDCl_3$): δ 3.4; 10.5; 26.7; 26.9; 27.0; 28.0; 28.1; 28.2; 28.9; 29.2; 29.5; 40.8; 43.8; 48.2; 48.3; 52.1; 79.0; 81.8; 82.9; 153.2; 156.0; 163.5; 165.2. LC-MS m/z (ES+) = 823.5 $[M + 2H]^{2+}$; 549.4 $[M + 3H]^{3+}$ Yellowish oil. Yield: 72%

***tert*-butyl *N*-{[(8-{[bis({8-[({[(*tert*-butoxy)carbonyl]amino}({[(*tert*-butoxy)carbonyl]imino})methyl)amino]octyl})carbamoyl]({8-[({[(*tert*-butoxy)carbonyl]amino}({[(*tert*-butoxy)carbonyl]imino})methyl)amino]octyl})amino}octyl)amino]({[(*tert*-butoxy)carbonyl]imino})methyl}-*N*-(cyclopropylmethyl)carbamate (80):**

Starting material: **79**. After hydrogenation LCMS m/z (ES+) = 865.7 $[M + H]^{+}$, 433.3 $[M + 2H]^{2+}$, 289.3 $[M + 3H]^{3+}$. The crude was purified through silica gel flash chromatography (PE/AcOEt 7/3). ^{1}H NMR (400 MHz, $CDCl_3$) δ (ppm): 0.25 (m, 2H), 0.45 (m, 2H), 1.04 (m, 1H), 1.28 (m, 32H), 1.48 (m, 72H), 1.49 (s, 36H), 1.57 (m, 16H), 3.07 (t, 8H, J = 7.2 Hz); 3.32 (t, 2H, J = 6.8 Hz); 3.39 (m, 6H), 3.55 (m, 2H); 8.28 (br, 3H), 11.50 (br, 3H). ^{13}C NMR (100 MHz, $CDCl_3$) δ (ppm): 3.5, 10.1, 23.1. 26.9, 27.0, 27.1, 27.9, 28.1, 28.3, 28.6, 29.6, 29.7, 41.3, 42.4, 47.2, 47.7, 79.4, 80.5, 82.0; 151.9, 153.1, 155.7, 157.5, 158.8, 164.3. LCMS m/z (ES+) = 807.8 $[M + H + Na]^{2+}$; 796.7 $[M + 2H]^{2+}$. Colorless oil. Yield: 63%.

6.3.18 General synthesis of guanylating agents GAa-o

N,N'-DiBoc-*1H*-pyrazole-1-carboxamidine (1.61 mmol) was dissolved in THF dry (6.2 mL). Then triphenylphosphine (2.41 mmol) and the suitable alcohol (2.09 mmol) were added. The reaction mixture was cooled at 0 °C and diisoporpyl azodicarboxylate (0.47 mL) was added dropwise. The temperature was increased to 70 °C and the reaction mixture was stirred at reflux for 16h. The reaction mixture was concentrated and then diluted with DCM and H_2O. The aqueous phase was extracted for three times with DCM; the organic phases were collected, washed with brine twice and dried over Na_2SO_4. Solvent was removed in vacuum and then the crude mixture was purified by flash chromatography on silica gel.

***N,N'*-Di-Boc-*N*-cyclopropylmethyl-pyrazole-1-carboxamidine (61):**

Alcohol used: cyclopropylmethanol. The crude product was purified with silica gel flash chromatography (PE/AcOEt 9:1) to afford compounds as a yellowish oils (yield 82%). ^{1H} NMR (400 MHz, $CDCI_3$) δ

(ppm): 0.45 (d, 2H, *J* = 4.8 Hz); 0.49 (d, *J* = 5.6Hz, 2H); 1.27 (s, 9H); 1.49 (s, 9H); 1.54 (s, *1H*); 3.60 (d, *J* = 6.8 Hz, 2H); 6.41 (t, , *J* =2.2 Hz, *1H*); 7.69 (d, *J* = 1 .2 Hz, *1H*); 7.95 (s, 1 H). ^{13}C NMR (100 MHz, $CDCl_3$) *δ* (ppm): 3.1; 18.2; 28.2; 28.3; 43.6; 80.5; 81.0; 107.7; 123.8; 141.6; 151.0; 151.7; 162.2. LCMS m/z (ES+) = 387.1 [M + Na]. Yield: 96%.

tert-butyl *N*-({[(tert-butoxy)carbonyl]imino}(*1H*-pyrazol-1-yl)methyl)-*N*-propylcarbamate (GAa):

Alcohol used: propanol. The crude was purified by silica gel flash chromatography (PE/AcOEt 9/1). ^{1H} NMR ($CDCl_3$) *δ* (ppm): 0.90 (t, 3H, *J*= 7.2 Hz); 1.26 (s, 9H); 1.49 (s, 9H); 1.74 (m, 2H); 3.62 (m, 2H); 6.40 (s, *1H*); 7.67 (s, *1H*); 7.93 (s, *1H*). ^{13}C NMR (100 MHz, $CDCl_3$) *δ* (ppm): 11.1; 21.6; 27.3; 27.6; 27.8; 50.5; 82.2; 82.4; 108.8; 129.8; 142.8; 152.4; 155.0; 157.5. LCMS *m/z* (ES+) = 353.0 $[M + H]^+$; 375.2 $[M + Na]^+$; 677.3 [2M-1Boc artifact + H]$^+$; 704.3 $[2M + H]^+$; 727.3 $[2M + Na]^+$. Colorless oil. Yield: 99%.

***N,N'*-Di-Boc-*N*-isopropyl-pyrazole-1-carboxamidine (GAb):**

Alcohol used: *i*-propanol. The crude was purified by silica gel flash chromatography (PE/AcOEt 9/1). ^{1H} NMR (400 MHz, $CDCl_3$) δ (ppm): 1.27 (s, 9H); 1.35 (d, 6H, *J* = 6.8 Hz); 1.52 (s, 9H); 4.27 (m, *1H*); 6.40 (s, *1H*); 7.68 (s, *1H*), 7.98 (s, *1H*). ^{13}C NMR (100 MHz, $CDCl_3$) δ (ppm): 20.3; 27.8; 27.9; 51.4; 81.8; 82.4; 109.0; 129.4; 143.0; 152.2; 157.4. LCMS *m/z* (ES+) = 353.1 $[M + H]^+$; 375.1 $[M + Na]^+$. Colorless oil. Yield: 95%.

tert-butyl *N*-({[(tert-butoxy)carbonyl]imino}(*1H*-pyrazol-1-yl)methyl)-*N*-butylcarbamate (GAc):

Alcohol used: *N*-butanol. The crude was purified by silica gel flash chromatography (PE/AcOEt 9/1). ^{1H} NMR (400 MHz, $CDCl_3$) *δ* (ppm): 0.90 (t, 3H, *J*= 7.2 Hz); 1.25 (s, 9H); 1.49 (s, 9H); 1.69 (m, 2H); 3.65 (m, 2H); 6.40 (s, *1H*); 7.67 (s, *1H*); 7.92 (s, *1H*). ^{13}C NMR (100 MHz, $CDCl_3$) *δ* (ppm): 13.6; 19.9; 27.3; 27.6; 27.8; 30.3; 48.6; 82.2; 82.4; 108.8; 129.8; 142.9; 152.4; 157.4. LCMS *m/z* (ES+) = 367.2 $[M + H]^+$; 389.2 $[M + Na]^+$; 705.3 [2M-1Boc artifact + Na]$^+$; 755.3 $[2M + Na]^+$. Yield: 95%.

tert-butyl *N*-({[(tert-butoxy)carbonyl]imino}(*1H*-pyrazol-1-yl)methyl)-*N*-(2-methylpropyl)carbamate (GAd):

Alcohol used: *i*-butanol. The crude was purified by silica gel flash chromatography (PE/AcOEt 9/1). ^{1H} NMR (400 MHz, $CDCl_3$) *δ* (ppm): 0.95 (d, 6H, *J*= 6.8 Hz); 1.23 (s, 9H); 1.47 (s, 9H); 2.10 (m, *1H*); 3.53 (d, 2H, *J*= 6.8 Hz); 6.39 (s, *1H*); 7.66 (s, *1H*); 7.89 (s, *1H*). ^{13}C NMR (100 MHz, $CDCl_3$) *δ* (ppm): 20.1; 27.5; 27.8; 28.1; 54.0; 55.8; 82.1; 82.5; 108.7; 129.9; 142.6; 152.3; 157.5. LCMS *m/z* (ES+) = 367.2 $[M + H]^+$; 389.2 $[M + Na]^+$; 705.3 [2M-1Boc artifact + Na]$^+$; 755.3 $[2M + Na]^+$. Colorless oil. Yield: 99%.

tert-butyl *N*-[(2E)-but-2-e*N*-1-yl]-*N*-({[(tert-butoxy)carbonyl]imino}(*1H*-pyrazol-1-yl)methyl)carbamate (GAe):

As reported in **Bioorganic and Medicinal Chemistry Letters**, **2017**, vol. 27, # 15, p. 3332 – 3336.

***N,N'*-Di-Boc-*N*-cyclopentyl-pyrazole-1-carboxamidine (GAf):**

Alcohol used: Cyclopentanol. The crude was purified by silica gel flash chromatography (PE/AcOEt 9/1). ^{1H} NMR (400 MHz, $CDCl_3$) δ (ppm): 1.30 (s, 9H); 1.53 (s, 9H); 1.73 (s, 6H); 1.95 (s, 2H); 4.12 (m, *1H*); 6.40 (s, *1H*); 7.67 (s, *1H*); 8.04 (s, *1H*). ^{13}C NMR (100 MHz, $CDCl_3$) δ (ppm): 23.5; 27.8; 27.9; 30.1; 60.3; 81.7; 82.4; 109.2; 129.2; 143.2. LCMS *m/z* (ES+) = 379.1 $[M + H]^+$; 401.1 = $[M + Na]^+$. White solid. Yield: 82%

tert-butyl *N*-[{[(tert-butoxy)carbonyl]imino}(*1H*-pyrazol-1-yl)methyl]-*N*-[(2E)-3,7-dimethylocta-2,6-die*N*-1-yl]carbamate (GAg):

Alcohol used: E-geraniol. The crude was purified by silica gel flash chromatography (PE/AcOEt 9/1). ^{1H} NMR (400 MHz, $CDCl_3$) *δ* (ppm): 1.27 (s, 9H); 1.48 (s, 9H); 1.54 (s, 3H); 1.58 (s, 3H); 1.62 (s, 3H); 1.96-2.00 (m, 4H); 4.29 (d, 2H, *J*= 6.8 Hz); 5.02 (m, *1H*); 5.36 (t, *1H, J*= 6.8 Hz);6.36 (s, *1H*); 7.64 (s, *1H*); 7.87 (s, *1H*). ^{13}C NMR (100 MHz, $CDCl_3$) *δ* (ppm): 26.3; 27.3; 27.5; 27.7; 28.0; 39.5; 46.4; 82.0; 82.4; 108.0; 108.7; 109.3; 118.3; 123.7; 124.0;129.6; 131.4; 140.7; 142.8; 143.0; 152.3; 157.3. LCMS *m/z* (ES+) = 447.0 $[M + H]^+$; 468.9 $[M + Na]^+$; 915.0 $[2M + Na]^+$. Colorless oil. Yield: 93%.

tert-butyl *N*-({[(tert-butoxy)carbonyl]imino}(*1H*-pyrazol-1-yl)methyl)-*N*-(2-methoxyethyl)carbamate (GAh):

Alcohol used: 2-methoxyethanol. The crude was purified by silica gel flash chromatography (PE/AcOEt 9/1). ^{1H} NMR (400 MHz, $CDCl_3$) δ (ppm): 1.27 (s, 9H); 1.51 (s, 9H); 3.29 (s, 3H); 3.67 (m, 2H); 3.93 (m, 2H); 6.40 (s, *1H*); 7.67 (s, *1H*); 7.95 (s, *1H*). ^{13}C NMR (100 MHz, $CDCl_3$) δ (ppm): 27.6; 27.8; 47.6; 58.3; 69.9; 82.2; 82.7; 108.5; 129.9; 142.9; 152.3; 157.3. LCMS *m/z* (ES+) = 369.1 $[M + H]^+$; 391.1 = $[M + Na]^+$. Colorless oil. Yield: 98 %

tert-butyl *N*-({[(tert-butoxy)carbonyl]imino}(*1H*-pyrazol-1-yl)methyl)-*N*-[2-(morpholin-4-yl)ethyl]carbamate (GAi):

Alcohol used: 4-(2-hydroxyethyl)morpholine. The crude was purified by silica gel flash chromatography (Et_2O/PE 6/4). ^{1H} NMR (400 MHz, $CDCl_3$) δ (ppm): 1.26 (s, 9H); 1.51 (s, 9H); 2.43 (m,4H); 2.65 (t, 2H, *J* = 5.6 Hz); 3,50 (m, 4H); 3.85 (m, 2H); 6.40 (s, *1H*); 7.66 (s, *1H*); 8.06 (s, *1H*). ^{13}C NMR (100 MHz, $CDCl_3$) δ (ppm): 27.6; 27.8; 44.8; 53.2; 56.7; 66.8; 82.1; 82.5; 108.3; 129.8; 142.6; 152.4; 157.5. LCMS *m/z* (ES+) = 424.3 $[M + H]^+$; 446.3 = $[M + Na]^+$. White solid. Yield: 96%.

***N*-({[(*tert*-butoxy)carbonyl]imino}(*1H*-pyrazol-1-yl)methyl)-*N*-[2-(methylsulfanyl)ethyl]carbamate (GAl):**

Alcohol used: 2-(methylthio)ethanol. The crude was purified by silica gel flash chromatography (PE/AcOET 95:5). ^{1H} NMR (400 MHz, $CDCl_3$) δ (ppm): 1.27 (s, 9H); 1.49 (s, 9H); 2.12 (s, 3H); 2.85 (m, 2H); 3.88 (t, *J* = 6.4 Hz, 2H); 6.41 (s, *1H*); 7.68 (s, *1H*); 8.00 (s, *1H*).^{13}C NMR (100 MHz, $CDCl_3$) δ (ppm): 15.6; 28.2; 28.3; 30.3; 53.1; 80.5; 81.0; 107.7; 123.1; 141.6; 150.6; 151.4; 162.3. LCMS *m/z* (ES+) = 407.1 $[M + Na]^+$. Colorless oil. Yield: 90%.

***tert*-butyl *N*-[2-(adamantan-1-yl)ethyl]-*N*-({[(*tert*-butoxy)carbonyl]imino}(*1H*-pyrazol-1-yl)methyl)carbamate (GAm):**

Alcohol used: 1-Adamantaneethanol. The crude was purified by silica gel flash chromatography (PE/AcOEt 95/5). ^{1H} NMR (400 MHz, $CDCl_3$) δ (ppm): 1.29 (m, 3H); 1.36 (s, 9H); 1.50 (s, 9H); 1.60 (m, 3H); 1.69 (m, 6H); 1.74 (m, 3H); 1.90 (m, 5H); 3.79 (t, *J* = 6.8 Hz, 2 H); 6.42 (s, *1H*); 7.78 (s, *1H*); 8.10 (s, *1H*).^{13}C NMR (100 MHz, $CDCl_3$) δ (ppm): 28.2; 28.3; 29.0; 32.4; 37.0; 37.5; 42.2; 47.2; 80.5; 81.0; 107.7; 124.3; 141.8; 150.5; 151.1; 162.4. LCMS *m/z* (ES+) = 473.2 $[M + H]^+$; 495.2 = $[M + Na]^+$. White solid. Yield: 86%.

***N,N'*-Di-Boc-*N*-methyl-pyrazole-1-carboxamidine (GAn)**

Alcohol used: methanol. The crude was purified by silica gel flash chromatography (PE/AcOEt 95/5). ^{1}H NMR (400 MHz, CDCl3) δ (ppm): 1.26 (s, 9H); 1.49 (s, 9H); 3.21 (s, 3H); 6.39 (s, 1H); 7.66 (s, 1H); 7.98 (s, 1H). ^{13}C NMR (100 MHz, CDCl3) δ (ppm): 27.63; 27.81; 35.53; 82.32; 82.57; 109.04; 129.76; 143.16; 152.41; 157.38. LCMS m/z (ES+) = 324.9 [M + H]+; 346.9 [M + Na]+ Yield: 95%

***N,N'*-Di-Boc-*N*-ethyl-pyrazole-1-carboxamidine (GAo)**

Alcohol used: ethanol. The crude was purified by silica gel flash chromatography (PE/AcOEt 95/5). ^{1}H NMR (400 MHz, CDCl3) δ (ppm): 1.27 (s, 9H); 1.28 (m, 3H); 1.50 (s, 9H); 3.73 (q, *J* = 6.8 Hz, 2H); 6.40 (s, 1H); 7.68 (s, 1H); 7.95 (s, 1H). ^{13}C NMR (100 MHz, CDCl3) δ (ppm): 13.34; 27.65; 27.83; 43.87; 82.25; 82.36; 108.86; 129.73; 142.94; 152.20; 157.43. LCMS m/z (ES+) = 339.0 [M + H]+; 361.0 [M + Na]+ Yield: 94%

6.3.19 General synthesis of monoguanylated diamine derivatives (87a-g):

tert-butyl *N*-{[(6-aminohexyl)amino]({[(tert-butoxy)carbonyl]imino})methyl}-*N*-(cyclopropylmethyl)carbamate (87a):

Starting materials: 1,6-diaminohexane and **61**. The crude was purified by silica gel flash chromatography (DCM/MeOH 9/1). ^{1}H NMR (600 MHz, $CDCl_3$) δ (ppm): 0.22 (m, 2H); 0.44 (m, 2H); 1.03 (m, 1H); 1.36 (m, 4H); 1.46 (s, 9H); 1.49 (s, 9H); 1.63 (m, 4H); 2.67 (t, *J* = 7.0 Hz, 2H); 3.28 (m, 2H); 3.52 (m, 2H). ^{13}C NMR (150 MHz, $CDCl_3$) δ (ppm): 3.5; 10.4; 26.5; 26.9; 28.2; 28.4; 28.6; 33.6; 42.0; 43.8; 52.1; 79.9; 82.5; 154.4; 157.7; 160.1; 164.4. LCMS *m/z* (ES+) = 413.3 $[M + H]^+$; 435.3 $[M + Na]^+$; 453.3 $[M + K]^+$. Colorless oil. Yield: 87%.

tert-butyl *N*-{[(8-aminooctyl)amino]({[(tert-butoxy)carbonyl]amino})methylidene}carbamate (87b):

Starting materials: 1,8-diaminooctane and 1,3-Bis(tert-butoxycarbonyl)-2-methyl-2-thiopseudourea. The crude was purified by silica gel flash chromatography (DCM/MeOH 9/1). ^{1}H NMR (600 MHz, $CDCl_3$) δ (ppm): 1.30 (m, 8H); 1.48 (s, 9H); 1.51 (s, 9H); 1.54 (m, 4H); 2.67 (t, *J* = 7.0 Hz, 2H); 3.38 (m, 2H). ^{13}C

NMR (150 MHz, $CDCl_3$) δ (ppm): 26.8; 28.0; 28.3; 29.6; 30.1; 33.8; 40.9; 42.2; 78.9; 83.0; 153.3; 156.2; 163.6. LCMS m/z (ES+) = 387.4 $[M + H]^+$; 409.4 $[M + Na]^+$. Colorless oil. Yield: 98%.

tert-butyl *N*-{[(8-aminooctyl)amino]({[(tert-butoxy)carbonyl]imino})methyl}-*N*-methylcarbamate (87c):

Starting materials: 1,8-diaminooctane and **GAn**. The crude was purified by silica gel flash chromatography (DCM/MeOH 9/1). ^1H NMR (600 MHz, $CDCl_3$) δ (ppm): 1.30 (m, 8H); 1.48 (s, 9H); 1.51 (s, 9H); 1.54 (m, 4H); 2.67 (t, J = 7.0 Hz, 2H); 3.06 (s, 3H); 3.38 (m, 2H). ^{13}C NMR (150 MHz, $CDCl_3$) δ (ppm): 26.8; 28.0; 28.3; 29.6; 30.1; 33.8; 37.9; 40.9; 42.2; 78.9; 83.0; 153.3; 156.2; 163.6. LCMS m/z (ES+) = 401.5 $[M + H]^+$; 423.4 $[M + Na]^+$. Colorless oil. Yield: 84%.

tert-butyl *N*-{[(8-aminooctyl)amino]({[(tert-butoxy)carbonyl]imino})ethyl}-*N*-ethylcarbamate (87d):

Starting materials: 1,8-diaminooctane and **GAn**. The crude was purified by silica gel flash chromatography (DCM/MeOH 9/1). ^1H NMR (600 MHz, $CDCl_3$) δ (ppm): 1.12 (t, J = 7.2 Hz, 3H); 1.30 (m, 8H); 1.48 (s, 9H); 1.51 (s, 9H); 1.54 (m, 4H); 2.67 (t, J = 7.0 Hz, 2H); 3.06 (s, 3H); 3.53 (q, J = 7.2 Hz, 2H). ^{13}C NMR (150 MHz, $CDCl_3$) δ (ppm): 12.7; 26.8; 28.0; 28.3; 29.6; 30.1; 33.8; 35.9; 40.9; 42.2; 78.9; 83.0; 153.3; 156.2; 163.6. LCMS m/z (ES+) = 415.5 $[M + H]^+$; 437.5 $[M + Na]^+$. Colorless oil. Yield: 70%.

tert-butyl *N*-{[(8-aminooctyl)amino]({[(tert-butoxy)carbonyl]imino})methyl}-*N*-(propan-2-yl)carbamate (87e):

Starting materials: 1,8-diaminooctane and **GAb**. The crude was purified by silica gel flash chromatography (DCM/MeOH 9/1). ^1H NMR (600 MHz, $CDCl_3$) δ (ppm): 1.18 (d, J = 6.4 Hz, 6H); 1.30 (m, 8H); 1.48 (s, 9H); 1.51 (s, 9H); 1.54 (m, 4H); 2.67 (t, J = 7.0 Hz, 2H); 3.38 (m, 2H); 3.63 (m, 1H). ^{13}C NMR (150 MHz, $CDCl_3$) δ (ppm): 19.8; 20.1; 26.8; 28.0; 28.3; 29.6; 30.1; 33.8; 40.9; 42.2; 48.9; 78.9; 83.0; 153.3; 156.2; 163.6. LCMS m/z (ES+) = 428.6 $[M + H]^+$; 451.6 $[M + Na]^+$. Colorless oil. Yield: 84%.

tert-butyl *N*-{[(8-aminooctyl)amino]({[(tert-butoxy)carbonyl]imino})methyl}-*N*-(but-2-en-1-yl)carbamate (87f):

Starting materials: 1,8-diaminooctane and **GAe**. The crude was purified by silica gel flash chromatography (DCM/MeOH 9/1). ^1H NMR (600 MHz, $CDCl_3$) δ (ppm): 1.30 (m, 8H); 1.48 (s, 9H); 1.51 (s, 9H); 1.54 (m, 4H); 1.76 (d, J = 6.4 Hz, 3H); 2.67 (t, J = 7.0 Hz, 2H); 3.38 (m, 2H); 3.63 (m, 1H); 4.15 (m, 2H); 5.48 (m, 1H); 5.63 (m, 1H). ^{13}C NMR (150 MHz, $CDCl_3$) δ (ppm): 17.8; 20.1; 26.8; 28.0; 28.3; 29.6; 30.1; 33.8; 41.2; 42.2; 43.3; 43.8; 78.9; 83.0; 126.5; 128.8; 153.3; 156.2; 163.6. LCMS m/z (ES+) = 441.6 $[M + H]^+$; 463.6 $[M + Na]^+$. Colorless oil. Yield: 75%.

***tert*-butyl *N*-[[(8-aminooctyl)amino]({[(*tert*-butoxy)carbonyl]imino})methyl]-*N*-(cyclopropylmethyl)carbamate (87g):**

To a stirred solution of 1,8-diaminooctane (3.47 mmol) in THF/MeOH 10/1 (17.0 mL), a solution of **61** (0.87 mmol) in THF (8.7 mL) was added dropwise through a syringe pump at room temperature over 16

h. The solvent was evaporated under reduced pressure and the crude product was purified by silica gel flash chromatography (AcOEt).[1]H NMR (400 MHz, $CDCl_3$) δ (ppm): 0.23 (m, 2H), 0.46 (m, 2H), 1.04 (m, 1H), 1.33 (m, 8H), 1.46 (s, 9H), 1.47 (s, 9H), 1.61 (m, 4H), 2.68 (t, 2H, J= 6.8 Hz), 3.31 (m, 2H), 3.55 (m, 2H), 4.66 (br, 1H), 8.06 (br, 1H). ^{13}C NMR (100 MHz, $CDCl_3$) δ (ppm): 3.5, 10.5, 26.6, 26.8, 28.1, 29.1, 33.2, 41.9, 43.8, 52.0, 78.8, 152.9, 158.0, 165.3. LCMS m/z (ES+) = 463.7 $[M + Na]^+$, 441.7 $[M + H]^+$. Colorless oil. Yield: 79%.

6.3.20 General synthesis of PMB-protected derivatives 88a-g:

To a stirred solution of triphosgene (0.31 mmol) in dry DCM (10.3 mL) under nitrogen atmosphere, dry DIPEA (162 μL) was added. The mixture was stirred at 0 °C and a solution of 4-methoxybenzylamine (40 μL) in dry DCM (10.3 mL) was added dropwise. The mixture was stirred at 0 °C for 10 min and then at room temperature for 30 min. When starting material disappeared, dry DIPEA (162 μL, 0.93 mmol) and a solution of **87a-g** (0.15 mmol) in dry DCM (1.2 mL) were added under nitrogen atmosphere. The mixture was stirred at room temperature for 16 h, then it was treated with $NaHCO_3$ s.s. and extracted three times with DCM. The combined organic phases were dried over Na_2SO_4, filtered and evaporated under reduced pressure. The oil obtained was purified through silica gel flash chromatography.

tert-butyl *N*-({[(tert-butoxy)carbonyl]imino}({[6-({[(4-methoxyphenyl)methyl]carbamoyl}amino)hexyl]amino})methyl)-*N*-(cyclopropylmethyl)carbamate (88a):

Starting material: **87a**. The crude product was purified through silica gel flash chromatography (AcOEt). ^{1}H NMR (600 MHz, $CDCl_3$) δ (ppm): 0.25 (m, 2H), 0.46 (m, 2H), 1.07 (m, 1H), 1.30 (m, 4H), 1.47 (s, 9H), 1.49 (s, 9H), 1.61 (m, 4H), 3.16 (m, 2H), 3.31 (m, 2H), 3.55 (m, 2H), 3.80 (s, 3H), 4.30 (m, 2H), 6.86 (d, 2H, J= 8.0 Hz), 7.22 (d, 2H, J= 8.0 Hz). ^{13}C NMR (150 MHz, $CDCl_3$) δ (ppm): 22.6, 26.7, 27.0, 28.2, 28.9, 29.3, 29.6, 30.0, 31.8, 43.8, 44.0, 52.1, 55.2, 113.9, 128.8, 131.1, 151.2, 158.0, 161.0. LCMS m/z (ES+) = 576.8 $[M + H]^+$, 598.7 $[M + Na]^+$. Colorless oil. Yield: 65%.

tert-butyl *N*-({[(tert-butoxy)carbonyl]amino}({[8-({[(4-methoxyphenyl)methyl]carbamoyl}amino)octyl]amino})methylidene)carbamate (88b):

Starting material: **87b**. The crude product was purified through silica gel flash chromatography (AcOEt/MeOH 98/2). ^{1}H NMR (600 MHz, $CDCl_3$) δ (ppm): 1.30 (m, 8H), 1.47 (s, 9H), 1.49 (s, 9H), 1.61 (m, 4H), 3.16 (m, 2H), 3.31 (m, 2H), 3.80 (s, 3H), 4.30 (m, 2H), 6.86 (d, 2H, J= 8.0 Hz), 7.22 (d, 2H, J= 8.0 Hz). ^{13}C NMR (150 MHz, $CDCl_3$) δ (ppm): 22.6, 26.7, 27.0, 28.2, 28.9, 29.3, 29.6, 30.0, 31.8, 44.0, 52.1, 55.2, 113.9, 128.8, 131.1, 151.2, 158.0, 161.0. LCMS m/z (ES+) = 550.7 $[M + H]^+$, 572.7 $[M + Na]^+$. Colorless oil. Yield: 60%.

tert-butyl *N*-({[(tert-butoxy)carbonyl]imino}({[8-({[(4-methoxyphenyl)methyl]carbamoyl}amino)octyl]amino})methyl)-*N*-methylcarbamate (88c):

Starting material: **87c**. The crude product was purified through silica gel flash chromatography (AcOEt). ^{1}H NMR (600 MHz, $CDCl_3$) δ (ppm): 1.30 (m, 8H), 1.47 (s, 9H), 1.49 (s, 9H), 1.61 (m, 4H), 3.03 (s, 1H), 3.18 (m, 2H), 3.31 (m, 2H), 3.80 (s, 3H), 4.30 (m, 2H), 6.86 (d, 2H, *J*= 8.0 Hz), 7.22 (d, 2H, *J*= 8.0 Hz). ^{13}C NMR (150 MHz, $CDCl_3$) δ (ppm): 22.6, 26.7, 27.0, 28.2, 28.9, 29.3, 29.6, 30.0, 31.8, 33.4, 44.0, 52.1, 55.2, 113.9, 128.8, 131.1, 150.7, 158.0, 161.0. LCMS *m/z* (ES+) = 564.7 $[M + H]^+$, 586.7 $[M + Na]^+$. Colorless oil. Yield: 62%.

tert-butyl *N*-({[(tert-butoxy)carbonyl]imino}({[8-({[(4-methoxyphenyl)methyl]carbamoyl}amino)octyl]amino})methyl)-*N*-ethylcarbamate (88d):

Starting material: **87d**. The crude product was purified through silica gel flash chromatography (AcOEt). ^{1}H NMR (600 MHz, $CDCl_3$) δ (ppm): 1.12 (t, *J* = 7.6 Hz, 3H), 1.30 (m, 8H), 1.47 (s, 9H), 1.49 (s, 9H), 1.61 (m, 4H), 3.16 (m, 2H), 3.31 (m, 2H), 3.51 (q, *J* = 7.6 Hz, 2H), 3.80 (s, 3H), 4.30 (m, 2H), 6.86 (d, 2H, *J*= 8.0 Hz), 7.22 (d, 2H, *J*= 8.0 Hz). ^{13}C NMR (150 MHz, $CDCl_3$) δ (ppm): 12.7, 22.6, 26.7, 27.0, 28.2, 28.9, 29.3, 29.6, 30.0, 31.8, 36,3, 44.0, 52.1, 55.2, 113.9, 128.8, 131.1, 151.2, 158.0, 161.0. LCMS *m/z* (ES+) = 578.8 $[M + H]^+$, 600.8 $[M + Na]^+$. Colorless oil. Yield: 70%.

tert-butyl *N*-({[(tert-butoxy)carbonyl]imino}({[8-({[(4-methoxyphenyl)methyl]carbamoyl}amino)octyl]amino})methyl)-*N*-(propan-2-yl)carbamate (88e):

Starting material: **87e**. The crude product was purified through silica gel flash chromatography (AcOEt). ^{1}H NMR (600 MHz, $CDCl_3$) δ (ppm): 1.20 (d, *J* = 7.0 Hz, 6H), 1.30 (m, 8H), 1.47 (s, 9H), 1.49 (s, 9H), 1.61 (m, 4H), 3.16 (m, 2H), 3.31 (m, 2H), 3.68 (m, 1H), 3.80 (s, 3H), 4.30 (m, 2H), 6.86 (d, 2H, *J*= 8.0 Hz), 7.22 (d, 2H, *J*= 8.0 Hz). ^{13}C NMR (150 MHz, $CDCl_3$) δ (ppm): 20.7, 22.6, 26.7, 27.0, 28.2, 28.9, 29.3, 29.6, 30.0, 31.8, 44.0, 49.1, 52.1, 55.2, 113.9, 128.8, 131.1, 151.2, 158.0, 161.0. LCMS *m/z* (ES+) = 592.7 $[M + H]^+$, 614.7 $[M + Na]^+$. Colorless oil. Yield: 60%.

tert-butyl *N*-(but-2-en-1-yl)-*N*-({[(tert-butoxy)carbonyl]imino}({[8-({[(4-methoxyphenyl)methyl]carbamoyl}amino)octyl]amino})methyl)carbamate (88f):

Starting material: **87f**. The crude product was purified through silica gel flash chromatography (AcOEt). ^{1}H NMR (600 MHz, $CDCl_3$) δ (ppm): 1.17 (d, *J* = 7.2 Hz, 3H), 1.30 (m, 8H), 1.47 (s, 9H), 1.49 (s, 9H), 1.61 (m, 4H), 3.16 (m, 2H), 3.31 (m, 2H), 3.80 (s, 3H), 4.02 (m, 2H), 4.30 (m, 2H), 5.62 (m, 1H), 5.66 (m, 1H), 6.86 (d, 2H, *J*= 8.0 Hz), 7.22 (d, 2H, *J*= 8.0 Hz). ^{13}C NMR (150 MHz, $CDCl_3$) δ (ppm): 22.6, 26.7, 27.0, 28.2, 28.9, 29.3, 29.6, 30.0, 31.8, 42.7, 44.0, 52.1, 55.2, 113.9, 125.6, 126.7, 128.8, 131.1, 151.2, 158.0, 161.0. LCMS *m/z* (ES+) = 603.8 $[M + H]^+$, 626.8 $[M + Na]^+$. Colorless oil. Yield: 68%.

tert-butyl *N*-({[(*tert*-butoxy)carbonyl]imino}({[8-({[(4-methoxyphenyl)methyl]carbamoyl}amino)octyl]amino})methyl)-*N*-(cyclopropylmethyl)carbamate (88g):

Starting material: **87g**. The crude product was purified through silica gel flash column chromatography (AcOEt). ^{1}H NMR (600 MHz, $CDCl_3$) δ (ppm): 0.25 (m, 2H), 0.46 (m, 2H), 1.07 (m, 1H), 1.30 (m, 4H), 1.47 (s, 9H), 1.49 (s, 9H), 1.61 (m, 4H), 3.16 (m, 2H), 3.31 (m, 2H), 3.55 (m, 2H), 3.80 (s, 3H), 4.30 (m, 2H), 6.86 (d, 2H, J= 8.0 Hz), 7.22 (d, 2H, J= 8.0 Hz). ^{13}C NMR (150 MHz, $CDCl_3$) δ (ppm): 3.5, 10.5, 14.0, 22.6, 26.7, 27.0, 28.2, 28.9, 29.3, 29.6, 30.0, 31.8, 43.8, 44.0, 52.1, 55.2, 113.9, 128.8, 131.1, 151.2, 158.0, 161.0. LCMS m/z (ES+) = 604.4 $[M + H]^+$, 626.4 $[M + Na]^+$. Colorless oil. Yield: 70%.

6.3.21 General synthesis for final Boc-cleavage

To a solution of the properly Boc-protected compound (0.02 mmol) in DCM (1.7 mL), freshly distilled TFA (final concentration 20%, 300 μL) was added. The reaction flask was sealed and the mixture was stirred at room temperature for 5-7 h. Then the mixture was treated with toluene and methanol and evaporated under reduced pressure to remove TFA residue. The crude was treated with PE and DCM, then decanted, and the solvents were pipetted off. This procedure was repeated several times until reaching the desired grade of purity of final compounds.

1,3-bis(8-carbamimidamidooctyl)-1,3-bis({8-[N'-(cyclopropylmethyl)carbamimidamido]octyl})urea trifluoroacetate salt (1):

Starting material **75.** ^{1}H NMR (400 MHz, CD_3OD): δ 0.26 (m, 4 H); 0.61 (m, 4 H); 1.06 (m, 2 H); 1.31 (m, 32 H); 1.51 (m, 8 H); 1.56 (m, 8 H); 3.05 (d, J = 6.8 Hz, 4 H); 3.16 (m, 12 H); 3.30 (m, 4 H). ^{13}C NMR (100 MHz, CD_3OD): δ 2.4; 9.5; 26.2; 26.5; 27.5; 28.4; 28.4; 28.8; 28.9; 29.2; 41.0; 41.1; 45.8; 46.9; 47.1; 47.3; 47.5; 47.7; 47.9; 48.1; 155.6; 165.4. LC-MS m/z (ES+) = 212.1 $[M + 4 H]^{4+}$; 282.5 $[M + 3 H]^{3+}$; 423.1 $[M + 2 H]^{2+}$; 845.8 $[M + H]^+$. Yield**:** quantitative.

1,3,3-tris(8-carbamimidamidooctyl)-1-{8-[*N'*-(cyclopropylmethyl)carbamimidamido]octyl}urea trifluoroacetate salt (39):

Starting material **80**. ^{1}H NMR (400 MHz, CD_3OD) δ (ppm): 0.28 (m, 2H); 0.59 (m, 2H); 1.06 (m, 1H); 1.33 (m, 32H); 1.52 (m, 8H); 1.59 (m, 8H); 3.06 (d, 2H, J = 6.8 Hz); 3.16 (m, 16H). ^{13}C NMR (100 MHz, CD3OD) δ (ppm): 2.4, 9.5, 26.2, 26.5, 27.5, 28.5, 28.8, 28.9, 41.0, 41.1, 45.8, 155.9, 157.2, 165.8. LCMS m/z (ES+) = m/z (ES+) = 792.2 $[M + H]^+$; 396.4 $[M + 2H]^{2+}$; 264.7 $[M + 3H]^{3+}$; 198.6 $[M + 4H]^{4+}$. Colorless oil. Yield: quantitative.

1,3-bis(7-carbamimidamidoheptyl)-1,3-bis({7-[*N'*-(cyclopropylmethyl)carbamimidamido]heptyl})urea trifluoroacetate salt (41):

Starting material: **64a**. ^{1}H NMR (400 MHz, CD_3OD) δ (ppm): 0.31 (m, 4H); 0.62 (m, 4H); 1.10 (m, 2H); 1.40 (m, 24H); 1.56 (m, 8H); 1.63 (m, 8H); 3.09 (d, 4H, J= 7.2 Hz); 3.19 (m, 16H). ^{13}C NMR (CD_3OD) δ (ppm): 2.5; 9.5; 26.0; 26.5; 27.5; 28.3; 28.8; 28.9; 29.2; 41.0; 41.1; 44.2, 46.9; 47.1; 48.1; 151.0; 155.6; 161.0; 165.4. LCMS m/z (ES+) = 198.2 $[M + 4H]^{4+}$, 264.0 $[M + 3H]^{3+}$, 395.5 $[M + 2H]^{2+}$. Yield: quantitative.

1,3-bis(9-carbamimidamidononyl)-3-{9-[*N'*-(cyclopropylmethyl)carbamimidamido]nonyl}-1-{8-[*N'*-(cyclopropylmethyl)carbamimidamido]octyl}urea trifluoroacetate salt (42):

Starting material: **64b**. ^{1}H NMR (100 MHz, CD_3OD) δ (ppm): 0.28 (m, 4H); 0.61 (m, 4H); 1.12 (m, 2H); 1.41 (m, 24H); 1.55 (m, 8H); 1.65 (m, 8H); 3.12 (d, 4H, *J*= 7.2 Hz); 3.23 (m, 16H). ^{13}C NMR (100 MHz, CD_3OD) δ (ppm): 2.3; 9.6; 26.0; 26.6; 27.5; 28.3; 28.8; 29.0; 29.3; 41.0; 41.3; 44.2, 47.0; 47.2; 48.1; 151.0; 155.7; 161.1; 165.4. LCMS m/z (ES+) = 223.3 $[M + 4H]^{4+}$, 297.4 $[M + 3H]^{3+}$, 444.7 $[M + 2H]^{2+}$. Yield: quantitative.

1,3-bis(6-carbamimidamidohexyl)-1,3-bis({8-[*N'*-(cyclopropylmethyl)carbamimidamido]octyl})urea trifluoroacetate salt (43):

Starting material: **72a**. ^{1}H NMR (400 MHz, CD_3OD) δ (ppm): 0.27 (m, 4H); 0.58 (m, 4H); 1.06 (m, 2H); 1.30 (m, 26H); 1.53-1.51-1.55 (m, 8H); 1.54-1.60 (overlapped, m, 8H); 3.06 (d, 4H, *J* = 7.2 Hz); 3.16 (m, 16H). ^{13}C NMR (100 MHz, CD_3OD) δ (ppm): 2.4; 9.5; 26.0; 26.2; 26.5; 27.4; 27.5; 28.4; 28.5; 28.8; 28.9; 41.0; 45.8; 156.0; 157.2; 161.6; 165.8. LCMS *m/z* (ES+) = 264.0 $[M + 3H]^{3+}$; 395.5 $[M + 2H]^{2+}$; 790.1 $[M + H]^{+}$. Colorless oil. Yield: quantitative.

1,3-bis(8-carbamimidamidooctyl)-1,3-bis({6-[*N'*-(cyclopropylmethyl)carbamimidamido]hexyl})urea trifluoroacetate salt (44):

Starting material: **72b**. ^{1}H NMR (400 MHz, CD_3OD) δ (ppm): 0.27 (m, 4H); 0.58 (q, 4H, *J* = 5.2 Hz); 1.06 (m, 2H); 1.31 (m, 26H); 1.52-1.55 (m, 8H); 1.54-1.59 (overlapped, m, 8H); 3.06 (d, 4H, *J* = 6.8 Hz); 3.16 (m, 16H). ^{13}C NMR (100 MHz, CD_3OD) δ (ppm): 2.4; 9.5; 26.0; 26.2; 26.5; 27.4; 27.5; 28.4; 28.5; 28.8; 28.9; 41.0; 45.8; 156.0; 157.2; 161.6; 165.8. LCMS *m/z* (ES+) = 264.0 $[M + 3H]^{3+}$; 395.5 $[M + 2H]^{2+}$; 790.1 $[M + H]^{+}$. Colorless oil. Yield: quantitative.

1-(6-carbamimidamidohexyl)-3-(8-carbamimidamidooctyl)-1,3-bis({8-[*N'*-(cyclopropylmethyl)carbamimidamido]octyl})urea trifluoroacetate salt (45):

Starting material: **72c**. ^{1}H NMR (400 MHz, CD_3OD) δ (ppm): 0.28 (m, 4H); 0.58 (m, 4H); 1.06 (m, 2H); 1.32 (m, 28H); 1.52-1.56 (m, 8H); 1.55-1.59 (overlapped, m, 8H); 3.06 (d, 4H, *J* = 6.8 Hz); 3.16 (m, 16H). ^{13}C NMR (100 MHz, CD_3OD) δ (ppm): 2.4; 9.5; 26.0; 26.2; 26.5; 27.5; 28.3; 28.4; 28.8; 28.9; 40.9; 41.0; 41.1; 45.8; 156.0; 157.2; 161.3; 165.8. LCMS *m/z* (ES+) = 273.3 $[M + 3H]^{3+}$; 409.4 $[M + 2H]^{2+}$; 817.7 $[M + H]^{+}$; 839.7 $[M + Na]^{+}$. Colorless oil. Yield: quantitative.

1,3-bis(8-carbamimidamidooctyl)-1-{6-[N'-(cyclopropylmethyl)carbamimidamido]hexyl}-3-{8-[N'-(cyclopropylmethyl)carbamimidamido]octyl}urea trifluoroacetate salt (46):

Starting material: **72d**. ^{1}H NMR (400 MHz, CD_3OD) *δ* (ppm): 0.28 (m, 4H); 0.59 (m, 4H); 1.07 (m, 2H); 1.36 (m, 28H); 1.53 (m, 8H); 1.59 (m, 8H); 3.06 (d, 2H, *J* = 6.8 Hz); 3.13-3.21 (m, 16H).^{13}C NMR (100 MHz, CD_3OD) *δ* (ppm): 2.6; 9.7; 26.1; 26.4; 26.6; 27.5; 28.3; 28.5; 28.9; 29.0; 41.1; 41.3; 41.4; 45.9; 156.2; 157.4; 161.4; 165.9. LCMS *m/z* (ES+) = 205.1 $[M + 4H]^{4+}$;273.2 $[M + 3H]^{3+}$; 409.3 $[M + 2H]^{2+}$, 817.7 $[M + H]^{+}$. Colorless oil. Yield: quantitative.

1,3-bis(8-azidooctyl)-1,3-bis(8-carbamimidamidooctyl)urea trifluoroacetate salt (48a):

Starting material: **73**. ^{1}H NMR (600 MHz, CD_3OD) δ (ppm): 1.35 (m, 32H); 1.51-1.54 (m, 8H); 1.55-1.61 (m, 12H); 3.16 (m, 12H); 3.26 (m, 4H). ^{13}C NMR (150 MHz, CD_3OD) δ (ppm): 26.2; 26.3; 26.4; 26.5; 27.4; 27.5; 28.4; 28.7; 28.8; 28.9; 29.0; 40.9; 50.9; 156.0; 157.6; 165.9. LCMS m/z (ES+) = 235.9 $[M + 3H]^{3+}$; 353.4 $[M + 2H]^{2+}$; 705.8 $[M + H]^{+}$. Colorless oil. Yield: quantitative.

1,3-bis(8-azidooctyl)-1,3-bis({8-[N'-(cyclopropylmethyl)carbamimidamido]octyl})urea trifluoroacetate salt (48b):

Starting material **76.** ^{1}H NMR (600 MHz, CD_3OD) δ (ppm): 0.27 (q, J = 4.8 Hz, 4H); 0.59 (q, J = 4.8 Hz, 4H); 1.08 (m, 2H); 1.33 (m, 32H); 1.52 (t, J = 6.6 Hz, 8H); 1.59 (t, J = 6.5 Hz, 8H); 3.05 (d, J = 7.8 Hz, 4H); 3.14 (m, 12H); 3.27 (t, J = 8 Hz, 4H). ^{13}C NMR (150 MHz, CD_3OD) δ (ppm): 3.1; 8.9; 26.7; 27.1; 27.3, 27.4; 29.3; 29.5; 29.8; 31.6; 41.0; 45.3; 47.6; 159.3; 163.6. LCMS m/z (ES+) = 407.3 $[M + 2H]^{2+}$; 813.9 $[M + H]^{+}$. Colorless oil. Yield: quantitative.

1,3-bis(8-carbamimidamidooctyl)-1,3-bis[8-(N'-propylcarbamimidamido)octyl]urea trifluoroacetate salt (47a):

Starting material: **74a**. ^{1}H NMR (400 MHz, CD_3OD) δ (ppm): 0.98 (t, 6H, J= 7.2 Hz); 1.36 (m, 32H); 1.50-1.54 (m, 8H); 1.57-1.64 (m, 12H); 3.13-3.20 (m, 20H). ^{13}C NMR (100 MHz, CD_3OD) δ (ppm): 21.8; 26.2; 26.5; 27.5; 28.4; 28.8; 41.0; 41.0; 42.7; 156.0; 157.2; 165.8. LCMS m/z (ES+) = 274.0 $[M + 3H]^{3+}$; 411.6 $[M + 2H]^{2+}$; 822.2 $[M + H]^{+}$. Colorless oil. Yield: quantitative.

1,3-bis(8-carbamimidamidooctyl)-1,3-bis({8-[N'-(propan-2-yl)carbamimidamido]octyl})urea trifluoroacetate salt (47b):

Starting material: **74b**. ^{1}H NMR (400 MHz, CD_3OD) δ (ppm): 1.23 (d, 12H, J = 6.4 Hz); 1.30 (m, 32H); 11.50-1.55 (m, 8H); 1.54-1.57 (overlapped, m, 8H); 3.16 (m, 16H); 3.73 (m, 2H). ^{13}C NMR (100 MHz, MeOD) δ (ppm): 21.2; 26.1; 26.2; 26.5; 27.5; 28.3; 28.4; 28.8; 28.9; 40.9; 41.0; 43.4; 46.8; 155.1; 157.4; 165.8. LCMS m/z (ES+) = 274.7 $[M + 3H]^{3+}$; 411.6 $[M + 2H]^{2+}$, 822.1 $[M + H]^{+}$. Colorless oil. Yield: quantitative.

1,3-bis[8-(N'-butylcarbamimidamido)octyl]-1,3-bis(8-carbamimidamidooctyl)urea trifluoroacetate salt (47c):

Starting material: **74c**. ^{1}H NMR (400 MHz, CD_3OD) δ (ppm): 0.97 (t, 6H, J= 7.2 hz), 1.36-1.44 (m, 32H), 1.49-1.61 (24H), 3.13-3.21 (m, 20H).^{13}C NMR (100 MHz, CD_3OD) δ (ppm): 22.8; 25.0; 26.2; 26.5; 26.8; 27.5; 28.4; 28.8; 29.0; 41.0; 43.0; 156.0; 157.2; 165.8. LCMS m/z (ES+) = 283.8 $[M + 3H]^{3+}$; 425.2 $[M + 2H]^{2+}$. Colorless oil. Yield: quantitative.

1,3-bis(8-carbamimidamidooctyl)-1,3-bis({8-[N'-(2-methylpropyl)carbamimidamido]octyl})urea trifluoroacetate salt (47d):

Starting material: **74d**. ^{1}H NMR (400 MHz, MeOD) δ = 0.97 (d, 12H, J= 6.4 Hz); 1.30-1.37 (m, 32H); 1.51-1.55 (m, 8H); 1.56-1.61 (m, 8H); 1.86 (m, 2H); 3.01 (d, 4H, J= 6.8 Hz); 3.13-3.21 (m, 16H). ^{13}C

NMR (100 MHz, CD_3OD) δ (ppm): 18.5; 18.8; 26.2; 26.5; 27.5; 28.0; 28.4; 28.8; 41.0; 156.2; 157.3; 165.7. LCMS m/z (ES+) = 283.8 $[M + 3H]^{3+}$; 425.2 $[M + 2H]^{2+}$. Colorless oil. Yield: quantitative.

1,3-bis(8-{N'-[(2E)-but-2-en-1-yl]carbamimidamido}octyl)-1,3-bis(8-carbamimidamidooctyl)urea trifluoroacetate salt (47e):

Starting material: **74e**. ^{1}H NMR (400 MHz, CD_3OD) δ (ppm): 1.36 (m, 32H); 1.53 (m, 8H); 1.59 (m, 8H); 1.73 (t, 6H, J= 6.4 Hz); 3.13-3.20 (m, 16H); 3.76 (d, 4H, , J= 5.6 Hz); 5.46-5.53 (m, 2H); 5.71-5.79 (m, 2H). ^{13}C NMR (100 MHz, CD_3OD) δ (ppm): 16.3; 26.2; 26.6; 27.5; 28.4; 28.4; 28.9; 29.0; 41.0; 41.1; 42.5; 124.9; 128.6; 155.8; 157.5; 165.8. LCMS m/z (ES+) = 282.6 $[M + 3H]^{3+}$; 423.3 $[M + 2H]^{2+}$; 845.7 $[M + H]^+$. Colorless oil. Yield: quantitative.

1,3-bis(8-carbamimidamidooctyl)-1,3-bis[8-(N'-cyclopentylcarbamimidamido)octyl]urea trifluoroacetate salt (47f)

Starting material: **74f**. ^{1}H NMR (400 MHz, CD_3OD) δ (ppm): 1.30 (m, 32H); 1.52-1.60 (m, 16H); 1.65 (m, 8H); 1.76 (m, 4H); 1.97-2.03 (m, 4H); 3.17 (m, 16H); 3.86 (m, 2H). ^{13}C NMR (100 MHz, CD_3OD) δ (ppm): 22.9; 26.2; 26.5; 27.5; 28.4; 28.5; 28.8; 31.9; 40.9; 45.8; 155.6; 157.2; 163.3; 165.8. LCMS m/z (ES+) = 292.0 $[M + 3H]^{3+}$; 437.6 $[M + 2H]^{2+}$, 873.2 $[M + H]^+$. Colorless oil. Yield: quantitative.

1,3-bis(8-carbamimidamidooctyl)-1,3-bis(8-{N'-[(2E)-3,7-dimethylocta-2,6-dien-1-yl]carbamimidamido}octyl)urea trifluoroacetate salt (47g):

Starting material:**74g**. ^{1}H NMR (400 MHZ, CD_3OD) δ (ppm): 1.36 (m, 32H); 1.48-1.64 (m, 8H); 1.56-1.62 (overlapped s, m, 20H); 1.71 (s, 6H); 1.84 (m, 4H); 2.10 (m, 4H); 3.13-3.20 (m, 16H); 3.83 (d, 2H, J= 6.8 Hz); 5.28 (m, 2H). ^{13}C NMR (100 MHz, CD_3OD) δ (ppm): 24.6; 26.2; 26.5; 27.5; 28.3; 28.4; 29.0; 38.9; 41.0; 118.5; 134.4; 137.5; 140.3; 156.1; 157.2; 161.3; 165.8. LCMS m/z (ES+) = 337.3 $[M + 3H]^{3+}$; 505.6 $[M + 2H]^{2+}$. Colorless oil. Yield: quantitative.

1,3-bis(8-carbamimidamidooctyl)-1,3-bis({8-[N'-(2-methoxyethyl)carbamimidamido]octyl})urea trifluoroacetate salt (47h):

Starting material: **74h**. ^{1}H NMR (400 MHz, CD_3OD) δ (ppm): 1.35 (m, 32H); 1.50 (m, 8H); 1.54 (m, 8H); 3.16 (m, 16H); 3.36-3.39 (m, 4H); 3.39 (overlapped, s, 6H); 3.52 (t, 4H, J = 5.2 Hz). ^{13}C NMR (100 MHz, CD_3OD) δ (ppm): 26.2; 26.6; 27.5; 28.3; 28.4; 28.8; 28.9; 40.9; 41.2; 41.4; 57.7; 78.7; 156.5; 1572; 165.8. LCMS m/z (ES+) = 285.4 $[M + 3H]^{3+}$; 427.5 $[M + 2H]^{2+}$; 876.2 $[M + Na]^+$. Colorless oil. Yield: quantitative.

1,3-bis(8-carbamimidamidooctyl)-1,3-bis(8-{N'-[2-(morpholin-4-yl)ethyl]carbamimidamido}octyl)urea trifluoroacetate salt (47i):

Starting material: **74i**. ^{1}H NMR (400 MHz, CD_3OD) δ (ppm): 1.33 (m, 32H); 1.52 (t, 8H, J = 7.3 Hz); 1.58 (m, 8H); 3.13-3.17 (m, 12H); 3.15-3.21 (overlapped, m, 8H); 3.20-3.25 (overlapped, m, 8H); 3.63 (m, 4H); 3.63 (m, 8H). ^{13}C NMR (100 MHz, CD_3OD) δ (ppm): 27.1; 27.3; 29.3; 29.5; 41.1; 41.8; 43.7; 53.2;

54.9; 66.8; 157.2; 163.6. LCMS m/z (ES+) = 241.8 $[M + 4H]^{4+}$; 322.1 $[M + 3H]^{3+}$; 482.6 $[M + 2H]^{2+}$; 964.2 $[M + H]^{+}$Colorless oil. Yield: quantitative.

1,3-bis(8-carbamimidamidooctyl)-1,3-bis(8-{N'-[2-(methylsulfanyl)ethyl]carbamimidamido}octyl)urea trifluoroacetate salt (47l):

Starting material: **74l**. ^{1}H NMR (600 MHz, CD_3OD) δ (ppm): 1.33 (m, 32H); 1.48-1.54 (m, 8H); 1.53-1.59 (overlapped, m, 8H); 2.11 (s, 6H); 2.68 (m, 4H); 3.16 (m, 20H); 3.87 (m, 4H). ^{13}C NMR (150 MHz, CD_3OD) δ (ppm): 15.6; 27.1; 27.3; 27.4; 29.3; 29.5; 30.3; 41.0; 41.1; 44.8; 47.6; 157.3; 158.2; 164.0. LCMS m/z (ES+) = 222.3 $[M + 4H]^{4+}$; 296.1 $[M + 3H]^{3+}$; 443.4 $[M + 2H]^{2+}$; 885.7 $[M + H]^{+}$Colorless oil. Yield: quantitative.

1,3-bis(8-{N'-[2-(adamantan-1-yl)ethyl]carbamimidamido}octyl)-1,3-bis(8-carbamimidamidooctyl)urea trifluoroacetate salt (47m):

Starting material: **47m**. ^{1}H NMR (600 MHz, 1CD_3OD) δ (ppm): 1.33 (m, 48H); 1.54 (m, 24H); 1.68 (m, 8H); 1.76 (m, 8H); 3.16 (m, 20H). ^{13}C NMR (150 MHz, CD_3OD) δ (ppm): 27.1; 27.3; 27.9; 28.9; 29.3; 29.5; 36.1; 37.2; 37.4; 41.1; 42.2; 47.6; 157.3; 158.0; 162.1. LCMS m/z (ES+) = 266.6 $[M + 4H]^{4+}$; 354.7 $[M + 3H]^{3+}$; 531.5 $[M + 2H]^{2+}$ Colorless oil. Yield: quantitative.

{6-[N'-(cyclopropylmethyl)carbamimidamido]hexyl}urea trifluoroacetate salt (49)

Starting material **88a**. ^{1}H NMR (600 MHz, CD_3OD) δ (ppm): 0.27 (q, J = 4.8 Hz, 2H); 0.59 (q, J = , 2H; 1.06 (m, 1H); 1.31 (m, 4H); 1.50 (m, 2H); 1.60 (m, 2H); 3.05 (d, J = 7.8 Hz, 2H); 3.10 (t, J = 7.2 Hz, 2H); 3.19 (t, J = 7.2 Hz, 2H). ^{13}C NMR (150 MHz, CD_3OD) δ (ppm): 3.6, 10.2, 26.2, 26.6, 27.5, 28.4, 29.0, 40.3, 41.1, 46.8, 159.3, 162.3. . LCMS m/z (ES+) = 256.1 $[M + H]^{+}$. Colorless oil. Yield: quantitative.

[8-(carbamoylamino)octyl]urea trifluoroacetate salt (50)

Starting material **88b**. ^{1}H NMR (600 MHz, CD_3OD) δ (ppm): 1.36 (m, 8H); 1.48 (m, 2H); 1.58 (m, 2H); 3.08 (t, J = 6.5 Hz, 2H); 3.16 (t, J = 6.6 Hz, 2H). ^{13}C NMR (150 MHz, CD_3OD) δ (ppm): 27.2, 27.3, 29.3, 29.5, 40.3, 41.1, 157.3, 163.3.LCMS m/z (ES+) = 230.2 $[M + H]^{+}$. Colorless oil. Yield: quantitative.

[8-(*N'*-methylcarbamimidamido)octyl]urea trifluoroacetate salt (51)

Starting material **88c**. ^{1}H NMR (600 MHz, CD_3OD) δ (ppm): 1.36 (m, 8H); 1.47 (m, 2H); 1.58 (m, 2H); 2.84 (s, 3H); 3.05 (d, J = 7.2 Hz, 2H); 3.16 (t, J = 7.2 Hz, 2H); 3.19 (t, J = 7.2 Hz, 2H). ^{13}C NMR (150 MHz, CD_3OD) δ (ppm): 27.2, 27.3, 29.3, 29.5, 38.7, 40.3, 41.1, 157.3, 163.3. LCMS m/z (ES+) = 244.4 $[M + H]^{+}$. Colorless oil. Yield: quantitative.

[8-(*N'*-ethylcarbamimidamido)octyl]urea trifluoroacetate salt (52)

Starting material **88d**. ^{1}H NMR (600 MHz, CD_3OD) δ (ppm): 1.21 (t, J = 7.2 Hz, 3H); 1.36 (m, 8H); 1.48 (m, 2H); 1.59 (m, 2H); 3.06 (t, J = 7.2 Hz, 2H); 3.17 (t, J = 7.2 Hz, 2H); 3.23 (q, J = 7.2 Hz, 2H). ^{13}C NMR (150 MHz, CD_3OD) δ (ppm): 14.6, 27.2, 27.3, 29.3, 29.5, 39.2, 40.3, 41.1, 157.3, 163.3. LCMS m/z (ES+) = 258.3 $[M + H]^{+}$. Colorless oil. Yield: quantitative.

{8-[N'-(propan-2-yl)carbamimidamido]octyl}urea trifluoroacetate salt (53)

Starting material **88e**. ^{1}H NMR (600 MHz, CD_3OD) δ (ppm): 1.22 (d, J = 6.6 Hz, 6H); 1.36 (m, 8H); 1.48 (m, 2H); 1.59 (m, 2H); 3.08 (t, J = 7.2 Hz, 2H); 3.18 (t, J = 7.2 Hz, 2H); 3.72 (m, 2H). ^{13}C NMR (150 MHz, CD_3OD) δ (ppm): 22.8, 27.2, 27.3, 29.3, 29.5, 40.3, 41.1, 47.1, 157.3, 163.3. LCMS m/z (ES+) = 272.1 $[M + H]^+$. Colorless oil. Yield: quantitative.

(8-{N'-[(2E)-but-2-en-1-yl]carbamimidamido}octyl)urea trifluoroacetate salt (54)

Starting material **88f**. ^{1}H NMR (600 MHz, CD_3OD) δ (ppm): 1.37 (m, 8H); 1.47 (m, 2H); 1.58 (m, 2H); 1.72 (d, J = 5.8 Hz, 2H); 3.08 (t, J = 7.2 Hz, 2H); 3.17 (t, J = 7.2 Hz, 2H); 3.74 (m, 2H); 5.49 (m, 1H); 5.73 (m, 1H).^{13}C NMR (150 MHz, CD_3OD) δ (ppm): 15.5, 27.2, 27.3, 29.3, 29.5, 40.3, 41.1, 44.7, 128.1, 128.4, 157.3, 163.3. LCMS m/z (ES+) = 284.2 $[M + H]^+$. Colorless oil. Yield: quantitative.

{8-[N'-(cyclopropylmethyl)carbamimidamido]octyl}urea trifluoroacetate salt (**20**)

Starting material: **88g**. ^{1}H NMR (600 MHz, CD_3OD) δ (ppm): 0.28 (m, 2H), 0.60 (m, 2H), 1.07 (m, 1H), 1.37 (m, 8H), 1.48 (m, 2H), 1.60 (m, 2H), 3.06 (d, 2H, J= 6.8 Hz), 3.09 (m, 2H), 3.19 (t, 2H, J= 7.2 Hz). ^{13}C NMR (150 MHz, CD_3OD) δ (ppm): 3.6, 10.0, 26.2, 26.6, 27.5, 28.4, 29.0, 41.0, 41.4, 42.8, 45.8, 46.9, 155.9, 157.2, 165.8. m/z (ES+) = 284.3 $[M + H]^+$. Colorless oil. Yield: quantitative.

6.3.22 Synthesis of 1,3-Bis(8-carbamimidamidooctyl)-1,3-bis({8-[*N'*-(cyclopropylmethyl)carbamimidamido]octyl})urea Hydrochloride Salt (40):

To a solution of **1** (0.035 mmol) in CH_3OH (5.8 mL), Amberlite IRA-400 Chloride-form (137.0 mg) was added and the reaction mixture was stirred through a rocker shaker at room temperature for 24h. Then, the mixture was diluted with CH_3OH and filtered through a 0.45 μm PTFE filter. The filtrate was evaporated *under vacuum* to furnish the desired product as a pale yellow oil. ^{1}H NMR (400 MHz, CD_3OD) δ (ppm): 0.31 (d, J = 5.0 Hz, 4H), 0.62 (d, J = 7.6 Hz, 4H), 1.09 (p, J = 5.6 Hz, 2H), 1.31 (m, 32H), 1.52 (m, 8H), 1.56 (m, 8H), 3.10 (d, J = 7.0 Hz, 4H), 3.17 (m, 16H). ^{13}C NMR (CD_3OD, 100 MHz) δ (ppm): 3.4, 9.5, 26.2, 26.5, 27.5, 28.4, 28.4, 28.8, 28.9, 29.2, 41.0, 41.1, 45.8, 46.9, 47.1, 47.3, 47.5, 47.7, 47.9, 48.1, 155.6, 165.4. LCMS(ES+) m/z = 212.1 $[M + 4H]^{4+}$, 282.5 $[M + 3H]^{3+}$,423.1 $[M + 2H]^{2+}$, 845.8 $[M + H]^+$, Pale yellow oil. Yield: quantitative.

6.3.23 Synthesis of 1,3-Bis(8-carbamimidamidooctyl)-1,3-bis({8-[*N'*-(cyclopropylmethyl)carbamimidamido]octyl})urea Free-Base (50)

To Boc-protected **75** (0.017 mmol), a solution of freshly distilled acetyl chloride (800 μL) in dry CH_3OH (7.2 mL) was added dropwise at 0 °C in an ice bath, under N_2. The reaction mixture was stirred at rt for 30 min. The completion of the reaction was assessed by LCMS analysis. Then, toluene and hexane were added and the mixture was evaporated. The crude was washed with hexane and DCM several times. Then, it was treated with a solution of sodium ethoxide in dry ethanol. Sodium ethoxide was prepared *in*

situ by adding sodium (3.2 mg) to dry absolute ethanol (4.25 mL) at 0 °C. The reaction mixture was stirred at room temperature for 1 h till precipitation of a white powder (NaCl). Then, the mixture was diluted with dry ethanol and filtered several times through 0.45 μm PTFE filters. Aliquots of the sample were analyzed with the *silver nitrate assay* to ensure the absence of chlorine atoms. After evaporation, the yellowish oil was treated with DCM and filtered again with a 0.45 μm PTFE filter. After evaporation, a colorless oil was obtained and again subjected to the silver nitrate assay. In brief, a 0.1 M solution of silver nitrate in deion. H_2O was freshly prepared and used to assess the complete conversion of **40** to **55** and the removal of residual NaCl. In presence of chloride ions, silver chloride is formed as a white precipitate. No evidence of precipitation was observed. Yield: 80%. ^{1}H NMR (600 MHz, CD_3OD) δ (ppm): 0.31 (d, J = 6.0 Hz, 4H), 0.61 (m, 4H), 1.10 (m, 1H), 1.31 (m, 8H), 1.38 (m, 24H), 1.53 (m, 8H), 1.60 (m, 8H), 3.09 (d, J = 7.0 Hz, 4H), 3.21 (m, 16H). ^{13}C NMR and LCMS(ES+) spectra are consistent with those of **1**.

CHAPTER II:

C(sp^3)-H allylation by a cooperative photocatalytical Hydrogen Atom Transfer and Palladium catalysis in the Tsuji-Trost protocol

1. Introduction

Tsuji-Trost reaction provides a milder approach to synthesize allylic compounds *via* palladium catalyzed alkylation of activated nucleophiles.[294]

Briefly, in this reaction, the allylic moiety is usually activated as an allyl halide, acetate or carbonate and the nucleophile often originates from aldehydes or ketones used in their corresponding enolates, silyl enolates or enamines.[294] Even though zerovalent, the catalytic cycle (Figure 35) involves a palladium specie coordinating the alkene to form the η^2 π-allyl-Pd^0 complex with subsequent oxidative addition to the metal to form a η^3 π-allyl-Pd^{II} complex in high yields. The Leaving Group (LG) on the allylic moiety is thus expelled and the oxidative addition proceed with inversion of configuration. Then, the nucleophile attacks the activated allyl, regenerating the η^2 π-allyl-Pd^0 complex , and thus the subsequent reductive elimination, exerted by the transition metal, affords the allylated product.

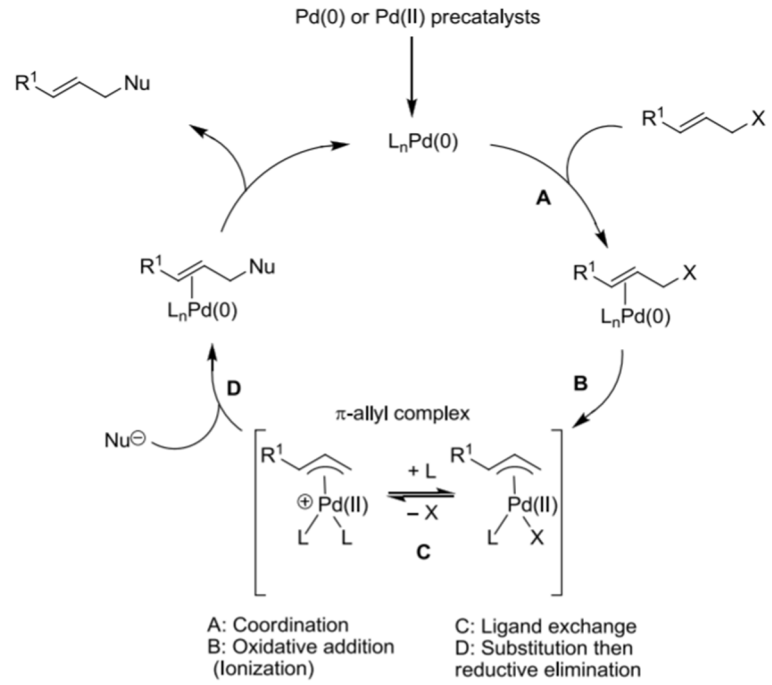

Figure 35. Catalytic cycle of the Tsuji.Trost allylation.[295]

Typically, pronucleophiles generate in situ the active specie. Stereoselectivity of the product is mainly ruled by the nature of the nucleophiles. Typically, pronucleophiles are employed to generate *in situ* their corresponding active species that can be divided into "hard" and "soft" nucleophiles.[296] Stabilized or "soft" nucleophiles invert the stereochemistry when forming the π-allyl complex, but along with the general inversion of configuration associated with the oxidative addition to palladium, a net retention of stereochemistry could be observed. Whereas, unstabilized or "hard" nucleophiles retain the configuration when forming the complex, but a net inversion of stereochemistry is generally observed after oxidative

addition to the metal.[297] This is due to the regioselectivity of the nucleophilic attack. In fact, hard nucleophiles tend to attack the metal center, whereas soft nucleophiles attack the LG bearing-carbon of the allyl moiety (Figure 36).[298]

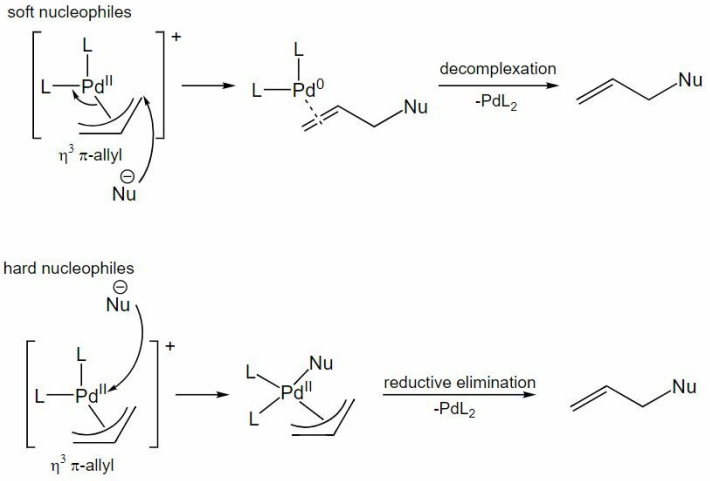

Figure 36. Hard vs soft nucleophiles in Tsuji-Trost allylation.

Moreover, phosphine ligands were widely employed to broaden the allylation scope and to afford enantioselectivity, providing asymmetrical control over the reaction. In fact, these ligands could actually modulate the electronic properties of the metal along with affecting the catalytic cicle providing steric hindrance effects.

The ability to achieve enantioselectivity in the formation of C-C, C-N, and C-O bonds under the mild conditions of Tsuji-Trost protocol, revealed to be particularly appealing for the synthesis of complex molecules, even in pharmaceutical field.[299,300]

To avoid the use of harsher conditions, employing stronger bases to promote the nucleophilic specie *in situ* formation, atom-economic and environmentally friendly approaches are preferred.[301] Thus, photocatalytic strategies could be involved to address this issue. To this concern, Hydrogen Atom Transfer (HAT) represents a versatile approach for substrate activation in photocatalyzed processes. HAT is a chemical transformation in which the concerted movement of a proton and an electron can occur between two substrates in a single kinetic step and with a radical pathway.[302,303] Indeed, HAT can be considered as a subclass of the Proton-Coupled Electron Transfer (PCET) processes in which the proton and the electron move together. However, while in PCET the elementary particles move one to another, in HAT the proton and electron start in the same shared orbital and then move together to the final one.[304]

In contrast to classic hydride abstraction, which usually employs strong bases, HAT processes feature mild conditions (e.g. room temperature, irradiations with soft-light sources, etc.) resulting in a precise

control of the reactivity of the generated radical intermediates.[305] Moreover, the activation of the C(sp^3)-H bond with the subsequent conversion into a C-X bond occurs with the net removal of the lightest atomic element from the substrate, namely the hydrogen. This scenario perfectly depicts the atom-economy profile of this process.[305]

Remarkable, HAT also represents a key step in a wide variety of bio- or chemical transformations: for instance, several metalloenzymes are known to operate through a HAT process, which is also the key step of antioxidants MoA.[304]

HAT allows the straightforward activation of aliphatic R-H bonds, proving to be an unique opportunity in organic synthesis to exploit the reactivity of unactivated substrates, tuning it by changing the reaction conditions.[306] Recently, photocatalysis contributed so far to this field. Namely, in this reactions a catalyst is excited upon light absorption and it results responsible for the activation of the reacting partners, restoring its general ground-state form at the end of the cycle. Thus, in HAT processes the amount of energy required for the transformation in delivered in the form of photons, which are made by pure energy. This results in a significant improvement of the process sustainability benefiting from the reduction of the amount of waste at the end of the transformation.[305]

A photocatalyst, upon excitation, could promote four different processes (Figure 37). Among them, in HAT (Figure 37, path *a*) the photocatalyst (PC) in its excited state (PC*) is able to abstract an hydrogen atom from a substrate R-H type, generating an activated specie with a high nucleophile tendency.

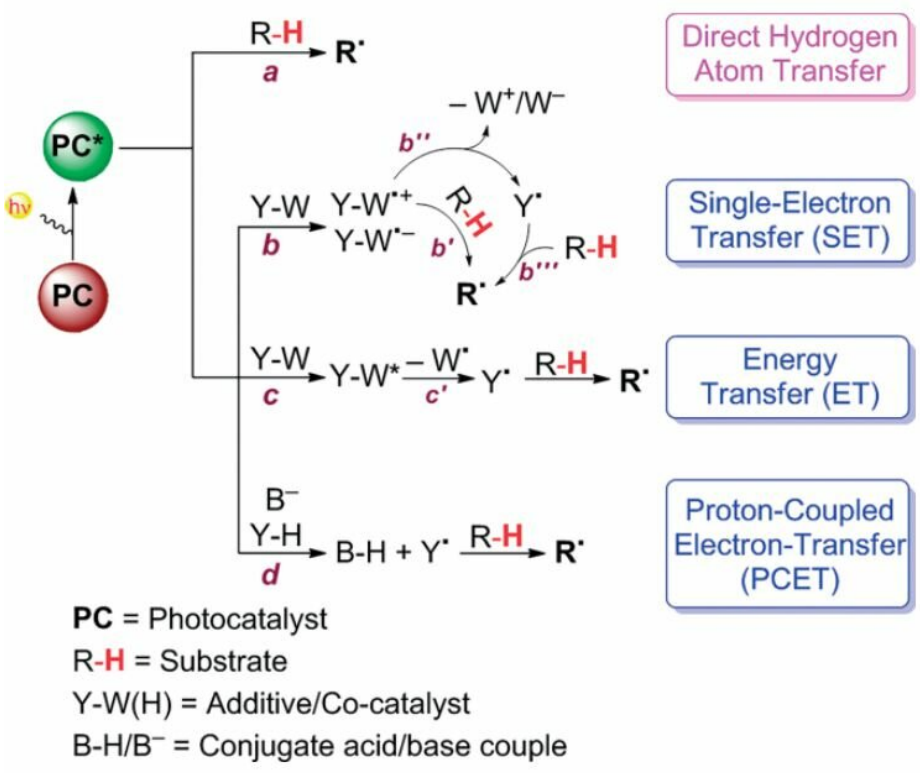

Figure 37. Substrate activation by photocatalytic processes.

On this basis, in this chapter will be presented a cooperative strategy, merging the traditional metal-catalysis with a photochemical HAT process in a Tsuji-Trost allylation protocol.

2. State of the Art

Synergistic catalysis is an emerging field wherein two catalytic cycles of two individual catalysts work together in a simultaneous way, to create a new chemical bond.[307] Generally, this strategy relies on the concomitant activation of both nucleophile and electrophile, using two different catalysts, to create their corresponding reacting species, one with a higher HOMO (Highest Occupied Molecular Orbital) and one with a lower LUMO (Lowest Unoccupied Molecular Orbital).[308] By this way, the reaction could be energetically feasible and favored. Synergistic strategies are thus potent tools to achieve high levels of atom- and step-economy. In fact, starting materials do not need to be activated and can be used as non-functionalized, replacing the conventional cross-coupling reaction approach in which reactants are generally converted in their most reactive forms (halides, boronic acids, organotins, etc.) before entering the cycle.[308]

On these basis, several research groups focused on merging different catalytic strategies. Concerning allylation, various approaches were reported, exploiting either photochemical Single Electron Transfer (SET) or HAT protocols to expand the nucleophile scope of Tsuji-Trost reaction.

For instance, a regioselective SET allylation was reported, disclosing a photoredox/nickel dual catalytic approach. In fact, a Ni-based radical mediated pathway was sought and proved to be crucial for the alkylation of allyl alcohols. 4-Alkyl 1,4-dihydropyridines (DHPs), used as latent radical precursors, are oxidized by a photocatalyst in its excited state, upon light absorption. The oxidation of these precursors generate radicals that can be subsequently captured by Ni(0). Then allyl carbonates or alcohols can oxidatively add to the Ni(I) intermediate, originating the active form Ni(III). Then, reductive elimination provides the new bond and the resulting Ni(I) species is reduced by the radical anion of the photocatalyst. By this way, both of the catalytic cycles are closed (Figure 38).[309]

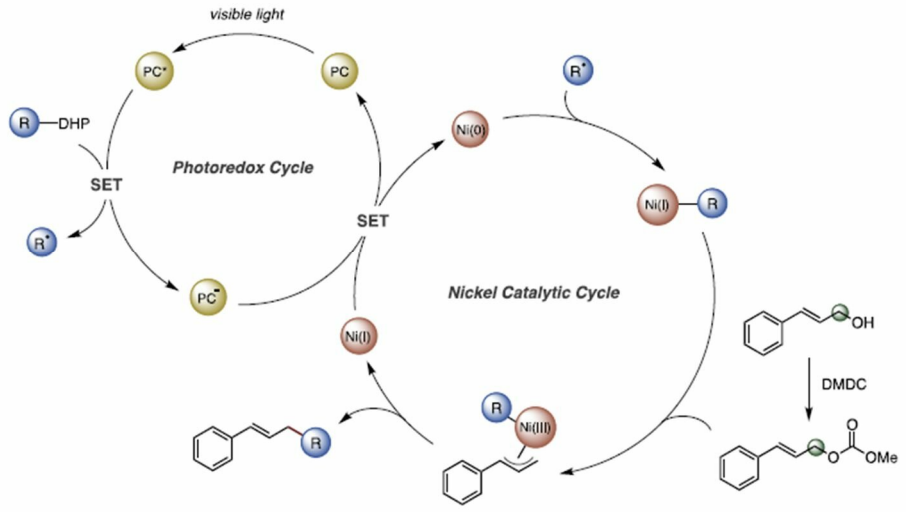

Figure 38. Regioselective cooperative photoredx/nickel-mediated catalytic cycle involving allyl alcohols and carbonates.[309]

Reaction conditions were finely tuned to favor regioselectivity in linear and E-isomer product and also the allylic scope was broaden with respect to the previous reported literature, extending also the range of Ni-catalyzed photoredox transformations.[309]

Decarboxylative allylation (DcA) is a subset of the Tsuji-Trost allylation, in which carboxylic acids are used as latent carbanions, bypassing the required harsh conditions when a base is needed. However, this transformation is only limited to acid substrates who can guarantee an effective stabilization of the resulting carbanion. To overcome this issue, the development of a photoredox/Pd dual catalytic strategy was conceived and reported.[310] Thus, an oxidative radical decarboxylation is mediated by an iridium photocatalyst and once the carbon radical is generated, the subsequent combination with a Pd-π-allyl intermediate furnished a new C(sp^3)-C(sp^3) bond (Figure 39).

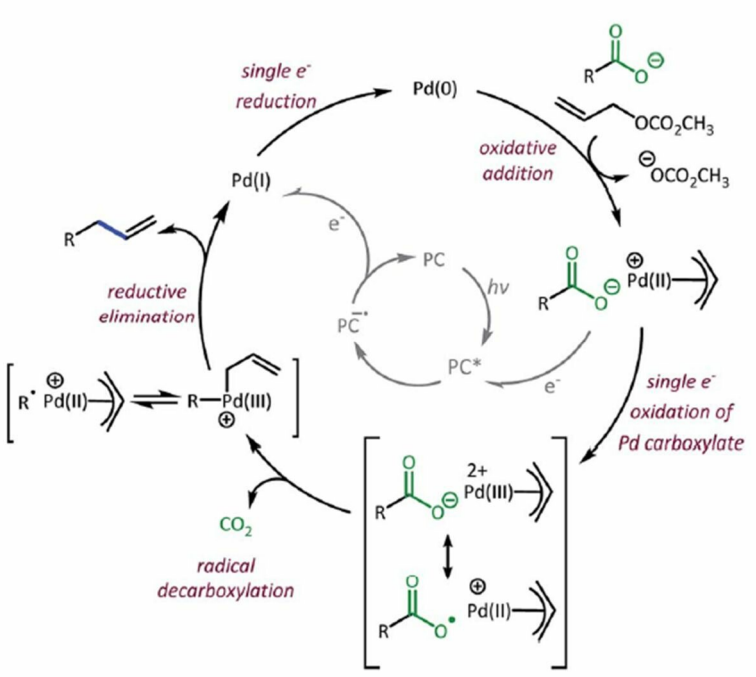

Figure 39. Catalytic dominant pathway of the decarboxylative allylation.[310]

The dominant catalytic pathway proceeds via a reductive quenching of excited 4CzlPN operated by a π-allyl-Pd-carboxylate complex. SET from the carboxylate to the Pd makes the decarboxylation efficient, forming the carbon centered radical. Coupling the π-allyl-Pd complex with the radical results overall in the formation of the allylated product. Pd(I) is thus produced and can be recuded by 4CzlPN to close both of the catalytic cycles.[310]

Moreover, a dehydrative allylation of alkyl amines was reported, in which the cooperation of photoredox and palladium catalysis proved to be efficient in promoting novel C(sp^3)-C(sp^3) bond formation.[311]

A range of alkyl amines were selected for the study which revealed that an *in situ* generated carboxylic acid activates an allylic alcohol, facilitating its oxidative addition to the palladium. Thus, a series of

homoallylic amines, which are versatile drug synthesis intermediates, have been reported with this synthetic approach.

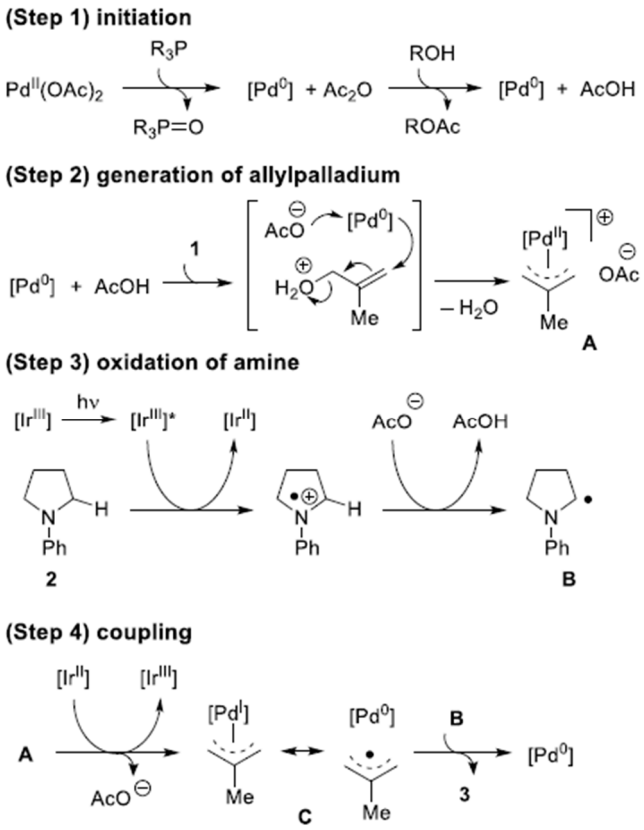

Figure 40. Proposed reaction pathway for the dehydrative allylation of C(sp3)−H bonds of alkylamines.[311]

Briefly, the phopshine ligand is able to reduce the $Pd(OAc)_2$ catalyst, generating Ac_2O and a Pd(0) species. Ac_2O reacts with the allylic alcohol producing acetic acid, which can now protonate the same alcohol, assisting its oxidative addition to the palladium, furnishing the π-allyl-complex. Then, an iridium catalyst is excited upon light absorption and induces a SET from the amine to the iridium complex, forming the amine radical cation and the iridium (II) species. A deprotonation occurring on the radical cation by the acetate, generates the α-aminoalkyl radical (Figure 40). Th Pd-complex is then reduced by the iridium (I) photocatalyst and can finally couple with the amino radical affording the desired derivative.[311]

The homolytic cleavage of an inert C(sp3)-H bond by a HAT photocatalyst was reported as successful strategy to perform a tandem Giese-Tsuji-Trost three-component protocol, to afford the final allylation product. Briefly, an HAT-mediated process, operated by the photocatalyst, gives rise to an alkyl radical able to undergo a Giese addition[312] to an electron-poor alkene. The so generated electron-deficient radical is then rapidly reduced by the photocatalyst furnishing a carbanionic nucleophile. The latter reacts then with the catalytically generated Pd- π-allyl-complex, leading to the allylation product (Figure 41).[301]

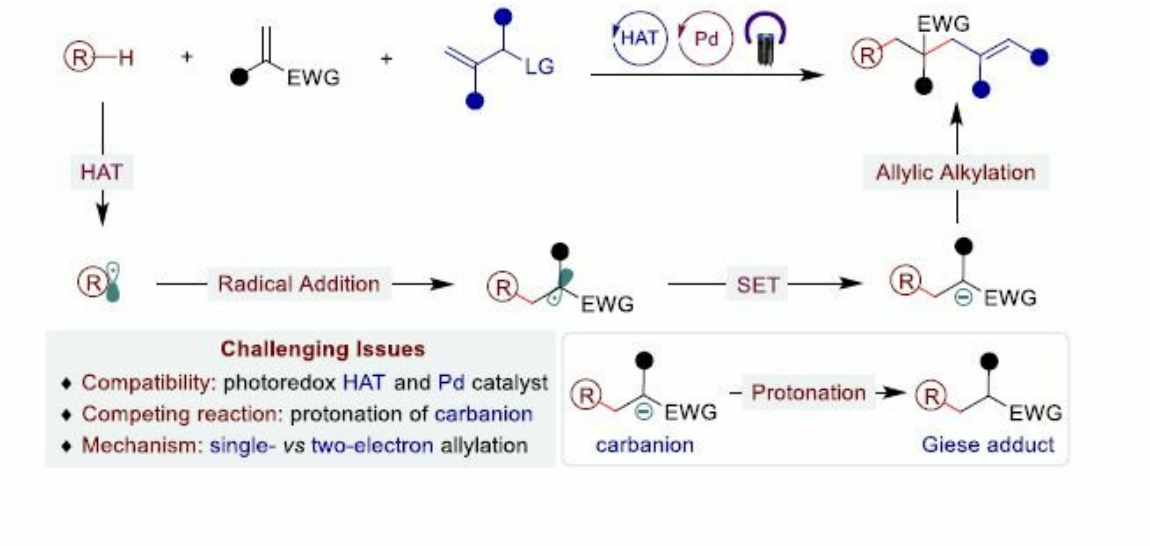

Figure 41. HAT-mediated three component Giese-Tsuji-Trost allylation.[301]

However, the compatibility of the HAT catalyst with palladium is poorly documented and a competing protonation of the so generated carbanion could actually occur when forming the Giese addiction product. Moreover, the direct coupling of the Pd- π-allyl-complex with the carbon-centered radical was not sorted out in this protocol, although the hypothesis of this additonal pathway occurring could not be avoided.

3. Results and Discussion

3.1 Aim of the work

To fill the gap in the HAT-mediated Tsuji-Trost allylation, and inspired by the three-component strategy previously reported,[301] a synergistic photochemical-mediated approach was developed.
Briefly, an HAT catalyst was selected to proper abstract, under light exposure, an hydrogen atom from a non-activated C(sp^3)-H bond of an alkyl radical precursor. The so generated radical species was supposed to act as nucleophile and couple with a π-allyl complex, originated from a metal transition catalyst and an electron-poor allyl, furnishing the desired allylated product (Figure 42).

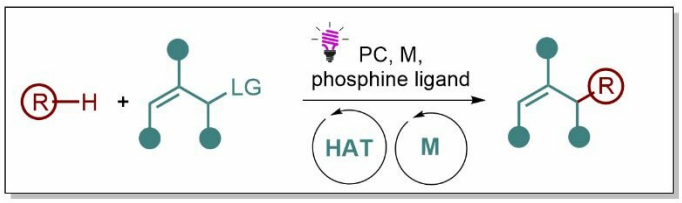

Figure 42. Aim of the work presented in this chapter.

3.2 Chemistry

To ensure the coupling, palladium and nickel catalyst were reported for photochemical-mediated approaches. However, first attempts to define a model reaction with optimized conditions involved a palladium catalyst as favored choice, since its well-known ability to ensure regio- and enantioselectivity through asymmetric induction by chiral ligands.[313]
To finely tune the reaction conditions, allyl methyl carbonate **89** was selected as allyl partner due to its small size and synthetical feasibility. Its synthesis has been achieved through a convenient and efficient path, showed in Scheme 11, using commercially available allyl alcohol.[314]

Scheme 11. Synthesis of the starting material allyl methyl carbonate **89**.

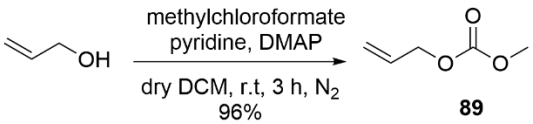

Moreover, THF and 1,3-benzodioxole were used as radical precursors, since the resulting radical species could benefit from the α- oxo stabilization.

Tris(dibenzylideneacetone)dipalladium was used as source of palladium (0) and triphenyl phosphine or tris(2,4,6-trimethylphenyl)phosphine as the phosphine ligands. Additionally, 5,7,12,14-pentacenetetrone (PT) was initially used as HAT photocatalyst.

Table 23. Experiment in presence and in absence of light.

Entry	PC	M	L		^{1}H-NMR yield[a]
1	PT	$Pd_2(dba)_3$	L1	390 nm	66%
2	PT	$Pd_2(dba)_3$	L1	no light	n.d.
3	PT	$Pd_2(dba)_3$	L1	456 nm	n.d.

[a] NMR yields were calculated using pyrazine or trichloroethylene as external standards.
PC: photocatalyst; **PT**: Pentacenetetrone; **M**: metal catalyst; **L**: ligand.

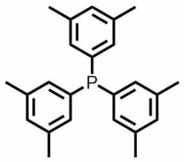

L1

First experiment was carried out in presence and in absence of light, to assess whether the reaction would work only under light exposure, and two different wavelengths were selected (Table 23). A full conversion of the starting materials was observed when the reaction was exposed to 390 nm *Kessil Lamp* (entry 1, Table 23), showing only a 30% yield of the desired compound **90**. As expected, any allylation product was detected when light was switched off (entry 2, Table 23), indicating that a radical pathway is likely to occur. However, no product was also observed under 456 nm *Kessil Lamp* exposure (entry 3, Table 23).

3.2.1 Optimization

Optimization of the protocol started from the solvent screening: five different aprotic solvents were evaluated (Table 24) and among them dry degassed acetonitrile (ACN) provided the best results (entry 4, Table 24).

Table 24. Solvent screening.

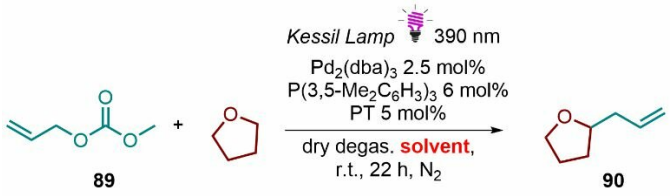

Entry	Solvent	^{1}H-NMR yield[a]
1	DCM	traces
2	DCE	n.d.
3	Acetone	n.d.
4	ACN	66%
5	BTF	n.d.

[a] ^{1}H-NMR yields are calculated using pyrazine or trichloroethylene as external standards.

Then, the optimization proceeded with the catalysts screening. Different sources of palladium (0) and palladium (II) were investigated, along with a nickel (I) catalyst that was properly synthesized as reported in literature[315] (Table 25).

Table 25. Catalyst screening.

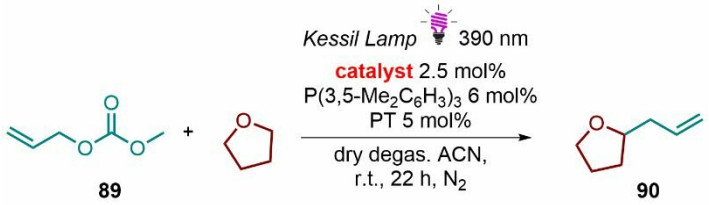

Entry	R-H	Catalyst	Ligand	^{1}H-NMR yields [a]
1	THF	$Pd_2(dba)_3$	L1	66%
2	1,3-Benzodioxole	$Pd_2(dba)_3$	L1	40%
3	THF	$Pd_2(dba)_3$	L2	69%
4	1,3-Benzodioxole	$Pd_2(dba)_3$	L2	36%
5	1,3-Benzodioxole	$Pd(dba)_2$	L2	37%
6	1,3-Benzodioxole	$Pd(PPh3)_2Cl_2$	L2	24%
7	1,3-Benzodioxole	$Pd(OAc)_2$	L2	16%
8	1,3-Benzodioxole	$PdCl_2$	L2	n.d.
9	1,3-Benzodioxole	$PdBr_2$	L2	12%
10	1,3-Benzodioxole	$(4,4'\text{-dtbbpy})NiCl_2$	L1	20%

[a] ^{1}H-NMR yields are calculated using pyrazine or trichloroethylene as external standards.

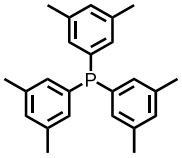

L1

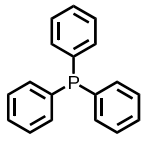

L2

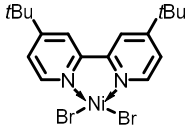

Ni(I) complex

Tris(dibenzylideneacetone)dipalladium (0) was confirmed as the most suitable catalyst for this transformation, either with THF or 1,3-benzodioxole as alkyl radical precursors R-H (entries 1 and 3, Table 25). Interestingly, reaction employing a Ni(I) complex as metal catalyst did not occur (entry 10, Table 25) revealing a key role for the palladium transition metal. Furthermore, palladium (II) catalysts provided only a worsening of the reaction profile (entries 7-9, Table 25).

Mono- and bi-dentate phosphine ligands, either bearing electronwithdrawing (EWG) or donating groups, were also investigated.

Table 26. Mono-dentate ligand screening.

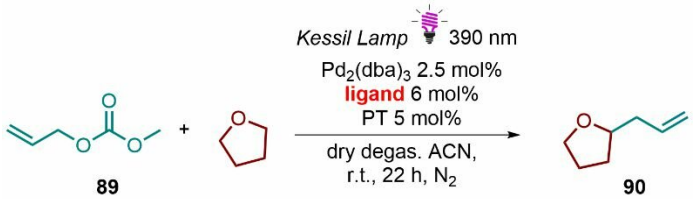

Entry	R-H	Catalyst	Ligand	^{1}H-NMR yields [a]
1	1,3-Benzodioxole	$Pd_2(dba)_3$	L3	n.d.
2	1,3-Benzodioxole	$Pd_2(dba)_3$	L4	n.d.
3	1,3-Benzodioxole	$Pd_2(dba)_3$	L5	traces
4	1,3-Benzodioxole	$Pd_2(dba)_3$	L6	16%
5	1,3-Benzodioxole	$Pd_2(dba)_3$	L7	n.d.
6	1,3-Benzodioxole	$Pd_2(dba)_3$	L8	35%
7	1,3-Benzodioxole	$Pd_2(dba)_3$	L9	n.d.

[a] ^{1}H-NMR yields are calculated using pyrazine or trichloroethylene as external standards.

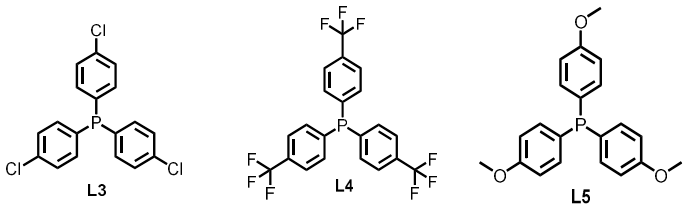

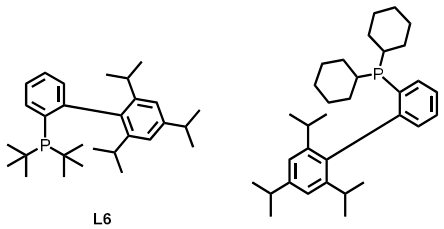

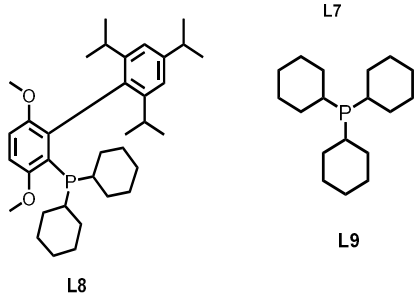

Mono-phosphine bearing EWG groups (entries 1 and 2, Table 26) or cyclic alkyl moieties (entry 7, Table 26) did not provide any product formation. On the contrary, bulky phosphine (entries 4 and 6, Table 26) displayed only scarce or moderate yields.

Table 27. Bi-dentate phosphine screening.

Entry	R-H	Catalyst	Ligand	^{1}H-NMR yields [a]
1	1,3-Benzodioxole	$Pd_2(dba)_3$	L10	n.d.
2	1,3-Benzodioxole	$Pd_2(dba)_3$	L11	55%
3	1,3-Benzodioxole	$Pd_2(dba)_3$	L12	24%
4	1,3-Benzodioxole	$Pd_2(dba)_3$	L13	22%
5	1,3-Benzodioxole	$Pd_2(dba)_3$	L14	51%
6	THF	$Pd_2(dba)_3$	L11	87%
7	1,3-Benzodioxole	$Pd_2(dba)_3$	L15	n.d.

[a] ^{1}H-NMR yields are calculated using pyrazine or trichloroethylene as external standards.

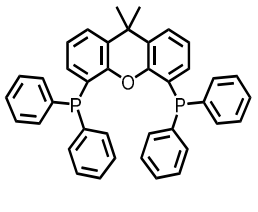
L10

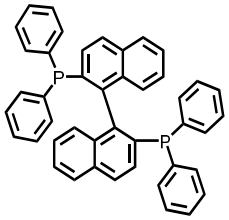
L11

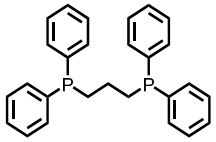
L12

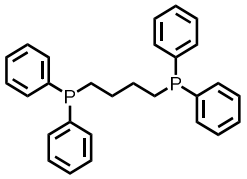
L13

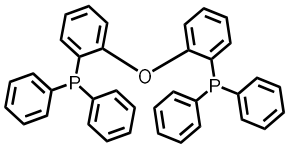
L14

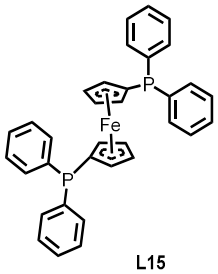
L15

Bi-dentate phosphine ligands provided overall promising results. Particularly, BINAP (2,2'-bis(diphenylphosphino)-1,1'-binaphthyl), an organophosphorus compound widely employed in asymmetrical synthesis, exerted the best reactivity towards THF and 1,3-benzodioxole, incrementing the yield up to 1.5 fold compared to the previous used tris(2,4,6-trimethylphenyl)phosphine or triphenylphosphine (entry 6, Table 27).

Keeping the BINAP unvaried, HAT photocatalysts were then screened: PT, benzophenones with both EWG or donating properties, and tetrabutylammonium decatungstate (TBADT) were investigated, as reported in Table 28.

Table 28. Photocatalyst screening.

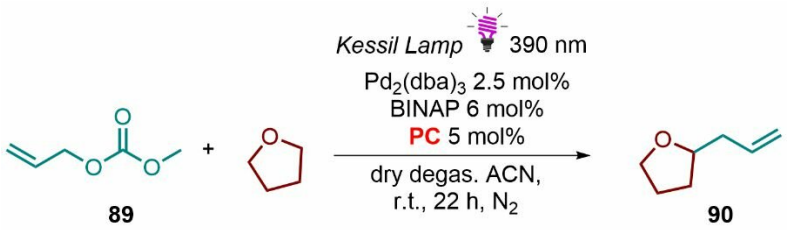

Entry	Ligand	PC	^{1}H-NMR yield [a]
1	L11	PC1	87%
2	L11	PC2	23%
3	L11	PC3	58%
4	L11	PC3	47%
5	L11	PC4	35%
6	L11	PC5	n.d.

[a] ^{1}H-NMR yields are calculated using pyrazine or trichloroethylene as external standards.

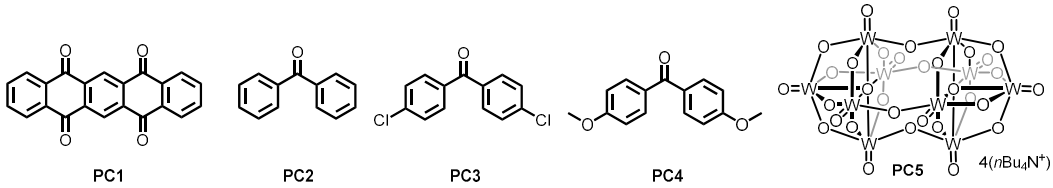

TBADT did not provide any product formation (entry 6, Table 28) and electron-poor or electron-rich benzophenones worsened the reactive profile, confirming that PT is the suitable catalyst for this transformation.[301,316]

Catalysts loading, both Pd and PT, and solution molarity were then evaluated as reported in Table 29.

Table 29. Varying the catalysts loading and the concentration of the reacting mixture.

Entry	R-H	Pd loading	PC loading	Final solution molarity	^{1}H-NMR yields [a]
1	1,3-benzodioxole	5 mol%	5 mol%	0.1 M	46%
2	1,3-benzodioxole	1.25 mol%	5 mol%	0.1 M	33%
3	1,3-benzodioxole	2.5 mol%	10 mol%	0.1 M	32%
4	1,3-benzodioxole	2.5 mol%	2.5 mol%	0.1 M	34%
5	1,3-benzodioxole	2.5 mol%	5 mol%	0.05 M	45%
6	1,3-benzodioxole	2.5 mol%	5 mol%	0.2 M	30%

[a] ^{1}H-NMR yields are calculated using pyrazine or trichloroethylene as external standards.

Doubling the catalysts loadings or reducing them of two fold resulted in any enhancement of the reaction profile and also varying the molar concentration of the reacting mixture did not provide any interesting breakthrough in reactivity.

Hence, optimization of the protocol led to the definition of the model reaction in which alkyl precursors, either THF or 1,3-benzodioxole, produced an alkyl radical upon photoexcitation PT-mediated. This radical could be added on the allyl moiety acting like a nucleophile, benefiting from Pd-mediated catalyst and BINAP auxiliary role, thus leading to the final allylated products **90** or **91** (Scheme 12).

Scheme 12. Model reaction with optimized final conditions.

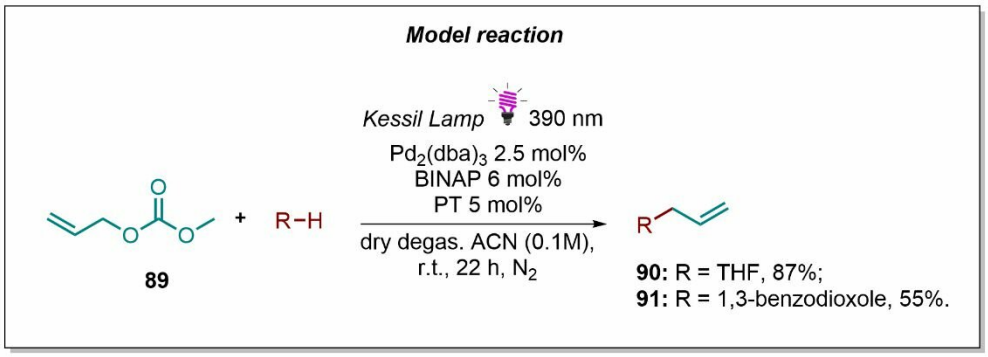

3.2.1 Scope of the alkyl radical precursors

Different radical precursors were selected for their electron and chemical properties to evaluate the reliability of the synthetic approach. In Table 30 are reported the (hetero) alkyl compounds selected for this study.

Table 30. Scope of the alkyl radical precursors.

Entry	R-H	^{1}H-NMR yields [a]
1	THF	87%
2	1,3-benzodioxole	55%
3	Cyclohexane	n.d.
4	Phtalan	12%
5	1,3-dioxolane	n.d.
6	*N*-Bocpyrrolidine	n.d.

[a] ^{1}H-NMR yields are calculated using pyrazine or trichloroethylene as external standards.

Since THF and 1,3-benzodioxole exerted an interesting reactivity towards HAT homolytic cleavage of their C(sp^3)-H bonds (entries 1 and 2, Table 30), cyclohexane was first selected to evaluate if the synergistic catalytic approach could also work towards less stabilized radical species (entry 3, Table 30).

Unfortunately, cyclohexane as the radical precursor did not provide the desired allylated compound. Switching to phtalan, worsened the overall yield of the transformation. However, even though allyl full conversion was still observed, also 1,3-dioxolane (entry 5, Table 30) and *N*-Bocpyrrolidine (entry 6, Table 30) proved to be unsuccessful. It is likely to hypothesize thus that α-oxo radical species are more responsive to this transformation than α-nitrogen radical ones, even though a broader scope is required to state this hypothesis. Moreover, a significant discrepancy was observed between 1,3-benzodioxole and 1,3-dioxolane. As common knowledge, they both could benefit from the anomeric effect, being heterocycles endowed with a five membered ring. However, the anomeric effect in 1,3-benzodioxole could affect the benzene ring planarity by lowering its barrier, resulting in a pucked aromatic cycle at an angle of 24°.[317] Hence, interactions between the *p* orbitals of oxygen atoms and the pucked benzene ring[317] could justify the greater stabilization of the benzodioxole free radical over the dioxolane one and thus the resulting reactivity.

3.2.2 Scope of the allyl partner

Different (hetero)alkyl or aromatic allyl partners (**92-100**, Figure 43) were selected for the scope and relative yields are reported in Table 31. The selection was made not only to assess their reactivity towards the novel catalytic approach, but also to reach the proper grade of polarity to achieve purification of the final products. In fact, purification of these allylation compounds resulted particularly challenging. The huge excess of highly-boiling radical precursors used in this approach (20 equivalents) along with their similar physicochemical properties with the achieved compounds, resulted in derivatives with close R_f and thus co-elution during isolation. Resorting to crystallization or distillation techniques also resulted in failed attempts. Moreover, the volatility of THF alkyl derivatives seriously hampered their isolation. To this concern, some compounds were conceived for being endowed with different polarity and higher molecular weights.

Figure 43. Allyl partners synthesized for this work.

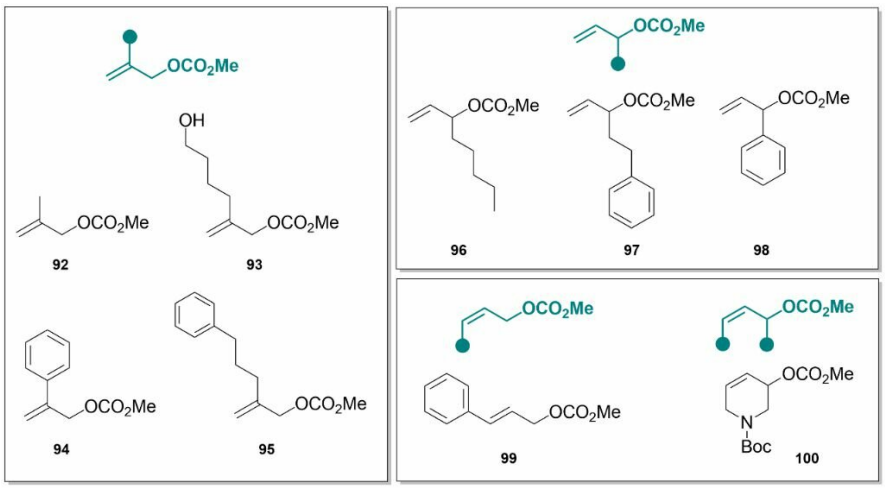

Allyl partners were properly synthesized as presented in Scheme 13-14. Briefly, the synthesis of derivatives **92**, **94**, **96**, **98-100** proceeded in one high yielding step, through carbonation of the corresponding commercially available allyl alcohols (Scheme 13).

Scheme 13. Synthesis of starting materials **92, 94**, **96**, **98-100**.

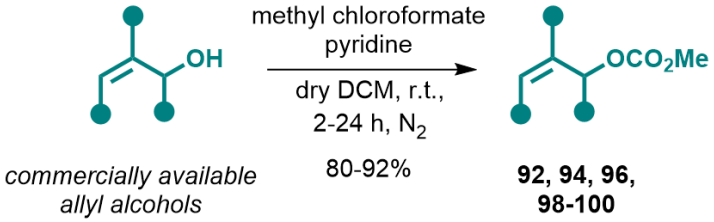

Synthesis of starting materials **93**, **95** and **97** proceeded instead following different approaches. Briefly, commercially available methallyl alcohol was treated with oxetane and butyl lithium in presence of tetramethylethylendiamin (TMEDA), affording intermediate **101**, which is then treated with methyl chloroformate furnishing starting material **93** (Scheme 14).[318]

Scheme 14. Synthesis of starting materials **93**, **95** and **97**.

Synthesis of starting material 93:

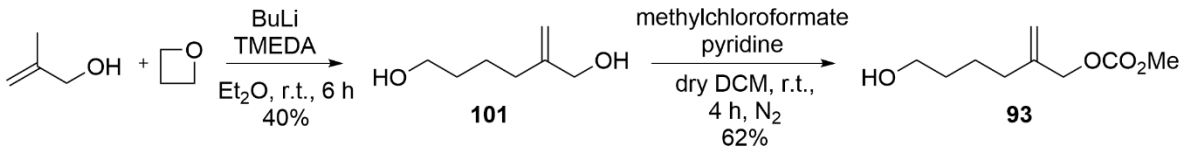

Synthesis of starting material 95:

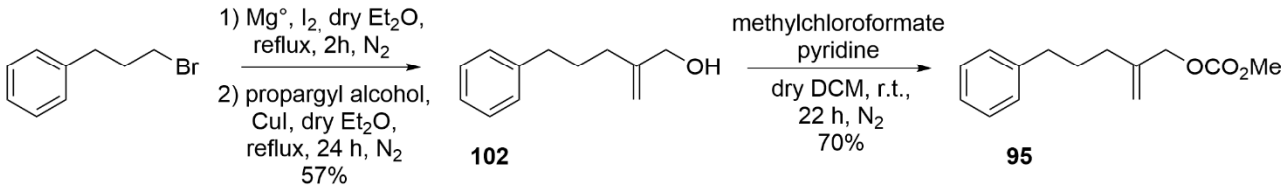

Synthesis of starting material 97:

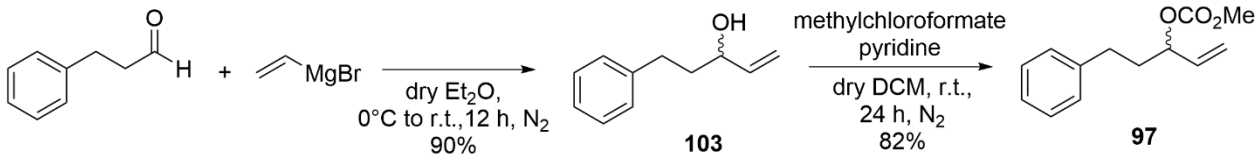

Then, commercially available 1-bromo-3-phenylpropane was first converted into its corresponding Grignard reagent and then reacted with propargyl alcohol, furnishing derivative **102** which is then converted into the carbonate **95** (Scheme 14).[319]

In the end, commercially available propionaldehyde is converted to the corresponding alcohol **103**, after addition of vinyl magnesium bromide to the carbonyl moiety, and then treated with methyl chloroformate to furnish starting material **97** (Scheme 14).[320]

Table 31. ^{1H}-NMR yields reported for allyl partners **92-100**.

Entry	Allyl partner	R-H	Ligand	💡	^{1}H-NMR yields [a]
1	92	1,3-benzodioxole	BINAP	390 nm	22%
2	92	1,3-benzodioxole	BIPHEP	390 nm	23%
3	92	THF	BINAP	390 nm	32%
4	92	THF	BIPHEP	390 nm	50%
5	93	1,3-benzodioxole	BINAP	390 nm	traces
6	93	1,3-benzodioxole	BIPHEP	390 nm	14%
7	93	THF	BINAP	390 nm	23%
8	93	THF	BIPHEP	390 nm	27%
9	94	1,3-benzodioxole	BINAP	390 nm	15%
10	94	1,3-benzodioxole	BINAP	456 nm	23%
11	94	THF	BINAP	390 nm	n.d. [b]
12	94	THF	BINAP	456 nm	traces
13	95	1,3-benzodioxole	BINAP	390 nm	traces
14	95	1,3-benzodioxole	BIPHEP	390 nm	n.d. [b]
15	95	THF	BINAP	390 nm	n.d. [b]
16	95	THF	BIPHEP	390 nm	n.d. [b]
17	96	1,3-benzodioxole	BINAP	390 nm	18%
18	96	1,3-benzodioxole	BIPHEP	390 nm	25%
19	96	THF	BINAP	390 nm	30%
20	96	THF	BIPHEP	390 nm	36%
21	97	1,3-benzodioxole	BINAP	390 nm	traces
22	97	1,3-benzodioxole	BINAP	456 nm	21%
23	97	THF	BINAP	390 nm	15%
23	97	THF	BINAP	456 nm	28%
24	98	1,3-benzodioxole	BINAP	390 nm	22%
25	98	1,3-benzodioxole	BIPHEP	390 nm	24%
26	98	THF	BINAP	390 nm	n.d. [b]
27	98	THF	BIPHEP	390 nm	n.d. [b]
28	99	1,3-benzodioxole	BINAP	390 nm	traces
29	99	1,3-benzodioxole	BIPHEP	390 nm	n.d. [b]
30	99	THF	BINAP	390 nm	traces
31	99	THF	BIPHEP	390 nm	n.d. [b]
32	100	1,3-benzodioxole	BINAP	390 nm	n.d.
33	100	1,3-benzodioxole	BIPHEP	390 nm	traces
34	100	THF	BINAP	390 nm	n.d.
35	100	THF	BIPHEP	390 nm	traces

[a] ^{1}H-NMR yields are calculated using pyrazine or trichloroethylene as external standards.

[b] Only the dimerization product was observed.

Keeping unvaried the optimized reaction conditions, THF and 1,3-benzodioxole were selected to proceed with the scope of the allyl partners, being the best shots among the alkyl radical precursors screened. Moreover, some aryl derivatives were also exposed to longer wavelengths under the 456 nm *Kessil Lamp*. Furthermore, (6,6'-Dimethoxybiphenyl-2,2'-diyl)bis-diphenylphosphine (BIPHEP) was also selected as ligand to broaden the acquired information about their cooperative action in the catalytic cycle of palladium. Unfortunately, poor yields were observed for all the screened allyl partners, with the exception of compound **92** (entry 4, Table 31) which however displayed lower yields compared to that of the model reaction. Additionally, when aryl derivatives were employed as allyl partner, competitive dimerization of their scaffold was observed and in some cases the dimerized product was the only one observed in the reaction mixture (entries 11, 14-16, 26-27, 29, 31, 34, Table 31). Nevertheless, interesting considerations could be made by observing the data set collected: BIPHEP seems to enhance the conversion of the starting materials in their corresponding final products with akyl allyl partners. Moreover, dimerization tend to occur prevalently in presence of THF rather than 1,3-benzodioxole. Varying the wavelength led to improved yields for compounds **94** and **97**, even though not significant. In the end, the extended conjugation which derivatives **94** and **99** provided (entries 9-12 and 28-31, Table 31) limited the reactivity towards the synergic protocol, probably due to a more persistent and stabilized π-allyl complex and thus a difficult reductive elimination. Overall, the allylation seems to be favored on less substituted substrates and only small alkylic substituents are tolerated, as confirmed by entry 4 in Table 31.

3.2.3 Limitations of the protocol

Isolation of coupled derivatives, as previously explained, resulted not trivial and particularly challenging and thus previous reported yields, also for model reaction, refer to quantitative ^{1H}-NMR calculations using pyrazine or trichloroethylene as external standard. However, questioning on how to improve the purification of allylated compounds, a one-pot-two step protocol was developed as showed in Scheme 15. Briefly, ACN from reaction mixture containing compound **91** was removed by rotary evaporation and then the excess of 1,3-benzodioxole was lowered by nitrogen flow. Then, epoxidation with m-chloroperbenzoic acid (mCPBA) resulted in compound **104** (Scheme 15). This epoxidation strategy resulted successful for the desired isolation of the coupled compound **91**, furnishing a 52% isolated yield over two steps.

Scheme 15. Epoxidation of compound **91**.

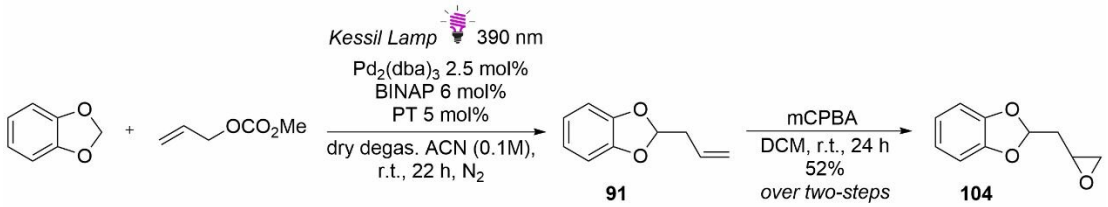

Moreover, the protocol proved to have only a limited applicability as confirmed by the scope of the allyl partners and alkyl radical precursors. However, only some representative derivatives were selected for the scope and further evaluations need to be done.

4. Conclusions

In this work a cooperative catalysis, merging a photochemical HAT process with a palladium-catalyzed cycle, was presented. Upon light exposure, an inert C(sp^3)-H bond is subjected to an homolytic HAT process, generating a radical specie that is then coupled, though a palladium-mediated strategy, with a suitable allyl partner to afford the allylation compound in a modified Tsuji-Trost approach.

The reliability of the process was first confirmed by carrying on the experiment in absence of light, which proved that the process is light-dependent. Optimization of the reaction conditions proved that BINAP, $Pd_2(dba)_3$, and PT are the favored ligand, palladium (0) source and photocatalyst, respectively, for this transformation. However, BIPHEP revealed to be more efficient with alkyl allyl partners (**92-93**, **96**). THF and 1,3-benzodioxole showed greater reactivity towards HAT activation than 1,3-dioxolane, cyclohexane, *N*-bocpyrrolidine and phtalan as proved by the alkyl radical precursors scope. Promising applicabilities of the protocol to allyl methyl carbonate **89** and methyl (2-methylallyl) carbonate **90** were not in agreement with what observed when the scope was broaden. Briefly, aryl derivatives were less tolerated, since in some selected cases (**94**, **99**) they could benefit from additional extended conjugation, challenging the reductive elimination step in palladium-catalytic cycle. Overall, poor yields were reported when scoping allyl partners and the cooperative catalysis seems to be promising only on less substituted substrates (**89** and **92**). The huge excess in terms of equivalents of the highly-boiling radical precursors hampered significantly the purification of the obtained compounds, whereas also the high-volatility of THF derivatives extended the purification issue. To this concern, epoxidation of the allylation product was pursued in a one-pot two steps protocol, affording the desired coupled derivative **104** in good yields over two steps. In the end, scopes of both allyl partners and alkyl radical precursors need to be extended to gain a deeper understanding of the real limitations and applicability of the protocol. Moreover, reaction parameters could be also re-screened to finely tune the conditions depending on the substrates involved in the transformation.

5. Materials and methods

5.1 General Chemistry

All commercially available chemicals and solvents were bought from Sigma Aldrich, TCI and Fluorochem. Technical solvents were bought from VWR International and used as received. Anhydrous solvents were purchased from Sigma Aldrich and used as such. Degassed dry ACN was prepared from dry ACN through cycles of atmosphere exchange under sonication and purging (nitrogen bubbling). Anhydrous reactions were performed into flame-dried glassware after three cycles of vacuum/dry nitrogen and were run under a positive pressure of dry nitrogen.

^{1H} (400 and 300 MHz), and ^{13}C (100 MHz) spectra were recorded at ambient temperature using Bruker AV 300-I, and AV 400. ^{1H} NMR spectra are reported in parts per million (ppm) downfield relative to CDCl3 (7.26 ppm) and all ^{13}C NMR spectra are reported in ppm relative to CDCl3 (77.16 ppm) unless stated otherwise. The multiplicities of signals are designated by the following abbreviations: s (singlet), d (doublet), t (triplet), q (quartet), m (multiplet), dd (doublet of doublets), dt (doublet of triplets), td (triplet of doublets), ddd (doublet of doublet of doublets). Coupling constants (*J*) are reported in hertz (Hz). NMR data was processed using the MestReNova 14 software package. Quantitative ^{1H}-NMR calculations were performed using the MestReNova 14 software package, using trichloroethylene or pyrazine, in a equimolar ratio to the desired product, as external standards.. Product isolation was performed manually, using silica (P60, SILICYCLE). TLC analysis was performed using Silica on aluminum foils TLC plates (F254, SILICYCLE) with visualization under ultraviolet light (254 nm and 365 nm) or appropriate TLC staining (Cerium Ammonium Molybdate, Potassium Permanganate). Organic solutions were concentrated under reduced pressure on a Büchi rotary evaporator (in vacuo at 40 °C, ~5 mbar).

5.2 Chemical procedures

5.2.1 General synthesis of allyl carbonates 89, 92, 94, 96, 98-100:

An oven-dryed round-bottom flask with a stirring bar inside, was capped with a septum cap and submitted to three cycles of vacuum/nitrogen. Then, methyl chloroformate (41.33 mmol) was added to a solution of allylic alcohol (34.44 mmol) and pyridine (103.3 mmol) in dry DCM (0.4 M) at 0°C, under nitrogen atmosphere. The reaction mixture was then warmed to room temperature, and stirred for 2-24 h. After reaction completion, the organic layer was washed three times with 1M HCl solution and finally with brine. The combined organic layers were dried over Na_2SO_4, filtered and then evaporated under reduced pressure, providing the desired allylic carbonates without further purifications.

Methyl allyl carbonate (89):

Allyl alcohol was used as starting material. ^{1H} NMR (400 MHz, $CDCl_3$) δ (ppm) 5.89 (m, *1H*), 5.33 (ddq, *J* = 17.2, 2.9, 1.5 Hz, *1H*), 5.23 (ddq, *J* = 10.4, 3.1, 1.3 Hz, *1H*), 4.60 (d, *J* = 5.8 Hz, 2H), 3.76 (d, *J* = 2.1 Hz, 3H). ^{13}C NMR ($CDCl_3$) δ (ppm) 54.7, 68.1, 118.0, 132.2, 155.7. Yellowish oil. Yield: 96%.

Methyl (2-methylallyl)carbonate (92):

Methallyl alcohol was used as starting material. ^{1H} NMR (400 MHz, CDCl3) δ (ppm) 5.10 (s, *1H*), 4.96 (s, *1H*), 4.51 (s, 2H), 3.79 (s, 3H), 1.75 (s, 3H). ^{13}C NMR (CDCl3) δ (ppm) 19.8, 54.7, 74.1, 112.9, 140.2, 155.7. Yellowish oil. Yield: 86%.

Methyl oct-1-en-3-yl carbonate (96):

Oct-1-en-3-ol was used as starting material. ^{1H} NMR (400 MHz, CDCl3) δ (ppm) 5.82 (ddd, *J* = 17.1 Hz, *J* =10.3 Hz, *J* = 7.2 Hz, *1H*), 5.29 (m, 2H), 4.78 (dt, *J* = 7.2 Hz, *J* = 1.0 Hz, *1H*), 3.79 (s, 3H), 0.92 (s, 9H). ^{13}C NMR ($CDCl_3$) δ (ppm) 14.4, 21.9, 25.6, 31.7, 34.2, 54.5, 86.3, 119.0, 133.3, 155.4. Yiellowish oil. Yield: 90%.

Methyl (1-phenylallyl) carbonate (98):

1-Phenyl-2-propen-1-ol was used as starting material. ^{1H} NMR (300 MHz, CDCl3) δ (ppm) 7.37 (s, 5H), 6.11 (m, 2H), 5.31 (m, 2H), 3.78 (s, 3H). ^{13}C NMR ($CDCl_3$) δ (ppm) 55.2, 86.1, 116.5, 127.1, 127.6, 128.8, 138.8, 155.7. Yiellowish oil. Yield: 91%.

Cinnamyl methyl carbonate (99):

Cinnamyl alcohol was used as starting material. ^{1H} NMR (400 MHz, CDCl3) δ (ppm) 7.39 (m, 2H), 7.32 (m, 2H), 7.25 (m, *1H*), 6.70 (d, *J* = 16.0 Hz, *1H*), 6.33 (dt, *J* = 16.0 Hz, *J* = 6.6 Hz, *1H*), 4.79 (dd, *J* = 6.6 Hz, *J* = 1.6 Hz, 2H), 3.80 (s, 3H). ^{13}C NMR ($CDCl_3$) δ (ppm) 54.7, 71.1, 121.1, 127.9, 128.3, 128.5, 128.6, 133.8, 136.7, 155.5. Yiellowish oil. Yields: 92%.

***tert*-butyl 3-((methoxycarbonyl)oxy)-3,6-dihydropyridine-1(2H)-carboxylate (100):**

N-Boc-3-hydroxy-1,2,3,6-tetrahydropyridine was used as starting material. ^{1H} NMR (400 MHz, CDCl3) δ (ppm) 1.46 (s, 9H), 5.01 (m, *1H*), 5.99 (m, *1H*), 5.90 (ddt, *J* = 10.2, 4.1, 2.1 Hz, *1H*), 4.97 (m, *1H*), 3.79 (s, 3H), 3.82 (m, 2H), 3.61 (m, *1H*). ^{13}C NMR ($CDCl_3$) δ (ppm) 28.2, 43.1, 44.5, 54.4, 69.9, 80.1, 123.4, 130.9, 154.5, 155.3. Yiellowish oil. Yield: 80%.

5.2.2 Synthesis of starting materials 93, 95 and 97:

2-methylenehexane-1,6-diol (101)

To a solution of 2-methylprop-2-en-1-ol (5 mmol) in anhydrous diethyl ether (0.4 M) at 0°C, BuLi 2.5 M in hexane (5 mL) and anhydrous TMEDA (2 mL) were added dropwise, under nitrogen atmosphere. The mixture was allowed to stir at room temperature for 30 minutes. Then, oxetane was added and the mixture was again stirred at room temperature for 6 hours. After reaction completion, the mixture was diluted

with diethyl ether and washed with 1M HCl solution three times. The organic layer was then dried over Na_2SO_4, filtered and evaporated under reduced pressure. The crude mixture was then purified by flash chromatography (DCM/MeOH 9/1). ^{1H} NMR (400 MHz, CDCl3) δ (ppm) 4.97 (s, *1H*), 4.80 (s, *1H*), 4.00 (b**s,** 2H), 3.59 (t, *J* = 5.0 Hz, 2H), 3.25 (b**s,** 2H), 2.06 (t, *J* = 5.0 Hz, 2H), 1.57 (m, 4H). ^{13}C NMR (CDCl3) δ (ppm) 23.9, 32-1, 32.6, 61.9, 65.0, 109.1, 148.6. Colorless oil. Yield: 40%.

6-hydroxy-2-methylenehexyl methyl carbonate (93):

An oven-dryed round-bottom flask with a stirring bar inside, was capped with a septum cap and submitted to three cycles of vacuum/nitrogen. Then, methyl chloroformate (1.4 mmol) was added to a solution of the allylic alcohol **101** (5.6 mmol) and pyridine (1.7 mmol) in dry DCM (0.4 M) at 0°C, under nitrogen atmosphere. The reaction mixture was then warmed to room temperature, and stirred for 4 h. After reaction completion, the organic layer was washed three times with 1M HCl solution and finally with brine. The combined organic layers were dried over Na_2SO_4, filtered and then evaporated under reduced pressure, providing the desired allylic carbonates without further purifications. ^{1H} NMR (400 MHz, CDCl3) δ (ppm) 5.08 (s, *1H*), 4.96 (s, *1H*), 4.55 (s, 2H), 3.83 (s, 3H), 3.61 (t, 2H, *J* = 5.2 Hz), 2.11 (br, *1H*), 2.08 (t, 2H, v*J* = 7.2 Hz), 1.57 (m, 4H). ^{13}C NMR (CDCl3) δ (ppm) 23.5, 32.3, 32.6, 54.6, 62.4, 70.1, 113.2, 143.1, 155.6. Colorless oil. Yield: 62%.

2-methylene-5-phenylpentan-1-ol (102):

An oven-dried flask was charged with magnesium turnings (9.60 mmol) and a small crystal of iodine. The flask was then purged with nitrogen and submitted to three cycle of vacuum/nitrogen. Then, 2.5 mL of dry THF were added and the mixture was refluxed. A solution of (3-bromopropyl)benzene (5.00 mmol) in dry THF (0.5mL) was added dropwise over the course of 30 min. The reaction was refluxed for 2 h and then cooled to room temperature.

A solution of CuI in dry THF (15 mol% in 10 mL) was then added. The reaction mixture was allowed to stir at room temperature for 0.5 h. Propargyl alcohol (2 mmol) in dry THF (2 mL) was then added dropwise at room temperature. The reaction was then heated to reflux for additional 24 h. After cooling to room temperature the crude, NH4Cl aqueous solution was added carefully. The organic layer was then separated and the aqueous phase extracted with diethyl ether. The reunited organic layers were dried over Na_2SO_4, filtered and evaporated under reduced pressure. Crude product was purified by silica gel column chromatography (Pentane/Diethyl ether 9/1). ^{1H} NMR (400 MHz, CDCl3) δ (ppm) 7.28 (m, 2H), 7.17 (m, 3H), 5.01 (s, *1H*), 4.90 (s *1H*), 4.07 (s, 2H), 2.63 (t, *J* = 7.7 Hz, 2H), 2.10 (t, *J* = 7.7 Hz, 2H), 1.79(m, 2H). ^{13}C NMR (CDCl3) δ (ppm) 27.7, 33.0, 36.2, 65.6, 110.1, 126.0, 128.1, 142.0, 148.2. Yiellowish oil. Yield: 57%.

Methyl (2-methylene-5-phenylpentyl) carbonate (95):

Same procedure of **5.2.1**, compound **102** used as starting material, stirring for 22 h. ^{1H} NMR (400 MHz, CDCl3) δ (ppm) 7.22 (m, 5H), 5.31 (s, *1H*), 5.19 (s, *1H*), 4.81 (s, 2H), 3.79 (s, 3H), 2.63 (t, *J* = 7.2 Hz,

2H), 2.19 (t, *J* = 7.2 Hz, 2H), 1.44 (m, 2H). ^{13}C NMR (CDCl3) δ (ppm) 27.4, 33.0, 35.8, 54.9, 72.3, 113.0, 126.2, 128.1, 128.8, 142.2, 143.6, 155.5. Yiellowish oil. Yield: 70%.

5-phenylpent-1-en-3-ol (103):

To a solution of 3-phenyl-propionaldehyde (4.2mmol) in dry diethyl ether (5mL) at 0°C was added slowly a solution of vinylmagnesium bromide 1 M in diethyl ether (5.0mmol). The resulting mixture was stirred at room temperature for 12h, under nitrogen atmosphere. After reaction completion, the reaction was quenched with a saturated solution of NH4Cl and extracted three times with diethylether. The organic layer was then washed with brine, dried over Na_2SO_4, filtered and evaporated under reduced pressure. Crude product was purified by silica gel column chromatography (Pentane/Diethyl ether 9/1). ^{1H} NMR (400 MHz, CDCl3) δ (ppm)7.30 (m, 2H), 7.25 (m, 2H), 7.22 (dd, *J* = 1.0, 0.5 Hz, *1H*), 5.93 (ddd, *J* = 17.2, 10.3, 6.0 Hz, *1H*), 5.27 (dt, *J* = 17.1, 1.3 Hz, *1H*), 5.19 (dt, *J* = 10.4, 1.3 Hz, *1H*), 4.13 (dd, *J* = 13.0, 6.0 Hz, *1H*), 2.75 (dd, *J* = 15.8, 7.0 Hz, 2H), 2.14 (br, *1H*), 1.89 (m, 2H). ^{13}C NMR (CDCl3) δ (ppm) 31.9, 39.2, 73.1, 115.7, 126.0, 128.1, 128.8, 139.1.

Methyl (5-phenylpent-1-en-3-yl) carbonate (97) :

Same procedure of **5.2.1**, compound **103** used as starting material, stirring for 24 h. ^{1H} NMR (400 MHz, CDCl3) δ (ppm) 7.27 (m, 2H), 7.19 (m, 3H), 5.80 (ddd, *J* = 17.4, 10.5, 6.7 Hz, *1H*), 5.29 (m, 3H), 3.79 (s, 3H), 2.67 (m, 2H), 1.98 (m, 2H). ^{13}C NMR (CDCl3) δ (ppm) 31.1, 35.8, 54.4, 78.1, 117.1, 126.0, 128.1, 128.2, 136.1, 141.3, 155.7. Colorless oil. Yield: 82%.

5.2.3 General procedure for the HAT-mediated Tsuji-Trost allylation

A glass vial capped with a septum was charged with the proper allyl methyl carbonate (0.1 mmol), tris(dibenzylideneacetone)dipalladium (2.5 μmol), 5,7,12,14-pentacenetetrone (6 μmol), and BINAP (5 μmol) and then purged with nitrogen and submitted to three cycle of nitrogen/vacuum. Then, the suitable alkyl radical precursor was added (2 mmol) under N_2 atmosphere along with dry degassed ACN (1 mL). Then the vial was sealed and placed in a photoreactor, showed in Figure 44, under a *Kessil Lamp* 390 nm 40 W exposure and stirred at room temperature for 22 h. After reaction completion, external standard was added (0.1 mmol) and the crude mixture was filtered over a plug of silica to remove palladium catalyst. Then, sample of 100 μL of reaction mixture was diluted with 400 μL of $CDCl_3$ and submitted to ^{1H}-NMR analysis.

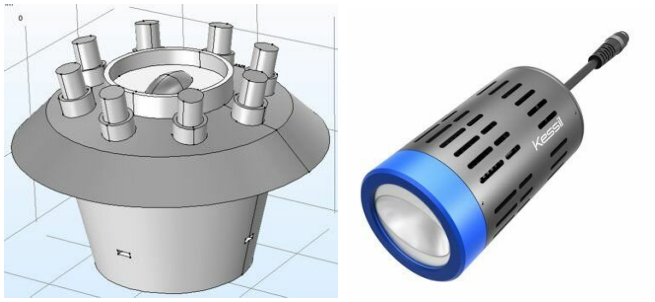

Figure 44. Photoreactor (on the left) endowed with Kessil Lamp 390 nm 40 W (on the right) for batch photocatalysis.

5.2.4 Epoxidation of 91 and synthesis of compound 104

2-(oxiran-2-ylmethyl)benzo[d][1,3]dioxole (104):

The crude mixture of compound **91** was filtered over a plug of celite and then evaporated under reduced pressure. The crude was redissolved in DCM (0.1 M) and mCPBA was added at 0°C in a 1:1 molar ration with **91**, based on the detected ^{1H}-NMR yield for the first step of the reaction. The reaction was then stirred at room temperature for 24 h. After reaction completion, the organic layer was first washed with a saturated $Na_2S_2O_3$ solution, then with a 1M NaOH solution and in the end with brine. The organic layer was dried over Na_2SO_4, filtered and evaporated under reduced pressure. Purification was made by flash chromatography (Pentane/Diethylether 95/5). ^{1H} NMR (400 MHz, CDCl3) δ (ppm) 2.23 (m, *1H*), 2.63 (dd, , *J* = 5.0, 2.6 Hz, *1H*), 2.86 (dd, *J* = 4.9, 4.0 Hz, *1H*), 5.32 (s, 2H), 6.30 (m, *1H*), 6.84 (s, *1H*). ^{13}C NMR (CDCl3) δ (ppm) 41.2, 44.1, 48.5, 101.3, 115.1, 121.2, 146.2. Colorless oil. Yield over two steps: 52%.

6. References Chapter I and Chapter II

(1) FAO. *The FAO Action Plan on Antimicrobial Resistance 2021–2025*; FAO: Rome, 2021. https://doi.org/10.4060/cb5545en.

(2) World Health Organization (WHO). Antimicrobial resistance https://www.who.int/news-room/fact-sheets/detail/antimicrobial-resistance (accessed Dec 11, 2021).

(3) Nieuwlaat, R.; Mbuagbaw, L.; Mertz, D.; Burrows, L. L.; Bowdish, D. M. E.; Moja, L.; Wright, G. D.; Schünemann, H. J. COVID-19 and Antimicrobial Resistance: Parallel and Interacting Health Emergencies. *Clin. Infect. Dis. An Off. Publ. Infect. Dis. Soc. Am.* **2021**, *72* (9), 1657–1659. https://doi.org/10.1093/CID/CIAA773.

(4) World Health Organization (WHO). Antimicrobial Resistance Benchmark - A research programme by the Access to Medicine Foundation https://www.amrbenchmark.org/amr-benchmark (accessed Dec 13, 2021).

(5) *2020 Antibacterial Agents in Clinical and Preclinical Development*; 2020.

(6) UNDP. Multi-Partner Trust Fund Office Gateway https://mptf.undp.org/factsheet/fund/AMR00?utm_source=EN&utm_medium=GSR&utm_content=US_UNDP_PaidSearch_Brand_English&utm_campaign=CENTRAL&c_src=CENTRAL&c_src2=GSR&gclid=CjwKCAiAtdGNBhAmEiwAWxGcUr8gilx74AsH3IiSckI4kcC_kczlxl_BIUv-BQcSw2oUfkaLASz-ThoCzn4QAv (accessed Dec 11, 2021).

(7) GARDP. Global Antibiotic Research & Development Partnership https://gardp.org/ (accessed Dec 11, 2021).

(8) Burrows, L. L. The conversation https://theconversation.com/drug-resistant-superbugs-a-global-threat-intensified-by-the-fight-against-coronavirus-135790 (accessed Dec 12, 2021).

(9) Mossialos, E.; Morel, C.; Edwards, S.; Berenson, J.; Gemmill-Toyama, M.; Brogan, D. Policies and Incentives for Promoting Innovation in Antibiotic Research. Geneva: World Health Organization for the European Observatory on Health Systems and Policies; 2010, 2010.

(10) World Health Organization (WHO). *2019 Antibacterial Agents in Clinical Development: An Analysis of the Antibacterial Clinical Development Pipeline.*; 2019.

(11) Food and Drugs Administration (FDA). FDA approves new antibacterial drug to treat complicated urinary tract infections as part of ongoing efforts to address antimicrobial resistance | FDA https://www.fda.gov/news-events/press-announcements/fda-approves-new-antibacterial-drug-treat-complicated-urinary-tract-infections-part-ongoing-efforts (accessed Dec 13, 2021).

(12) Veve, M. P.; Wagner, J. L. Lefamulin: Review of a Promising Novel Pleuromutilin Antibiotic. *Pharmacotherapy* **2018**, *38* (9), 935–946. https://doi.org/10.1002/phar.2166.

(13) FDA approves new antibiotic to treat community-acquired bacterial pneumonia | FDA.

(14) United Nations Organization (ONU). World Health Leaders Agree on Action to Combat Antimicrobial Resistance, Warning of Nearly 10 Million Deaths Annually If Left Unchecked | Meetings Coverage and Press Releases https://www.un.org/press/en/2016/ga11825.doc.htm (accessed Dec 13, 2021).

(15) The World Bank. Drug-Resistant Infections: A Threat to Our Economic Future https://www.worldbank.org/en/topic/health/publication/drug-resistant-infections-a-threat-to-our-economic-future (accessed Dec 13, 2021).

(16) O 'neill, J. Tackling Drug-Resistant Infections Globally: Final Report and Recommendations the Review on Antimicrobial Resistance. **2016**, No. May.

(17) Li, J.; Xie, S.; Ahmed, S.; Wang, F.; Gu, Y.; Zhang, C.; Chai, X.; Wu, Y.; Cai, J.; Cheng, G. Antimicrobial Activity and Resistance: Influencing Factors. *Front. Pharmacol.* **2017**, *8* (JUN), 364. https://doi.org/10.3389/FPHAR.2017.00364.

(18) Lobie, T. A.; Roba, A. A.; Booth, J. A.; Kristiansen, K. I.; Aseffa, A.; Skarstad, K.; Bjørås, M. Antimicrobial Resistance: A Challenge Awaiting the Post-COVID-19 Era. *Int. J. Infect. Dis.* **2021**, *111*, 322–325. https://doi.org/10.1016/j.ijid.2021.09.003.

(19) Gautret, P.; Lagier, J. C.; Parola, P.; Hoang, V. T.; Meddeb, L.; Mailhe, M.; Doudier, B.; Courjon, J.; Giordanengo, V.; Vieira, V. E.; Tissot Dupont, H.; Honoré, S.; Colson, P.; Chabrière, E.; La Scola, B.; Rolain, J. M.; Brouqui, P.; Raoult, D. Hydroxychloroquine and Azithromycin as a Treatment of COVID-19: Results of an Open-Label Non-Randomized Clinical Trial. *Int. J. Antimicrob. Agents* **2020**, *56* (1), 105949. https://doi.org/10.1016/J.IJANTIMICAG.2020.105949.

(20) Nori, P.; Cowman, K.; Chen, V.; Bartash, R.; Szymczak, W.; Madaline, T.; Punjabi Katiyar, C.; Jain, R.; Aldrich, M.; Weston, G.; Gialanella, P.; Corpuz, M.; Gendlina, I.; Guo, Y. Bacterial and Fungal Coinfections in COVID-19 Patients Hospitalized during the New York City Pandemic Surge. *Infect. Control Hosp. Epidemiol.* **2021**, *42* (1), 84–88. https://doi.org/10.1017/ice.2020.368.

(21) Huang, C.; Wang, Y.; Li, X.; Ren, L.; Zhao, J.; Hu, Y.; Zhang, L.; Fan, G.; Xu, J.; Gu, X.; Cheng, Z.; Yu, T.; Xia, J.; Wei, Y.; Wu, W.; Xie, X.; Yin, W.; Li, H.; Liu, M.; Xiao, Y.; Gao, H.; Guo, L.; Xie, J.; Wang, G.; Jiang, R.; Gao, Z.; Jin, Q.; Wang, J.; Cao, B. Clinical Features of Patients Infected with 2019 Novel Coronavirus in Wuhan, China. *Lancet* **2020**, *395* (10223), 497–506. https://doi.org/10.1016/S0140-6736(20)30183-5.

(22) Ripa, M.; Galli, L.; Poli, A.; Oltolini, C.; Spagnuolo, V.; Mastrangelo, A.; Muccini, C.; Monti, G.; De Luca, G.; Landoni, G.; Dagna, L.; Clementi, M.; Rovere Querini, P.; Ciceri, F.; Tresoldi, M.; Lazzarin, A.; Zangrillo, A.; Scarpellini, P.; Castagna, A.; Andolina, A.; Redaelli, M. B.; Bigai, G.; Bigoloni, A.; Borio, G.; Bossolasco, S.; Bruzzesi, E.; Calabrò, M. G.; Calvisi, S.; Campochiaro, C.; Canetti, D.; Canti, V.; Castellani, J.; Castiglioni, B.; Cavalli, G.; Cavallo, L.; Cernuschi, M.;

Chiurlo, M.; Cilla, M.; Cinel, E.; Cinque, P.; Conte, C.; Da Prat, V.; Danise, A.; De Lorenzo, R.; Dell'Acqua, A.; Dell'Acqua, R.; Della Torre, E.; Della Torre, L.; Di Terlizzi, G.; Dumea, I.; Farolfi, F.; Ferrante, M.; Frangi, C.; Fumagalli, L.; Gallina, G.; Germinario, B.; Gianotti, N.; Guffanti, M.; Hasson, H.; Lalla, F.; Lanzillotta, M.; Li Voti, R.; Messina, E.; Molinari, C.; Moizo, E.; Montagna, M.; Morsica, G.; Nozza, S.; Pascali, M.; Patrizi, A.; Pieri, M.; Poloniato, A.; Prestifilippo, D.; Ramirez, G.; Ranzenigo, M.; Sapienza, J.; Seghi, F.; Tambussi, G.; Tassan Din, C.; Turi, S.; Uberti-Foppa, C.; Vinci, C. Secondary Infections in Patients Hospitalized with COVID-19: Incidence and Predictive Factors. *Clin. Microbiol. Infect.* **2021**, *27* (3), 451–457. https://doi.org/10.1016/j.cmi.2020.10.021.

(23) Moser, D.; Biere, K.; Han, B.; Hoerl, M.; Schelling, G.; Choukér, A.; Woehrle, T. COVID-19 Impairs Immune Response to Candida Albicans. *Front. Immunol.* **2021**, *12*. https://doi.org/10.3389/FIMMU.2021.640644/FULL.

(24) Song, G.; Liang, G.; Liu, W. Fungal Co-Infections Associated with Global COVID-19 Pandemic: A Clinical and Diagnostic Perspective from China. *Mycopathologia* **2020**, *185* (4), 1. https://doi.org/10.1007/S11046-020-00462-9.

(25) Koehler, P.; Cornely, O. A.; Böttiger, B. W.; Dusse, F.; Eichenauer, D. A.; Fuchs, F.; Hallek, M.; Jung, N.; Klein, F.; Persigehl, T.; Rybniker, J.; Kochanek, M.; Böll, B.; Shimabukuro-Vornhagen, A. COVID-19 Associated Pulmonary Aspergillosis. *Mycoses* **2020**, *63* (6), 528. https://doi.org/10.1111/MYC.13096.

(26) Garcia-Vidal, C.; Sanjuan, G.; Moreno-García, E.; Puerta-Alcalde, P.; Garcia-Pouton, N.; Chumbita, M.; Fernandez-Pittol, M.; Pitart, C.; Inciarte, A.; Bodro, M.; Morata, L.; Ambrosioni, J.; Grafia, I.; Meira, F.; Macaya, I.; Cardozo, C.; Casals, C.; Tellez, A.; Castro, P.; Marco, F.; García, F.; Mensa, J.; Martínez, J. A.; Soriano, A.; Rico, V.; Hernández-Meneses, M.; Agüero, D.; Torres, B.; González, A.; de la Mora, L.; Rojas, J.; Linares, L.; Fidalgo, B.; Rodriguez, N.; Nicolas, D.; Albiach, L.; Muñoz, J.; Almuedo, A.; Camprubí, D.; Angeles Marcos, M.; Cilloniz, C.; Fernández, S.; Nicolas, J. M.; Torres, A. Incidence of Co-Infections and Superinfections in Hospitalized Patients with COVID-19: A Retrospective Cohort Study. *Clin. Microbiol. Infect.* **2021**, *27* (1), 83–88. https://doi.org/10.1016/J.CMI.2020.07.041.

(27) Tracking the Global Pipeline of Antibiotics in Development, March 2021 | The Pew Charitable Trusts https://www.pewtrusts.org/en/research-and-analysis/issue-briefs/2021/03/tracking-the-global-pipeline-of-antibiotics-in-development (accessed Dec 13, 2021).

(28) Rogers, G. B.; Carroll, M. P.; Bruce, K. D. Enhancing the Utility of Existing Antibiotics by Targeting Bacterial Behaviour? *Br. J. Pharmacol.* **2012**, *165* (4), 845. https://doi.org/10.1111/J.1476-5381.2011.01643.X.

(29) World Health Organization (WHO). Antibiotic resistance https://www.who.int/news-

room/fact-sheets/detail/antibiotic-resistance (accessed Dec 13, 2021).

(30) Pendleton, J. N.; Gorman, S. P.; Gilmore, B. F. Clinical Relevance of the ESKAPE Pathogens. *Expert Rev. Anti. Infect. Ther.* **2013**, *11* (3), 297–308. https://doi.org/10.1586/ERI.13.12.

(31) Mulani, M. S.; Kamble, E. E.; Kumkar, S. N.; Tawre, M. S.; Pardesi, K. R. Emerging Strategies to Combat ESKAPE Pathogens in the Era of Antimicrobial Resistance: A Review. *Front. Microbiol.* **2019**, *10* (APR), 539. https://doi.org/10.3389/FMICB.2019.00539/BIBTEX.

(32) Magiorakos, A. P.; Srinivasan, A.; Carey, R. B.; Carmeli, Y.; Falagas, M. E.; Giske, C. G.; Harbarth, S.; Hindler, J. F.; Kahlmeter, G.; Olsson-Liljequist, B.; Paterson, D. L.; Rice, L. B.; Stelling, J.; Struelens, M. J.; Vatopoulos, A.; Weber, J. T.; Monnet, D. L. Multidrug-Resistant, Extensively Drug-Resistant and Pandrug-Resistant Bacteria: An International Expert Proposal for Interim Standard Definitions for Acquired Resistance. *Clin. Microbiol. Infect.* **2012**, *18* (3), 268–281. https://doi.org/10.1111/J.1469-0691.2011.03570.X.

(33) Gajdács, M. The Concept of an Ideal Antibiotic: Implications for Drug Design. *Mol. 2019, Vol. 24, Page 892* **2019**, *24* (5), 892. https://doi.org/10.3390/MOLECULES24050892.

(34) Spellberg, B. The Future of Antibiotics. *Crit. Care* **2014**, *18* (3). https://doi.org/10.1186/CC13948.

(35) Spellberg, B.; Talbot, G. H.; Brass, E. P.; Bradley, J. S.; Boucher, H. W.; Gilbert, D. N. Position Paper: Recommended Design Features of Future Clinical Trials of Antibacterial Agents for Community-Acquired Pneumonia. *Clin. Infect. Dis.* **2008**, *47* (Suppl 3), S249. https://doi.org/10.1086/591411.

(36) Lewis, K. Platforms for Antibiotic Discovery. *Nat. Rev. Drug Discov. 2013 125* **2013**, *12* (5), 371–387. https://doi.org/10.1038/nrd3975.

(37) Plackett, B. Why Big Pharma Has Abandoned Antibiotics. *Nature* **2020**, *586* (7830), S50–S52. https://doi.org/10.1038/D41586-020-02884-3.

(38) Maier, M. E. Design and Synthesis of Analogues of Natural Products. *Org. Biomol. Chem.* **2015**, *13* (19), 5302–5343. https://doi.org/10.1039/C5OB00169B.

(39) DiMasi, J. A.; Hansen, R. W.; Grabowski, H. G. The Price of Innovation: New Estimates of Drug Development Costs. *J. Health Econ.* **2003**, *22* (2), 151–185. https://doi.org/10.1016/S0167-6296(02)00126-1.

(40) Boggs, A. F.; Miller, G. H. Antibacterial Drug Discovery: Is Small Pharma the Solution? *Clin. Microbiol. Infect.* **2004**, *10 Suppl 4* (4), 32–36. https://doi.org/10.1111/J.1465-0691.2004.1008.X.

(41) Van Duijn, P. J.; Bonten, M. J. Antibiotic Rotation Strategies to Reduce Antimicrobial Resistance in Gram-Negative Bacteria in European Intensive Care Units: Study Protocol for a Cluster-Randomized Crossover Controlled Trial. *Trials* **2014**, *15* (277). https://doi.org/10.1186/1745-6215-15-277.

(42) Wright, G. D. Antibiotic Adjuvants: Rescuing Antibiotics from Resistance. *Trends Microbiol.* **2016**, *24* (11), 862–871. https://doi.org/10.1016/J.TIM.2016.06.009.

(43) Annunziato, G. Strategies to Overcome Antimicrobial Resistance (AMR) Making Use of Non-Essential Target Inhibitors: A Review. *Int. J. Mol. Sci.* **2019**, *20* (23). https://doi.org/10.3390/IJMS20235844.

(44) Beeuwkes, H.; Rutgers, V. H. A Combination of Amoxicillin and Clavulanic Acid in the Treatment of Respiratory Tract Infections Caused by Amoxicillin-Resistant Haemophilus Influenzae. *Infection* **1981**, *9* (5), 244–248. https://doi.org/10.1007/BF01640725.

(45) Hartzell, J. D.; Neff, R.; Ake, J.; Howard, R.; Olson, S.; Paolino, K.; Vishnepolsky, M.; Weintrob, A.; Wortmann, G. Nephrotoxicity Associated with Intravenous Colistin (Colistimethate Sodium) Treatment at a Tertiary Care Medical Center. *Clin. Infect. Dis.* **2009**, *48* (12), 1724–1728. https://doi.org/10.1086/599225.

(46) Odds, F. C. Synergy, Antagonism, and What the Chequerboard Puts between Them. *J. Antimicrob. Chemother.* **2003**, *52* (1), 1. https://doi.org/10.1093/JAC/DKG301.

(47) Taccone, F. S.; Rodriguez-Villalobos, H.; De Backer, D.; De Moor, V.; Deviere, J.; Vincent, J. L.; Jacobs, F. Successful Treatment of Septic Shock Due to Pan-Resistant Acinetobacter Baumannii Using Combined Antimicrobial Therapy Including Tigecycline. *Eur. J. Clin. Microbiol. Infect. Dis.* **2006**, *25* (4), 257–260. https://doi.org/10.1007/S10096-006-0123-1/FIGURES/1.

(48) Sakoulas, G.; Moise, P. A.; Casapao, A. M.; Nonejuie, P.; Olson, J.; Okumura, C. Y. M.; Rybak, M. J.; Kullar, R.; Dhand, A.; Rose, W. E.; Goff, D. A.; Bressler, A. M.; Lee, Y.; Pogliano, J.; Johns, S.; Kaatz, G. W.; Ebright, J. R.; Nizet, V. Antimicrobial Salvage Therapy for Persistent Staphylococcal Bacteremia Using Daptomycin plus Ceftaroline. *Clin. Ther.* **2014**, *36* (10), 1317–1333. https://doi.org/10.1016/J.CLINTHERA.2014.05.061.

(49) Davis, J. S.; Network, and for the A. S. for I. D. C. R.; Sud, A.; Network, and for the A. S. for I. D. C. R.; O'Sullivan, M. V. N.; Network, and for the A. S. for I. D. C. R.; Robinson, J. O.; Network, and for the A. S. for I. D. C. R.; Ferguson, P. E.; Network, and for the A. S. for I. D. C. R.; Foo, H.; Network, and for the A. S. for I. D. C. R.; van Hal, S. J.; Network, and for the A. S. for I. D. C. R.; Ralph, A. P.; Network, and for the A. S. for I. D. C. R.; Howden, B. P.; Network, and for the A. S. for I. D. C. R.; Binks, P. M.; Network, and for the A. S. for I. D. C. R.; Kirby, A.; Network, and for the A. S. for I. D. C. R.; Tong, S. Y. C.; Network, and for the A. S. for I. D. C. R.; group, for the C. A. for Me. R. S. aureus (CAMERA) study; group, for the C. A. for Me. R. S. aureus (CAMERA) study; Tong, S.; Davis, J.; Binks, P.; Majumdar, S.; Ralph, A.; Baird, R.; Gordon, C.; Jeremiah, C.; Leung, G.; Brischetto, A.; Crowe, A.; Dakh, F.; Whykes, K.; Kirkwood, M.; Sud, A.; Menon, M.; Somerville, L.; Subedi, S.; Owen, S.; O'Sullivan, M.; Liu, E.; Zhou, F.; Robinson, O.; Coombs, G.; Ferguson, P.; Ralph, A.; Liu, E.; Pollet, S.; Van Hal, S.;

Foo, H.; Van Hal, S.; Davis, R. Combination of Vancomycin and β-Lactam Therapy for Methicillin-Resistant Staphylococcus Aureus Bacteremia: A Pilot Multicenter Randomized Controlled Trial. *Clin. Infect. Dis.* **2016**, *62* (2), 173–180. https://doi.org/10.1093/CID/CIV808.

(50) Aktas, G.; Derbentli, S. In Vitro Activity of Daptomycin Combined with Dalbavancin and Linezolid, and Dalbavancin with Linezolid against MRSA Strains. *J. Antimicrob. Chemother.* **2017**, *72* (2), 441–443. https://doi.org/10.1093/JAC/DKW416.

(51) Bush, K. Antimicrobial Agents Targeting Bacterial Cell Walls and Cell Membranes. *Rev. Sci. Tech.* **2012**, *31* (1), 43–56. https://doi.org/10.20506/RST.31.1.2096.

(52) Spapen, H.; Jacobs, R.; Gorp, V. Van; Troubleyn, J.; Honoré, P. M. Renal and Neurological Side Effects of Colistin in Critically Ill Patients. *Ann. Intensive Care* **2011**. https://doi.org/10.1186/2110-5820-1-14.

(53) Nation, R. L.; Li, J. Colistin in the 21 St Century. *Curr. Opin. Infect. Dis.* **2009**. https://doi.org/10.1097/QCO.0b013e328332e672.

(54) Corona, A.; Cattaneo, D. Dosing Colistin Properly: Let's Save "Our Last Resort Old Drug!" *Clin. Infect. Dis.* **2017**, *65* (5), 870. https://doi.org/10.1093/CID/CIX388.

(55) Bialvaei, A. Z.; Samadi Kafil, H. Colistin, Mechanisms and Prevalence of Resistance. *Curr. Med. Res. Opin.* **2015**, *31* (4), 707–721. https://doi.org/10.1185/03007995.2015.1018989.

(56) Rossi, F.; Girardello, R.; Cury, A. P.; Di Gioia, T. S. R.; Almeida, J. N. de; Duarte, A. J. da S. Emergence of Colistin Resistance in the Largest University Hospital Complex of São Paulo, Brazil, over Five Years. *Braz. J. Infect. Dis.* **2017**, *21* (1), 98–101. https://doi.org/10.1016/J.BJID.2016.09.011.

(57) Monaco, M.; Giani, T.; Raffone, M.; Arena, F.; Garcia-Fernandez, A.; Pollini, S.; Grundmann, H.; Pantosti, A.; Rossolini, G. M. Colistin Resistance Superimposed to Endemic Carbapenem-Resistant Klebsiella Pneumoniae: A Rapidly Evolving Problem in Italy, November 2013 to April 2014. *Euro Surveill.* **2014**, *19* (42), 20939.

(58) Cannatelli, A.; D'Andrea, M. M.; Giani, T.; Di Pilato, V.; Arena, F.; Ambretti, S.; Gaibani, P.; Rossolini, G. M. In Vivo Emergence of Colistin Resistance in Klebsiella Pneumoniae Producing KPC-Type Carbapenemases Mediated by Insertional Inactivation of the PhoQ/PhoP MgrB Regulator. *Antimicrob. Agents Chemother.* **2013**, *57* (11), 5521–5526. https://doi.org/10.1128/AAC.01480-13.

(59) Hjort, K.; Nicoloff, H.; Andersson, D. I. Unstable Tandem Gene Amplification Generates Heteroresistance (Variation in Resistance within a Population) to Colistin in Salmonella Enterica. *Mol. Microbiol.* **2016**, *102* (2), 274–289. https://doi.org/10.1111/MMI.13459.

(60) Minrovic, B. M.; Jung, D.; Melander, R. J.; Melander, C. A New Class of Adjuvants Enables Lower Dosing of Colistin Against Acinetobacter Baumannii. *ACS Infect. Dis.* **2018**, *4* (9), 1368–

1376.

(61) Kubo, A.; Lunde, C. S.; Kubo, I. Indole and (E)-2-Hexenal, Phytochemical Potentiators of Polymyxins against Pseudomonas Aeruginosa and Escherichia Coli. *Antimicrob. Agents Chemother.* **1996**, *40* (6), 1438–1441. https://doi.org/10.1128/AAC.40.6.1438.

(62) Pollini, S.; Boncompagni, S.; DI Maggio, T.; DI Pilato, V.; Spanu, T.; Fiori, B.; Blasi, F.; Aliberti, S.; Sergio, F.; Rossolini, G. M.; Pallecchi, L. In Vitro Synergism of Colistin in Combination with N-Acetylcysteine against Acinetobacter Baumannii Grown in Planktonic Phase and in Biofilms. *J. Antimicrob. Chemother.* **2018**, *73* (9), 2388–2395. https://doi.org/10.1093/JAC/DKY185.

(63) Zarrilli, R.; Bagattini, M.; Berisio, R.; Rossolini, G. M.; Cannatelli, A.; Principato, S.; Colavecchio, O. L.; Pallecchi, L. Synergistic Activity of Colistin in Combination With Resveratrol Against Colistin-Resistant Gram-Negative Pathogens. *Front. Microbiol. | www.frontiersin.org* **2018**, *1*, 1808. https://doi.org/10.3389/fmicb.2018.01808.

(64) Domalaon, R.; Malaka De Silva, P.; Kumar, A.; Zhanel, G. G.; Schweizer, F. The Anthelmintic Drug Niclosamide Synergizes with Colistin and Reverses Colistin Resistance in Gram-Negative Bacilli. *Antimicrob. Agents Chemother.* **2019**, *63* (4). https://doi.org/10.1128/AAC.02574-18.

(65) Stokes, J. M.; Macnair, C. R.; Ilyas, B.; French, S.; Côté, J.-P.; Bouwman, C.; Farha, M. A.; Sieron, A. O.; Whitfield, C.; Coombes, B. K.; Brown, E. D. Pentamidine Sensitizes Gram-Negative Pathogens to Antibiotics and Overcomes Acquired Colistin Resistance. *Nat. Microbiol.* **2017**, *2* (17028). https://doi.org/10.1038/nmicrobiol.2017.28.

(66) Matoke Holdings - Reactive Oxygen Technology https://matokeholdings.com/ (accessed Dec 15, 2021).

(67) Could these therapies make antimicrobial resistance a thing of the past? https://www.labiotech.eu/in-depth/antimicrobial-resistance-new-therapies/ (accessed Dec 15, 2021).

(68) Lin, D. M.; Koskella, B.; Lin, H. C. Phage Therapy: An Alternative to Antibiotics in the Age of Multi-Drug Resistance. *World J. Gastrointest. Pharmacol. Ther.* **2017**, *8* (3), 162–173. https://doi.org/10.4292/wjgpt.v8.i3.162.

(69) Mariathasan, S.; Tan, M. W. Antibody–Antibiotic Conjugates: A Novel Therapeutic Platform against Bacterial Infections. *Trends Mol. Med.* **2017**, *23* (2), 135–149. https://doi.org/10.1016/J.MOLMED.2016.12.008.

(70) Lehar, S. M.; Pillow, T.; Xu, M.; Staben, L.; Kajihara, K. K.; Vandlen, R.; DePalatis, L.; Raab, H.; Hazenbos, W. L.; Hiroshi Morisaki, J.; Kim, J.; Park, S.; Darwish, M.; Lee, B. C.; Hernandez, H.; Loyet, K. M.; Lupardus, P.; Fong, R.; Yan, D.; Chalouni, C.; Luis, E.; Khalfin, Y.; Plise, E.; Cheong, J.; Lyssikatos, J. P.; Strandh, M.; Koefoed, K.; Andersen, P. S.; Flygare, J. A.; Wah Tan, M.; Brown, E. J.; Mariathasan, S. Novel Antibody–Antibiotic Conjugate Eliminates Intracellular

S. Aureus. *Nat. 2015 5277578* **2015**, *527* (7578), 323–328. https://doi.org/10.1038/nature16057.

(71) Zhou, C.; Lehar, S.; Gutierrez, J.; Rosenberger, C. M.; Ljumanovic, N.; Dinoso, J.; Koppada, N.; Hong, K.; Baruch, A.; Carrasco-Triguero, M.; Saad, O.; Mariathasan, S.; Kamath, A. V. Pharmacokinetics and Pharmacodynamics of DSTA4637A: A Novel THIOMAB™ Antibody Antibiotic Conjugate against Staphylococcus Aureus in Mice. *https://doi.org/10.1080/19420862.2016.1229722* **2016**, *8* (8), 1612–1619. https://doi.org/10.1080/19420862.2016.1229722.

(72) Rosini, R.; Nicchi, S.; Pizza, M.; Rappuoli, R. Vaccines Against Antimicrobial Resistance. *Front. Immunol.* **2020**, *11*. https://doi.org/10.3389/FIMMU.2020.01048.

(73) Kwong, J. C.; Maaten, S.; Upshur, R. E. G.; Patrick, D. M.; Marra, F. The Effect of Universal Influenza Immunization on Antibiotic Prescriptions: An Ecological Study. *Clin. Infect. Dis.* **2009**, *49* (5), 750–756. https://doi.org/10.1086/605087.

(74) Zasloff, M. Antimicrobial Peptides of Multicellular Organisms. *Nat. 2002 4156870* **2002**, *415* (6870), 389–395. https://doi.org/10.1038/415389a.

(75) Zhang, N.; Ma, S. Recent Development of Membrane-Active Molecules as Antibacterial Agents. *Eur. J. Med. Chem.* **2019**, *184*. https://doi.org/10.1016/J.EJMECH.2019.111743.

(76) Yang, T.; Moreira, W.; Nyantakyi, S. A.; Chen, H.; Aziz, D. binte; Go, M. L.; Dick, T. Amphiphilic Indole Derivatives as Antimycobacterial Agents: Structure-Activity Relationships and Membrane Targeting Properties. *J. Med. Chem.* **2017**, *60* (7), 2745–2763. https://doi.org/10.1021/ACS.JMEDCHEM.6B01530/SUPPL_FILE/JM6B01530_SI_002.CSV .

(77) Mingeot-Leclercq, M. P.; Décout, J. L. Bacterial Lipid Membranes as Promising Targets to Fight Antimicrobial Resistance, Molecular Foundations and Illustration through the Renewal of Aminoglycoside Antibiotics and Emergence of Amphiphilic Aminoglycosides. *Medchemcomm* **2016**, *7* (4), 586–611. https://doi.org/10.1039/c5md00503e.

(78) Epand, R. M.; Epand, R. F. Domains in Bacterial Membranes and the Action of Antimicrobial Agents. *Mol. Biosyst.* **2009**, *5* (6), 580–587. https://doi.org/10.1039/B900278M.

(79) Epand, R. M.; Walker, C.; Epand, R. F.; Magarvey, N. A. Molecular Mechanisms of Membrane Targeting Antibiotics. *Biochim. Biophys. Acta* **2016**, *1858* (5), 980–987. https://doi.org/10.1016/J.BBAMEM.2015.10.018.

(80) Vance, J. E. Phospholipid Synthesis and Transport in Mammalian Cells. *Traffic* **2015**, *16* (1), 1–18. https://doi.org/10.1111/TRA.12230.

(81) Ghosh, C.; Haldar, J. Membrane-Active Small Molecules: Designs Inspired by Antimicrobial Peptides. *ChemMedChem* **2015**, *10* (10), 1606–1624. https://doi.org/10.1002/CMDC.201500299.

(82) Hickey, S. M.; Ashton, T. D.; Boer, G.; Bader, C. A.; Thomas, M.; Elliott, A. G.; Schmuck, C.;

Yu, H. Y.; Li, J.; Nation, R. L.; Cooper, M. A.; Plush, S. E.; Brooks, D. A.; Pfeffer, F. M. Norbornane-Based Cationic Antimicrobial Peptidomimetics Targeting the Bacterial Membrane. *Eur. J. Med. Chem.* **2018**, *160*, 9–22. https://doi.org/10.1016/J.EJMECH.2018.09.072.

(83) Alborn, W. E.; Allen, N. E.; Preston, D. A. Daptomycin Disrupts Membrane Potential in Growing Staphylococcus Aureus. *Antimicrob. Agents Chemother.* **1991**, *35* (11), 2282–2287. https://doi.org/10.1128/AAC.35.11.2282.

(84) FDA. DAPTOMYCIN FOR INJECTION safely and effectively. LABEL https://www.accessdata.fda.gov/drugsatfda_docs/label/2020/208385s005lbl.pdf (accessed Dec 21, 2021).

(85) Lim, L. M.; Ly, N.; Anderson, D.; Yang, J. C.; Macander, L.; Jarkowski, A.; Forrest, A.; Bulitta, J. B.; Tsuji, B. T. Resurgence of Colistin: A Review of Resistance, Toxicity, Pharmacodynamics, and Dosing. *Pharmacotherapy* **2010**, *30* (12), 1279–1291. https://doi.org/10.1592/PHCO.30.12.1279.

(86) Pajerski, W.; Ochonska, D.; Brzychczy-Wloch, M.; Indyka, P.; Jarosz, M.; Golda-Cepa, M.; Sojka, Z.; Kotarba, A. Attachment Efficiency of Gold Nanoparticles by Gram-Positive and Gram-Negative Bacterial Strains Governed by Surface Charges. *J. Nanoparticle Res.* **2019**, *21* (8), 1–12. https://doi.org/10.1007/S11051-019-4617-Z/FIGURES/8.

(87) FDA. MACROBID - nitrofurantoin monohydrate/macrocrystals LABEL https://www.accessdata.fda.gov/drugsatfda_docs/label/2009/020064s019lbl.pdf (accessed Dec 21, 2021).

(88) Su, M.; Xia, D.; Teng, P.; Nimmagadda, A.; Zhang, C.; Odom, T.; Cao, A.; Hu, Y.; Cai, J. Membrane-Active Hydantoin Derivatives as Antibiotic Agents. *J. Med. Chem.* **2017**, *60* (20), 8456–8465. https://doi.org/10.1021/ACS.JMEDCHEM.7B00847/SUPPL_FILE/JM7B00847_SI_002.CSV.

(89) Wang, J.; Ansari, M. F.; Zhou, C. H. Unique Para-Aminobenzenesulfonyl Oxadiazoles as Novel Structural Potential Membrane Active Antibacterial Agents towards Drug-Resistant Methicillin Resistant Staphylococcus Aureus. *Bioorg. Med. Chem. Lett.* **2021**, *41*. https://doi.org/10.1016/J.BMCL.2021.127995.

(90) Hoque, J.; Konai, M. M.; Gonuguntla, S.; Manjunath, G. B.; Samaddar, S.; Yarlagadda, V.; Haldar, J. Membrane Active Small Molecules Show Selective Broad Spectrum Antibacterial Activity with No Detectable Resistance and Eradicate Biofilms. *J. Med. Chem.* **2015**, *58* (14), 5486–5500. https://doi.org/10.1021/ACS.JMEDCHEM.5B00443/SUPPL_FILE/JM5B00443_SI_002.CSV.

(91) Raulji, C. M.; Clay, K.; Velasco, C.; Yu, L. C. Daily Bathing with Chlorhexidine and Its Effects on Nosocomial Infection Rates in Pediatric Oncology Patients. *Pediatr. Hematol. Oncol.* **2015**, *32* (5), 315–321. https://doi.org/10.3109/08880018.2015.1013588.

(92) FDA. PerioChip ® 2.5mg - CHLORHEXEDINE gluconate LABEL https://www.accessdata.fda.gov/drugsatfda_docs/label/2012/020774s012lbl.pdf (accessed Dec 21, 2021).

(93) Cheung, H. Y.; Wong, M. M. K.; Cheung, S. H.; Liang, L. Y.; Lam, Y. W.; Chiu, S. K. Differential Actions of Chlorhexidine on the Cell Wall of Bacillus Subtilis and Escherichia Coli. *PLoS One* **2012**, *7* (5), 36659. https://doi.org/10.1371/JOURNAL.PONE.0036659.

(94) Teng, P.; Nimmagadda, A.; Su, M.; Hong, Y.; Shen, N.; Li, C.; Tsai, L. Y.; Cao, J.; Li, Q.; Cai, J. Novel Bis-Cyclic Guanidines as Potent Membrane-Active Antibacterial Agents with Therapeutic Potential. *Chem. Commun.* **2017**, *53* (87), 11948–11951. https://doi.org/10.1039/C7CC07285F.

(95) Datta, S.; Roy, A. Antimicrobial Peptides as Potential Therapeutic Agents: A Review. *Int. J. Pept. Res. Ther. 2020 271* **2020**, *27* (1), 555–577. https://doi.org/10.1007/S10989-020-10110-X.

(96) Bahar, A. A.; Ren, D. Antimicrobial Peptides. *Pharmaceuticals* **2013**, *6* (12), 1543. https://doi.org/10.3390/PH6121543.

(97) Jenssen, H.; Hamill, P.; Hancock, R. E. W. Peptide Antimicrobial Agents. *Clin. Microbiol. Rev.* **2006**, *19* (3), 491–511. https://doi.org/10.1128/CMR.00056-05/ASSET/885405EA-2BFA-4A39-AF5E-1A0445AEA662/ASSETS/GRAPHIC/ZCM0030621790002.JPEG.

(98) Lee, T. H.; Hofferek, V.; Separovic, F.; Reid, G. E.; Aguilar, M. I. The Role of Bacterial Lipid Diversity and Membrane Properties in Modulating Antimicrobial Peptide Activity and Drug Resistance. *Curr. Opin. Chem. Biol.* **2019**, *52*, 85–92. https://doi.org/10.1016/J.CBPA.2019.05.025.

(99) Huang, H. W.; Charron, N. E. Understanding Membrane-Active Antimicrobial Peptides. *Q. Rev. Biophys.* **2017**, *50*, e10. https://doi.org/10.1017/S0033583517000087.

(100) Li, S.; Wang, Y.; Xue, Z.; Jia, Y.; Li, R.; He, C.; Chen, H. The Structure-Mechanism Relationship and Mode of Actions of Antimicrobial Peptides: A Review. *Trends Food Sci. Technol.* **2021**, *109*, 103–115. https://doi.org/10.1016/J.TIFS.2021.01.005.

(101) Jamal, M.; Ahmad, W.; Andleeb, S.; Jalil, F.; Imran, M.; Nawaz, M. A.; Hussain, T.; Ali, M.; Rafiq, M.; Kamil, M. A. Bacterial Biofilm and Associated Infections. *J. Chin. Med. Assoc.* **2018**, *81* (1), 7–11. https://doi.org/10.1016/J.JCMA.2017.07.012.

(102) Koehbach, J.; Craik, D. J. The Vast Structural Diversity of Antimicrobial Peptides. *Trends Pharmacol. Sci.* **2019**, *40* (7), 517–528. https://doi.org/10.1016/J.TIPS.2019.04.012.

(103) Otvos, L. The Short Proline-Rich Antibacterial Peptide Family. *Cell. Mol. Life Sci. C. 2002 597* **2002**, *59* (7), 1138–1150. https://doi.org/10.1007/S00018-002-8493-8.

(104) Chan, D. I.; Prenner, E. J.; Vogel, H. J. Tryptophan- and Arginine-Rich Antimicrobial Peptides: Structures and Mechanisms of Action. *Biochim. Biophys. Acta - Biomembr.* **2006**, *1758* (9), 1184–1202. https://doi.org/10.1016/J.BBAMEM.2006.04.006.

(105) Kim, C. H.; Go, H. J.; Oh, H. Y.; Park, J. B.; Lee, T. K.; Seo, J. K.; Elphick, M. R.; Park, N. G. Identification of a Novel Antimicrobial Peptide from the Sea Star Patiria Pectinifera. *Dev. Comp. Immunol.* **2018**, *86*, 203–213. https://doi.org/10.1016/J.DCI.2018.05.002.

(106) Baumann, T.; Kämpfer, U.; Schürch, S.; Schaller, J.; Largiadèr, C.; Nentwig, W.; Kuhn-Nentwig, L. Ctenidins: Antimicrobial Glycine-Rich Peptides from the Hemocytes of the Spider Cupiennius Salei. *Cell. Mol. Life Sci. 2010 6716* **2010**, *67* (16), 2787–2798. https://doi.org/10.1007/S00018-010-0364-0.

(107) Lee, T.-H.; N. Hall, K.; Aguilar, M.-I. Antimicrobial Peptide Structure and Mechanism of Action: A Focus on the Role of Membrane Structure. *Curr. Top. Med. Chem.* **2016**, *16* (1), 25–39. https://doi.org/10.2174/1568026615666150703121700.

(108) Bogdanova, L. R.; Valiullina, Y. A.; Faizullin, D. A.; Kurbanov, R. K.; Ermakova, E. A. Spectroscopic, Zeta Potential and Molecular Dynamics Studies of the Interaction of Antimicrobial Peptides with Model Bacterial Membrane. *Spectrochim. Acta. A. Mol. Biomol. Spectrosc.* **2020**, *242*. https://doi.org/10.1016/J.SAA.2020.118785.

(109) Chen, C.; Li, G.; Cui, X.; Chen, J.; Yu, Q.; Zong, C.; Zhao, Y.; Xu, M.; Zhou, S.; Xu, H. Mechanistic Investigation of a Self-Assembling Peptide against Escherichia Coli. *Langmuir* **2020**, *36* (33), 9800–9809. https://doi.org/10.1021/ACS.LANGMUIR.0C01311/SUPPL_FILE/LA0C01311_SI_001.PDF.

(110) Perrin, B. S.; Pastor, R. W. Simulations of Membrane-Disrupting Peptides I: Alamethicin Pore Stability and Spontaneous Insertion. *Biophys. J.* **2016**, *111* (6), 1248–1257. https://doi.org/10.1016/J.BPJ.2016.08.014.

(111) Mihajlovic, M.; Lazaridis, T. Antimicrobial Peptides in Toroidal and Cylindrical Pores. *Biochim. Biophys. Acta - Biomembr.* **2010**, *1798* (8), 1485–1493. https://doi.org/10.1016/J.BBAMEM.2010.04.004.

(112) Sun, Y.; Shang, D. Inhibitory Effects of Antimicrobial Peptides on Lipopolysaccharide-Induced Inflammation. *Mediators Inflamm.* **2015**, *2015*. https://doi.org/10.1155/2015/167572.

(113) Bhattacharjya, S.; Straus, S. K. Design, Engineering and Discovery of Novel α-Helical and β-Boomerang Antimicrobial Peptides against Drug Resistant Bacteria. *Int. J. Mol. Sci. 2020, Vol. 21, Page 5773* **2020**, *21* (16), 5773. https://doi.org/10.3390/IJMS21165773.

(114) Sohlenkamp, C.; Geiger, O. Bacterial Membrane Lipids: Diversity in Structures and Pathways. *FEMS Microbiol. Rev.* **2015**, *40* (1), 133–159. https://doi.org/10.1093/femsre/fuv008.

(115) Strahl, H.; Errington, J. Bacterial Membranes: Structure, Domains, and Function. *Annu. Rev. Microbiol.* **2017**, *71*, 519–538. https://doi.org/10.1146/annurev-micro-102215-095630.

(116) Desriac, F.; Luiz Franco, O.; Yannick Fleury, B.; Wenzel, M.; Schäfer, A.-B. A How-To Guide for Mode of Action Analysis of Antimicrobial Peptides. *Front. Cell. Infect. Microbiol. | www.frontiersin.org* **2020**, *10*, 540898. https://doi.org/10.3389/fcimb.2020.540898.

(117) Voievoda, N.; Schulthess, T.; Bechinger, B.; Seelig, J. Thermodynamic and Biophysical Analysis of the Membrane-Association of a Histidine-Rich Peptide with Efficient Antimicrobial and Transfection Activities. *J. Phys. Chem. B* **2015**, *119* (30), 9678–9687. https://doi.org/10.1021/acs.jpcb.5b04543.

(118) Voievoda, N.; Schulthess, T.; Bechinger, B.; Seelig, J. Thermodynamic and Biophysical Analysis of the Membrane-Association of a Histidine-Rich Peptide with Efficient Antimicrobial and Transfection Activities. *J. Phys. Chem. B* **2015**, *119* (30), 9678–9687. https://doi.org/10.1021/ACS.JPCB.5B04543/SUPPL_FILE/JP5B04543_SI_001.PDF.

(119) Li, H.; Zhao, T.; Sun, Z. Analytical Techniques and Methods for Study of Drug-Lipid Membrane Interactions. *Rev. Anal. Chem.* **2018**, *37* (1). https://doi.org/10.1515/revac-2017-0012.

(120) Farkas, A.; Maróti, G.; Kereszt, A.; Kondorosi, É. Comparative Analysis of the Bacterial Membrane Disruption Effect of Two Natural Plant Antimicrobial Peptides. *Front. Microbiol.* **2017**, *8* (JAN), 51. https://doi.org/10.3389/fmicb.2017.00051.

(121) Chan, Y. H. M.; Boxer, S. G. Model Membrane Systems and Their Applications. *Curr. Opin. Chem. Biol.* **2007**, *11* (6), 581–587. https://doi.org/10.1016/J.CBPA.2007.09.020.

(122) Knobloch, J.; Suhendro, D. K.; Zieleniecki, J. L.; Shapter, J. G.; Köper, I. Membrane-Drug Interactions Studied Using Model Membrane Systems. *Saudi J. Biol. Sci.* **2015**, *22* (6), 714–718. https://doi.org/10.1016/j.sjbs.2015.03.007.

(123) Savini, F.; Bobone, S.; Roversi, D.; Mangoni, M. L.; Stella, L. From Liposomes to Cells: Filling the Gap between Physicochemical and Microbiological Studies of the Activity and Selectivity of Host-Defense Peptides. *Pept. Sci.* **2020**, *110* (5), e24041. https://doi.org/10.1002/pep2.24041.

(124) Agadi, N.; Vasudevan, S.; Kumar, A. Structural Insight into the Mechanism of Action of Antimicrobial Peptide BMAP-28(1-18) and Its Analogue MutBMAP18. *J. Struct. Biol.* **2018**, *204* (3), 435–448. https://doi.org/10.1016/J.JSB.2018.10.003.

(125) Hollmann, A.; Martinez, M.; Maturana, P.; Semorile, L. C.; Maffia, P. C. Antimicrobial Peptides: Interaction with Model and Biological Membranes and Synergism with Chemical Antibiotics. *Front. Chem.* **2018**, *6* (JUN), 204. https://doi.org/10.3389/fchem.2018.00204.

(126) Kyrychenko, A. Using Fluorescence for Studies of Biological Membranes: A Review. *Methods Appl. Fluoresc.* **2015**, *3* (4), 042003. https://doi.org/10.1088/2050-6120/3/4/042003.

(127) Berglund, N. A.; Piggot, T. J.; Jefferies, D.; Sessions, R. B.; Bond, P. J.; Khalid, S. Interaction of the Antimicrobial Peptide Polymyxin B1 with Both Membranes of E. Coli: A Molecular Dynamics Study. *PLOS Comput. Biol.* **2015**, *11* (4), e1004180. https://doi.org/10.1371/JOURNAL.PCBI.1004180.

(128) Skvortsova, P.; Valiullina, Y.; Baranova, N.; Faizullin, D.; Zuev, Y.; Ermakova, E. Spectroscopic Study of Antimicrobial Peptides: Structure and Functional Activity. *Spectrochim. Acta. A. Mol. Biomol. Spectrosc.* **2022**, *264*. https://doi.org/10.1016/J.SAA.2021.120273.

(129) Avitabile, C.; D'Andrea, L. D.; Romanelli, A. Circular Dichroism Studies on the Interactions of Antimicrobial Peptides with Bacterial Cells. *Sci. Reports 2014 41* **2014**, *4* (1), 1–7. https://doi.org/10.1038/srep04293.

(130) Lombardi, L.; Stellato, M. I.; Oliva, R.; Falanga, A.; Galdiero, M.; Petraccone, L.; D'Errico, G.; De Santis, A.; Galdiero, S.; Del Vecchio, P. Antimicrobial Peptides at Work: Interaction of Myxinidin and Its Mutant WMR with Lipid Bilayers Mimicking the P. Aeruginosa and E. Coli Membranes. *Sci. Reports 2017 71* **2017**, *7* (1), 1–15. https://doi.org/10.1038/srep44425.

(131) Hartmann, M.; Berditsch, M.; Hawecker, J.; Ardakani, M. F.; Gerthsen, D.; Ulrich, A. S. Damage of the Bacterial Cell Envelope by Antimicrobial Peptides Gramicidin S and PGLa as Revealed by Transmission and Scanning Electron Microscopy. *Antimicrob. Agents Chemother.* **2010**, *54* (8), 3132–3142. https://doi.org/10.1128/AAC.00124-10.

(132) Kaur, P.; Li, Y.; Cai, J.; Song, L. Selective Membrane Disruption Mechanism of an Antibacterial γ-AApeptide Defined by EPR Spectroscopy. *Biophys. J.* **2016**, *110* (8), 1789. https://doi.org/10.1016/J.BPJ.2016.02.038.

(133) Porcelli, F.; Ramamoorthy, A.; Barany, G.; Veglia, G. On the Role of NMR Spectroscopy for Characterization of Antimicrobial Peptides. *Methods Mol. Biol.* **2013**, *1063*, 159. https://doi.org/10.1007/978-1-62703-583-5_9.

(134) Pazderková, M.; Maloň, P.; Zíma, V.; Hofbauerová, K.; Kopecký, V.; Kočišová, E.; Pazderka, T.; Čeřovský, V.; Bednárová, L. Interaction of Halictine-Related Antimicrobial Peptides with Membrane Models. *Int. J. Mol. Sci.* **2019**, *20* (3). https://doi.org/10.3390/IJMS20030631.

(135) Stone, M. R. L.; Masi, M.; Phetsang, W.; Pagès, J. M.; Cooper, M. A.; Blaskovich, M. A. T. Fluoroquinolone-Derived Fluorescent Probes for Studies of Bacterial Penetration and Efflux. *Medchemcomm* **2019**, *10* (6), 901–906. https://doi.org/10.1039/C9MD00124G.

(136) Stone, M. R. L.; Butler, M. S.; Phetsang, W.; Cooper, M. A.; Blaskovich, M. A. T. Fluorescent Antibiotics: New Research Tools to Fight Antibiotic Resistance. *Trends Biotechnol.* **2018**, *36* (5), 523–536. https://doi.org/10.1016/J.TIBTECH.2018.01.004.

(137) Scheinpflug, K.; Wenzel, M.; Krylova, O.; Bandow, J. E.; Dathe, M.; Strahl, H. Antimicrobial Peptide CWFW Kills by Combining Lipid Phase Separation with Autolysis. *Sci. Reports 2017 71*

2017, *7* (1), 1–15. https://doi.org/10.1038/srep44332.

(138) Wenzel, M.; Vischer, N.; Strahl, H.; Hamoen, L. Assessing Membrane Fluidity and Visualizing Fluid Membrane Domains in Bacteria Using Fluorescent Membrane Dyes. *Bio-protocol* **2018**, *8* (20). https://doi.org/10.21769/BIOPROTOC.3063.

(139) Raheem, N.; Straus, S. K. Mechanisms of Action for Antimicrobial Peptides With Antibacterial and Antibiofilm Functions. *Front. Microbiol.* **2019**, *10*. https://doi.org/10.3389/FMICB.2019.02866.

(140) te Winkel, J. D.; Gray, D. A.; Seistrup, K. H.; Hamoen, L. W.; Strahl, H. Analysis of Antimicrobial-Triggered Membrane Depolarization Using Voltage Sensitive Dyes. *Front. Cell Dev. Biol.* **2016**, *4* (APR), 29. https://doi.org/10.3389/FCELL.2016.00029/BIBTEX.

(141) Sass, V.; Schneider, T.; Wilmes, M.; Körner, C.; Tossi, A.; Novikova, N.; Shamova, O.; Sahl, H. G. Human β-Defensin 3 Inhibits Cell Wall Biosynthesis in Staphylococci. *Infect. Immun.* **2010**, *78* (6), 2793–2800. https://doi.org/10.1128/IAI.00688-09/ASSET/D6B5F4E1-5897-4A83-9E11-BBC4643FD671/ASSETS/GRAPHIC/ZII9990986530006.JPEG.

(142) Müller, A.; Wenzel, M.; Strahl, H.; Grein, F.; Saaki, T. N. V.; Kohl, B.; Siersma, T.; Bandow, J. E.; Sahl, H. G.; Schneider, T.; Hamoen, L. W. Daptomycin Inhibits Cell Envelope Synthesis by Interfering with Fluid Membrane Microdomains. *Proc. Natl. Acad. Sci. U. S. A.* **2016**, *113* (45), E7077–E7086. https://doi.org/10.1073/PNAS.1611173113/-/DCSUPPLEMENTAL.

(143) Wenzel, M.; Dekker, M. P.; Wang, B.; Burggraaf, M. J.; Bitter, W.; Weering, J. R. T. van; Hamoen, L. W. New Flat Embedding Method for Transmission Electron Microscopy Reveals an Unknown Mechanism of Tetracycline. *bioRxiv* **2019**, 820191. https://doi.org/10.1101/820191.

(144) Mori, A.; Cohen, B. D. (Burton D. .; Lowenthal, A. (Armand); Japan Guanidino Compounds Research Association. Meeting (6th : 1983 : Tokyo, J. *Guanidines : Historical, Biological, Biochemical, and Clinical Aspects of the Naturally Occurring Guanidino Compounds*; Springer US, 1985.

(145) Castagnolo, D.; Schenone, S.; Botta, M. Guanylated Diamines, Triamines, and Polyamines: Chemistry and Biological Properties. *Chem. Rev.* **2011**, *111* (9), 5247–5300. https://doi.org/10.1021/CR100423X.

(146) Menor-Salván, C.; Marín-Yaseli, M. R. Prebiotic Chemistry in Eutectic Solutions at the Water–Ice Matrix. *Chem. Soc. Rev.* **2012**, *41* (16), 5404–5415. https://doi.org/10.1039/C2CS35060B.

(147) Bera, S.; Zhanel, G. G.; Schweizer, F. Antibacterial Activity of Guanidinylated Neomycin B- and Kanamycin A-Derived Amphiphilic Lipid Conjugates. *J. Antimicrob. Chemother.* **2010**, *65* (6), 1224–1227. https://doi.org/10.1093/JAC/DKQ083.

(148) Feichtinger, K.; Zapf, C.; Sings, H. L.; Goodman, M. Diprotected Triflylguanidines: A New Class of Guanidinylation Reagents. *J. Org. Chem.* **1998**, *63* (12), 3804–3805.

https://doi.org/10.1021/JO980425S/SUPPL_FILE/JO3804.PDF.

(149) Saczewski, F.; Balewski, Ł. Biological Activities of Guanidine Compounds, 2008 - 2012 Update. *Expert Opin. Ther. Pat.* **2013**, *23* (8), 965–995. https://doi.org/10.1517/13543776.2013.788645.

(150) Luo, X.; Jiang, Z.; Zhang, N.; Yang, Z.; Zhou, Z. Interactions of Biocidal Polyhexamethylene Guanidine Hydrochloride and Its Analogs with POPC Model Membranes. *Polymers (Basel).* **2017**, *9* (10). https://doi.org/10.3390/POLYM9100517.

(151) FDA. Catapres ® https://www.accessdata.fda.gov/drugsatfda_docs/label/2009/017407s034lbl.pdf (accessed Dec 22, 2021).

(152) FDA. MIDAMOR - Amiloride hydrochloride LABEL https://www.accessdata.fda.gov/drugsatfda_docs/nda/2002/18-200S024_Midamor_Prntlbl.pdf (accessed Dec 22, 2021).

(153) fda; cder. GLUCOPHAGE ® (metformin hydrochloride) LABEL https://www.accessdata.fda.gov/drugsatfda_docs/label/2017/020357s037s039,021202s021s023lbl.pdf (accessed Dec 22, 2021).

(154) FDA. Cimetidine Label https://www.accessdata.fda.gov/scripts/cder/daf/index.cfm?event=overview.process&ApplNo=017920 (accessed Dec 22, 2021).

(155) fda. Pepcid - famotidine LABEL https://www.accessdata.fda.gov/drugsatfda_docs/label/2018/019462s039lbl.pdf (accessed Dec 22, 2021).

(156) Kaplan, D. L. *Biopolymers from Renewable Resources*; Springer Berlin Heidelberg, 1998. https://doi.org/10.1007/978-3-662-03680-8.

(157) Kim, S.-H.; Semenya, D.; Castagnolo, D. Antimicrobial Drugs Bearing Guanidine Moieties: A Review | Elsevier Enhanced Reader. *Eur. J. Med. Chem.* **2021**, *216*, 113293. https://doi.org/10.1016/j.ejmech.2021.113293.

(158) Dantas, N.; de Aquino, T. M.; de Araújo-Júnior, J. X.; da Silva-Júnior, E.; Gomes, E. A.; Gomes, A. A. S.; Siqueira-Júnior, J. P.; Mendonça Junior, F. J. B. Aminoguanidine Hydrazones (AGH's) as Modulators of Norfloxacin Resistance in Staphylococcus Aureus That Overexpress NorA Efflux Pump. *Chem. Biol. Interact.* **2018**, *280*, 8–14. https://doi.org/10.1016/J.CBI.2017.12.009.

(159) Kaul, M.; Parhi, A. K.; Zhang, Y.; Lavoie, E. J.; Tuske, S.; Arnold, E.; Kerrigan, J. E.; Pilch, D. S. A Bactericidal Guanidinomethyl Biaryl That Alters the Dynamics of Bacterial FtsZ Polymerization. *J. Med. Chem.* **2012**, *55* (22), 10160–10176. https://doi.org/10.1021/JM3012728.

(160) Coqueiro, A.; Regasini, L. O.; Stapleton, P.; Da Silva Bolzani, V.; Gibbons, S. In Vitro Antibacterial Activity of Prenylated Guanidine Alkaloids from Pterogyne Nitens and Synthetic

Analogues. *J. Nat. Prod.* **2014**, *77* (8), 1972–1975. https://doi.org/10.1021/NP500281C/SUPPL_FILE/NP500281C_SI_001.PDF.

(161) Fair, R. J.; Hensler, M. E.; Thienphrapa, W.; Dam, Q. N.; Nizet, V.; Tor, Y. Selectively Guanidinylated Aminoglycosides as Antibiotics. *ChemMedChem* **2012**, *7* (7), 1237–1244. https://doi.org/10.1002/CMDC.201200150.

(162) Nizalapur, S.; Kimyon, O.; Yee, E.; Ho, K.; Berry, T.; Manefield, M.; Cranfield, C. G.; Willcox, M.; Black, D. S. C.; Kumar, N. Amphipathic Guanidine-Embedded Glyoxamide-Based Peptidomimetics as Novel Antibacterial Agents and Biofilm Disruptors. *Org. Biomol. Chem.* **2017**, *15* (9), 2033–2051. https://doi.org/10.1039/C7OB00053G.

(163) Nizalapur, S.; Ho, K. K. K.; Kimyon, Ö.; Yee, E.; Berry, T.; Manefield, M.; Cranfield, C. G.; Willcox, M.; Black, D. S. C.; Kumar, N. Synthesis and Biological Evaluation of N-Naphthoyl-Phenylglyoxamide-Based Small Molecular Antimicrobial Peptide Mimics as Novel Antimicrobial Agents and Biofilm Inhibitors. *Org. Biomol. Chem.* **2016**, *14* (14), 3623–3637. https://doi.org/10.1039/C6OB00298F.

(164) Andreev, K.; Bianchi, C.; Laursen, J. S.; Citterio, L.; Hein-Kristensen, L.; Gram, L.; Kuzmenko, I.; Olsen, C. A.; Gidalevitz, D. Guanidino Groups Greatly Enhance the Action of Antimicrobial Peptidomimetics against Bacterial Cytoplasmic Membranes. *Biochim. Biophys. Acta - Biomembr.* **2014**, *1838* (10), 2492–2502. https://doi.org/10.1016/j.bbamem.2014.05.022.

(165) Yang, C. H.; Chen, Y. C.; Peng, S. Y.; Tsai, A. P. Y.; Lee, T. J. F.; Yen, J. H.; Liou, J. W. An Engineered Arginine-Rich α-Helical Antimicrobial Peptide Exhibits Broad-Spectrum Bactericidal Activity against Pathogenic Bacteria and Reduces Bacterial Infections in Mice. *Sci. Reports 2018 81* **2018**, *8* (1), 1–14. https://doi.org/10.1038/s41598-018-32981-3.

(166) Strecker, A. Untersuchungen Über Die Chemischen Beziehungen Zwischen Guanin, Xanthin, Theobromin, Caffeïn Und Kreatinin. *Justus Liebigs Ann. Chem.* **1861**, *118* (2), 151–177. https://doi.org/10.1002/JLAC.18611180203.

(167) Göbel, M.; Klapötke, T. M. First Structural Characterization of Guanidine, HNC(NH2)2. *Chem. Commun.* **2007**, No. 30, 3180–3182. https://doi.org/10.1039/B705100J.

(168) Marcus, Y. The Guanidinium Ion. *J. Chem. Thermodyn.* **2011**, *48*, 70–74. https://doi.org/10.1016/j.jct.2011.11.031.

(169) Wexselblatt, E.; Esko, J. D.; Tor, Y. On Guanidinium and Cellular Uptake. **2014**. https://doi.org/10.1021/jo501101s.

(170) Antol, I.; Glasovac, Z.; Margetić, D.; Crespo-Otero, R.; Barbatti, M. Insights on the Auxochromic Properties of the Guanidinium Group. *J. Phys. Chem. A* **2016**, *120* (36), 7088–7100. https://doi.org/10.1021/acs.jpca.6b05180.

(171) Rozas, I.; Alkorta, I.; Elguero, J. Hydrogen Bonds and Ionic Interactions in

Guanidine/Guanidinium Complexes: A Computational Case Study. *Struct. Chem.* **2008**, *19* (6), 923–933. https://doi.org/10.1007/S11224-008-9377-9.

(172) Ferretti, V.; Bertolasi, V.; Pretto, L. Supramolecular Aggregation by Means of Charge-Assisted Hydrogen Bonds in Acid-Base Adducts Containing Amidinium Cations. *New J. Chem.* **2004**, *28* (5), 646–651. https://doi.org/10.1039/B314143H.

(173) Braga, D.; Rubini, K.; Maini, L. Transition from a Charge-Opposed(+)N-H–N(+) Inter-Cation Hydrogen Bonded Form of the Salt [HN(CH2CH2)3N][OOC(HCCH) COOH] to the More Traditional Charge-Assisted(+)N-H–O(−) Cation-Anion Hydrogen Bonded Pseudo-Polymorph upon Hydration. *CrystEngComm* **2004**, *6* (41), 236–238. https://doi.org/10.1039/B409904B.

(174) Gund, P. Guanidine, Trimethylenemethane, and "Y-Delocalization." Can Acyclic Compounds Have "Aromatic" Stability? *J. Chem. Educ.* **1972**, *49* (2), 100–103. https://doi.org/10.1021/ED049P100.

(175) Tobey, S. L.; Anslyn, E. V. Energetics of Phosphate Binding to Ammonium and Guanidinium Containing Metallo-Receptors in Water. *J. Am. Chem. Soc.* **2003**, *125* (48), 14807–14815. https://doi.org/10.1021/JA030507K/SUPPL_FILE/JA030507K_S1.PDF.

(176) Savelli, C.; Salvio, R. Guanidine-Based Polymer Brushes Grafted onto Silica Nanoparticles as Efficient Artificial Phosphodiesterases. *Chemistry* **2015**, *21* (15), 5856–5863. https://doi.org/10.1002/CHEM.201406526.

(177) Salvio, R. The Guanidinium Unit in the Catalysis of Phosphoryl Transfer Reactions: From Molecular Spacers to Nanostructured Supports. *Chemistry* **2015**, *21* (31), 10960–10971. https://doi.org/10.1002/CHEM.201500789.

(178) Villanueva, M. E.; González, J. A.; Rodríguez-Castellón, E.; Teves, S.; Copello, G. J. Antimicrobial Surface Functionalization of PVC by a Guanidine Based Antimicrobial Polymer. *Mater. Sci. Eng. C. Mater. Biol. Appl.* **2016**, *67*, 214–220. https://doi.org/10.1016/J.MSEC.2016.05.052.

(179) Ghamrawi, S.; Bouchara, J. P.; Tarasyuk, O.; Rogalsky, S.; Lyoshina, L.; Bulko, O.; Bardeau, J. F. Promising Silicones Modified with Cationic Biocides for the Development of Antimicrobial Medical Devices. *Mater. Sci. Eng. C. Mater. Biol. Appl.* **2017**, *75*, 969–979. https://doi.org/10.1016/J.MSEC.2017.03.013.

(180) Choi, H.; Kim, K. J.; Lee, D. G. Antifungal Activity of the Cationic Antimicrobial Polymer-Polyhexamethylene Guanidine Hydrochloride and Its Mode of Action. *Fungal Biol.* **2017**, *121* (1), 53–60. https://doi.org/10.1016/J.FUNBIO.2016.09.001.

(181) Donalisio, M.; Ranucci, E.; Cagno, V.; Civra, A.; Manfredi, A.; Cavalli, R.; Ferruti, P.; Lembo, D. Agmatine-Containing Poly(Amidoamine)s as a Novel Class of Antiviral Macromolecules: Structural Properties and in Vitro Evaluation of Infectivity Inhibition. *Antimicrob. Agents*

Chemother. **2014**, *58* (10), 6315–6319. https://doi.org/10.1128/AAC.03420-14.

(182) Mogaki, R.; Hashim, P. K.; Okuro, K.; Aida, T. Guanidinium-Based "Molecular Glues" for Modulation of Biomolecular Functions. *Chemical Society Reviews*. Royal Society of Chemistry November 7, 2017, pp 6480–6491. https://doi.org/10.1039/c7cs00647k.

(183) Springs, B.; Haake, P. Equilibrium Constants for Association of Guanidinium and Ammonium Ions with Oxyanions: The Effect of Changing Basicity of the Oxyanion. *Bioorg. Chem.* **1977**, *6* (2), 181–190. https://doi.org/10.1016/0045-2068(77)90019-0.

(184) Stelmakh, S. A.; Grigor'eva, M. N.; Garkusheva, N. M.; Lebedeva, S. N.; Ochirov, O. S.; Mognonov, D. M.; Zhamsaranova, S. D.; Batoev, V. B. Studies of New Biocidal Polyguanidines: Antibacterial Action and Toxicity. *Polym. Bull. 2020 784* **2020**, *78* (4), 1997–2008. https://doi.org/10.1007/S00289-020-03197-1.

(185) Pasero, C.; D'Agostino, I.; De Luca, F.; Zamperini, C.; Deodato, D.; Truglio, G. I.; Sannio, F.; Del Prete, R.; Ferraro, T.; Visaggio, D.; Mancini, A.; Guglielmi, M. B.; Visca, P.; Docquier, J.-D. D.; Botta, M.; D'Agostino, I.; De Luca, F.; Zamperini, C.; Deodato, D.; Truglio, G. I.; Sannio, F.; Del Prete, R.; Ferraro, T.; Visaggio, D.; Mancini, A.; Guglielmi, M. B.; Visca, P.; Docquier, J.-D. D.; Botta, M.; D'Agostino, I.; De Luca, F.; Zamperini, C.; Deodato, D.; Truglio, G. I.; Sannio, F.; Del Prete, R.; Ferraro, T.; Visaggio, D.; Mancini, A.; Guglielmi, M. B.; Visca, P.; Docquier, J.-D. D.; Botta, M.; D'Agostino, I.; De Luca, F.; Zamperini, C.; Deodato, D.; Truglio, G. I.; Sannio, F.; Del Prete, R.; Ferraro, T.; Visaggio, D.; Mancini, A.; Guglielmi, M. B.; Visca, P.; Docquier, J.-D. D.; Botta, M.; D'Agostino, I.; De Luca, F.; Zamperini, C.; Deodato, D.; Truglio, G. I.; Sannio, F.; Del Prete, R.; Ferraro, T.; Visaggio, D.; Mancini, A.; Guglielmi, M. B.; Visca, P.; Docquier, J.-D. D.; Botta, M. Alkyl-Guanidine Compounds as Potent Broad-Spectrum Antibacterial Agents: Chemical Library Extension and Biological Characterization. *J. Med. Chem.* **2018**, *61* (20), acs.jmedchem.8b00619. https://doi.org/10.1021/acs.jmedchem.8b00619.

(186) Zamperini, C.; Maccari, G.; Deodato, D.; Pasero, C.; D'Agostino, I.; Orofino, F.; De Luca, F.; Dreassi, E.; Docquier, J. D. D.; Botta, M.; D'Agostino, I.; Orofino, F.; De Luca, F.; Dreassi, E.; Docquier, J. D. D.; Botta, M.; D'Agostino, I.; Orofino, F.; De Luca, F.; Dreassi, E.; Docquier, J. D. D.; Botta, M. Identification, Synthesis and Biological Activity of Alkyl-Guanidine Oligomers as Potent Antibacterial Agents. *Sci. Rep.* **2017**, *7* (1), 8251. https://doi.org/10.1038/s41598-017-08749-6.

(187) BOTTA, M.; MACCARI, G.; SANFILIPPO, S.; DE LUCA, F.; DOCQUIER, J.-D.; DEODATO, D. LINEAR GUANIDINE DERIVATIVES, METHODS OF PREPARATION AND USES THEREOF. WO/2016/055644, April 2016.

(188) Goncharova, I.; Orlov, S.; Urbanová, M. The Location of the High- and Low-Affinity Bilirubin-Binding Sites on Serum Albumin: Ligand-Competition Analysis Investigated by Circular

Dichroism. *Biophys. Chem.* **2013**, *180–181*, 55–65. https://doi.org/10.1016/J.BPC.2013.06.004.

(189) Silvestro, L.; Weiser, J. N.; Axelsen, P. H. Antibacterial and Antimembrane Activities of Cecropin A in Escherichia Coli. *Antimicrob. Agents Chemother.* **2000**, *44* (3), 602. https://doi.org/10.1128/AAC.44.3.602-607.2000.

(190) Lehrer, R. I.; Barton, A.; Daher, K. A.; Harwig, S. S. L.; Ganz, T.; Selsted, M. E. Interaction of Human Defensins with Escherichia Coli. Mechanism of Bactericidal Activity. *J. Clin. Invest.* **1989**, *84* (2), 553–561. https://doi.org/10.1172/JCI114198.

(191) Breeuwer, P.; Abee, T. Assessment of Viability of Microorganisms Employing Fluorescence Techniques. *Int. J. Food Microbiol.* **2000**, *55* (1–3), 193–200. https://doi.org/10.1016/S0168-1605(00)00163-X.

(192) Wang, B.; Pachaiyappan, B.; Gruber, J. D.; Schmidt, M. G.; Zhang, Y.-M.; Woster, P. M.; Zhang, Y. M. Antibacterial Diamines Targeting Bacterial Membranes Graphical Abstract Corresponding Authors: HHS Public Access. *J Med Chem* **2016**, *59* (7), 3140–3151. https://doi.org/10.1021/acs.jmedchem.5b01912.

(193) D'Agostino, I.; Ardino, C.; Poli, G.; Sannio, F.; Lucidi, M.; Poggialini, F.; Visaggio, D.; Rango, E.; Filippi, S.; Petricci, E.; Visca, P.; Botta, L.; Docquier, J.-D.; Dreassi, E. Antibacterial Alkylguanidino Ureas: Molecular Simplification Approach, Searching for Membrane-Based MoA. *Eur. J. Med. Chem.* **2022**, 114158. https://doi.org/10.1016/J.EJMECH.2022.114158.

(194) Zamperini, C.; Maccari, G.; Deodato, D.; Pasero, C.; D'Agostino, I.; Orofino, F.; De Luca, F.; Dreassi, E.; Docquier, J. D.; Botta, M. Identification, Synthesis and Biological Activity of Alkyl-Guanidine Oligomers as Potent Antibacterial Agents. *Sci. Rep.* **2017**, *7* (July), 1–11. https://doi.org/10.1038/s41598-017-08749-6.

(195) Pinacho Crisóstomo, F. R.; Carrillo, R.; León, L. G.; Martín, T.; Padrón, J. M.; Martín, V. S. Molecular Simplification in Bioactive Molecules: Formal Synthesis of (+)-Muconin. *J. Org. Chem.* **2006**, *71* (6), 2339–2345. https://doi.org/10.1021/JO0524674.

(196) Wang, S.; Dong, G.; Sheng, C. Structural Simplification: An Efficient Strategy in Lead Optimization. *Acta Pharm. Sin. B* **2019**, *9* (5), 880–901. https://doi.org/10.1016/J.APSB.2019.05.004.

(197) Ghosh, A. K.; Brindisi, M. Urea Derivatives in Modern Drug Discovery and Medicinal Chemistry. *J. Med. Chem.* **2020**, *63* (6), 2751–2788. https://doi.org/10.1021/acs.jmedchem.9b01541.

(198) Khalaf, M.; Zageer, D.; Hussain, Z.; Adil, H.; Mohammed, S.; Yousif, E. Guanidine Group: Definition and Pharmaceutical Applications. *Res. J. Pharm. Biol. Chem. Sci.* **2016**, *7* (5), 1026–1031.

(199) D'Agostino, I. Polyalkylguanidines: New Weapons To Tackle Bacterial Resistance, University of Siena, 2018.

(200) Cornish, J.; Callon, K. E.; Lin, C. Q. X. Q.-X.; Xiao, C. L.; Mulvey, T. B.; Cooper, G. J. S. S.; Reid, I. R. Trifluoroacetate, a Contaminant in Purified Proteins, Inhibits Proliferation of Osteoblasts and Chondrocytes. **1999**, *277*, E779–E783.

(201) Tipps, M. E.; Iyer, S. V.; John Mihic, S. Trifluoroacetate Is an Allosteric Modulator with Selective Actions at the Glycine Receptor. *Neuropharmacology* **2012**, *63* (3), 368–373. https://doi.org/10.1016/j.neuropharm.2012.04.011.

(202) Ma, T. G.; Ling, Y. H.; McClure, G. D.; Tseng, M. T. Effects of Trifluoroacetic Acid, a Halothane Metabolite, on C6 Glioma Cells. *J. Toxicol. Environ. Health* **1990**, *31* (2), 147–158. https://doi.org/10.1080/15287399009531444.

(203) Han, G.; Tamaki, M.; Hruby, V. J. Fast, Efficient and Selective Deprotection of the Tert-Butoxycarbonyl (Boc) Group Using HCl/Dioxane (4 M). *J. Pept. Res.* **2001**, *58* (4), 338–341. https://doi.org/10.1034/J.1399-3011.2001.00935.X.

(204) Nudelman, A.; Bechor, Y.; Falb, E.; Fischer, B.; Wexler, B. A.; Nudelman, A. Acetyl Chloride-Methanol as a Convenient Reagent for: A) Quantitative Formation of Amine Hydrochlorides B) Carboxylate Ester Formation C) Mild Removal of N-t-Boc-Protective Group. *Synth. Commun.* **2006**, *28* (3), 471–474. https://doi.org/10.1080/00397919808005101.

(205) Nagle, P. S.; Rodriguez, F.; Kahvedžić, A.; Quinn, S. J.; Rozas, I. Asymmetrical Diaromatic Guanidinium/2-Aminoimidazolinium Derivatives: Synthesis and DNA Affinity. *J. Med. Chem.* **2009**, *52* (22), 7113–7121. https://doi.org/10.1021/JM901017T/SUPPL_FILE/JM901017T_SI_001.PDF.

(206) Bachand, B.; DiMaio, J.; Siddiqui, M. A. Synthesis and Structure-Activity Relationship of Potent Bicyclic Lactam Thrombin Inhibitors. *Bioorg. Med. Chem. Lett.* **1999**, *9* (7), 913–918. https://doi.org/10.1016/S0960-894X(99)00130-4.

(207) Diez-Cecilia, E.; Kelly, B.; Perez, C.; Zisterer, D. M.; Nevin, D. K.; Lloyd, D. G.; Rozas, I. Guanidinium-Based Derivatives: Searching for New Kinase Inhibitors. *Eur. J. Med. Chem.* **2014**, *81*, 427–441. https://doi.org/10.1016/J.EJMECH.2014.05.025.

(208) Rizzello, C. G.; Losito, I.; Gobbetti, M.; Carbonara, T.; De Bari, M. D.; Zambonin, P. G. Antibacterial Activities of Peptides from the Water-Soluble Extracts of Italian Cheese Varieties. *J. Dairy Sci.* **2005**, *88* (7), 2348–2360. https://doi.org/10.3168/jds.S0022-0302(05)72913-1.

(209) Gaussier, H.; Morency, H.; Lavoie, M. C.; Subirade, M. Replacement of Trifluoroacetic Acid with HCl in the Hydrophobic Purification Steps of Pediocin PA-1: A Structural Effect. *Appl. Environ. Microbiol.* **2002**, *68* (10), 4803–4808. https://doi.org/10.1128/AEM.68.10.4803-4808.2002.

(210) Greber, K. E.; Dawgul, M.; Kamysz, W.; Sawicki, W. Cationic Net Charge and Counter Ion Type as Antimicrobial Activity Determinant Factors of Short Lipopeptides. *Front. Microbiol.* **2017**,

8 (FEB), 123. https://doi.org/10.3389/fmicb.2017.00123.

(211) Zhang, C.; Jiang, Y.; Ju, H.; Wang, Y.; Geng, T. "Organic Counterion" Modified Quaternary Ammonium Salt: Impact on Antibacterial Activity & Application Properties. *J. Mol. Liq.* **2017**, *241*, 638–645. https://doi.org/10.1016/j.molliq.2017.06.062.

(212) Dutta, S.; Shome, A.; Kar, T.; Das, P. K. Counterion-Induced Modulation in the Antimicrobial Activity and Biocompatibility of Amphiphilic Hydrogelators: Influence of in-Situ-Synthesized Ag-Nanoparticle on the Bactericidal Property. *Langmuir* **2011**, *27* (8), 5000–5008. https://doi.org/10.1021/la104903z.

(213) Kan, T.; Fukuyama, T. Ns Strategies: A Highly Versatile Synthetic Method for Amines. *Chem. Commun.* **2004**, *4* (4), 353–359. https://doi.org/10.1039/b311203a.

(214) Fujiwara, A.; Kan, T.; Fukuyama, T. Total Synthesis of Lipogrammistin-A: Efficient Macrocyclization with 2-Nitrobenzenesulfonamide. *Synlett* **2000**, No. 11, 1667–1669. https://doi.org/10.1055/s-2000-7950.

(215) Kurosawa, W.; Kan, T.; Fukuyama, T. Preparation of Secondary Amines From Primary Amines Via 2-Nitrobenzenesulfonamides: N-(4-Methoxybenzyl)-3-Phenylpropylamine. *Org. Synth.* **2003**, *79*.

(216) Patil, M.; Noonikara-Poyil, A.; Joshi, S. D.; Patil, S. A.; Patil, S.; Bugarin, A. New Urea Derivatives as Potential Antimicrobial Agents: Synthesis, Biological Evaluation, and Molecular Docking Studies. *Antibiot.* **2019**, *8* (4), 178. https://doi.org/10.3390/antibiotics8040178.

(217) Benfield, A. H.; Henriques, S. T. Mode-of-Action of Antimicrobial Peptides: Membrane Disruption vs. Intracellular Mechanisms. *Front. Med. Technol.* **2020**, *2* (December), 25–28. https://doi.org/10.3389/fmedt.2020.610997.

(218) Kumar, L.; Amin, A.; Bansal, A. K. Salt Selection in Drug Development. *Pharm. Technol.* **2008**, *32* (3).

(219) Acharya, P. C.; Marwein, S.; Mishra, B.; Ghosh, R.; Vora, A.; Tekade, R. K. *Role of Salt Selection in Drug Discovery and Development*; Elsevier Inc., 2018. https://doi.org/10.1016/B978-0-12-814423-7.00013-7.

(220) Katritzky, A. R.; Pleynet, D. P. M.; Yang, B. A General Synthesis of Unsymmetrical Tetrasubstituted Ureas. *J. Org. Chem.* **1997**, *62* (12), 4155–4158. https://doi.org/10.1021/jo962245t.

(221) Burke, M. D.; Schreiber, S. L. . A Planning Strategy for Diversity-Oriented Synthesis. *Angew. Chemie Int. Ed.* **2003**, *43* (1), 46–58. https://doi.org/10.1002/anie.200300626.

(222) Kan, T.; Fukuyama, T. Ns Strategies: A Highly Versatile Synthetic Method for Amines. *Chem. Commun.* **2004**, *4* (4), 353–359. https://doi.org/10.1039/b311203a.

(223) Zamperini, C.; MacCari, G.; Deodato, D.; Pasero, C.; D'Agostino, I.; Orofino, F.; De Luca, F.;

Dreassi, E.; Docquier, J. D.; Botta, M. Identification, Synthesis and Biological Activity of Alkyl-Guanidine Oligomers as Potent Antibacterial Agents. *Sci. Rep.* **2017**, *7* (1), 1–11. https://doi.org/10.1038/s41598-017-08749-6.

(224) Fukuyama Amine Synthesis | Chem-Station Int. Ed. https://en.chem-station.com/reactions-2/2014/03/fukuyama-amine-synthesis.html (accessed Jan 2, 2022).

(225) Topliss, J. G. Utilization of Operational Schemes for Analog Synthesis in Drug Design. *J. Med. Chem.* **1972**, *15* (10), 1006–1011.

(226) Asghari, G.; Jalali, M.; Sadoughi, E. Antimicrobial Activity and Chemical Composition of Essential Oil From the Seeds of Artemisia Aucheri Boiss. *Jundishapur J. Nat. Pharm. Prod.* **2012**, *7* (1), 11. https://doi.org/10.5812/jjnpp.3530.

(227) Sugamoto, K.; Matsusita, Y. I.; Matsui, K.; Kurogi, C.; Matsui, T. Synthesis and Antibacterial Activity of Chalcones Bearing Prenyl or Geranyl Groups from Angelica Keiskei. *Tetrahedron* **2011**, *67* (29), 5346–5359. https://doi.org/10.1016/J.TET.2011.04.104.

(228) Maccari, G.; Deodato, D.; Fiorucci, D.; Orofino, F.; Truglio, G. I.; Pasero, C.; Martini, R.; De Luca, F.; Docquier, J. D.; Botta, M. Design and Synthesis of a Novel Inhibitor of T. Viride Chitinase through an in Silico Target Fishing Protocol. *Bioorganic Med. Chem. Lett.* **2017**, *27* (15), 3332–3336. https://doi.org/10.1016/j.bmcl.2017.06.016.

(229) Shakeel, A. Thiourea Derivatives in Drug Design and Medicinal Chemistry: A Short Review. *J. Drug Des. Med. Chem.* **2016**, *2* (1), 10. https://doi.org/10.11648/j.jddmc.20160201.12.

(230) Abd Halim, A. N.; Ngaini, Z. Synthesis and Bacteriostatic Activities of Bis(Thiourea) Derivatives with Variable Chain Length. *J. Chem.* **2016**, *2016*, 2739832. https://doi.org/10.1155/2016/2739832.

(231) Zhong, Z.; Xing, R.; Liu, S.; Wang, L.; Cai, S.; Li, P. Synthesis of Acyl Thiourea Derivatives of Chitosan and Their Antimicrobial Activities in Vitro. *Carbohydr. Res.* **2008**, *343* (3), 566–570. https://doi.org/10.1016/J.CARRES.2007.11.024.

(232) Huang, M.; Sun, Y.; Yang, W.; Hou, H.; Fabrycki, I.; Nie, X.; Sanchez, A.; Zao, Y.; Phadke, A.; Deshpande, M. ACH-806: A Potent Inhibitor of HCV Replication with a Novel Mechanism of Action. *J. Hepatol.* **207AD**, *46* (1), S221. https://doi.org/10.1016/S0168-8278(07)62181-3.

(233) Saeed, S.; Rashid, N.; Jones, P. G.; Ali, M.; Hussain, R. Synthesis, Characterization and Biological Evaluation of Some Thiourea Derivatives Bearing Benzothiazole Moiety as Potential Antimicrobial and Anticancer Agents. *Eur. J. Med. Chem.* **2010**, *45* (4), 1323–1331. https://doi.org/10.1016/j.ejmech.2009.12.016.

(234) Reddy, N. S.; Rao, A. S.; Chari, M. A.; Kumar, V. R.; Jyothy, V.; Himabindu, V. Synthesis and Antibacterial Activity of Sulfonamide Derivatives at C-8 Alkyl Chain of Anacardic Acid Mixture Isolated from a Natural Product Cashew Nut Shell Liquid (CNSL). *J. Chem. Sci. 2012 1243* **2012**,

124 (3), 723–730. https://doi.org/10.1007/S12039-012-0253-1.

(235) Ozturk, T.; Ertas, E.; Mert, O. Use of Lawesson's Reagent in Organic Syntheses. *Chemical Reviews*. American Chemical Society November 2007, pp 5210–5278. https://doi.org/10.1021/cr040650b.

(236) Messeri, T.; Sternbach, D. D.; Tomkinson, N. C. O. A Novel Deprotection I Functionalisation Sequence Using 2,4-Dinitrobenzenesulfonamide : Part 2. *Tetrahedron Lett.* **1998**, *39*, 1673–1676.

(237) Messeri, T.; Sternbach, D. D.; Tomkinson, N. C. O. A Novel Deprotection/Functionalisation Sequence Using 2,4- Dinitrobenzenesulfonamide: Part 1. *Tetrahedron Lett.* **1998**, *39* (13), 1669–1672. https://doi.org/10.1016/S0040-4039(98)00017-3.

(238) White, R. W. The Structure of the Thiuram Oxides. *Can. J. Chem.* **1954**, *32* (9), 867–871. https://doi.org/10.1139/v54-110.

(239) Kardon, F.; Mörtl, M.; Magyarfalvi, G. Preparation of Mixed Carbamic/Dithiocarbamic Anhydrides via Silyl Carbamates or Silyl Dithiocarbamates. *http://dx.doi.org/10.1080/00397910701693658* **2008**, *38* (2), 192–199. https://doi.org/10.1080/00397910701693658.

(240) McMaster, C.; Bream, R. N.; Grainger, R. S. Radical-Mediated Reduction of the Dithiocarbamate Group under Tin-Free Conditions. *Org. Biomol. Chem.* **2012**, *10* (24), 4752–4758. https://doi.org/10.1039/C2OB25434D.

(241) Suresh Babu, V. V.; Patil, B. S.; Vasanthakumar, G. R. MW-Enhanced High-Speed Deprotection of Boc Group Using P-TsOH and Concommitant Formation of N-Me-Amino Acid Benzyl Ester P-TsOH Salts. *Synth. Commun.* **2006**, *35* (13), 1795–1802. https://doi.org/10.1081/SCC-200063953.

(242) Bose, D. S.; Lakshmiriarayana, V. An Efficient and Highly Selective Cleavage of N-Tert-Butoxycarbonyl Group under Microwave Irradiation. *Tetrahedron Lett.* **1998**, *39* (31), 5631–5634. https://doi.org/10.1016/S0040-4039(98)01094-6.

(243) Yousuf, S. K.; Mukherjee, D.; L, M.; Taneja, S. C. Highly Regio-and Stereoselective One-Pot Synthesis of Carbohydrate-Based Butyrolactones. *Org. Lett.* **2011**, *13* (4), 576–579. https://doi.org/10.1021/OL102723C/SUPPL_FILE/OL102723C_SI_001.PDF.

(244) Pavan Kumar, G.; Rambabu, D.; Basaveswara Rao, M. V.; Pal, M. Iodine-Mediated Neutral and Selective N-Boc Deprotection. *J. Chem.* **2013**. https://doi.org/10.1155/2013/916960.

(245) Zinelaabidine, C.; Souad, O.; Zoubir, J.; Malika, B.; Nour-Eddine, A. A Simple and Efficient Green Method for the Deprotection of N-Boc in Various Structurally Diverse Amines under Water-Mediated Catalyst-Free Conditions. *Int. J. Chem.* **2012**, *4* (3), p73. https://doi.org/10.5539/IJC.V4N3P73.

(246) George, N.; Ofori, S.; Parkin, S.; Awuah, S. G. Mild Deprotection of the N-Tert-

Butyloxycarbonyl (N-Boc) Group Using Oxalyl Chloride. *RSC Adv.* **2020**, *10* (40), 24017–24026. https://doi.org/10.1039/D0RA04110F.

(247) Rahman, A.; Stipaničev, N.; Keogh, A. P.; Twamley, B.; Rozas, I. Selective Carbamate Conversion of Protected Guanidines. *Tetrahedron Lett.* **2021**, *74*, 153160. https://doi.org/10.1016/J.TETLET.2021.153160.

(248) Choy, J.; Jaime-Figueroa, S.; Jiang, L.; Wagner, P. Novel Practical Deprotection of N-Boc Compounds Using Fluorinated Alcohols. *http://dx.doi.org/10.1080/00397910802238718* **2008**, *38* (21), 3840–3853. https://doi.org/10.1080/00397910802238718.

(249) Bégué, J. P.; Bonnet-Delpon, D.; Crousse, B. Fluorinated Alcohols: A New Medium for Selective and Clean Reaction. *Synlett* **2004**, *2004* (1), 18–29. https://doi.org/10.1055/S-2003-44973/ID/5.

(250) Srinivasan, N.; Yurek-George, A.; A, G. Rapid Deprotection of N-Boc Amines by TFA Combined with Freebase Generation Using Basic Ion-Exchange Resins. *Mol. Divers.* **2005**, *9*, 291–293. https://doi.org/10.1007/s11030-005-4386-8.

(251) Taglang, C.; Martínez-Prieto, L. M.; del Rosal, I.; Maron, L.; Poteau, R.; Philippot, K.; Chaudret, B.; Perato, S.; Sam Lone, A.; Puente, C.; Dugave, C.; Rousseau, B.; Pieters, G. Enantiospecific C-H Activation Using Ruthenium Nanocatalysts. *Angew. Chemie* **2015**, *127* (36), 10620–10623. https://doi.org/10.1002/ANGE.201504554.

(252) Kumar, A. B.; Tipton, J. D.; Manetsch, R. 3-Trifluoromethyl-3-Aryldiazirine Photolabels with Enhanced Ambient Light Stability. *Chem. Commun.* **2016**, *52* (13), 2729–2732. https://doi.org/10.1039/C5CC09518B.

(253) Roux, S.; Zékri, E.; Rousseau, B.; Cintrat, J. C.; Fay, N. Elimination and Exchange of Trifluoroacetate Counter-Ion from Cationic Peptides: A Critical Evaluation of Different Approaches. *J. Pept. Sci.* **2008**, *14* (3), 354–359. https://doi.org/10.1002/PSC.951.

(254) Trummal, A.; Lipping, L.; Kaljurand, I.; Koppel, I. A.; Leito, I. Acidity of Strong Acids in Water and Dimethyl Sulfoxide. *J. Phys. Chem. A* **2016**, *120* (20), 3663–3669. https://doi.org/10.1021/ACS.JPCA.6B02253/SUPPL_FILE/JP6B02253_SI_001.PDF.

(255) Sweis, R.; Edmondson, S.; Kaelin, D. SUBSTITUTED AMINOPYRIMIDINES AS CHOLECYSTOKININ-I RECEPTOR MODULATORS BACKGROUND OF THE INVENTION. WO2008091631A1, 2008.

(256) Pinho, S. P.; Macedo, E. A. Solubility of NaCl, NaBr, and KCl in Water, Methanol, Ethanol, and Their Mixed Solvents. *J. Chem. Eng. Data* **2004**, *50* (1), 29–32. https://doi.org/10.1021/JE049922Y.

(257) Physicochemical Properties of Derivatives Were Predicted Using SwissADME and Marvin Sketch ChemAxon Tools.

(258) Marquardt, D.; Geier, B.; Pabst, G. Asymmetric Lipid Membranes: Towards More Realistic Model Systems. *Membr. 2015, Vol. 5, Pages 180-196* **2015**, *5* (2), 180–196. https://doi.org/10.3390/MEMBRANES5020180.

(259) Salton, M. R. J. Structural and Functional Asymmetry of Bacterial Membranes. *Membr. Transp.* **1982**, 277–282. https://doi.org/10.1007/978-1-4684-4082-9_34.

(260) Bonikowski, R.; Świtakowska, P.; Sienkiewicz, M.; Zaklos-Syzda, M. Selected Compounds Structurally Related to Acyclic Sesquiterpenoids and Their Antibacterial and Cytotoxic Activity. *Molecules* **2015**, *20* (6), 11272–11296. https://doi.org/10.3390/molecules200611272.

(261) Collins, K. D.; Washabaugh, M. W. The Hofmeister Effect and the Behaviour of Water at Interfaces. *Q. Rev. Biophys.* **1985**, *18* (4), 323–422. https://doi.org/10.1017/S0033583500005369.

(262) You, Q.; Cheng, L.; Reilly, T. P.; Wegmann, D.; Ju, C. Role of Neutrophils in a Mouse Model of Halothane-Induced Liver Injury. *Hepatology* **2006**, *44* (6), 1421–1431. https://doi.org/10.1002/hep.21425.

(263) Trudell, J. R.; Ardies, C. M.; Anderson, W. R. Antibodies Raised against Trifluoroacetyl-Protein Adducts Bind to N-Trifluoroacetyl-Phosphatidylethanolamine in Hexagonal Phase Phospholipid Micelles. *J. Pharmacol. Exp. Ther.* **1991**, *257* (2).

(264) You, Q.; Cheng, L.; Ju, C. Generation of T Cell Responses Targeting the Reactive Metabolite of Halothane in Mice. *Toxicol. Lett.* **2010**, *194* (3), 79–85. https://doi.org/10.1016/j.toxlet.2010.02.009.

(265) Boullerne, A. I.; Polak, P. E.; Braun, D.; Sharp, A.; Pelligrino, D.; Feinstein, D. L. Effects of Peptide Fraction and Counter Ion on the Development of Clinical Signs in Experimental Autoimmune Encephalomyelitis. *J. Neurochem.* **2014**, *129* (4), 696–703. https://doi.org/10.1111/jnc.12664.

(266) Sikora, K.; Jaśkiewicz, M.; Neubauer, D.; Migoń, D.; Kamysz, W. The Role of Counter-Ions in Peptides—an Overview. *Pharmaceuticals* **2020**, *13* (12), 1–26. https://doi.org/10.3390/ph13120442.

(267) Patel, J. B.; Eliopoulos, G. M.; Jenkins, S. G.; James Lewis II, F. S.; Brandi Limbago, P.; Nicolau, D. P.; Robin Patel, F.; Powell, M.; Sandra Richter, Frcp. S.; Jana Swenson, D. M.; Maria Traczewski, Mms. M.; John Turnidge, M. D.; Weinstein, M. P.; Zimmer, B. L.; April Bobenchik, D. M.; Shelley Campeau, D.; Sharon Cullen, D. K.; Marcelo Galas Howard Gold, R. F.; Romney Humphries, F. M.; Thomas Kirn, D. J.; Lewis II, J. S.; Brandi Limbago, F.; Mathers, A. J.; Tony Mazzulli, D.; Sandra Richter, F. S.; Michael Satlin, F.; Audrey Schuetz, M. N.; Pranita Tamma, Mms. D. Performance Standards for Antimicrobial Susceptibility Testing Performance Standards for Antimicrobial Susceptibility Testing Suggested Citation. **2016**, 100–125.

(268) EUCAST: MIC determination

https://www.eucast.org/ast_of_bacteria/mic_determination/?no_cache=1 (accessed Jan 16, 2022).

(269) Hu, X.; Tam, K. Biomembrane Mimics and Their Roles in Anti-Bacterial Drug Discovery. *ADMET DMPK* **2017**, *5* (1), 9–13. https://doi.org/10.5599/admet.5.1.375.

(270) Deleu, M.; Crowet, J. M.; Nasir, M. N.; Lins, L. Complementary Biophysical Tools to Investigate Lipid Specificity in the Interaction between Bioactive Molecules and the Plasma Membrane: A Review. *Biochim. Biophys. Acta* **2014**, *1838* (12), 3171–3190. https://doi.org/10.1016/J.BBAMEM.2014.08.023.

(271) Moyano, F.; Molina, P. G.; Silber, J. J.; Sereno, L.; Correa, N. M. An Alternative Approach to Quantify Partition Processes in Confined Environments: The Electrochemical Behavior of PRODAN in Unilamellar Vesicles. *ChemPhysChem* **2010**, *11* (1), 236–244. https://doi.org/10.1002/cphc.200900557.

(272) Andrushchenko, V. V.; Aarabi, M. H.; Nguyen, L. T.; Prenner, E. J.; Vogel, H. J. Thermodynamics of the Interactions of Tryptophan-Rich Cathelicidin Antimicrobial Peptides with Model and Natural Membranes. *Biochim. Biophys. Acta - Biomembr.* **2008**, *1778* (4), 1004–1014. https://doi.org/10.1016/j.bbamem.2007.12.022.

(273) Pérez-Peinado, C.; Dias, S. A.; Domingues, M. M.; Benfield, A. H.; Freire, J. M.; Rádis-Baptista, G.; Gaspar, D.; Castanho, M. A. R. B.; Craik, D. J.; Henriques, S. T.; Veiga, A. S.; Andreu, D. Mechanisms of Bacterial Membrane Permeabilization by Crotalicidin (Ctn) and Its Fragment Ctn(15–34), Antimicrobial Peptides from Rattlesnake Venom. *J. Biol. Chem.* **2018**, *293* (5), 1536–1549. https://doi.org/10.1074/jbc.RA117.000125.

(274) Lin, T. Y.; Weibel, D. B. Organization and Function of Anionic Phospholipids in Bacteria. *Appl. Microbiol. Biotechnol.* **2016**, *100* (10), 4255–4267. https://doi.org/10.1007/s00253-016-7468-x.

(275) Epand, R. M.; Epand, R. F. Lipid Domains in Bacterial Membranes and the Action of Antimicrobial Agents. *Biochim. Biophys. Acta - Biomembr.* **2009**, *1788* (1), 289–294. https://doi.org/10.1016/j.bbamem.2008.08.023.

(276) Grau-Campistany, A.; Manresa, Á.; Pujol, M.; Rabanal, F.; Cajal, Y. Tryptophan-Containing Lipopeptide Antibiotics Derived from Polymyxin B with Activity against Gram Positive and Gram Negative Bacteria. *Biochim. Biophys. Acta - Biomembr.* **2016**, *1858* (2), 333–343. https://doi.org/10.1016/j.bbamem.2015.11.011.

(277) Schmid, F.-X. Biological Macromolecules: UV-Visible Spectrophotometry. *Encycl. Life Sci.* **2001**. https://doi.org/10.1038/npg.els.0003142.

(278) Pereira, F.; Figueiredo, T.; de Almeida, R. F. M.; Antunes, C. A. C.; Garcia, C.; Reis, C. P.; Ascensão, L.; Sobral, R. G.; Rijo, P. Unveiling the Mechanism of Action of 7α-Acetoxy-6β-Hydroxyroyleanone on an Mrsa/Visa Strain: Membrane and Cell Wall Interactions. *Biomolecules*

2020, *10* (7), 1–17. https://doi.org/10.3390/biom10070983.

(279) Greenspan, P.; Fowler, S. D. Spectrofluorometric Studies of the Lipid Probe, Nile Red. *J. Lipid Res.* **1985**, *26* (7), 781–789. https://doi.org/10.1016/s0022-2275(20)34307-8.

(280) Berben, P.; Bauer-Brandl, A.; Brandl, M.; Faller, B.; Flaten, G. E.; Jacobsen, A. C.; Brouwers, J.; Augustijns, P. Drug Permeability Profiling Using Cell-Free Permeation Tools: Overview and Applications. *Eur. J. Pharm. Sci.* **2018**, *119*, 219–233. https://doi.org/10.1016/j.ejps.2018.04.016.

(281) Orofino, F.; Truglio, G. I.; Fiorucci, D.; D'Agostino, I.; Borgini, M.; Poggialini, F.; Zamperini, C.; Dreassi, E.; Maccari, L.; Torelli, R.; Martini, C.; Bernabei, M.; Meis, J. F.; Khandelwal, N. K.; Prasad, R.; Sanguinetti, M.; Bugli, F.; Botta, M. In Vitro Characterization, ADME Analysis, and Histological and Toxicological Evaluation of BM1, a Macrocyclic Amidinourea Active against Azole-Resistant Candida Strains. *Int. J. Antimicrob. Agents* **2020**, *55* (3). https://doi.org/10.1016/j.ijantimicag.2019.105865.

(282) Wohnsland, F.; Faller, B. High-Throughput Permeability PH Profile and High-Throughput Alkane/Water Log P with Artificial Membranes. *J. Med. Chem.* **2001**, *44* (6), 923–930. https://doi.org/10.1021/jm001020e.

(283) Décout, J. Bacterial Lipid Membranes as Promising Targets to Fight Antimicrobial Resistance, Molecular Foundations and Illustration through the Renewal of Aminoglycoside Antibiotics and Emergence of Amphiphilic Aminoglycosides. *Medchemcomm* **2016**, *7*, 586–611. https://doi.org/10.1039/C5MD00503E.

(284) Masungi, C.; Mensch, J.; Van Dijck, A.; Borremans, C.; Willems, B.; Mackie, C.; Noppe, M.; Brewster, M. E. Parallel Artificial Membrane Permeability Assay (PAMPA) Combined with a 10-Day Multiscreen Caco-2 Cell Culture as a Tool for Assessing New Drug Candidates. *Pharmazie* **2008**, *63* (3), 194–199. https://doi.org/10.1691/ph.2008.7327.

(285) He, S.; Zhiti, A.; Barba-Bon, A.; Hennig, A.; Nau, W. M. Real-Time Parallel Artificial Membrane Permeability Assay Based on Supramolecular Fluorescent Artificial Receptors. *Front. Chem.* **2020**, *8*. https://doi.org/10.3389/fchem.2020.597927.

(286) Balimane, P. V.; Pace, E.; Chong, S.; Zhu, M.; Jemal, M.; Van Pelt, C. K. A Novel High-Throughput Automated Chip-Based Nanoelectrospray Tandem Mass Spectrometric Method for PAMPA Sample Analysis. *J. Pharm. Biomed. Anal.* **2005**, *39* (1–2), 8–16. https://doi.org/10.1016/j.jpba.2005.03.043.

(287) Sugano, K.; Hamada, H.; Machida, M.; Ushio, H.; Saitoh, K.; Terada, K. Optimized Conditions of Bio-Mimetic Artificial Membrane Permeation Assay. *Int. J. Pharm.* **2001**, *228* (1–2), 181–188. https://doi.org/10.1016/S0378-5173(01)00845-6.

(288) Khondker, A.; Dhaliwal, A.; Alsop, R. J.; Tang, J.; Backholm, M.; Shi, A. C.; Rheinstädter, M. C. Partitioning of Caffeine in Lipid Bilayers Reduces Membrane Fluidity and Increases Membrane

Thickness. *Phys. Chem. Chem. Phys.* **2017**, *19* (10), 7101–7111. https://doi.org/10.1039/c6cp08104e.

(289) Waters, M. L. Aromatic Interactions in Peptides: Impact on Structure and Function. *Biopolym. - Pept. Sci. Sect.* **2004**, *76* (5), 435–445. https://doi.org/10.1002/bip.20144.

(290) Blanco, F.; Kelly, B.; Alkorta, I.; Rozas, I.; Elguero, J. Cation-π Interactions: Complexes of Guanidinium and Simple Aromatic Systems. *Chem. Phys. Lett.* **2011**, *511* (1–3), 129–134. https://doi.org/10.1016/j.cplett.2011.06.012.

(291) Li, Y.; Liu, J.; Gumbart, J. C. Preparing Membrane Proteins for Simulation Using CHARMM-GUI. In *Methods in Molecular Biology*; Humana Press Inc., 2021; Vol. 2302, pp 237–251. https://doi.org/10.1007/978-1-0716-1394-8_13.

(292) Bankier, C.; Cheong, Y.; Mahalingam, S.; Edirisinghe, M.; Ren, G.; Cloutman-Green, E.; Ciric, L. A Comparison of Methods to Assess the Antimicrobial Activity of Nanoparticle Combinations on Bacterial Cells. *PLoS One* **2018**, *13* (2), e0192093. https://doi.org/10.1371/JOURNAL.PONE.0192093.

(293) Rajamanickam, R.; Kim, H.; Park, J.-W. Tuning Organic Carbon Dioxide Absorbents for Carbonation and Decarbonation. *Sci. Rep.* **2015**, *5*, 10688.

(294) Wang, Z. Tsuji-Trost Reaction. *Compr. Org. Name React. Reagents* **2010**, 2812–2816. https://doi.org/10.1002/9780470638859.CONRR630.

(295) Li, J. J. Tsuji-Trost Reaction. *Name React.* **2021**, 543–546. https://doi.org/10.1007/978-3-030-50865-4_151.

(296) Kürti, L.; Czakó, B. Strategic Applications of Named Reactions in Organic Synthesis - Negishi Cross Coupling. *Strateg. Appl. Named React. Org. Synth.* **2005**, 310.

(297) Luparia, M.; Oliveira, M. T.; Audisio, D.; Frébault, F.; Goddard, R.; Maulide, N. Catalytic Asymmetric Diastereodivergent Deracemization. *Angew. Chemie Int. Ed.* **2011**, *50* (52), 12631–12635. https://doi.org/10.1002/ANIE.201106321.

(298) Aggarwal, V. K.; Monteiro, N.; Tarver, G. J.; McCague, R. Scope and Limitations in Palladium-Catalyzed Substitution Reactions of Unsaturated Fused Lactones. *J. Org. Chem.* **1997**, *62* (14), 4665–4671. https://doi.org/10.1021/JO962106B/SUPPL_FILE/JO4665.PDF.

(299) Jansen, D. J.; Shenvi, R. A. Synthesis of (-)-Neothiobinupharidine. *J. Am. Chem. Soc.* **2013**, *135* (4), 1209–1212. https://doi.org/10.1021/JA310778T/SUPPL_FILE/JA310778T_SI_002.CIF.

(300) Trost, B. M.; Tang, W.; Toste, D. F. Divergent Enantioselective Synthesis of (−)-Galanthamine and (−)-Morphine. *J. Am. Chem. Soc.* **2005**, *127* (42), 14785–14803.

(301) Shen, Y.; Dai, Z.-Y.; Zhang, C.; Wang, P.-S. Palladium-Catalyzed Allylic Alkylation via Photocatalytic Nucleophile Generation. *ACS Catal.* **2021**, 6757–6762. https://doi.org/10.1021/acscatal.1c01500.

(302) Ludwig, R. Hydrogen-Transfer Reactions.Edited by J. T. Hynes, J. P. Klinman, H.-H. Limbach and R. L. Schowen. *ChemPhysChem* **2007**, *8* (17), 2539–2539. https://doi.org/10.1002/CPHC.200700637.

(303) *Encyclopedia of Radicals in Chemistry, Biology and Materials*; John Wiley & Sons, Ltd, 2012. https://doi.org/10.1002/9781119953678.

(304) Capaldo, L.; Ravelli, D. Hydrogen Atom Transfer (HAT): A Versatile Strategy for Substrate Activation in Photocatalyzed Organic Synthesis. *European J. Org. Chem.* **2017**, *2017* (15), 2056–2071. https://doi.org/10.1002/EJOC.201601485.

(305) Capaldo, L.; Quadri, L. L.; Ravelli, D. Photocatalytic Hydrogen Atom Transfer: The Philosopher's Stone for Late-Stage Functionalization? *Green Chem.* **2020**, *22* (11), 3376–3396. https://doi.org/10.1039/D0GC01035A.

(306) Salamone, M.; Bietti, M. Tuning Reactivity and Selectivity in Hydrogen Atom Transfer from Aliphatic C–H Bonds to Alkoxyl Radicals: Role of Structural and Medium Effects. *Acc. Chem. Res.* **2015**, *48* (11), 2895–2903. https://doi.org/10.1021/ACS.ACCOUNTS.5B00348.

(307) Allen, A. E.; MacMillan, D. W. C. Synergistic Catalysis: A Powerful Synthetic Strategy for New Reaction Development. *Chem. Sci.* **2012**, *3* (3), 633–658. https://doi.org/10.1039/C2SC00907B.

(308) Shee, M.; Singh, N. D. P. Cooperative Photoredox and Palladium Catalysis: Recent Advances in Various Functionalization Reactions. *Catal. Sci. Technol.* **2021**, *11* (3), 742–767. https://doi.org/10.1039/D0CY02071K.

(309) Wang, Z. J.; Zheng, S.; Romero, E.; Matsui, J. K.; Molander, G. A. Regioselective Single-Electron Tsuji-Trost Reaction of Allylic Alcohols: A Photoredox/Nickel Dual Catalytic Approach. *Org. Lett.* **2019**, *21* (16), 6543–6547. https://doi.org/10.1021/acs.orglett.9b02473.

(310) Cartwright, K. C.; Tunge, J. A. Organophotoredox/Palladium Dual Catalytic Decarboxylative Csp3-Csp3coupling of Carboxylic Acids and π-Electrophiles. *Chem. Sci.* **2020**, *11* (31), 8167–8175. https://doi.org/10.1039/d0sc02609c.

(311) Masuda, Y.; Ito, M.; Murakami, M. Dehydrative Allylation of α C(Sp3)-H Bonds of Alkylamines with Allylic Alcohols. *Org. Lett.* **2020**, *22* (11), 4467–4470. https://doi.org/10.1021/acs.orglett.0c01464.

(312) Margrey, K. A.; Czaplyski, W. L.; Nicewicz, D. A.; Alexanian, E. J. A General Strategy for Aliphatic C-H Functionalization Enabled by Organic Photoredox Catalysis. *J. Am. Chem. Soc.* **2018**, *140* (12), 4213–4217. https://doi.org/10.1021/JACS.8B00592/SUPPL_FILE/JA8B00592_SI_001.PDF.

(313) Zhang, H. H.; Zhao, J. J.; Yu, S. Enantioselective Allylic Alkylation with 4-Alkyl-1,4-Dihydro-Pyridines Enabled by Photoredox/Palladium Cocatalysis. *J. Am. Chem. Soc.* **2018**, *140* (49), 16914–16919. https://doi.org/10.1021/jacs.8b10766.

(314) Trost, B. M.; Miller, J. R.; Hoffman, C. M. A Highly Enantio- and Diastereoselective Molybdenum-Catalyzed Asymmetric Allylic Alkylation of Cyanoesters. *J. Am. Chem. Soc.* **2011**, *133* (21), 8165–8167. https://doi.org/10.1021/JA2029602/SUPPL_FILE/JA2029602_SI_002.PDF.

(315) Mazzarella, D.; Pulcinella, A.; Bovy, L.; Broersma, R.; No l, T.; Mazzarella, [D; Pulcinella,] A; Bovy,] L; No l, T.; Broersma, R. Rapid and Direct Photocatalytic C(Sp3)−H Acylation and Arylation in Flow. *Angew. Chemie Int. Ed.* **2021**, *60* (39), 21277–21282. https://doi.org/10.1002/ANIE.202108987.

(316) Kamijo, S.; Kamijo, K.; Maruoka, K.; Murafuji, T. Aryl Ketone Catalyzed Radical Allylation of C(Sp3)-H Bonds under Photoirradiation. *Org. Lett.* **2016**, *18* (24), 6516–6519. https://doi.org/10.1021/ACS.ORGLETT.6B03586/SUPPL_FILE/OL6B03586_SI_001.PDF.

(317) Ocola, E. J.; Laane, J. Anomeric Effect in Five-Membered Ring Molecules: Comparison of Theoretical Computations and Experimental Spectroscopic Results. *J. Phys. Chem. A* **2021**, *125* (1), 327–337. https://doi.org/10.1021/ACS.JPCA.0C10158/SUPPL_FILE/JP0C10158_SI_001.PDF.

(318) Szeimies, G.; Miinchen, U. Synthese von [n.1.1]Propellanen (n = 2,3,4). **1992**, *12*, 8–11.

(319) Duan, Z. C.; Hu, X. P.; Zhang, C.; Wang, D. Y.; Yu, S. B.; Zheng, Z. Highly Enantioselective Rh-Catalyzed Hydrogenation of β,γ- Unsaturated Phosphonates with Chiral Ferrocene-Based Monophosphoramidite Ligands. *J. Org. Chem.* **2009**, *74* (23), 9191–9194. https://doi.org/10.1021/JO901619C/SUPPL_FILE/JO901619C_SI_001.PDF.

(320) Lafrance, M.; Roggen, M.; Carreira, E. M. Direct, Enantioselective Iridium-Catalyzed Allylic Amination of Racemic Allylic Alcohols. *Angew. Chemie Int. Ed.* **2012**, *51* (14), 3470–3473. https://doi.org/10.1002/ANIE.201108287.

APPENDIX I: Scientific production

Part of the work herein present has been recently approved as research article and published in *European Journal of Medicinal Chemistry*.

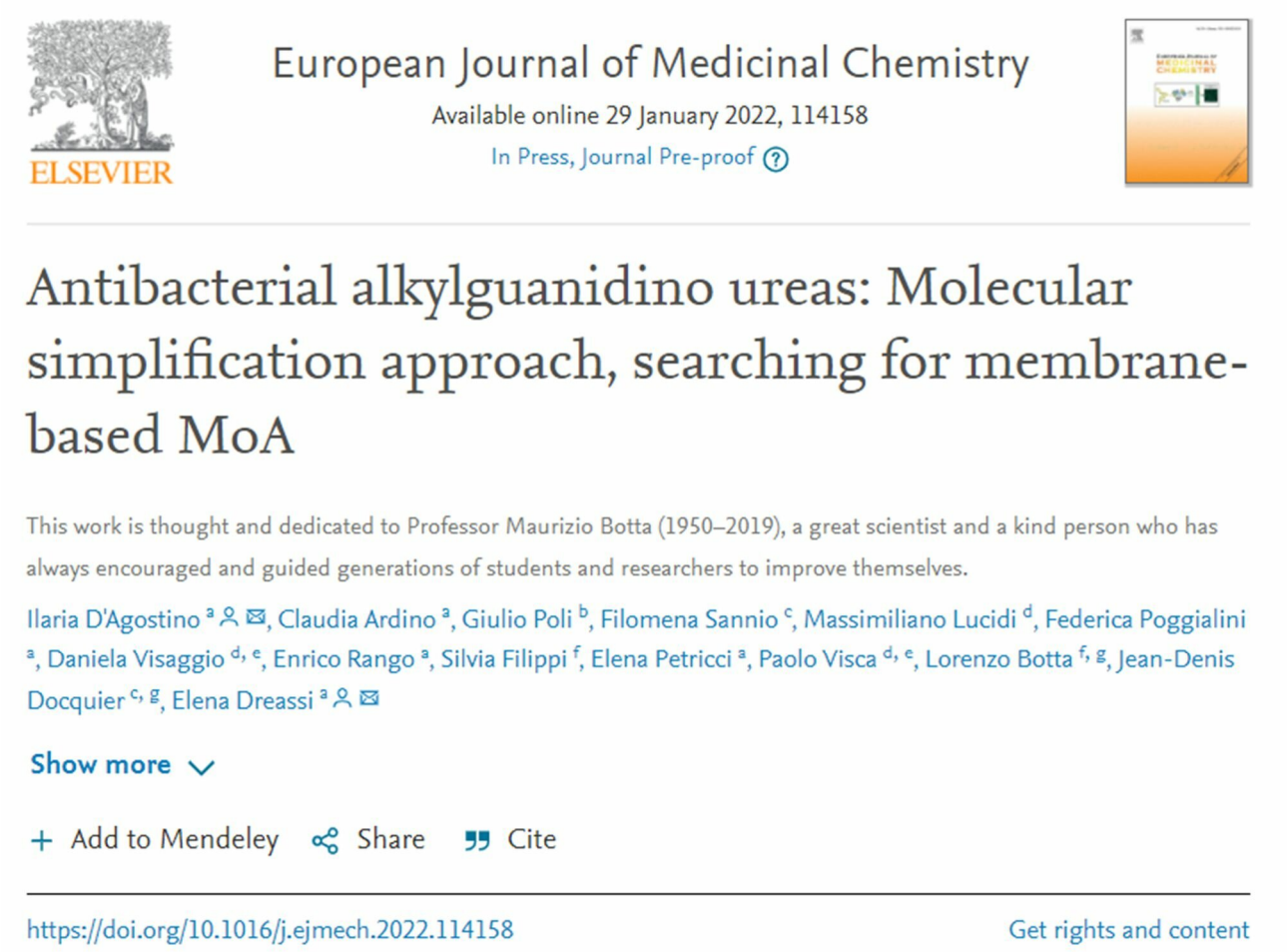

European Journal of Medicinal Chemistry

Available online 29 January 2022, 114158

In Press, Journal Pre-proof

Antibacterial alkylguanidino ureas: Molecular simplification approach, searching for membrane-based MoA

This work is thought and dedicated to Professor Maurizio Botta (1950–2019), a great scientist and a kind person who has always encouraged and guided generations of students and researchers to improve themselves.

Ilaria D'Agostino [a], Claudia Ardino [a], Giulio Poli [b], Filomena Sannio [c], Massimiliano Lucidi [d], Federica Poggialini [a], Daniela Visaggio [d, e], Enrico Rango [a], Silvia Filippi [f], Elena Petricci [a], Paolo Visca [d, e], Lorenzo Botta [f, g], Jean-Denis Docquier [c, g], Elena Dreassi [a]

Show more

+ Add to Mendeley Share Cite

https://doi.org/10.1016/j.ejmech.2022.114158

Get rights and content

Eur. J. Med. Chem. **2022**, 114158.
doi:10.1016/J.EJMECH.2022.114158. **Pre-proof version available online.**

The remaining parts of this work will be subjects of two more research papers currently under authors revision and ready to be submitted:

1. Ardino, C.; D'Agostino, I.; Sannio, F.; Petricci, E.; Botta, L.; Docquier, J.; Dreassi, E. *An Update on New AlkylGuanidino Ureas and Second-Generation Derivatives Endowed with Antibacterial Activity.*
2. D'Agostino, I.; Ardino, C.; Sannio, F.; Pasero, C.; Botta, L.; Dreassi, E.; Docquier, J. *The Impact of Counterions in Biological Activity: Case Study of Antibacterial Alkylguanidino Ureas.*